

AD-A199 220

E (When Data Entered)

STATION PAGE

READ INSTRUCTIONS
BEFORE COMPLETING FORM

1. REPORT NUMBER AFIT/CI/NR 88-190	2. GOVT ACCESSION NO. DTIC FILE COPY	3. RECIPIENT'S CATALOG NUMBER
4. TITLE (and Subtitle) GLOBAL POSITIONING SATELLITE SYSTEM NAVIGATION ACCURACY WITH UPDATED EPHEMERIDES		5. TYPE OF REPORT & PERIOD COVERED PHD THESIS
7. AUTHOR(s) DOUGLAS HAYWARD KIRKPATRICK		6. PERFORMING ORG. REPORT NUMBER
9. PERFORMING ORGANIZATION NAME AND ADDRESS AFIT STUDENT AT: UNIVERSITY OF TEXAS AT AUSTIN		8. CONTRACT OR GRANT NUMBER(s)
11. CONTROLLING OFFICE NAME AND ADDRESS		10. PROGRAM ELEMENT, PROJECT, TASK AREA & WORK UNIT NUMBERS
14. MONITORING AGENCY NAME & ADDRESS (if different from Controlling Office) AFIT/NR Wright-Patterson AFB OH 45433-6583		12. REPORT DATE 1988
		13. NUMBER OF PAGES 291
		15. SECURITY CLASS. (of this report) UNCLASSIFIED
		15a. DECLASSIFICATION/DOWNGRADING SCHEDULE
16. DISTRIBUTION STATEMENT (of this Report) DISTRIBUTED UNLIMITED: APPROVED FOR PUBLIC RELEASE		
17. DISTRIBUTION STATEMENT (of the abstract entered in Block 20, if different from Report) SAME AS REPORT		
18. SUPPLEMENTARY NOTES Approved for Public Release: IAW AFR 190-1 LYNN E. WOLAVER <i>Lynn Wolaver</i> 26 AUG 88 Dean for Research and Professional Development Air Force Institute of Technology Wright-Patterson AFB OH 45433-6583		
19. KEY WORDS (Continue on reverse side if necessary and identify by block number)		
20. ABSTRACT (Continue on reverse side if necessary and identify by block number) ATTACHED		

88 9 6 20 5

DD FORM 1 JAN 73 1473

EDITION OF 1 NOV 65 IS OBSOLETE

UNCLASSIFIED

SECURITY CLASSIFICATION OF THIS PAGE (When Data Entered)

GLOBAL POSITIONING SATELLITE SYSTEM
NAVIGATION ACCURACY WITH UPDATED
EPHEMERIDES

Publication No.

Douglas Hayward Kirkpatrick, Ph.D.
The University of Texas at Austin, 1988

Supervising Professor: Bob E. Schutz

The Department of Defense is developing a space-based navigation system called the Global Positioning System(GPS). The system is composed of three segments: the control segment operated by the Master Control Station(MCS), the space segment with 21 satellites at semi-synchronous altitude, and the user segment which consists of any number of receivers that can process four satellite transmissions for a navigation solution. The MCS performs many vital functions such as creating and uploading each satellite ephemeris. If the MCS were unable to perform these functions, the system accuracy would degrade gracefully over two weeks. After two weeks with no uploaded ephemerides, the satellites would begin broadcasting empty messages which could be used to form pseudorange measurements, although no ephemeris would be

available. By using old ephemerides from other sources and current pseudoranges, updated ephemerides could be formed and used to navigate. GPS system tests, run by the Jet Propulsion Laboratory in April and November, 1985, provided ephemerides and raw pseudoranges from the constellation of seven test satellites for this evaluation of navigation accuracy using old broadcast ephemerides and current pseudoranges. The resulting navigation accuracy appears to be comparable to normal system accuracy, though there are numerous variables affecting the accuracy.

DOUGLAS H. KIRKPATRICK, Lt Col, USAF
306 pages.

Accession For	
NTIS GRA&I	<input checked="" type="checkbox"/>
DTIC TAB	<input type="checkbox"/>
Unannounced	<input type="checkbox"/>
Justification	
By	
Distribution/	
Availability Codes	
Dist	Avail and/or Special
A-1	

GLOBAL POSITIONING SATELLITE SYSTEM

NAVIGATION ACCURACY WITH UPDATED

EPHEMERIDES

by

Douglas Hayward Kirkpatrick, B.S., M.S.

DISSERTATION

Presented to the Faculty of the Graduate School of

The University of Texas at Austin

in Partial Fulfillment

of the Requirements

for the Degree of

DOCTOR OF PHILOSOPHY

THE UNIVERSITY OF TEXAS AT AUSTIN

August 1988

ACKNOWLEDGMENTS

My name appears alone on the cover of this dissertation but many people helped. First of all, I want to thank all of my professors at The University of Texas for their encouragement and technical advice. Particularly Bob E. Schultz was patient with my early stumblings and directed me toward the current work. I greatly appreciate the help of P.A.M. Abusali who gave technical advice and acquired all of the raw data for me.

Credit for the finished report goes to Ms Catherine Richard at the Air Force Academy who labored through typing all of the equations, forming all of the tables and typing all of the words inbetween on a persnickity machine.

Finally, and most importantly, I thank my wife, [REDACTED] and children, [REDACTED] who stuck by me throughout this work and to whom I am eternally dedicated.

GLOBAL POSITIONING SATELLITE SYSTEM
NAVIGATION ACCURACY WITH UPDATED
EPHEMERIDES

Publication No.

Douglas Hayward Kirkpatrick, Ph.D.
The University of Texas at Austin, 1988

Supervising Professor: Bob E. Schutz

The Department of Defense is developing a space-based navigation system called the Global Positioning System(GPS). The system is composed of three segments: the control segment operated by the Master Control Station(MCS), the space segment with 21 satellites at semi-synchronous altitude, and the user segment which consists of any number of receivers that can process four satellite transmissions for a navigation solution. The MCS performs many vital functions such as creating and uploading each satellite ephemeris. If the MCS were unable to perform these functions, the system accuracy would degrade gracefully over two weeks. After two weeks with no uploaded ephemerides, the satellites would begin broadcasting empty messages which could be used to form

pseudorange measurements, although no ephemeris would be available. By using old ephemerides from other sources and current pseudoranges, updated ephemerides could be formed and used to navigate. GPS system tests, run by the Jet Propulsion Laboratory in April and November, 1985, provided ephemerides and raw pseudoranges from the constellation of seven test satellites for this evaluation of navigation accuracy using old broadcast ephemerides and current pseudoranges. The resulting navigation accuracy appears to be comparable to normal system accuracy, though there are numerous variables affecting the accuracy.

TABLE OF CONTENTS

	<u>Page</u>
Acknowledgements	iii
Abstract	iv
List of Figures	x
List of Tables	xiv
Chapter One - History of Navigation by Satellite . .	1
1.1 Introduction	1
1.2 The Global Positioning Satellite System. . . .	3
A. The Control Segment.	6
B. The Space Segment.	7
C. The User Segment	8
D. GPS Error Sources.	10
1.3 Purpose of the Study.	13
Chapter Two - GPS Broadcast Ephemeris	15
2.1 Introduction	15
2.2 The Broadcast Ephemeris Model.	15
A. Overview	15
B. The Broadcast Ephemeris Algorithm.	19
C. The Broadcast Ephemeris Estimator.	27
D. Validation of the Broadcast Ephemeris Parameter Determination.	37
D.1 Determination of the Predicted Ephemeris.	44

D.2	Ill-Conditioning in the Normal Matrix. . .	77
2.3	Summary	79
Chapter Three - Broadcast Ephemeris Update Processor 80		
3.1	Introduction.	80
3.2	The Broadcast Ephemeris Update Algorithm. . .	85
3.3	Test Data	92
3.4	Update Algorithm Observability.	99
3.5	Experiments with the Ephemeris Update Estimator	100
A.	Validation Tests.	101
B.	Long Range Ephemeris Updates.	115
3.6	Summary	136
Chapter Four - User Navigation Algorithm. 139		
4.1	Introduction.	139
4.2	The Differential Correction Algorithm	140
A.	Experiments with Differential Correction Algorithm	150
4.3	The Extended Kalman Filter.	162
A.	Experiments with the Extended Kalman Filter.	167
4.4	Summary	186
Chapter Five - Navigation Accuracy Using Updated Ephemerides 188		
5.1	Introduction	188
5.2	System and Algorithm Characteristics	189
5.3	Experiments in Navigation Using Updated Ephemerides	197

A.	Navigation Accuracy with Broadcast Ephemerides on 21 November	197
B.	Navigation Accuracy with Updated Ephemerides on 21 November	201
B.1	11 October Ephemerides Updated on 21 November.	203
B.2	13 September Ephemerides Updated on 21 November.	207
B.3	Three, Five, and Seven Month Old Ephemerides Updated on 21 November	210
C.	Navigation Accuracy with the Broadcast Ephemerides on 20 November	216
D.	Navigation Accuracy with Updated Ephemerides on 20 November	218
D.1	11 October Ephemerides Updated on 20 November.	220
D.2	13 September Ephemerides Updated on 20 November	221
D.3	Three, Five, and Seven Month Old Ephemerides Updated on 20 November	222
E.	Navigation Accuracy at Richmond, FL, with Broadcast Ephemerides on 21 November . . .	226
E.1	Navigation Accuracy at Richmond with Updated Ephemerides from Fort Davis. . . .	229
E.2	One to Seven Month Old Ephemerides Updated on 21 November at Fort Davis and Used at Richmond	230
5.4	Summary	234
5.5	Aerospace Corporation Autonomous User Study .	235
Chapter Six -	Conclusions and Recommendations	237
6.1	Conclusions	238

6.2 Recommendations	239
Appendix A - Formulation of the Longitude of Longitude of Ascending Node in the ECF Coordinate System.	241
Appendix B - Summary of the Broadcast Ephemeris Algorithm.	243
Appendix C - The Measurement Sensitivity Matrix for the Broadcast Ephemeris Algorithm . . .	246
Appendix D - The Measurement Sensitivity Matrix for the Ephemeris Update Algorithm	272
Appendix E - Propagating the Broadcast Parameters to the Update Time	277
Appendix F - Derivation of the Filter Gain and Covariance Matrix for the Extended Kalman Filter	280
References	286
Vita	

LIST OF FIGURES

	<u>Page</u>
2-1 RMS of Residuals Plot	52
2-2 Change in Mean Anomaly Plot	53
2-3 Change in Mean Motion Plot	54
2-4 Square Root of Semimajor Axis Plot.	55
2-5 Eccentricity Plot	56
2-6 Ascending Node Plot	57
2-7 Inclination Plot	58
2-8 Argument of Perigee Plot	59
2-9 Ascending Node Rate Plot	60
2-10 Inclination Rate Plot	61
2-11 Change in Argument of Latitude Plot	62
2-12 C_{uc} Zonal Parameter Plot	64
2-13 C_{us} Zonal Parameter Plot	64
2-14 C_{rc} Zonal Parameter Plot	65
2-15 C_{rs} Zonal Parameter Plot	66
2-16 C_{ic} Zonal Parameter Plot	67
2-17 C_{is} Zonal Parameter Plot	68
2-18 X Residuals Plot	70
2-19 Y Residuals Plot.	70
2-20 Z Residuals Plot.	71
2-21 Radial Difference Between Broadcast Ephemeris and UTOPIA Orbits	73

2-22	Transverse Difference Between Broadcast Ephemeris and UTOPIA Orbits	74
2-23	Normal Difference Between Broadcast Ephemeris and UTOPIA Orbits	75
3-1	Comparison of RMS of Residuals, Updated Ephemerides	132
3-2	Comparison of Position Errors, Updated Ephemerides	133
3-3	Comparison of Updated Mean Anomaly One Sigma Values	134
3-4	Comparison of Changes in Updated Values of the Square Root of the Semimajor Axis, Mean Anomaly and Argument of Latitude	135
4-1	Position Error Versus Time, Fort Davis, TX . . .	153
4-2	Position Error Versus Time, Richmond, FL . . .	153
4-3	Position Error Versus Time, Haystack, MA . . .	154
4-4	User Clock Bias Versus Time, Fort Davis, TX . . .	156
4-5	User Clock Bias Versus Time, Richmond, FL . . .	157
4-6	User Clock Bias Versus Time, Haystack, MA . . .	157
4-7	GDOP Versus Time, Fort Davis, TX	159
4-8	GDOP Versus Time, Richmond, FL	160
4-9	GDOP Versus Time, Haystack, MA	160
4-10	Position Error at Fort Davis, 1 April 1985 . .	172
4-11	Position Error at Fort Davis, 2 April 1985 . .	173
4-12	Position Error at Fort Davis, 3 April 1985 . .	173
4-13	Position Error at Richmond, 1 April 1985. . . .	177
4-14	Position Error at Haystack, 1 April 1985 . . .	178
4-15	GDOP at Fort Davis, 1 April 1985	179

4-16	Clock Bias at Fort Davis, 1 April 1985	180
4-17	GDOP at Fort Davis, 2 April 1985	180
4-18	Clock Bias at Fort Davis, 2 April 1985	181
4-19	GDOP at Fort Davis 3 April 1985	181
4-20	Clock Bias at Fort Davis, 3 April 1985	182
4-21	GDOP at Richmond, 1 April 1985	182
4-22	Clock Bias at Richmond, 1 April 1985	183
4-23	GDOP at Haystack, 1 April 1985	183
4-24	Clock Bias at Haystack, 1 April 1985	184
5-1	Position Error - Broadcast Ephemerides - 21 November 1985	200
5-2	GDOP - Broadcast Ephemerides - 21 November 1985	200
5-3	Position Error - Updated Ephemerides - 21 November 1985	202
5-4	Position Error - Updated Ephemerides - 11 October 1985, No Earth Rate Correction . . .	206
5-5	Position Error - Updated Ephemerides - 11 October 1985, With Earth Rate Correction . .	206
5-6	Position Error - Updated Ephemerides - 13 September 1985, No Earth Rate Correction . .	209
5-7	Position Error - Updated Ephemerides - 13 September 1985, With Earth Rate Correction .	209
5-8	Position Error - Updated Ephemerides - 13 August 1985, No Earth Rate Correction . . .	212
5-9	Position Error - Updated Ephemerides - 13 August 1985, With Earth Rate Correction . .	212
5-10	Position error - Updated Ephemerides - 11 June 1985, No Earth Rate Correction	213

5-11	Position Error - Updated Ephemerides - 11 June 1985, With Earth Rate Correction . . .	213
5-12	Position Error - Updated Ephemerides - 5 April 1985, With Earth Rate Correction . . .	214
5-13	Position Error - Updated Ephemerides - 5 April 1985, With Earth Rate Correction . . .	214
5-14	Position Error - Broadcast Ephemerides - 20 November 1985	218
5-15	Position Error - Updated Ephemerides - No Earth Rate Correction	224
5-16	Position Error - Richmond - Broadcast Ephemerides - 21 November 1985	227
5-17	GDOP - Richmond - Broadcast Ephemerides - 21 November 1985	228
5-18	Clock Bias - Richmond - Broadcast Ephemerides - 21 November 1985	228
5-19	Position Error - Updated Ephemerides - Richmond - 21 November 1985	230
5-20	Position Error - Updated Ephemerides - Richmond - 11 October 1985	232
5-21	Position Error - Updated Ephemerides - Richmond - 13 September 1985	232
5-22	Position Error - Updated Ephemerides - Richmond - 13 August 1985	233
5-23	Position Error - Updated Ephemerides - Richmond - 11 June 1985	233
5-24	Position Error - Updated Ephemerides - Richmond - 5 April 1985	234
A-1	Longitude of the Ascending Node	242

LIST OF TABLES

	<u>Page</u>
1-1 GPS Range Error	12
2-1 Broadcast Ephemeris Parameters with GEL Ephemeris	42
2-2 Perturbed Initial Conditions for Creating Broadcast Ephemerides	43
2-3 UTOPIA Orbit Perturbations.	44
2-4 Broadcast Ephemeris Parameters from UTOPIA Ephemeris	46
2-5 Variances of the Estimated Ephemeris Parameters	47
2-6 GPS Perturbing Accelerations	50
2-7 Comparison of Broadcast Ephemeris Estimates . . .	76
2-8 Comparison of Broadcast Ephemeris Estimates . . .	77
3-1 Range of Values for the Accuracy Criteria	83
3-2 Observation Sets for Fort Davis, TX, April 1985 .	98
3-3 Observation Sets for Richmond, FL, April 1985 . .	98
3-4 Validation Test - Fort Davis, TX, April 1985. . .	105
3-5 Validation Tests - Richmond, FL, April 1985 . . .	106
3-6 Validation Tests - Fort Davis, TX, November 1985.	108
3-7 SV11 Parameter Differences (750 obs) Fort Davis, TX, 3 April 1985.	110
3-8 SV11 Parameter Differences (750 obs) Richmond, FL, 3 April 1985.	111
3-9 SV11 Parameter Differences (750 obs) Fort Davis, TX, 20 November 1985.	111

3-10	Updated SV11 Parameter One Sigma Values, Fort Davis, TX, 3 April 1985.	113
3-11	Updated SV11 Parameter One Sigma Values, Richmond, FL, 3 April 1985.	113
3-12	Updated SV11 Parameters One Sigma Values, Fort Davis, TX, 20 November 1985.	114
3-13	Propagated Ephemeris Position Errors Before Applying the Ephemeris Update Algorithm SV11. . .	117
3-14	Position Errors Caused by Holding the Perturbation Parameters Constant to 20 November - SV11.	119
3-15	October Ephemeris Updates on 20 November 1985, Fort Davis, TX	121
3-16	Updated SV11 Parameter Differences (600 obs) 11 October 1985	122
3-17	Updated SV11 Parameter One Sigma Values, 11 October 1985	122
3-18	September Ephemeris Updates on 20 November 1985, Fort Davis, TX	124
3-19	Updated SV11 Parameter Differences (600 obs), 13 September 1985	124
3-20	Updated SV11 Parameter One Sigma Values, 13 September 1985	125
3-21	August Ephemeris Updates on 20 November 1985, Fort Davis, TX	126
3-22	Updated SV11 Parameter Differences (600 obs), 13 August 1985	126
3-23	Updated SV11 Parameter One Sigma Values, 13 August 1985	127
3-24	June Ephemeris Updates on 20 November 1985, Fort Davis, TX	128
3-25	Updated SV11 Parameter Differences (600 obs), 11 June 1985	128

3-26	Updated SV11 Parameter One Sigma Values, 11 June 1985	129
3-27	April Ephemeris Updates on 20 November 1985, Fort Davis, TX	129
3-28	Updated SV11 Parameter Differences (600 obs), 5 April 1985	130
3-29	Updated SV11 Parameter One Sigma Values, 5 April 1985	130
3-30	Ephemeris Update Estimator Assumptions.	137
3-31	Significant Results of the Ephemeris Update Algorithm	138
4-1	Initial and Final Variances of the State	161
4-2	X_u Position Variances	186
5-1	Satellite Updated Position Errors, Radial Com- ponents, Subsequent Navigation Position Error	225

Chapter One History of Navigation by Satellite

1.1 Introduction

Accurate surface navigation using space-based transmitters has been a goal of the United States Department of Defense since the late 1950's. This goal was a natural outgrowth of navigating by the stars, except with modern satellites, the stars could be man-made. Because these modern stars were man-made, they were built to transmit useful navigation signals to a variety of users. Early users were naval vessels which needed worldwide coverage in all types of weather conditions. More recent users include land and air craft which require both position and velocity as well as a highly accurate time. This first chapter will give a brief history of the Navstar Global Positioning System, as the current system is known, describe the operation during the Phase One Tests, and discuss the purpose of this study of navigation accuracy using old satellite ephemerides.

The first space-based navigation system was the Navy Transit system which was funded in December 1958 and became operational in January 1964. This system evolved from the need for position updates to the inertial navigation equipment used on the Polaris submarines. The concept for the satellite system came from early studies

done at the Applied Physics Laboratory, Johns Hopkins University, of the radio transmissions by the Sputnik I satellite. Under the leadership of Richard B. Kershner, the concept of determining a position using Doppler measurements from a satellite with an accurately known orbit was developed.

The result of the navigation satellite studies performed in the early 1960's was the current system of five Transit satellites in circular, polar orbits, at about 1,075 kilometers altitude. With the system, two-dimensional position fixes could be obtained every 35 to 100 minutes, depending on the latitude of the receiver. Although some of the satellites have been in operation for 20 years, the Transit system is still a significant contribution to satellite navigation.

The Transit system is operated by the Navy Astronautics Group at Point Mugu, California. At this computing center, tracking data from three sites in the United States are used to form navigation messages for transmission to each satellite. The satellites, in turn, transmit their messages to users on the surface for navigation. The transmitted messages allow users to calculate the satellite position as a function of time. The user navigation algorithm then uses the satellite position and about 15 minutes of Doppler measurements to estimate the

user position. Typical accuracies are on the same order as short range radio beacons[Stansell,1979]. The Transit system is expected to continue operation into the 1990's [Sentman,et.al.,1986].

The next space-based navigation system was another Navy project known as Timation, which is an acronym for Time Navigation[Easton,1979]. The Naval Research Laboratory was tasked by the Bureau of Naval Weapons in September, 1964, to develop a passive ranging process for a surface navigation system. The heart of the new system was two highly accurate atomic clocks, synchronized between the satellite and the user so that range measurements could be taken passively, just by receiving a timed signal from a satellite. The navigation process was similar to the Transit system except for the passive ranging. The first Timation satellite was launched into an 800 kilometer orbit in May 1967, with successful navigation results. Timation experience acquired about atmospheric drag and radio frequency signal propagation through the ionosphere, as well as advancements in atomic clocks, prompted later improvements in the Timation satellites.

1.2 The Global Positioning Satellite System

At the same time the Navy was improving the Timation

system, the Air Force was designing a three-dimensional worldwide system called Project 621B with similar objectives. On 17 April, 1973, the Deputy Secretary of Defense announced a merging of the Navy and Air Force plans into the Navstar Global Positioning System (GPS) to serve all of the Department of Defense [Joint Program Office, 1984]. One more Timation satellite was launched which was designated Navigation Technology Satellite One (NTS-1), a research vehicle for the new GPS design. This satellite carried GPS experiments including the signal encoder and two new rubidium clocks which would be the heart of the early GPS development satellites. All of the follow-on satellites were designed to test GPS concepts for the benefit of all the armed services and a new, growing civilian clientele [Easton, 1979].

The GPS joint service project incorporated all of the best features of the three previous systems to provide a continuous, worldwide, all-weather, three-dimensional, highly accurate navigation capability. As a military system it was required to be survivable and jam-resistant, as well. All of these critical requirements were met in a joint system concept.

The current GPS concept provides for a constellation of 18 satellites and three operating spares positioned in six evenly spaced orbit planes at 55 degrees inclination.

The orbits are at semi-synchronous altitude (20,183 km) so that at least four satellites are visible to users located anywhere in the world at any time[Kruh,1981]. With at least four satellites in view, a user can receive a transmitted message from each satellite, providing data to enable calculation of the satellite positions. Along with the four satellite positions, the user can compute ranges to the satellites by multiplying the signal transit time by the speed of light. Several small errors in these range calculations make them inexact and the term "pseudorange" is applied.

The navigation algorithm uses four pseudoranges and estimates the user position as the intersection of the four spheres centered at the four satellites with radii equal to the four pseudoranges. Three spheres could be used to estimate the user position, but the fourth allows estimation of the user clock bias which is critical for synchronizing the user clock with GPS time. This clock synchronization satisfies the requirement for passive ranging which permits any number of users to receive signals and navigate simultaneously[Milliken and Zoller,1980]. The resulting navigation solution will yield 15 meter position, 0.1 meter per second velocity, and 100 nanosecond time accuracy, assuming that three system segments operate nominally[Joint Program

Office,1984]. These segments are the Control Segment, the Space Segment, and the User Segment.

A. The Control Segment

The Control Segment consists of the Master Control Station (MCS) and five Monitor Stations (MS). Early tests included an Upload Station and a computation center which are now incorporated in the MCS. The MCS controls all of the GPS operations from its location at Falcon Air Force Station, Colorado. The primary MCS functions are to compute all of the satellite messages and upload the messages to the satellites. Other tasks include maintaining the satellite health information, reporting system status to users, and controlling the satellite attitude and momentum dumping. The message process begins with measurements of pseudorange and delta-pseudorange, or integrated Doppler, from all the satellites, taken at the five Monitor Stations, located at Wahiawa, Hawaii, Ascension Island, Diego Garcia, Kwajalein Atoll, and Falcon Air Force Station, Colorado[Conley,1987]. These unmanned Monitor Stations also collect meteorological conditions for future computation of the tropospheric delay to the signal propagation. The pseudorange and delta-pseudorange measurements are sent to the MCS for generating the hourly ephemerides for the 21 satellites

(discussed in Section 2.2.A). The hourly ephemeris messages contain 15 parameters for computing the satellite position; two clock parameters for synchronizing the satellite clock with the GPS time kept at the MCS, satellite health codes, and an ephemeris almanac for initial position calculation. At least once a day, the MCS transmits the ephemeris messages to each satellite which stores a two week supply of its own messages. When an accurate set of messages are on board each satellite, the ground segment has completed its primary task[Hurley, et.al.,1978].

B. The Space Segment

The Space Segment of the system consists of the 21 satellites which store and continuously transmit the current-hour messages. The constellation as described previously guarantees at least four satellites are more than five degrees above the horizon everywhere on the Earth. This arrangement provides continuous navigation coverage almost everywhere in the world, except for short periods in relatively small areas at mid-latitudes where the visible satellites experience a geometry that results in a degraded navigation solution[Kruh,1981].

The ephemeris messages are transmitted on two radio frequency channels, L_1 and L_2 , and are formatted into

five 300-bit subframes which require a total of 30 seconds to transmit. The L_1 signal is modulated on a long precision code known as the P-code, and a short code known as the C/A-code (coarse/acquisition). The L_2 signal is modulated only on the P-code. The two codes help identify each spacecraft since code patterns are vehicle-specific, and help measure the signal transit time by measuring the phase shift required to match the codes. Because the P-code is transmitted on both channels, users who receive both frequencies can calculate an ionospheric delay correction term which improves the accuracy of the navigation solution. Thus, receivers with a dual frequency capability are considered to be precision user systems[Milliken and Zoller,1980].

C. The User Segment

The user systems, whether on the land, in the air, at sea, or in space, make up the third segment of the GPS System. The myriad of possible receiver configurations must be capable of performing the following functions: satellite selection, signal acquisition, tracking and measurement, and data recovery. To perform these functions the User Equipment (UE) consists of an antenna, receiver, computer, and input/output devices.

The antenna must be able to receive the appropriate

transmission frequencies from any quadrant above the unit. Antenna placement on the unit must allow a clear view of the sky and be free of reflected multipath signals that may interfere with the reception.

The receiver architecture depends on the type of navigation process required for the vehicle. The simplest, for a stationary unit, processes one C/A signal at a time. More complex receivers may process the C/A and both P signals from four satellites simultaneously. The more maneuverable the vehicle and the more accurate the navigation, the more elaborate the receiver must be.

The computer controls the unit operation and calculates the navigation solution. The computer must select the satellites (when more than four are visible), correct the measurements for propagation effects, and communicate with the input/output devices.

Finally, the input/output devices depend on the vehicle and type of data links that may be required. For instance, for a stationary unit, simple digital displays of longitude, latitude, and altitude may suffice, but for a unit linked to a fighter aircraft flight control computer the requirements will include data transfer busses, an attitude reference system, an antenna offset figure and an altitude feedback loop[Glazer,1980].

D. GPS Error Sources

Several error sources in the range measurements limit the accuracy of the GPS system. Table 1-1 shows the error sources and expected range errors. The first of these errors is the space vehicle clock errors which are generally small because of the stability in the atomic clocks. However, since the clocks do wander slightly and may deviate as much as 976 microseconds from the official GPS system time, the MCS computes a satellite clock bias and drift rate which are transmitted in the ephemeris message so user equipment can apply the correction[Milliken and Zoller,1980].

The second error source is a time delay due to the transmitted signal being refracted by the ionosphere and the troposphere. The ionospheric delay is approximated by the inverse of the square of the frequency, so when receiving both L_1 and L_2 signals the user equipment can calculate an accurate correction. Single frequency receivers will not be able to make as accurate a correction, however. The tropospheric delay is frequency independent but is modelled using atmospheric density and the elevation angle of the satellite[Milliken and Zoller,1980].

Group delays are the next error sources, defined as

errors caused by signal processing and passage through the satellite equipment. These delays must be calibrated during ground tests and included in the satellite clock bias and drift rate[Milliken and Zoller,1980].

Next are ephemeris errors which are satellite position errors caused by inaccuracies in the 15 parameters that comprise the broadcast ephemeris. Because the MCS creates the ephemerides by fitting a week of satellite pseudorange measurements from five monitor stations, then predicts the satellite position two weeks into the future and finally, uses same-day pseudorange measurements in an optimal filter, the ephemerides are highly accurate. Yet, satellite positions may be several meters in error. Range errors are more significant than along-orbit (transverse) or cross-orbit (normal) errors, since the user position is calculated as the intersection of four spheres. The effect of the range errors on the navigation solution is reduced somewhat in the user equipment by the user clock bias estimate.

Another error source is due to multipath effects caused by receiving data from more than one propagation path. Reflective surfaces near the user antenna produce the multiple signal paths. These errors are expected to be less than one meter[Milliken and Zoller,1980].

The next error sources are the receiver noise and

resolution. Receiver hardware and software capabilities will determine the size of these errors. The need for highly accurate solutions will encourage the use of high resolution equipment[Milliken and Zoller,1980].

Finally, the receiver vehicle dynamics will produce the last of the range errors. High-speed, low-altitude aircraft will need special receivers and Kalman processing to reduce these errors. Because of the variety of users, no specific error value is attributed to the vehicle dynamics[Milliken and Zoller,1980].

Table 1-1
GPS Range Error

Source	User Range Error (1σ)
Satellite Clock + Ephemeris Errors	1.5 meters
Atmospheric delays	2.4-5.2 meters
Group delays	1.0 meters
Multipath	1.2-2.7 meters
Receiver noise, resolution + vehicle dynamics	1.5 meters
Root Sum Square	<u>3.6-6.3 meters</u>

[Milliken and Zoller,1980].

1.3 Purpose of the Study

This study of the GPS navigation accuracy using old broadcast ephemerides was prompted by the GPS system dependence on the Control Segment. As described earlier, the Master Control Station manages a multitude of critical functions at one site, Falcon Air Force Station, Colorado. The loss of certain functions at the MCS may prevent the uploading of the ephemeris messages. Without new messages, the satellites will continue to broadcast the supply of stored messages from the last upload (a 14 day supply in the operational satellites) [Moller, 1984]. When the satellites exhaust their storage, timed signals continue to be broadcast so pseudorange measurements can be received. The pseudoranges from four satellites can be used to update their old broadcast ephemerides to the pseudorange time and then be reused with the updated ephemerides to navigate. The actual availability of old broadcast ephemerides and mechanization of the hardware in this scenario was not considered. This study analyzes certain broadcast ephemeris characteristics, the broadcast ephemeris update process, and the navigation process with current broadcast ephemerides and updated ephemerides. No attempt is made to generalize by suggesting that the update or navigation test cases represent all

possible conditions. On the contrary, very specific test cases are described and the results presented.

As previously mentioned the early tests of the GPS concept were highly successful. In October 1978, the first of the Phase One test satellites was launched to begin a small constellation to validate the system. By April of 1985 seven operating satellites were available for system tests. The Jet Propulsion Laboratory organized a Spring 1985 High Precision Baseline Test with receivers located at many surveyed sites around the United States. Another similar test was conducted in November 1985. Pseudorange measurements and broadcast ephemerides were collected at the sites and made available for research. The Applied Research Laboratory at the University of Texas at Austin made available data from Fort Davis, Texas, Richmond, Florida, and Haystack, Massachusetts, for this study of navigation accuracy using old broadcast ephemerides. The test conditions for this study, including the satellites, the site locations, and the receiver equipment are presented in Section 3.1

The results of this study show that the old broadcast ephemerides can be updated with reasonable accuracy and that navigation accuracy with the updated ephemerides depends on many variables but, for certain test cases, was comparable to normal GPS operations.

Chapter Two GPS Broadcast Ephemeris

2.1 Introduction

This analysis of the GPS system begins with a batch linearized least squares estimator used to determine the satellite broadcast ephemeris parameters. This discussion introduces the GPS orbit parameters, the ephemeris representation, and the estimation process, all of which play important parts in the GPS system analysis described in later chapters. To study the GPS system, one must be familiar with the fifteen orbit parameters, the mathematical model used for the ephemeris representation, and the sensitivities of the estimation process in the GPS system. This chapter establishes the foundation for the following chapters.

2.2 The Broadcast Ephemeris Model

A. Overview

The Broadcast Ephemeris consists of a set of 15 Keplerian-like parameters which are produced by the Master Control Station(MCS), transmitted to the satellite, and broadcast by the satellite for GPS users. The parameters permit users to locate each satellite at any time as part of the user navigation process. Creation of each

ephemeris requires a three-step process for the MCS.

The first step in the process is a batch, least squares fit of one week of pseudorange measurements from the five Monitor Stations to produce a reference ephemeris. This reference ephemeris is extrapolated two weeks into the future to serve as a basis around which perturbations are computed.

The perturbations are computed in step two, which requires current measurements of each satellite [Russell and Schaibly, 1978]. These measurements are also pseudorange measurements taken at 1.5 second intervals and transmitted immediately to the MCS through dedicated phone lines. The MCS collects 15 minutes of pseudorange measurements for each satellite, then smooths the data so that one pseudorange measurement is available for processing in a Kalman estimator. The Kalman estimator produces current estimates of the six element satellite state (\bar{r}, \bar{v}) , two solar pressure parameters, three satellite clock states (bias, frequency offset, and drift rate), and two clock states for each of the Monitor Stations. So, every 15 minutes a new satellite state is available. At the same time the current estimate is made, the MCS again extrapolates the satellite state two weeks into the future, yielding predictions of \bar{r} and \bar{v} at 15-minute intervals.

The final step fits the predicted state vectors with an appropriate approximation function, namely the mathematical model that uses the 15 broadcast ephemeris parameters. The fitting process uses four hours of state vectors to estimate the broadcast ephemeris parameters at the middle of the four-hour period. This estimate of the parameters is valid for only one hour, starting at the beginning of the third hour of the four-hour period. Another set of parameters, valid for the next hour, is estimated using the next four-hour block of state vectors. In other words, the four-hour blocks of predicted state vectors slide forward one hour to obtain each new hour's broadcast ephemeris. By this method, 24 one-hour broadcast ephemerides are calculated and made available for uploading to the satellite.

After 24 hours of ephemerides are generated the fitting process changes to six hours of predicted state vectors to formulate future ephemerides that are valid for four hours each. This extended process saves computer time at the MCS, since the ephemerides beyond 24 hours are not expected to be used, but serve as a backup in case the formulation process fails. The broadcast ephemeris generation and satellite upload occur every six to eight hours with each satellite storing approximately three and a half days of ephemerides to be broadcast each

hour.

In summary, the broadcast ephemerides that the user receives from the GPS satellites are created in the MCS through four-hour fits of satellite state vectors which are generated by extrapolating current Kalman filter estimates of the state vectors. The Kalman estimates are computed as perturbations to the reference ephemeris which is created by a batch least squares estimator using measurements from the previous week[Brown,1987].

The broadcast ephemerides are approximations to the actual predicted ephemerides and describe elliptical orbits with secular and periodic perturbations. The broadcast ephemeris parameters are Keplerian in appearance, however even with terms that represent secular and periodic perturbations, they are accurate for only a few hours. Consequently, new orbit parameters are available for each hour and broadcast by the individual satellites. Each ephemeris, composed of the 15 constants, is broadcast for an hour and then replaced in the broadcast message by the next hour's ephemeris. The accuracy of the constant parameter ephemerides drifts during the hour of applicability, but is sufficiently accurate to meet the required navigation specifications [Van Dierendonck, et.al., 1978].

The coordinate system for the mathematical model of

the broadcast ephemeris is Earth-centered, Earth-fixed (ECF). The origin is the center of mass of the earth and the x-axis is located at the Prime Meridian in the equatorial plane. The y-axis is 90 degrees east of the x axis in the equatorial plane and the z-axis is assumed to be coincident with the rotation axis of the Earth. The coordinate system rotates with the Earth, which necessitates the Earth-rate adjustment to the longitude of the ascending node. As will be seen in the next section, the broadcast ephemeris parameter for longitude of the ascending node is Ω_0 which is the only reference among the parameters to the Earth-centered, nonrotating coordinate system. The Ω_0 parameter relates the ascending node of the orbit plane to an inertial coordinate system [Van Dierendonck, et.al., 1978].

B. The Broadcast Ephemeris Algorithm

The algorithm used to compute the satellite position from the broadcast information, which consists of the 15 ephemeris parameters, is described by Van Dierendonck, et.al., [1978] and will be referred to as the Broadcast Ephemeris Algorithm (BEA) throughout this paper. Although the algorithm now uses 15 parameters, 14 parameters were used in the original version. In addition to the ephemeris parameters, an epoch time at the

beginning of the hour in which the parameters apply is broadcast.

Of the 15 ephemeris parameters, six are Keplerian in nature and the remaining nine are associated with corrections required to account for orbit perturbations. All 15 parameters are constant for one hour that starts at the epoch time. The Keplerian parameters are as follows:

- M_0 - Mean anomaly at epoch time
- e - Eccentricity
- \sqrt{A} - Square root of the semimajor axis
- Ω_0 - Longitude of the ascending node at epoch time
(with respect to Earth-centered Nonrotating coordinates) (see Appendix A for how Ω_0 is related to the GPS rotating coordinates)
- i_0 - Inclination at epoch time
- u - Argument of perigee

The nine correction terms are:

- Δn - Change in mean motion
- $\dot{\Omega}$ - Rate of longitude of ascending node
- di/dt - Inclination rate
- C_{uc}, C_{us} - Amplitudes of the cosine and sine harmonic correction to the argument of latitude.
- C_{rc}, C_{rs} - Amplitudes of the cosine and sine harmonic correction to the orbit radius.
- C_{ic}, C_{is} - Amplitudes of the cosine and sine harmonic correction to the inclination.

These parameters enable computation of an ephemeris during the interval following the epoch time, t_{oe} . The t_{oe} is the beginning of a one-hour interval during which the constant parameters are valid, expressed in seconds past 00:00 Sunday, GPS time. It is reset to zero each Sunday at 00:00, so it never exceeds 604,800 seconds. Examples of t_{oe} are the following:

- * 36,000 seconds for 10:00 Sunday
- * 104,400 seconds for 05:00 Monday
- * 450,000 seconds for 05:00 Friday

Because these ephemeris parameters locate the satellite at t_{oe} only, the three ephemeris rate parameters must be used to locate the satellite after t_{oe} . The rate terms, $\dot{\Omega}$, \dot{i} , and \dot{n} (mean motion), are multiplied by the time since epoch, t_k , and added to their respective epoch parameters, Ω_0 , i_0 , and M_0 , to update the satellite position between t_{oe} 's. The other 12 parameters remain constant for one hour until the next epoch when another complete parameter set represents the orbit for an hour. Thus, with 12 sets of parameters a GPS satellite can be located at any time in its semi-synchronous orbit [Van Dierendonck, et.al., 1978].

The six Keplerian parameters differ slightly from what is regarded as the classic Keplerian set since

time-of-perigee is not the reference time. Because of the need for hourly parameter sets, the pair (M_o, t_{oe}) replace the time-of-perigee. According to Van Dierendonck, et.al., [1978] the use of the pair (M_o, t_{oe}) facilitates the broadcast ephemeris formulation at the MCS. The change to M_o and t_{oe} also aids the least squares fitting of the estimated ephemeris to the predicted ephemeris in this work, since the argument of perigee values vary widely during the fitting process.

The BEA enables reconstruction of the GPS orbits, which include the two-body forces, the nonspherical part of the Earth gravity field, lunar-solar gravity, solar radiation pressure, polar motion and variability in Earth rotation rate. The algorithm and considerations given to its selection are described in detail by Van Dierendonck, et.al., [1978].

The first quantity computed is the mean motion, n_o , using the square root of the semimajor axis, \sqrt{A} .

$$A = (\sqrt{A})^2 \quad (2-1)$$

$$n_o = \sqrt{\frac{\mu_e}{A^3}} \quad (2-2)$$

Here, μ_e is the gravitational parameter for the earth. The second parameter, Δn , is the first perturbation term and it adjusts the mean motion.

$$n = n_0 + \Delta n \quad (2-3)$$

The time, t_k , since the ephemeris epoch, t_{oe} , is computed as

$$t_k = t - t_{oe} \quad , \quad (2-4)$$

where t is the current time of interest, measured from 00:00 Sunday. The time t_k is used to update the angles which have rate corrections such as mean anomaly, M_k , during the hour of applicability, i.e.,

$$M_k = M_0 + nt_k. \quad (2-5)$$

With this value of M_k , Kepler's equation is solved by Newton iteration [Bate, Mueller, and White, 1971] for eccentric anomaly, E_k , which is used to find true anomaly, V_k ,

$$M_k = E_k - e \sin E_k \quad , \quad (2-6)$$

$$V_k = \arccos[(\cos E_k - e)/(1 - e \cos E_k)] \quad (2-7)$$

To compute the correct quadrant the model also uses $\arcsin [\sqrt{1-e^2} \sin E_k / (1 - e \cos E_k)]$ for true anomaly. Because the GPS orbits are nearly circular, the true anomaly is added to the argument of perigee, u , to form the argument of latitude, ϕ_k , namely,

$$\phi_k = V_k + u \quad . \quad (2-8)$$

Then ϕ_k , with the estimated zonal harmonic constants, is used to find orbit corrections to the argument of

latitude, (δu_k) , the orbit radius, (δr_k) , and the inclination, (δi_k) , as follows:

$$\delta u_k = C_{uc} \cos 2\phi_k + C_{us} \sin 2\phi_k , \quad (2-9)$$

$$\delta r_k = C_{rc} \cos 2\phi_k + C_{rs} \sin 2\phi_k , \quad (2-10)$$

$$\delta i_k = C_{ic} \cos 2\phi_k + C_{is} \sin 2\phi_k . \quad (2-11)$$

The corrected terms are:

$$u_k = \phi_k + \delta u_k , \quad (2-12)$$

$$r_k = A(1 - e \cos E_k) + \delta r_k , \quad (2-13)$$

and
$$i_k = i_0 + \delta i_k + \frac{di}{dt} t_k . \quad (2-14)$$

The current satellite position components in the orbit plane , x'_k , y'_k are obtained as follows:

$$x'_k = r_k \cos u_k , \quad (2-15)$$

$$y'_k = r_k \sin u_k . \quad (2-16)$$

The quantities x'_k and y'_k locate the satellite position in an intermediate coordinate system that has its origin at the Earth's center, the x' axis collocated with the ascending node vector, and the y' axis in the orbit plane, 90 degrees from the x' axis in the direction of the orbit. The z' axis is perpendicular to the orbit plane forming a right hand orthogonal coordinate system. Next, Ω_0 is updated with $\dot{\Omega}$ and the rotation rate of the Earth $\dot{\Omega}_e$,

$$\Omega_k = \Omega_0 + (\dot{\Omega} - \dot{\Omega}_e) t_k - \dot{\Omega}_e t_{oe} , \quad (2-17)$$

as described in more detail in Appendix A. Finally, the satellite position in ECF coordinates is computed as

$$x_k = x'_k \sin \Omega_k + y'_k \cos i_k \sin \Omega_k, \quad (2-18)$$

$$y_k = x'_k \cos \Omega_k + y'_k \cos i_k \cos \Omega_k, \quad (2-19)$$

$$z_k = y'_k \sin i_k. \quad (2-20)$$

This position is a two body position corrected for a variety of perturbations [Van Dierendonck, et.al., 1978]. (see Appendix B for a summary of the equations.)

The perturbation terms account for the various forces acting on GPS satellites other than the two-body force. For example, Δn absorbs the secular drift in du/dt due to the second zonal harmonic [Van Dierendonck, et.al., 1978]. It also absorbs other effects, such as the long period sun and moon gravity effects and solar radiation pressure. The $\dot{\Omega}$ estimate accounts for secular drift caused by the second zonal harmonic, but it also absorbs other effects including variations in the Earth rotation rate. The di/dt term, added during GPS system tests as the fifteenth parameter, adjusts inclination for the second zonal harmonic. Finally, the six coefficients which are the amplitudes of the sine and cosine second zonal harmonic terms correct the argument of latitude u_k , orbit radius r_k , and inclination i_k , for the second zonal harmonic effect. They also account for

short term effects of the moon's gravity and non-zero phase angles due to terms other than the second zonal harmonics.

These nine correction terms are estimated constants that describe the orbit for only a short time. During this short time, the algorithm uses these constants to calculate the satellite position and thus, eliminates the complicated, nonlinear equations that more accurately describe the motion. Because some constants absorb several effects, the algorithm is as simple as possible. One of the goals of the Van Dierendonck team was to calculate the satellite position with minimum computer execution time, an important consideration for user equipment.

The constants required in the BEA were the World Geodetic System (WGS) constants. Originally, WGS-72[Seppelin,1974] constants were used and in 1986, WGS-84[Decker, 1986] constants were partially incorporated in the MCS. Since early 1987 the MCS operates with the WGS-84. Since the research discussed in this paper used actual satellite transmissions data from 1985, the WGS-72 constants were employed. Values for the WGS-72 constants are as follows:

$$\mu_e = 3.986008 \times 10^{14} \text{ meters}^3/\text{sec}^2,$$

$$\dot{\Omega}_e = 7.292115147 \times 10^{-5} \text{ rads/sec},$$

$$c = 2.99792458 \times 10^8 \text{ meters/sec} \\ (\text{speed of light}).$$

For comparison, the WGS-84 values are:

$$\mu_e = 3.986005 \times 10^{14} \text{ meters}^3/\text{sec}^2, \\ \dot{\Omega}_e = 7.292115 \times 10^{-5} \text{ rads/sec}, \\ c = 2.99792458 \times 10^8 \text{ meters/sec}.$$

C. The Broadcast Ephemeris Estimator

To investigate the broadcast ephemeris characteristics, an estimator was used to generate the ephemeris parameters from a set of satellite position measurements. This batch estimator, analogous to the MCS formulation of the broadcast ephemerides, was an unweighted, least squares, batch processor using satellite position quadruples (x, y, z, t) for measurements and solving for the 15 ephemeris parameters at an epoch time, t_{oe} . This section discusses the estimator initialization, measurements, measurement residuals, the measurement sensitivity matrix, the state corrections, the state transition matrix, convergence, observability, the covariance matrix, and the estimated ephemeris.

The estimator was initialized with reasonable values for each of the 15 parameters, the set of which was represented by X . Since the GPS satellites are in specified orbits, the Keplerian parameters were all set to

typical values[Porter,1978]. For example, one set of elements is given by the following:

$$\begin{aligned}
 X_1 &= 137 \text{ deg} & (M_O) \\
 X_2 &= .1 \times 10^{-7} \text{ deg/sec} & (\Delta n) \\
 X_3 &= .002 & (e) \\
 X_4 &= 5153.62 \text{ meters}^{1/2} & (\sqrt{A}) \\
 X_5 &= 30 \text{ deg} & (\Omega_O) \\
 X_6 &= 55 \text{ deg} & (i_O) \\
 X_7 &= 0 \text{ deg} & (u) \\
 X_8 &= -.6 \times 10^{-8} \text{ rads/sec} & (\dot{\Omega}) \\
 X_9 &= -.15 \times 10^{-9} \text{ rads/sec} & (di/dt)
 \end{aligned}$$

Note that X_9 was not in the original parameter set but was added during GPS testing. The amplitudes of the sine and cosine terms have values taken from preliminary analysis. Typical values were:

$$\begin{aligned}
 X_{10} &= -.8 \times 10^{-5} \text{ rads} & (C_{uc}) \\
 X_{11} &= .1 \times 10^{-5} \text{ rads} & (C_{us}) \\
 X_{12} &= 348.0 \text{ meters} & (C_{rc}) \\
 X_{13} &= -71.0 \text{ meters} & (C_{rs}) \\
 X_{14} &= -4 \times 10^{-7} \text{ rads} & (C_{ic}) \\
 X_{15} &= -.2 \times 10^{-8} \text{ rads} & (C_{is})
 \end{aligned}$$

Other, perturbed sets of initial conditions were used in the validation tests discussed in Section 2.2.D. The

epoch time, t_{oe} , for this initial set of parameters was set to the beginning of an hour past 00:00 Sunday. After initializing the parameters, the estimator accepted the first measurements.

The measurements were simulated position and time quadruples in the ECF coordinate system, at time t_k , i.e.,

$$B = \begin{bmatrix} x & y & z & t \\ & & & k \end{bmatrix}^T$$

Twenty such measurements per hour were used for the study, a trade-off between ensuring enough observations for a solution and spacing the data too closely for observability. The total number of measurements per solution varied for different cases from three hours (61 measurements) to six hours (121 measurements) with only minor variations in the results. Previous analysis in this work indicated that more than six hours of observations caused a loss of accuracy in the root-mean-square (RMS) of residuals.

There were two sources of the simulated observations: a computer program (GEL) which used the BEA to generate position quadruples from typical broadcast ephemerides, and the University of Texas Orbit Processor (UTOPIA) which numerically integrated the satellite equations of motion including a complete representation of

all forces, to obtain orbit positions. The first method helped to verify the software used to determine the broadcast parameters. When the estimation process converged accurately to the same broadcast ephemeris parameters that produced the observations, the verification aspect was regarded as satisfied.

To simulate the MCS operation, more realistic measurements were provided by the UTOPIA program which numerically integrated the two body force, the sun and moon gravity, solar radiation pressure, a user-specified truncation of the earth gravity potential, solid earth and ocean tides, and polar motion[Schutz and Tapley,1980]. This program has been validated with a variety of tracking data, particularly laser range measurements, and compared with other, similar programs. These more realistic position measurements tested the BEA ability to represent a realistic ephemeris. In essence, the GEL program produced data that was consistent with the BEA, but not completely consistent with UTOPIA. The values for the RMS of the residuals for both types of observations are very reasonable. (see part D of this chapter for results'.

The two sources of observations did not include measurement bias, so the curve fitting assumed that any error present was uncorrelated in time and Gaussian with zero mean. The measurements were equally weighted in the

estimation process.

The measurement residual vector, y , contained the differences between the observed and the calculated satellite positions in the ECF coordinates,

$$y = \dot{Y}_O - Y_C \quad (2-21)$$

At time, t_k , the estimator calculated the satellite coordinates using the BEA. These calculated coordinates were subtracted from the input measurements, producing the residuals. During estimator operation, the residuals generally decreased in the root-mean-square (RMS) sense, indicating that the fit was better with each iteration. The change in the RMS of the residuals on successive iterations served as the convergence criterion for the estimator. During each iteration, after the residuals were computed, the estimation routine computed the measurement sensitivity matrix.

The measurement sensitivity matrix, H , consists of the partial derivatives of the Earth-fixed position components (x , y , z) with respect to the ephemeris parameters, evaluated on the reference trajectory, X^* , the most current estimate of the ephemeris, that is,

$$H = \frac{\partial G(X^*, t)}{\partial X} \quad , \quad (2-22)$$

where $G(X,t) = \begin{vmatrix} x \\ y \\ z \end{vmatrix}$ calculated (2-23)

This partial derivative matrix is a (3 x 15) matrix which describes the sensitivity of the position, G , to small changes in the state, X , namely

$$H = \begin{vmatrix} \frac{\partial x_k}{\partial M_0} & \frac{\partial x_k}{\partial \Delta n} & \dots & \frac{\partial x_k}{\partial C_{is}} \\ \frac{\partial y_k}{\partial M_0} & \frac{\partial y_k}{\partial \Delta n} & \dots & \frac{\partial y_k}{\partial C_{is}} \\ \frac{\partial z_k}{\partial M_0} & \frac{\partial z_k}{\partial \Delta n} & \dots & \frac{\partial z_k}{\partial C_{is}} \end{vmatrix} \quad (2-24)$$

The elements of this matrix are presented in Appendix C. The measurement sensitivity matrix is used in the normal matrix ($H^T H$) and with the residuals in the least squares best estimate of the state corrections, \hat{x} , given by

$$\hat{x} = (H^T H)^{-1} H^T y, \quad (2-25)$$

the normal equation [Tapley and Born, 1985].

The state correction vector, \hat{x} , is the difference between the current state, X , and the reference trajectory, X^* . The \hat{x} vector results from the solution of the normal equation. Two methods were used to solve the normal equation, namely, the method of Gentleman [Gentleman, 1973], and the Cholesky algorithm. The method of Gentleman used Givens transformations and the QR decomposition, which eliminated square roots and reduced

multiplications. The Cholesky algorithm decomposed the normal matrix into upper and lower triangular matrices using square root factoring. Both methods improved speed and accuracy over a direct inversion method. The Gentleman method was programmed in a software library called GIVLIB[Wilson, 1979]. The Cholesky decomposition came from the International Mathematical and Statistical Library(IMSL) subroutine LEQT2P[IMSL, 1986]. Before calling LEQT2P, the estimator first normalized the H^TH matrix, according to Marquardt[1980] to improve accuracy.

During iteration toward convergence the estimator added the \hat{x} vector to the previous state vector to improve the estimate of the state. At convergence, \hat{x} changed very little between successive iterations. The resulting estimate of the state vector was the broadcast ephemeris for the hour beginning at time t_{oe} . This ephemeris also served as the initial condition for the next hour ephemeris estimation[Tapley and Born,1985].

One of the advantageous features of using the constant ephemeris in this estimator was the constant state transition matrix. For a typical least squares process, the state transition matrix is a function of the state sensitivity matrix, $A(t)$, and can be obtained from the following equation:

$$\dot{\Phi}(t, t_k) = A(t) \Phi(t, t_k), \Phi(t_{k-1}) = I, \quad (2-26)$$

$$\text{where } A(t) = \frac{\partial F(X^*, t)}{\partial X}, \quad (2-27)$$

$$\text{and } F(X, t) = \dot{X}(t); \quad (2-28)$$

F being the mathematical model. For this estimator the state elements are all constants, valid at the beginning of the applicable hour. Consequently, their time derivatives, \dot{X} , are all zero, that is,

$$F(X, t) = \dot{X}(t) = [0] \quad (2-29)$$

Therefore the state sensitivity matrix is the null matrix,

$$A(t) = [0]. \quad (2-30)$$

Finally, the state transition matrix is the constant identity matrix,

$$\Phi(t, t_k) = I \quad (2-31)$$

This simplification eliminates the integration of the matrix differential equation for $\dot{\Phi}$, Equations (2-26), which streamlines the process. For each measurement time the state need not be propagated forward by the state transition matrix. Instead, the state vector rate terms are updated to the measurement time and all others remain constant. In this way, all measurements relate back to the epoch time, t_{oe} , where the best estimate

occurs[Tapley and Born,1985].

After the estimator processes all of the measurements, a solution to the normal equation, \hat{x} , results. The elements of the first such \hat{x} may have large values due to the linearization process and the RMS of the residuals may be large also. The estimator then updates the state vector, x , with \hat{x} , and iterates to calculate another \hat{x} with smaller residuals[Tapley and Born,1985]. The residual RMS of this convergent process continues to decrease until the relative difference between successive iterations drops below a specified tolerance. At this point, the estimator is converged and the ephemeris at epoch is printed.

To obtain a solution to the normal equation and thus have an ephemeris estimate, the state must be "observable". Mathematically, the normal matrix must be non-singular which means it must have the same rank as there are parameters (rank 14 for the initial 14 parameter set, or rank 15 when 15 parameters are used). The minimum number of observations to allow a solution is the same as the rank, however, 61 or more observations (position quadruples) were used to meet this criteria and to overcome some ill-conditioning discussed in section D.2. For the current study, the spacing between ephemeris points was three minutes. With a sufficient number of linearly

independent observations, the ephemeris parameters are observable [Tapley and Born, 1985]. With observable parameters, the estimator produced two outputs: the converged state and the covariance matrix.

The covariance matrix, P , is the inverse of the normal matrix,

$$P = (H^T H)^{-1} \quad (2-32)$$

A unique P matrix always exists if the system is observable. The diagonal terms in P are the variances of the state vector elements, and the off-diagonal terms are the covariances. Since a unit weighting matrix was used, there were no weighting factors for the normal and P matrices, leaving high confidence in the variances and covariances [Tapley and Born, 1985].

The main output was the estimated satellite state, X , at each epoch hour, t_{oe} ; however, some of the estimates were obtained at the beginning of the observation time and others obtained at the midpoint of the observation interval for comparison. The state in both cases approximates the orbit accurately for several hours, but is changed at each hour for continuity. Because all of the parameters are constant for the hour and the actual orbit is perturbed, the accuracy of the ephemeris changes. However, the RMS of the residuals indicated

that the change was not excessive. In addition, the user navigation algorithm of Chapter Four demonstrates that the broadcast ephemerides can produce accurate results.

D. Validation of the Broadcast Ephemeris Parameter Determination

Various experiments were performed to validate the software used in the determination of the broadcast ephemeris parameters and to investigate the behavior of the parameter estimation in an environment simulating actual operation. The dual Cyber computers at the University of Texas at Austin were used for the experiments. The software was run in single precision which carries 15 significant digit accuracy. Two methods for solving the normal equation (Cholesky decomposition and the method of Gentleman) produced nearly identical results. Also, numerical partial derivatives were used to validate the analytic partial derivatives. Slight indications of ill-conditioning in the normal matrix were found, caused by a high correlation between the parameters M_0 and w . This section will summarize the various test cases, followed by an analysis of the ill-conditioned cases.

The first test cases used simulated observations from the program GEL (described in Section 2.2.C), and a

14 parameter state. The simulated position and time quadruples were obtained by selecting a typical set of broadcast parameters, such as those in Section 2.2.C, and evaluating the Broadcast Ephemeris Algorithm in the GEL program. The output of this process was an ephemeris of ECF positions and time, at three minutes intervals for three to six hours. The output ephemerides were then used in blocks of three to six hours to estimate the broadcast ephemeris parameters. The three to six hour blocks were used because they were typical of the MCS operation. Only one set of parameters was estimated in these initial test cases, but later cases estimated many hourly ephemerides, similar to the MCS operation. Since the parameters were being estimated in a model identical to that which generated the observations, problems of model error were eliminated, thereby enabling validation of the software. In contrast to this case, the UTOPIA-generated measurements resulted in model error, making software validation impossible.

In these early tests, the rate of change of inclination, di/dt , was not included in the state. Early GPS system tests also did not include di/dt , and as is shown with the UTOPIA-produced measurements, some errors resulted. These errors were reduced to acceptable levels when the inclination rate term was included in the

continuous cases discussed later in this chapter. The accuracy obtained with the GEL data in the converged parameters was between eight and twelve significant digits, depending on the parameter. For example, in all the various cases, the square root of A used to create the observation sets was 5153.620087 meters^{1/2} and the converged value was identical. For the case that used a perturbed initial condition for \sqrt{A} , the converged value was still the value used to create the observation set, to twelve significant digits. The eccentricity and inclination also converged to the same values as the those used for the observation sets in all cases. The worst converged values were the sine and cosine harmonic coefficients which were accurate to six significant digits for all the validation cases. These cases involved several variations to aid the validation.

The first variations involved fitting observations for three to six hours. With three to six hour fits, the normalized Cholesky decomposition of the normal matrix produced an RMS of residuals (combined x, y, z) on the order of 10^{-6} meters. Cases using the Gentleman solution produced an RMS of residuals on the same order of magnitude. These tests used analytic partials in the measurement sensitivity matrix. The same cases computed using numerical partials yielded an RMS of residuals on the

order of 10^{-4} meters. Because of the numerical approximation, the numerical partial derivatives were expected to be less accurate than correctly formed and implemented analytical partial derivatives. Individual parameters, produced by the Gentleman method, matched the normalized Cholesky cases for nine to twelve significant digits.

Variations in the initial conditions were used to aid the software validation. The first variation was to set the parameters M_0 , \sqrt{A} , Ω_0 , i and u to exact values and all others to zero. Thus, Δn , e , $\dot{\Omega}$, and all the harmonic coefficients were zero. The results using the Cholesky solution and three, four, and six hours of observations were nearly identical, converging in six iterations to the same values used to create the observation set, with an accuracy of six significant digits for the harmonic coefficients and twelve for M_0 , \sqrt{A} , Ω_0 , and i . The other parameters varied from seven to eleven significant digit accuracy.

Other variations to the initial conditions included perturbing the M_0 , \sqrt{A} , Ω_0 , and i parameters individually while holding the other parameters zero. First, the M_0 initial condition was perturbed two degrees, from 137 degrees to 135 degrees, which was a 927,119 meter in-plane position perturbation. Although the processor required 14 iterations to converge, the resulting

parameter estimates using 61 observations were virtually identical to those used to create the observation set. Perturbing the \sqrt{A} initial condition by 54 meters^{1/2} changed the semimajor axis by 559,900 meters, but the estimated parameters were the same after eight iterations as the previous case. Perturbations of Ω_0 and i by five degrees and two degrees, respectively, again resulted in RMS of residuals on the order of 10^{-6} meters and parameter estimates that were nearly identical to the parameters used to create the observations. Thus, in each case the estimator was able to reproduce the parameter values that were input to the GEL program.

These results indicate excellent accuracy, however, as expected the accuracy in the RMS of residuals is limited by the computer precision of a 48-bit mantissa, particularly during the Cholesky decomposition and the Givens orthogonalization processes. The test results which compared the Cholesky and Gentleman methods, analytic and numerical partials, and from three to six-hour fits are shown in Table 2-1. In Table 2-2 is a summary of the results of perturbing the initial conditions off of nominal. Based on these results, it was concluded that the software prepared for the estimation of the broadcast ephemeris parameters was implemented correctly.

Table 2-1
Broadcast Ephemeris Parameters with GEL Ephemeris

Hours of Observations	Type of Solution	Partial Derivations	RMS of Residuals (meters)
3	Cholesky	Analytic	$.44 \times 10^{-6}$
3	Gentleman	Analytic	$.45 \times 10^{-6}$
3	Cholesky	Numerical	$.13 \times 10^{-4}$
4	Cholesky	Analytic	$.56 \times 10^{-6}$
4	Gentleman	Analytic	$.10 \times 10^{-4}$
4	Cholesky	Numerical	$.24 \times 10^{-4}$
6	Cholesky	Analytic	$.59 \times 10^{-6}$
6	Gentleman	Analytic	$.59 \times 10^{-6}$

Table 2-2
Perturbed Initial Conditions
for Creating Broadcast Ephemerides

Hours of Obs	Perturbed Parameters	Perturbed Values	No. of Iterations	RMS of Residuals(m)
3	$\Delta n, e, w, \dot{\Omega}, C_{uc}, C_{uc},$ $C_{rc}, C_{rs}, C_{ic}, C_{is}$	0	6	$.57 \times 10^{-6}$
4	$\Delta n, e, w, \dot{\Omega}, C_{uc}, C_{us},$ $C_{rc}, C_{rs}, C_{ic}, C_{is}$	0	6	$.61 \times 10^{-6}$
6	$\Delta n, e, w, \dot{\Omega}, C_{uc}, C_{us},$ $C_{rc}, C_{rs}, C_{ic}, C_{is}$	0	6	$.98 \times 10^{-6}$
3	M_0	135°	14	$.50 \times 10^{-6}$
	$\Delta n, e, w, \dot{\Omega}, C_{uc}, C_{us},$ $C_{rc}, C_{rs}, C_{ic}, C_{is}$	0		
3	\sqrt{A}	$5099.62m^{1/2}$	8	$.62 \times 10^{-6}$
	$\Delta n, e, w, \dot{\Omega}, C_{uc}, C_{us},$ $C_{rc}, C_{rs}, C_{ic}, C_{is}$	0		
3	Ω	35°	10	$.60 \times 10^{-6}$
	$\Delta n, e, w, \dot{\Omega}, C_{uc}, C_{us},$ $C_{rc}, C_{rs}, C_{ic}, C_{is}$	0		
3	i	53°	8	1.0×10^{-6}
	$\Delta n, e, w, \dot{\Omega}, C_{uc}, C_{us},$ $C_{rc}, C_{rs}, C_{ic}, C_{is}$	0		

D.1. Determination of the Predicted Ephemeris

The 14-parameter estimator was also used with the more realistic observation set produced by the UTOPIA program. As mentioned previously, the UTOPIA measurements included a variety of orbit perturbations. The UTOPIA orbit processor produced satellite positions given a set of initial conditions (position and velocity at a specified time) and the specified perturbations. The activated UTOPIA perturbations are shown in Table 2-3.

<p>Table 2-3 UTOPIA Orbit Perturbations</p>

- | |
|--|
| <ol style="list-style-type: none">1. WGS 72 Earth Gravity Field Truncated at Degree and Order Eight.2. Luni-Solar Gravity.3. Solar Radiation Pressure. |
|--|

The UTOPIA-generated satellite positions were input to the broadcast ephemeris estimator which produced hourly ephemerides. The estimator converged smoothly in the various test cases to an RMS of residuals in the range of two to forty one meters. Test cases using Cholesky and Gentleman solutions and fit periods between three and six hours were investigated. Only analytic partials were used in the measurement sensitivity matrix for UTOPIA studies, since the numerical partial derivatives were

used only to aid in the validation of the analytical partial derivatives and they had been shown to be less accurate. The initial conditions in the estimator using the UTOPIA observations were similar to the GEL data.

For a three-hour fit using the Cholesky solution, the RMS of residuals at convergence was 9.41 meters. The Gentlemen solution for a three-hour fit produced a 4.0 meter RMS of residuals. The other cases are presented in Table 2-4. The differences between the Gentleman and Cholesky converged values of RMS of residuals are possibly due to the lack of the di/dt term in these initial ephemeris estimates. The ill-conditioning in the normal matrix (discussed later in this chapter) may contribute to the RMS of residual differences. The differences disappear when the di/dt term is included in the ephemeris, as is seen in the 24 hour cases.

Table 2-4
Broadcast Ephemeris Parameters from
UTOPIA Ephemeris

Hours of Observations	Types of Solutions	RMS of Residuals (meters)
3	Cholesky	9.4
3	Gentleman	4.0
4	Cholesky	25.4
4	Gentleman	12.3
5	Cholesky	2.1
5	Gentleman	23.1
6	Cholesky	2.5
6	Gentleman	41.1

These results for the UTOPIA-observation cases indicate that the broadcast ephemeris estimator can approximate the GPS orbit using the 14 constant parameters to an accuracy of two to forty one meters. With the addition of the fifteenth parameter, the estimator produced better results which will be evident in the following covariance discussion.

The diagonal elements of the covariance matrix are the variances of the estimated ephemeris parameters, and as such provide an indication about the accuracy of the solution. Typical variances from 10^{-5} to 10^{-18} show that the estimator accuracy and confidence in the estimated parameters are high. For instance, the variance for M_0 is $.102 \times 10^{-9}$ radians², which converts to a one sigma

value of $.101 \times 10^{-4}$ radians. The variance for $\sqrt{|\bar{A}|}$ is $.1394 \times 10^{-5}$ meters which represents a one sigma value of $.118 \times 10^{-2}$ meters^{1/2}, or 12.2 meters in A. Both of these variances suggest high confidence in the estimates. Table 2-5 is a list of the variances of all estimated parameters in the 14-parameter estimator.

Table 2-5 Variances of the Estimated Ephemeris Parameters			
Parameter	Variance	Parameter	Variance
M_0	$.1020 \times 10^{-9} \text{ (rad)}^2$	$\dot{\Omega}$	$.1764 \times 10^{-18} \text{ (r/s)}^2$
Δn	$.5952 \times 10^{-19} \text{ (r/s)}^2$	C_{uc}	$.1880 \times 10^{-14} \text{ (rad)}^2$
e	$.4169 \times 10^{-12}$	C_{us}	$.3583 \times 10^{-13} \text{ (rad)}^2$
$\sqrt{ \bar{A} }$	$.1394 \times 10^{-5} \text{ meters}$	C_{rc}	$.2489 \times 10^{+2} \text{ meters}^2$
Ω	$.4654 \times 10^{-11} \text{ (rad)}^2$	C_{rs}	$.1327 \times 10^{+1} \text{ meters}^2$
I	$.3479 \times 10^{-11} \text{ (rad)}^2$	C_{ic}	$.2799 \times 10^{-12} \text{ (rad)}^2$
ω	$.1000 \times 10^{-9} \text{ (rad)}^2$	C_{is}	$.3691 \times 10^{-15} \text{ (rad)}^2$

All the estimates to this point have been single estimates for one hour, based on one set of observations. Next, the investigation expanded to 24 hour sequential estimates using the 15-parameter state. This sequential operation over two revolutions used sliding, four-hour blocks of observations to estimate the ephemeris parame-

ters in a manner similar to the MCS operation described in Section 2.2.A. Like the MCS formulation of the parameters, this process used four hours of observations to estimate the ephemeris, then dropped the first hour of observations, added a new fourth hour of observations, and estimated the parameters, one hour after the last estimate. This moving window of observation blocks continued through 24 epoch times, producing 24 sets of parameters. Unlike the MCS, the estimates were at the beginning of the observation block and the observations were spaced three minutes apart and not edited, whereas, the MCS uses estimates at the midpoint of the observation block and edited measurements at 15 minute intervals. Also, unlike the MCS operation, this processor estimated both M_0 and w individually, while the MCS estimates the combination of the two, $M_0 + w$ and another term, $e \sin w$. Then the MCS separates values for M_0 and w for inclusion in the upload message. These differences from the MCS operation caused the RMS of residuals to be higher than the MCS-created RMS of residuals (.3-.4 meters) but not so high as to prevent the study of the broadcast ephemeris characteristics. [Brown, 1987]

Expanding to the 24-hour time frame and the 15-parameter set aided the analysis of the GPS broadcast ephemeris. These hourly estimates used UTOPIA-generated

position measurements and the Cholesky and Gentleman formulations, which produced almost identical results. For example, the sequential four-hour fit using the Gentleman method converged to values for the RMS of residuals between 1.1 and 6.1 meters. The Cholesky solutions yielded the same values of RMS to seven significant digits. Typically, the number of iterations to converge was between seven and twelve, with one being 23 iterations. These iteration numbers are higher than the MCS iteration numbers (2-3 iterations), due to the ill-conditioning in the normal matrix. The estimated parameter values for each hour were essentially the same for both methods. Realizing that the two methods produced nearly identical estimates, it was informative to investigate individual characteristics of the estimated parameters over the 24-hour period.

The parameter characteristics that appear during two revolutions are secular and periodic. Because the parameters are constant and absorb a variety of perturbations during the fitting process, it is difficult to identify specific perturbations, other than the dominant influence of earth oblateness without a more detailed analysis. To illustrate the relative importance of the various perturbation, Table 2-6 lists the approximate accelerations given by Van Dierendonck, et.al., [1978].

Table 2-6
GPS Perturbing Accelerations

Source	Maximum Acceleration (m/sec ²)
Two body	5.65×10^{-2}
J_2	5.3×10^{-5}
Lunar gravity	5.5×10^{-6}
Solar gravity	3×10^{-6}
J_4	10^{-7}
Solar radiation pressure	10^{-7}
Gravity anomalies	10^{-8}
All other forces	10^{-8}

The J_2 effect is absorbed in several parameters and the Δn parameter absorbs secular drift in du/dt due to J_2 , $\dot{\Omega}$ accounts for secular drift in the longitude of the ascending node, and C_{uc} , C_{us} , C_{rc} , C_{rs} , C_{ic} , C_{is} accommodate other effects on the orbit caused by the nonspherical Earth and the lunar-solar gravity. Some of these effects are clearly visible in the estimated parameters plotted over two revolutions.

Figures 2-1 through 2-10 show the hourly values of the RMS of residuals and the first nine ephemeris parameters. The abscissa of each figure presents both the hour

and the u_0 value (argument of latitude at epoch), to indicate the satellite position relative to the ascending node. The figures clearly show an effect at twice per revolution, predominantly produced by J_2 . The GPS orbits are at semi-synchronous altitude so the magnitude of the oblateness effect is small, but it is the dominant perturbation. The first figure, 2-1, plots the RMS of residuals for two revolutions and shows a dependence on satellite position relative to the nodes. That is, minimum values occur at the nodes where the estimator fits the observations best, since the satellite is directly over the Earth bulge. The largest RMS value, halfway between the nodes, is 6.13 meters, which is nevertheless, a satisfactory value.

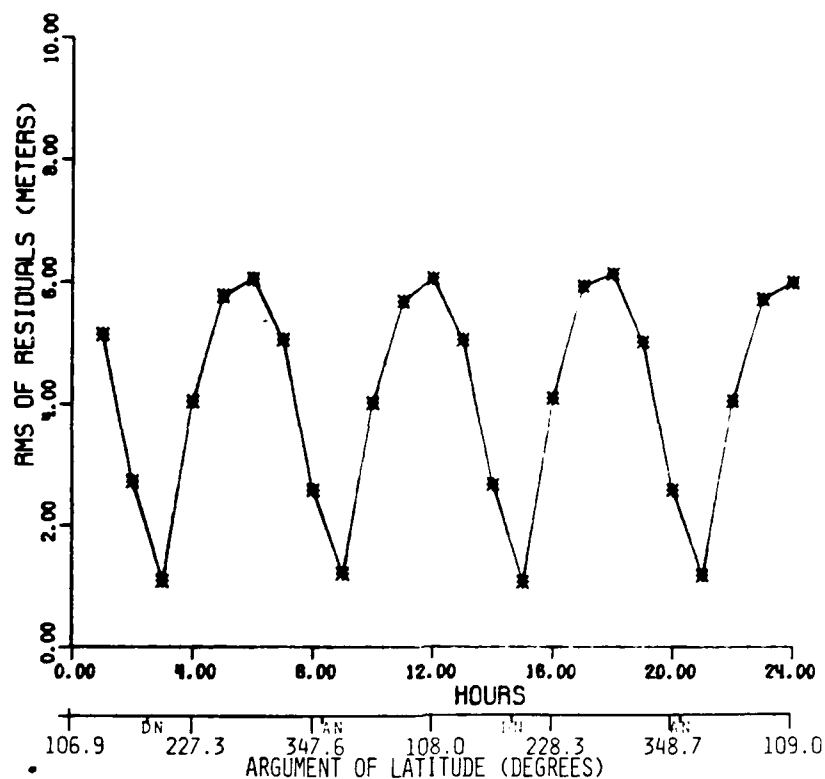


FIGURE 2-1 RMS OF RESIDUALS (METERS) - TWO REVOLUTIONS

Figure 2-2 shows the twice-per-revolution effect in the change of the mean anomaly. This change is the amount the satellite moves in one hour; approximately 30 degrees. The effect is periodic with minimum values located close to the node.

Quantifying the ΔM_0 values in terms of known secular and periodic perturbations is difficult because the argument of perigee correlates so highly with M_0 (see Figure 2-8). However, the combined value, u_0 , Figure 2-11, exhibits a periodic effect that can be attributed to other perturbations.

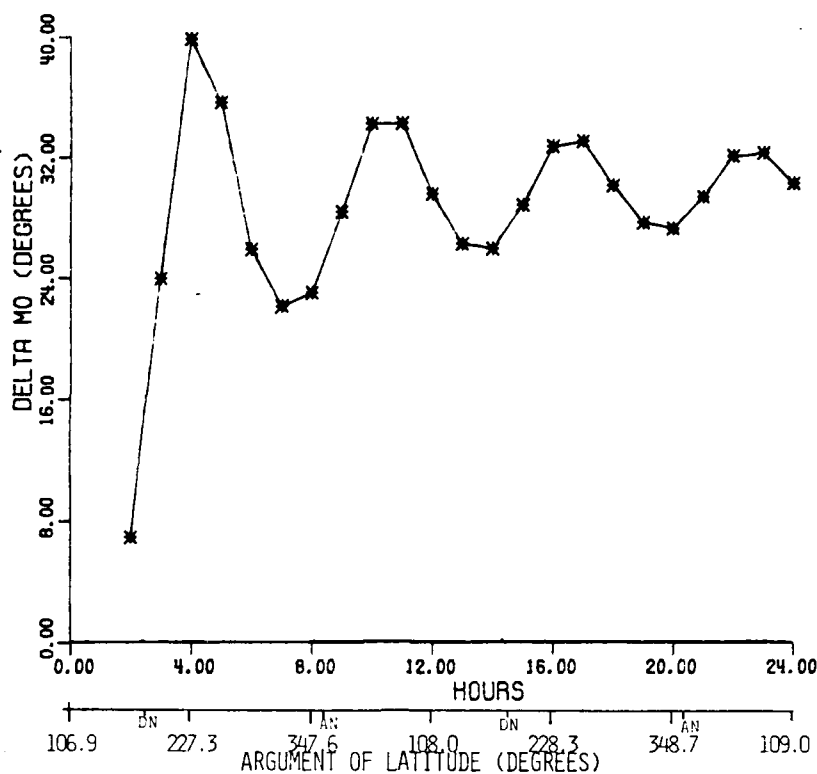


FIGURE 2-2 ΔM_0 (DEGREES) - TWO REVOLUTIONS

The change in mean motion, Δn , is shown in Figure 2-3. The periodic effect in Δn with minima at the ascending node is clear. However, because Δn is included in the parameter list to absorb secular growth in du/dt , two effects must be noted. First, the average value of Δn in the figure is nearly equal to the expected value of \dot{u}_{J_2} from analytic computation. From the figure, the average value of Δn is 2.53×10^{-7} deg/sec. Kaula's [1966] equation for \dot{u}_{J_2} yields 2.52×10^{-7} deg/sec; nearly identical. The second effect is the periodicity that must be caused by a perturbation other than J_2 since it occurs

once-per-revolution. According to Van Dierendonck, et.al., [1978], the Δn parameter also absorbs the influence of lunar and solar gravity and solar radiation pressure which cause the proper periodic effect. Therefore, the earth oblateness causes a constant bias for the Δn plot and the lunar-solar gravity and solar radiation pressure impose a periodic effect.

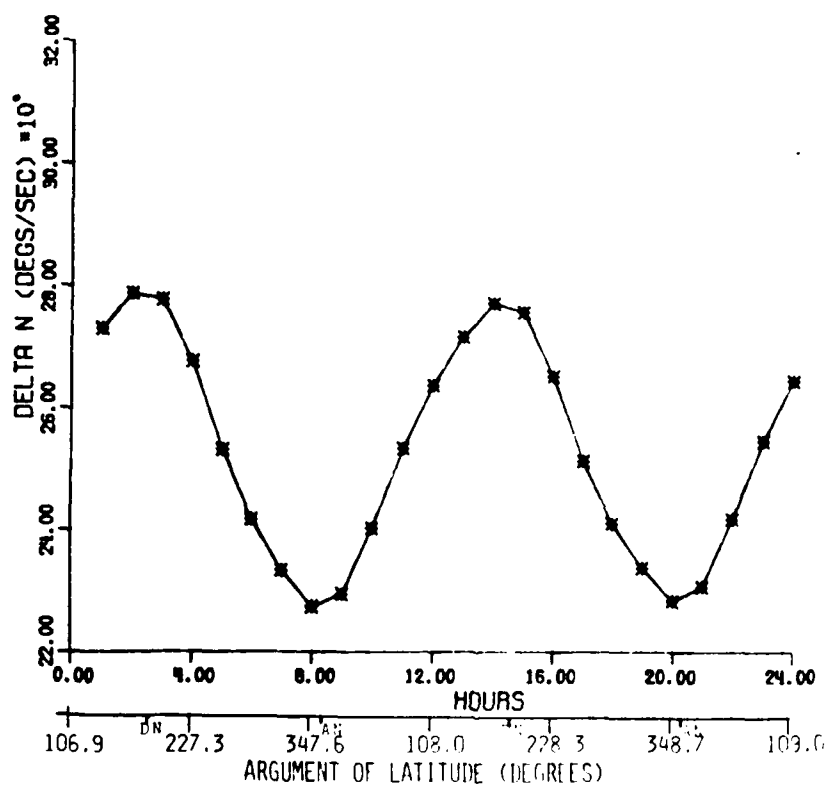


FIGURE 2-3 $\Delta n \text{ (DEGS/SEC)} \times 10^8$ - TWO REVOLUTIONS

The $\sqrt{|\bar{A}|}$ is shown in Figure 2-4. This figure displays a once-per-revolution periodic effect with maxima occurring at the ascending nodes. The maximum excu-

sion from the average is $0.099 \text{ meters}^{1/2}$, which is the same as 1021.5 meters for A. The twelve-hour period is most likely due to the lunar-solar gravity and solar radiation pressure. An expected short-term periodic effect caused by J_2 is absent, probably due to the effect being absorbed by another parameter, remembering that these parameters are estimated.

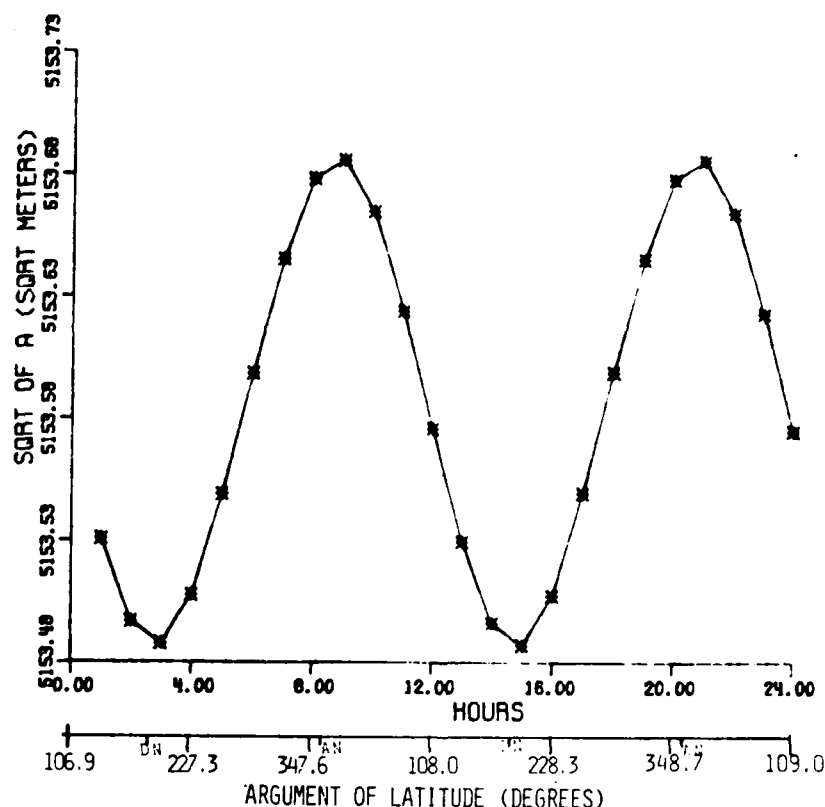


FIGURE 2-4 SQUARE ROOT OF A ($\sqrt{\text{METERS}}$) - TWO REVOLUTIONS

The next figure is 2-5, the eccentricity. The eccentricity shows a secular growth over two revolutions, but also a leveling trend at each node, probably due to

the oblateness. The secular growth is unusual and may be a long term periodic effect caused by lunar or solar gravity or solar radiation pressure. Regardless of the cause, the change is very small (0.00029) over two revolutions and there is no apparent effect on the fitting of the orbit.

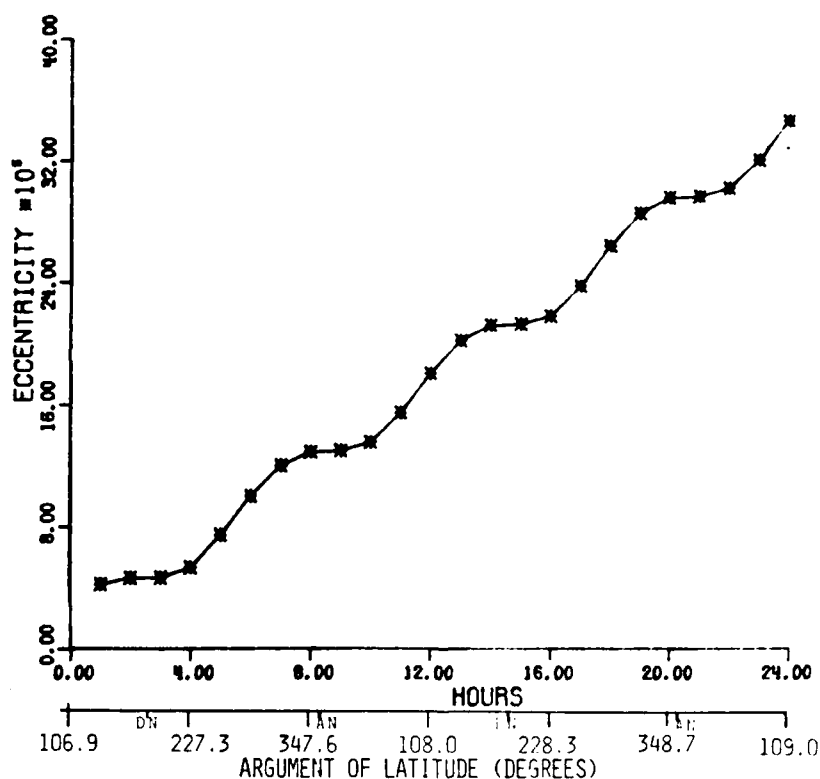


FIGURE 2-5 ECCENTRICITY $\times 10^5$ - TWO REVOLUTIONS

The longitude of the ascending node values in Figure 2-6 show the classic regression of the node; the magnitude of the rate being consistent with the $\dot{\Omega}$ plot in Figure 2-9. Figure 2-6 exhibits a rate of -4.38×10^{-7}

deg/sec, while the rate in Figure 2-9 averages about -4.60×10^{-7} deg/sec. Checking the rate with Kaula's equation[1966] for $\dot{\Omega}_{J_2}$, yields a similar result: -4.48×10^{-7} deg/sec. Compared with the effect of lunar gravity, this rate is over two orders of magnitude larger. From Kozai[1963] the nodal regression rate caused by the moon is -9.67×10^{-9} deg/sec. Thus, the estimated values for Ω closely match the expected values.

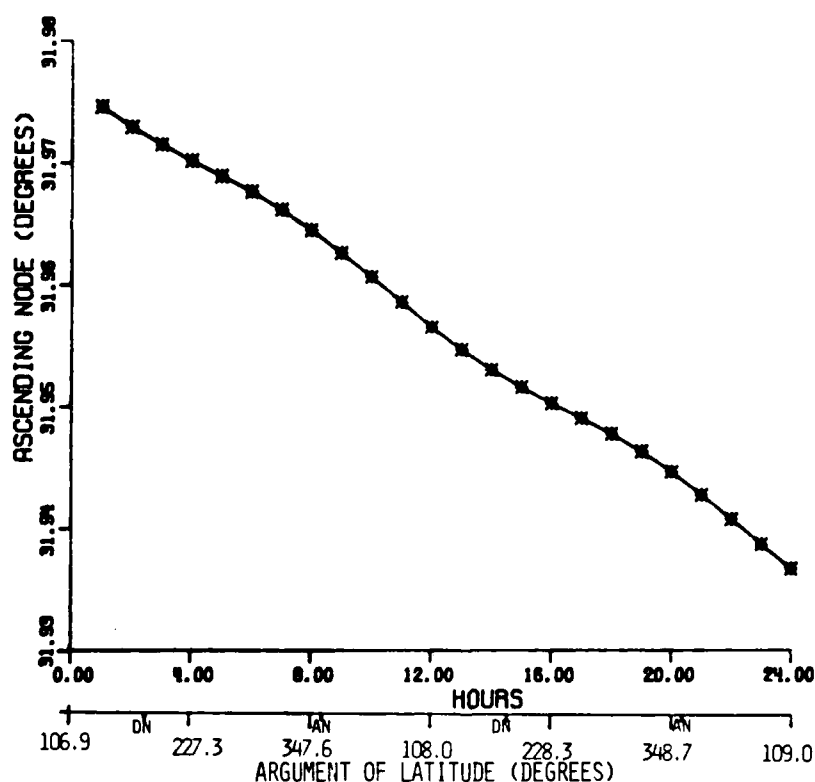


FIGURE 2-6 ASCENDING NODE (DEGREES) - TWO REVOLUTIONS

Figure 2-7 shows the variation in inclination from the nominal 55 degrees. The peak-to-peak variation is

about 0.0012 degrees with the average being about 0.001 degrees off nominal. The small magnitude emphasizes how little the oblateness affects the orbit. Note that the maxima and minima are not located at the nodes, but much closer to the northern-most or southern-most points on the orbit. For inclination this effect is expected since J_2 will not change inclination while the satellite is over the equator.

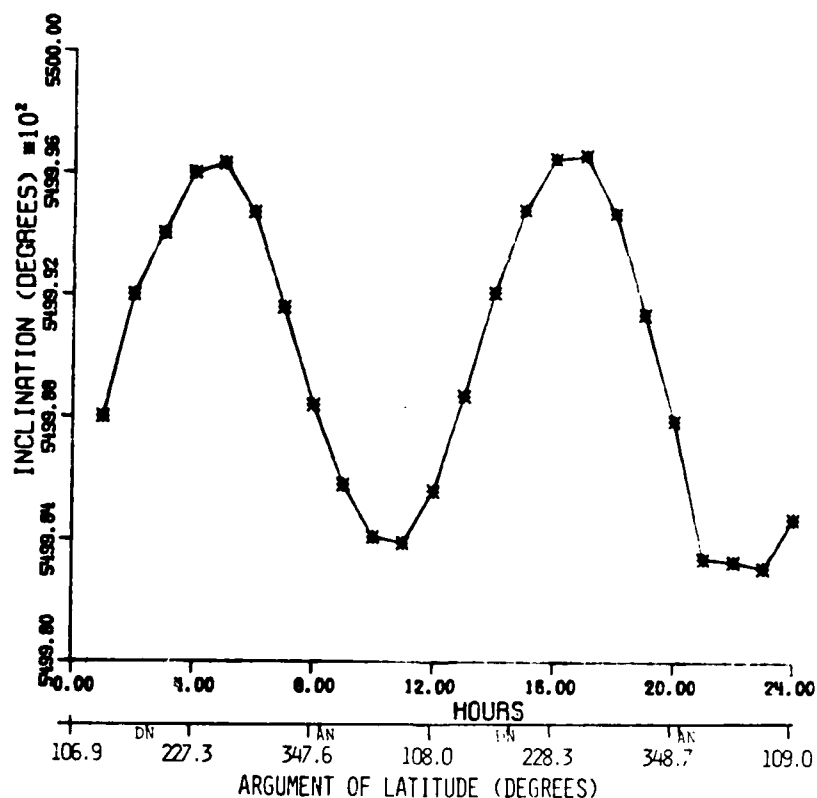


FIGURE 2-7 INCLINATION (DEGS $\times 10^2$) - TWO REVOLUTIONS

The argument of perigee displays a short-periodic effect coupled with a long-term periodic effect. Figure

2-8 presents w with maxima occurring at the nodes, probably due to the oblateness. The small secular growth expected in w due to J_2 is absorbed in the Δn parameter. As mentioned previously about ΔM_0 (Figure 2-2), tying the long-term periodic effect to a specific perturbation is difficult. The M_0 and w parameters have such high negative correlation that only their combination, u_0 , shows an effect attributable to the lunar-solar gravity and solar pressure.

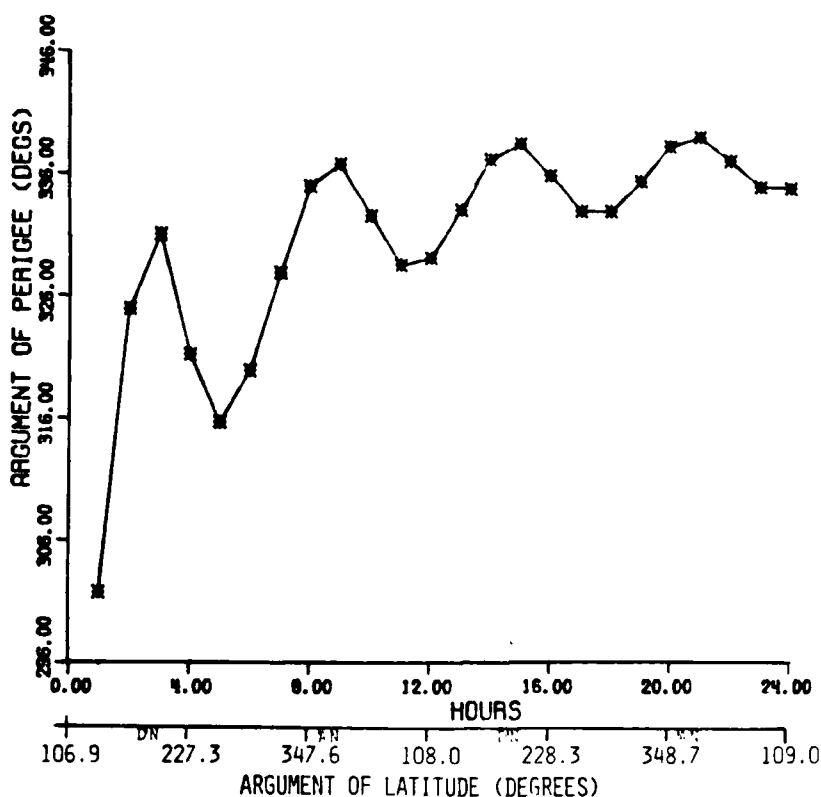


FIGURE 2-8 ARGUMENT OF PERIGEE (DEGS) - TWO REVOLUTIONS

Figure 2-9 presents the ascending node rate. As

reported previously, the average value is -4.60×10^{-7} deg/sec which agrees with the rate in Figure 2-6. Thus, the $\dot{\Omega}$ parameter absorbs secular drift in Ω caused by J_2 .

Van Dierendonck, et.al. [1978] reports that the $\dot{\Omega}$ parameter also absorbs polar wander and earth rate variations. These two effects are long-term periodic with small amplitudes, so they do not appear here. The once-per-revolution effect exhibited by $\dot{\Omega}$ has an amplitude of 5.85×10^{-8} deg/sec which is a 12.7 percent variation from the average. The 12-hour period indicates again that lunar-solar gravity and solar radiation are likely causes.

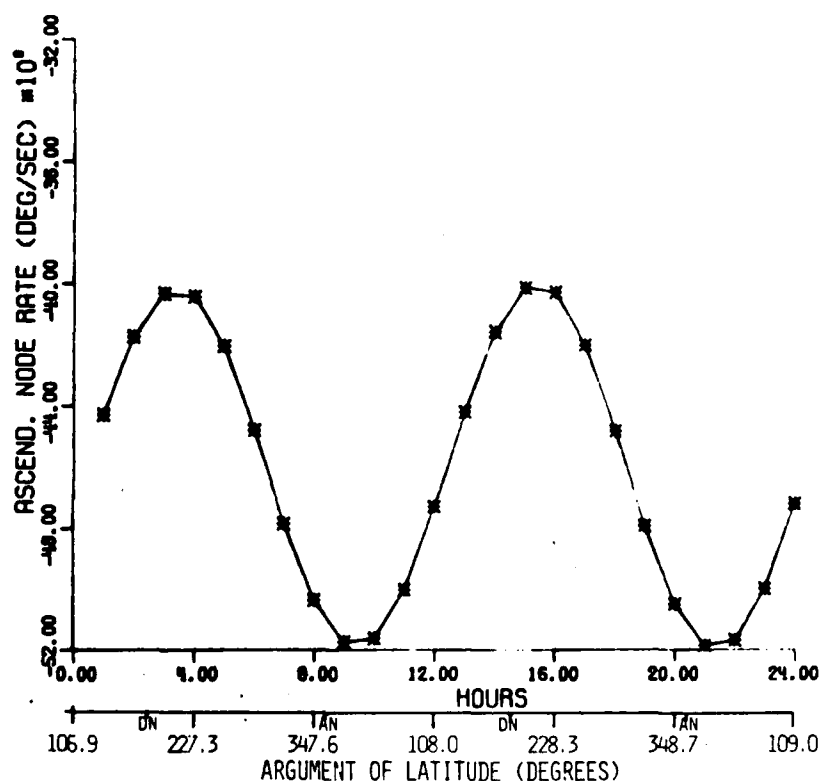


FIGURE 2-9 ASCENDING NODE RATE (DEG/SEC) $\times 10^8$
TWO REVOLUTIONS

The inclination rate is next, Figure 2-10. Originally omitted from the parameter set by the system developers, it absorbs out-of-plane perturbations not absorbed by the $\dot{\Omega}$ parameter. By the 12-hour period, it appears that lunar-solar gravity and solar radiation pressure are the perturbations. Note that the average value is very close to zero, -1.13×10^{-9} deg/sec, so that little secular change in inclination occurs. This near-zero rate is expected since analytic results by Kozai[1963] also show zero rate.

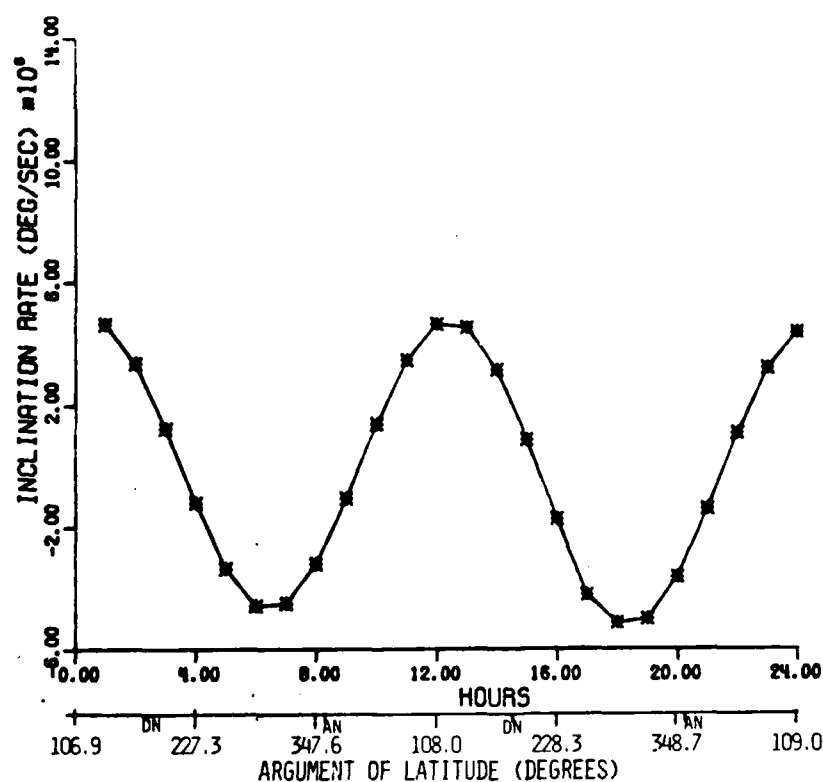


FIGURE 2-10 INCLIN. RATE (DEG/SEC) $\times 10^8$ TWO REVOLUTIONS

The next plot, Figure 2-11, is Δu_0 , the change in the argument of latitude, which shows how far the satellite moves from the ascending node each hour; approximately 30 degrees. Because M_0 and u are interrelated, their individual characteristics are not clear. However, when combined in u_0 , the lack of secular growth and the presence of periodic variations are clear. The average value is 30.087 degrees which means the satellite completes one revolution in 12 sidereal hours, and returns to the same ground track in 24 sidereal hours [Van Dierendonck, et.al., 1978]. The 12-hour period in Figure 2-11 is most likely caused by the lunar-solar gravity and solar pressure.

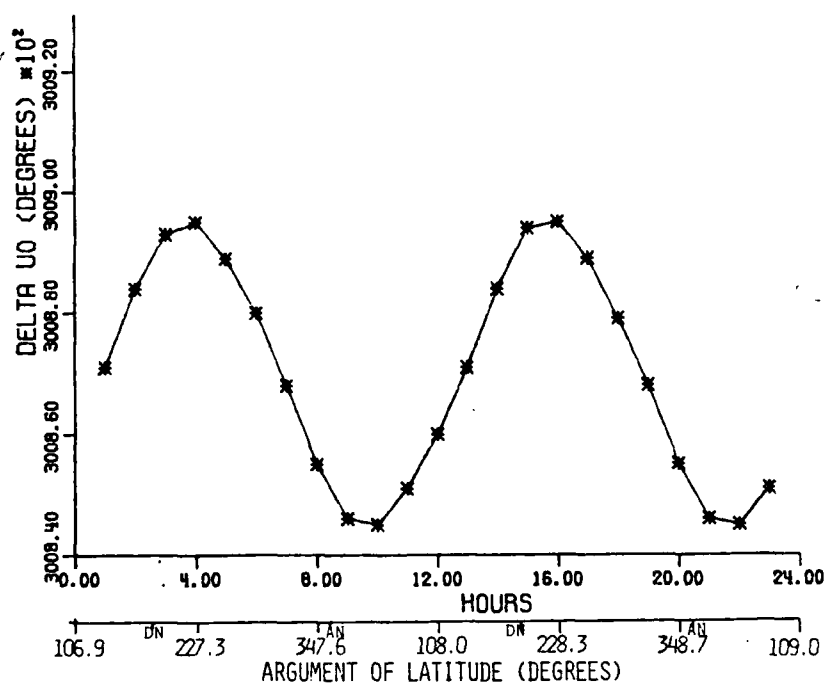


FIGURE 2-11 Δ ARG. OF LATITUDE (DEG) -- TWO REVOLUTIONS

The last six figures, 2-12 through 2-17, plot the estimated second zonal harmonic coefficients. These coefficients, like the other parameters, absorb a variety of perturbations, the dominant one being J_2 . Van Dierendonck, et.al., [1978] reports that short term effects of the closest approach to the moon are also significant in these parameters. They are included to correct mean anomaly, semimajor axis, and inclination. Again, identifying specific perturbations from the plots is difficult. However, the periodicity indicates generally which perturbations are absorbed. The first two harmonic coefficients, C_{uc} and C_{us} are in Figures 2-12 and 2-13.

The C_{uc} and C_{us} parameters exhibit a 12-hour period with opposing maxima and minima. Both vary from positive to negative with C_{uc} being biased slightly below zero and C_{us} slightly above zero. Both parameters show dependence on the nodal crossing with leveling trends at the nodes. Because of the 12-hour period, the most likely perturbation causing the variations is lunar gravity at closest approach. The biases are probably due to the J_2 effect.

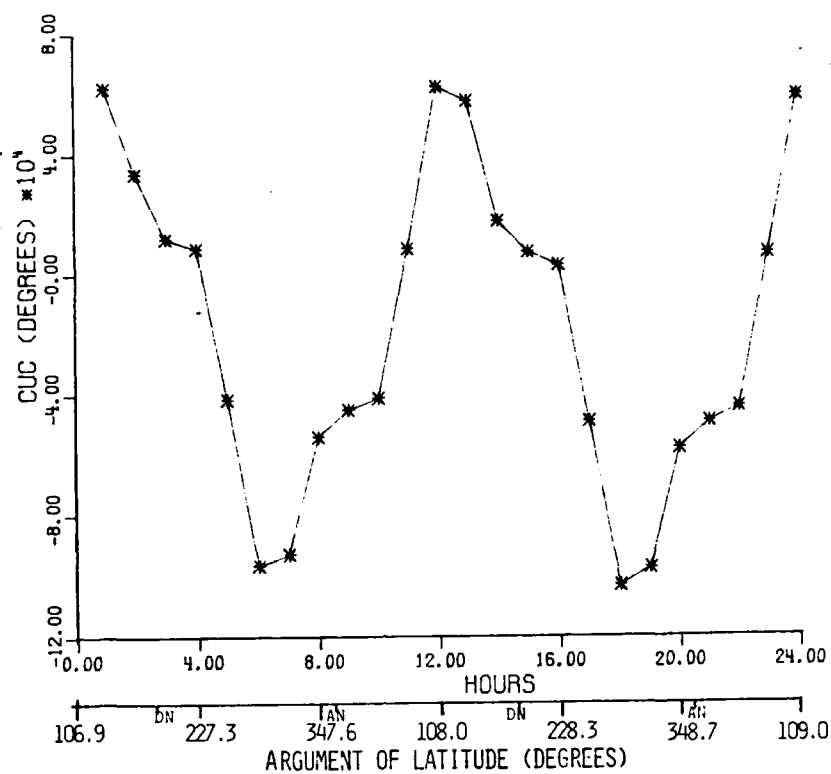


FIGURE 2-12 C_{uc} ZONAL PARAMETER (DEGS) TWO REVOLUTIONS

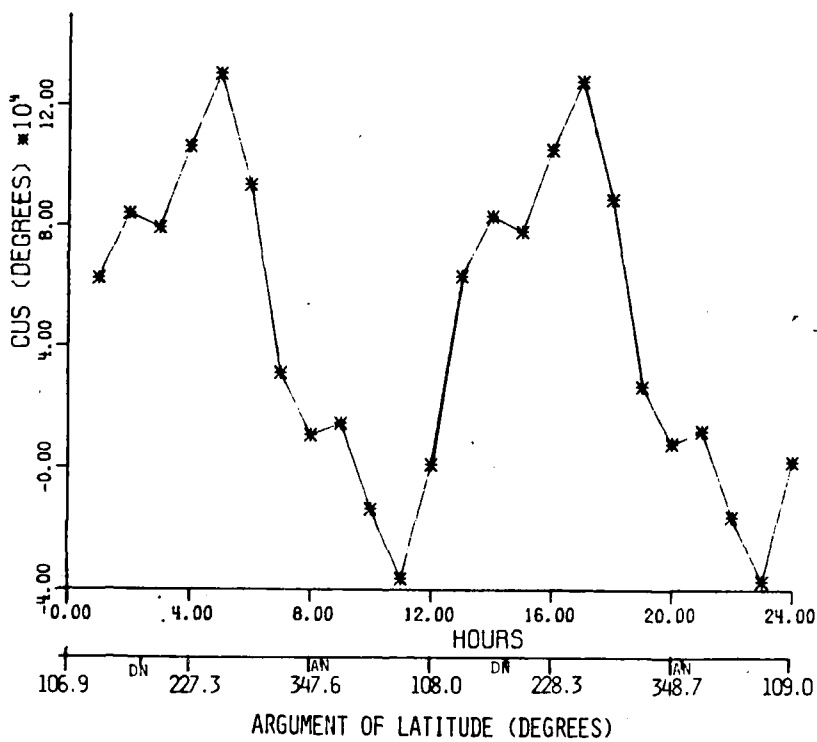


FIGURE 2-13 C_{us} ZONAL PARAMETER (DEGS) TWO REVOLUTIONS

The C_{rc} and C_{rs} parameters, Figures 2-14 and 2-15, have the same 12-hour period with coinciding maxima and minima. The C_{rc} parameter has a positive bias and C_{rs} a negative bias. The slight leveling trend at the nodes is present also. Consequently, the expected perturbations are the same as the C_{uc} and C_{us} parameter; i.e., J_2 causes the biases while the lunar gravity at closest approach causes the periodic effect.

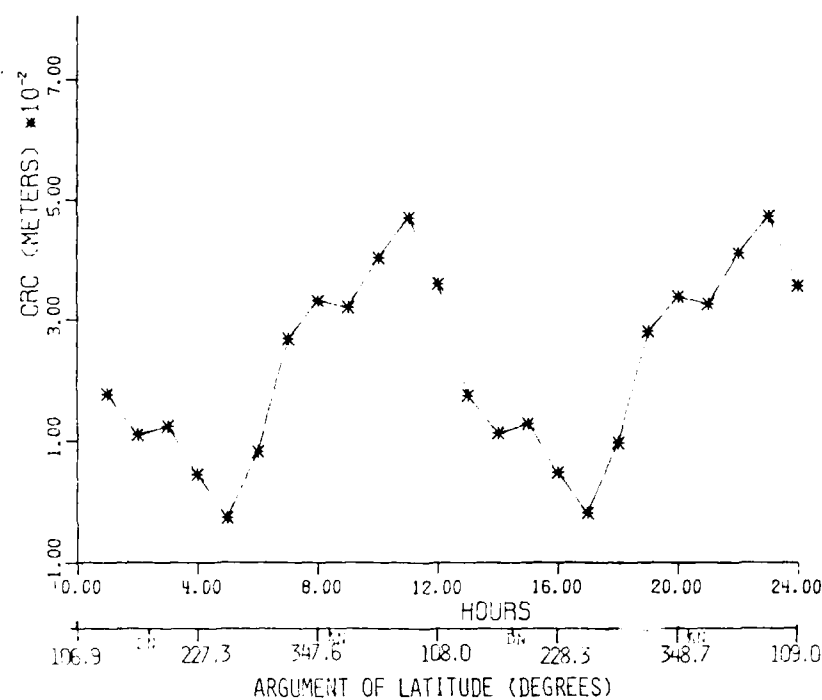


FIGURE 2-14 C_{rc} ZONAL PARAMETER (METERS) TWO REVOLUTIONS

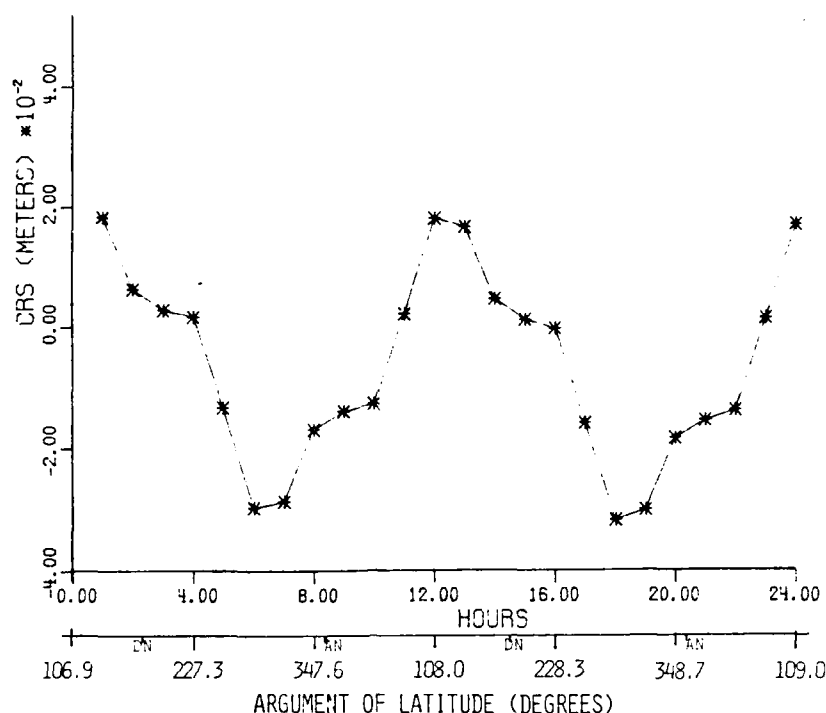


FIGURE 2-15 C_{rs} ZONAL PARAMETER (METERS) TWO REVOLUTIONS

The last two figures, 2-16 and 2-17, exhibit quite different characteristics. According to Kopitzke[private communication,1986], the C_{ic} and C_{is} parameters are included to aid the fitting process, since there is no expected secular change and very little periodic change in inclination due to J_2 . In other words, C_{ic} and C_{is} help absorb out-of-plane perturbations not accounted for by the di/dt parameter. The plots exhibit a four-hour periodic effect with mixed maxima and minima. Both have near-zero biases which supports the expected lack of secular growth. There is no indicated dependence on the nodal crossings. Consequently, the J_2 perturbation is minimal and the lunar gravity may cause the periodic

variation, however, the four-hour period is unusual.

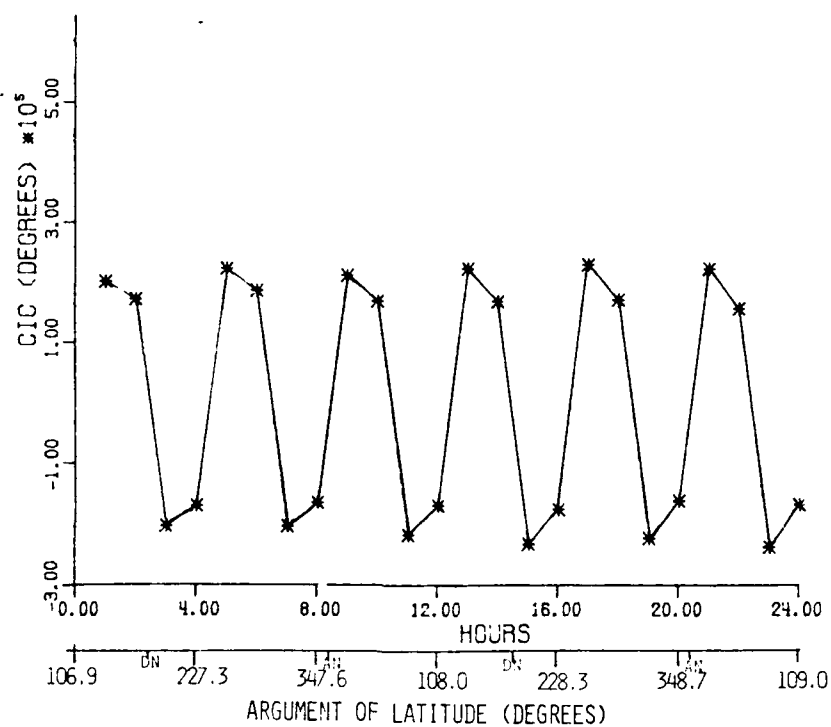


FIGURE 2-16 C_{ic} ZONAL PARAMETER (DEGS) TWO REVOLUTIONS

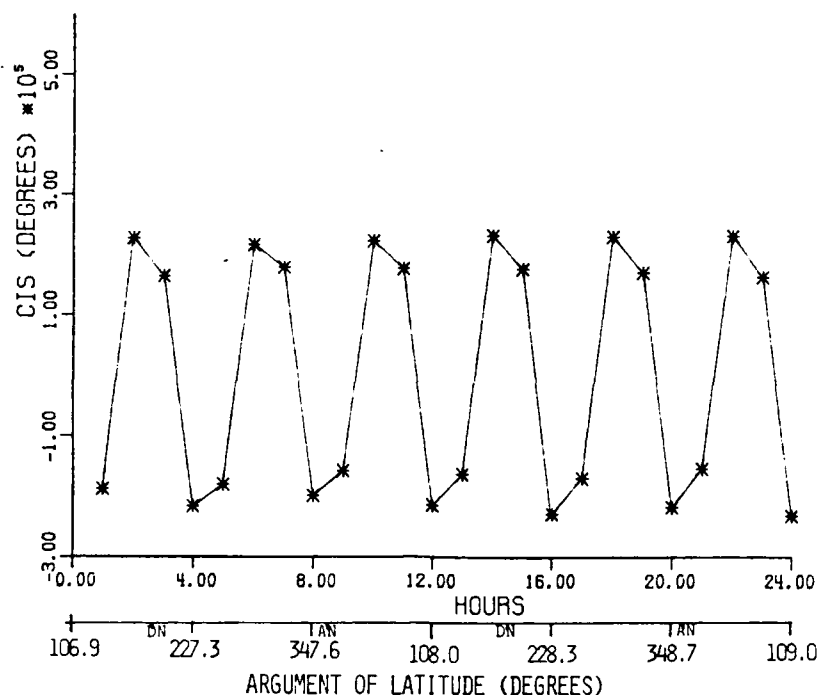


FIGURE 2-17 C_{1s} ZONAL PARAMETER (DEGS) TWO REVOLUTIONS

This set of results has shown typical parameter characteristics that appear during the fit of the UTOPIA-generated orbit. Effects due to Earth oblateness, lunar and solar gravity, and solar radiation pressure are present, while smaller effects due to J_4 , and polar wander, do not appear. It is important to realize several parameters absorb different perturbations during the fit, so isolating one characteristic is difficult and, perhaps, not essential. The conclusion that can be drawn is that this set of 15 constant parameters fits the perturbed orbit well, i.e., to less than ten meters in the RMS of the combined x, y, z residuals.

The accuracy of the sequential estimator is demonstrated further in Figures 2-18 through 2-20, plots of the x, y, and z components of the residual vector over two revolutions. Each figure shows how the broadcast ephemeris drifts each hour compared to the UTOPIA orbit. The broadcast ephemeris model cannot match the perturbed orbit precisely. However, these four-hour fits, with twenty points per hour, do indicate that the broadcast ephemeris describes the UTOPIA-generated orbit very well for each hour. The curves are centered around zero meters which demonstrates that the 15-parameter ephemerides accurately account for orbit perturbations.

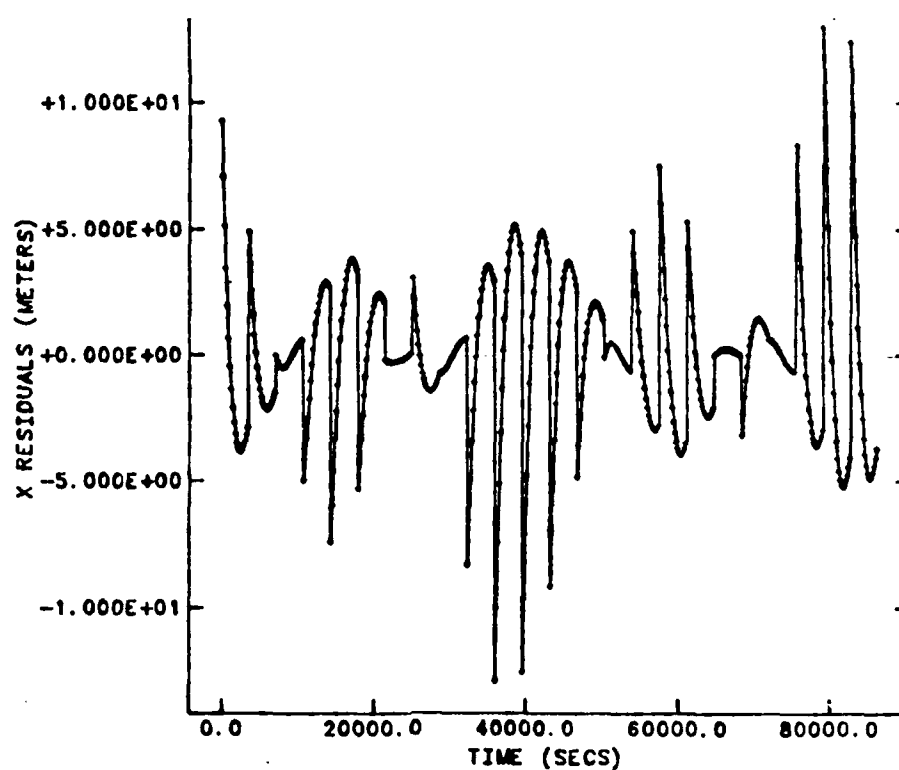


FIGURE 2-18 X RESIDUALS (METERS) - TWO REVOLUTIONS

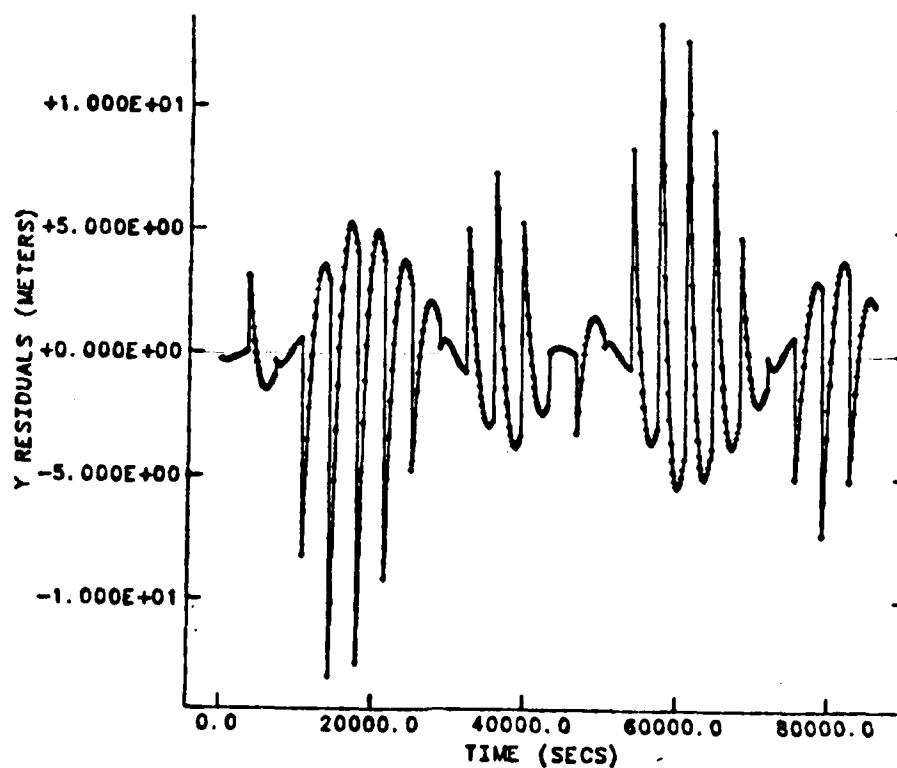


FIGURE 2-19 Y RESIDUALS (METERS) - TWO REVOLUTIONS

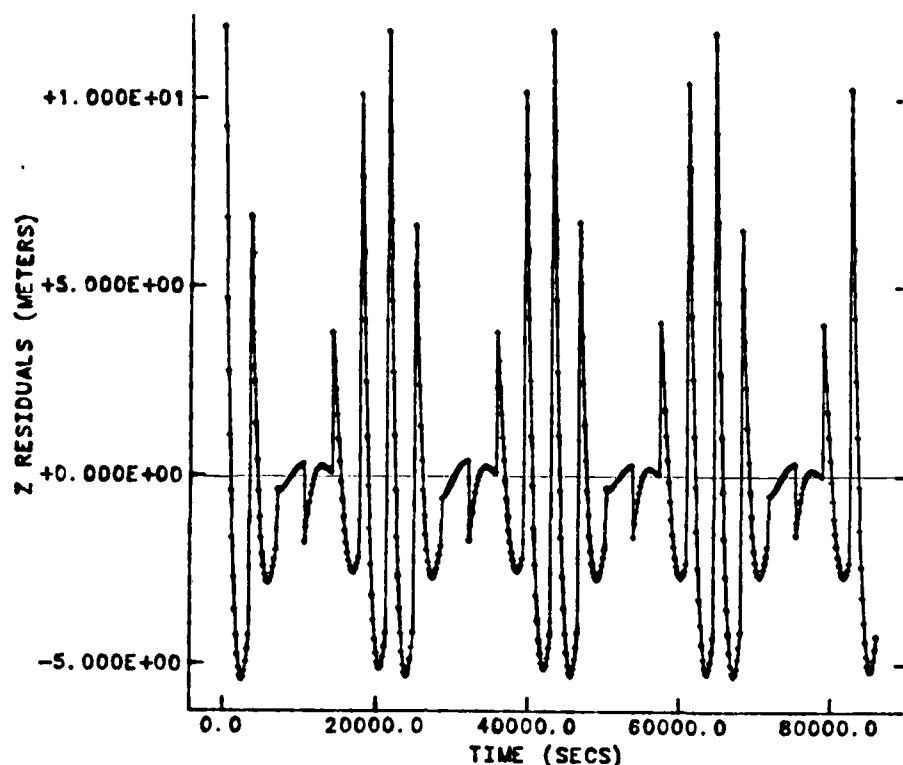


FIGURE 2-20 Z RESIDUALS (METERS) - TWO REVOLUTIONS

Several other characteristics of the broadcast ephemeris are shown in Figures 2-21 through 2-23. These plots compare how the estimated ephemeris fits the UTOPIA-generated orbit in the radial, transverse, and normal directions. The plots were created by first producing position quadruples (x, y, z, t) with the UTOPIA orbit processor for two revolutions. Then the Broadcast Ephemeris estimator fit the UTOPIA positions with hourly ephemerides, based on four-hour fits. Finally, satellite positions were computed from the hourly ephemerides using the Broadcast Ephemeris Algorithm and compared with the original UTOPIA orbit positions. The differences, taken

every three minutes, show how the estimator models the UTOPIA orbit. The large spikes in each figure show the discontinuity of the fit at the beginning of each hour when a new broadcast ephemeris attempts to model the UTOPIA orbit. The fit improves quickly in the first few points, then overshoots the UTOPIA orbit at the middle of the hour, but returns toward the UTOPIA orbit as the hour ends. The best fits in Figures 2-21 and 2-22 occur every six hours, at the nodes. The largest spikes occur at the northern-most and southern-most points of the orbits. Figure 2-23 shows very little out-of-plane sensitivity to the nodal crossing, plus very small errors in the fit. These characteristics support the parameter plot discussions earlier in the chapter, where the J_2 perturbation caused most of the parameter variations. The nine meter bound on the radial, 15 meter on the transverse, and the .3 meter on the normal differences further indicate the ephemeris accuracy.

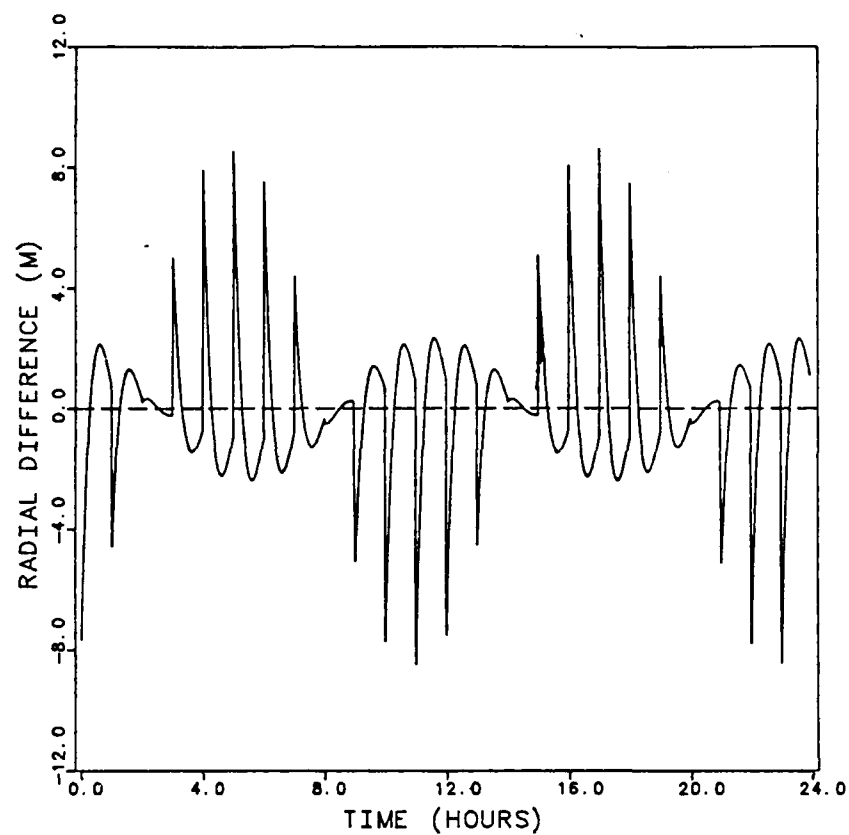


FIGURE 2-21 RADIAL DIFFERENCE BETWEEN BROADCAST EPHEMERIS AND UTOPIA ORBITS

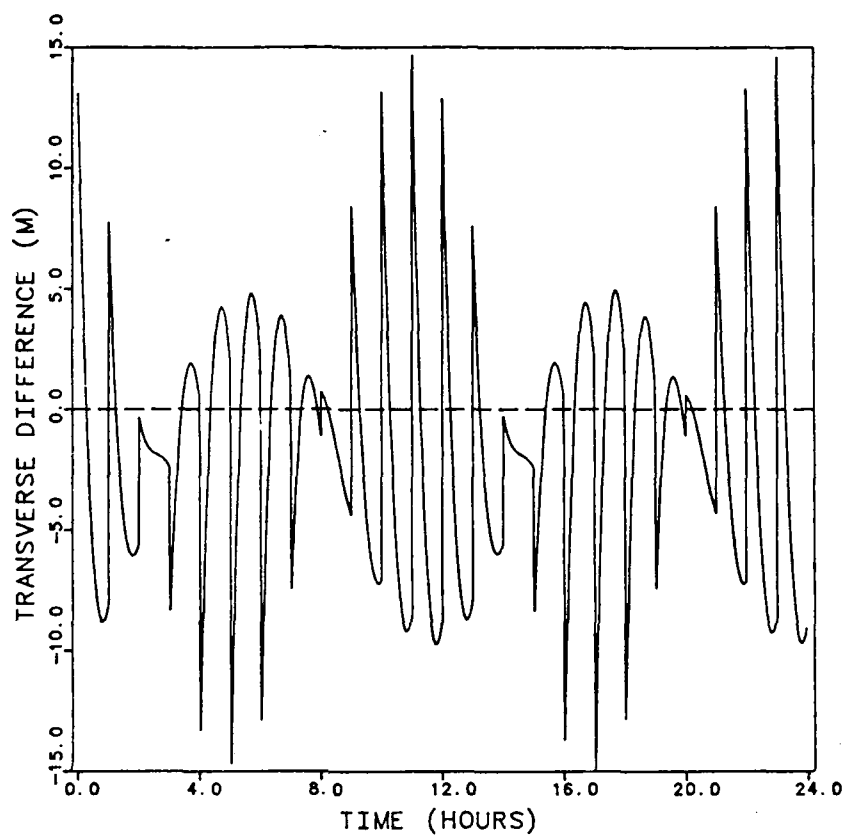


FIGURE 2-22 TRANSVERSE DIFFERENCE BETWEEN BROADCAST EPHEMERIS AND UTOPIA ORBITS

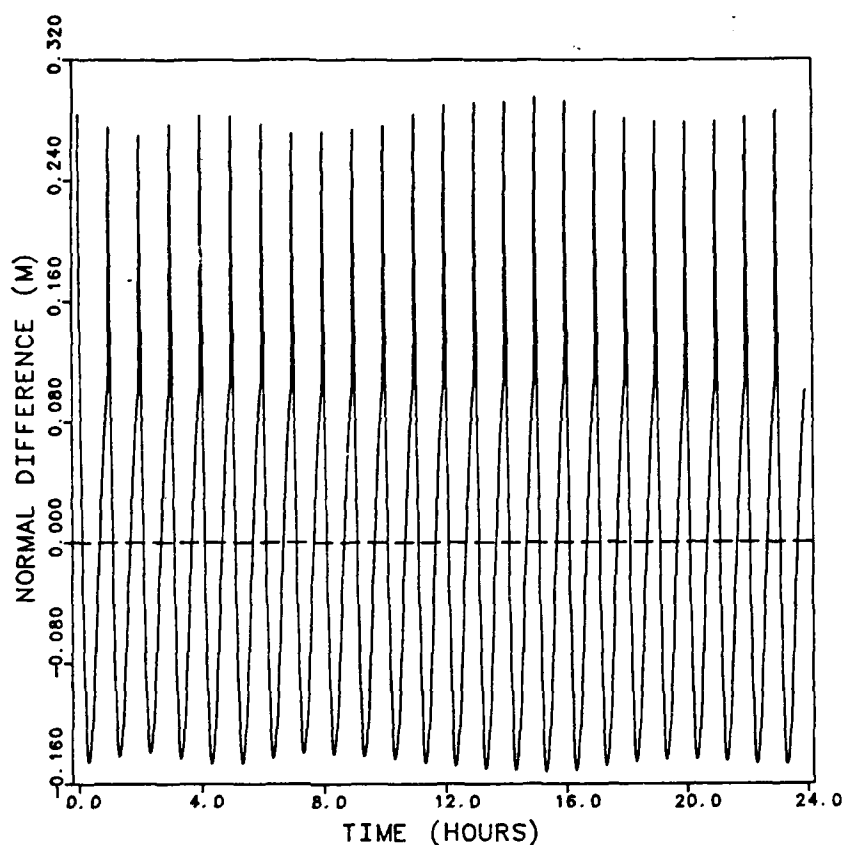


FIGURE 2-23 NORMAL DIFFERENCE BETWEEN BROADCAST EPHEMERIS AND UTOPIA ORBITS

One other version of the estimator used two and four-hour fits to estimate the state at the midpoint of the observations, instead of at the beginning. This timing was an attempt to improve the accuracy of the ephemerides, expecting less drift in the ephemeris by keeping the observations within one and two hours either side of the epoch. The estimator used the Gentleman formulation to process sliding, two and four-hour measurement blocks.

The results are similar to the previous cases for the four-hour blocks, with a much improved RMS of residuals for the two-hour blocks. For example, the RMS of

residuals is 5.14 meters for the first four-hour case. For the same epoch, the two-hour estimate yields .286 meters. All of the two-hour estimates for the 24 hour test cases are at least one order of magnitude better than the four-hour cases. However, the two-hour estimates generally take longer to converge and their variances are two to three orders of magnitude larger, indicating less confidence in the converged state.

Tables 2-7 and 2-8 compare the two cases along with the original case for RMS of residual, number of iterations, and variances of M_0 .

Table 2-7 Comparison of Broadcast Ephemeris Estimates			
Hour	RMS of Residual (meters)/Iterations		
	Beginning-of-the-Hour Estimate	Two-Hour Mid-Point Estimate	Four-Hour Mid-Point Estimate
1	1.09 / 8	.286 / 12	5.14 / 7
2	6.05 / 9	.150 / 14	2.72 / 12
3	5.77 / 9	.053 / 11	1.09 / 9
4	6.05 / 10	.228 / 10	4.05 / 14
5	5.06 / 8	.320 / 13	5.77 / 9
6	2.58 / 8	.333 / 12	6.05 / 12
7	1.21 / 17	.283 / 15	5.06 / 10
8	4.03 / 9	.143 / 11	2.58 / 11
9	5.69 / 23	.063 / 10	1.21 / 9
10	6.05 / 11	.226 / 10	4.03 / 10
11	5.05 / 7	.315 / 9	5.69 / 8
12	2.67 / 9	.335 / 8	6.05 / 8

Table 2-8
Comparison of Broadcast Ephemeris Estimates

Hour	Variance of M_0 (radians ²)		
	Beginning-of-the-Hour Estimate	Two-Hour Mid-Point Estimate	Four-Hour Mid-Point Estimate
1	.475 x 10 ⁻⁴	.360 x 10 ⁻¹	.578 x 10 ⁻⁴
2	.130 x 10 ⁻⁴	.304 x 10 ⁻¹	.504 x 10 ⁻⁴
3	.305 x 10 ⁻⁶	.291 x 10 ⁻¹	.474 x 10 ⁻⁴
4	.239 x 10 ⁻⁵	.843 x 10 ⁻²	.130 x 10 ⁻⁴
5	.443 x 10 ⁻⁵	.499 x 10 ⁻⁴	.305 x 10 ⁻⁶
6	.601 x 10 ⁻⁵	.129 x 10 ⁻²	.239 x 10 ⁻⁵
7	.635 x 10 ⁻⁵	.258 x 10 ⁻²	.443 x 10 ⁻⁵
8	.309 x 10 ⁻⁵	.355 x 10 ⁻²	.601 x 10 ⁻⁵
9	.241 x 10 ⁻⁶	.379 x 10 ⁻²	.635 x 10 ⁻⁵
10	.381 x 10 ⁻⁶	.186 x 10 ⁻²	.309 x 10 ⁻⁵
11	.136 x 10 ⁻⁵	.128 x 10 ⁻³	.241 x 10 ⁻⁶
12	.219 x 10 ⁻⁵	.195 x 10 ⁻³	.381 x 10 ⁻⁶

D.2 Ill-Conditioning in the Normal Matrix

There is evidence of ill-conditioning in the broadcast ephemeris algorithm due to the correlation between the parameters M_0 and u . For the near circular GPS orbits, M_0 and u correlate at almost -1.0. As the estimate of M_0 changes between iterations and between epochs, the value of u changes the same amount in the opposite direction. The sum of the two, u_0 , the argument of latitude, remains steady. The MCS uses u_0 for creating the ephemerides instead of estimating both M_0 and u , to avoid the ill-conditioning. However, for this study u_0 and u

remain separate, resulting in some ill-conditioning. The evidence of the ill-conditioning comes in two of the outputs, the first being the correlation matrix where the correlation coefficient, $\mu_{1,7}$, is always very close to -1.0. Here

$$\mu_{1,7} = \frac{P_{1,7}}{\sqrt{P_{1,1}} \sqrt{P_{7,7}}} \quad (2-33)$$

The elements, $P_{1,1}$, $P_{7,7}$ and $P_{1,7}$ are the variances and covariance of M_0 and w , respectively. The other evidence is in the normal matrix condition number, computed as the square root of the largest eigenvalue divided by the smallest eigenvalue in the Gentleman-formulated cases. A typical value for the condition number in these cases is 10^{12} , indicating that a large change in the state may result from a small change in the observations[Strang,1980].

The ill-conditioning does not prevent convergence in any of the test cases. Rather, each case shows smooth iteration to convergence with acceptable values for the RMS of residuals. All values for the converged state are reasonable and yield excellent navigation results in Chapters Four and Five.

2.3 Summary

This chapter has investigated the GPS Broadcast Ephemeris Parameters and their formulation. The software to determine the broadcast ephemerides has been validated by comparing numerical and analytical partial derivatives in the measurement sensitivity matrix, and by considering the accuracy of the converged state in several cases with no model error. Application of the software to realistic ephemerides has shown that the estimated parameters reflect unmodelled periodic errors, but that accuracy to ten meters is possible (reconstructing the position ephemeris in the x, y, z frame) or in the RTN frame: nine, fifteen, and one meter, respectively.

The caveat for these tests is that the results are obtained for one typical satellite on a specified day. Other satellites on other days may produce different results, but are not expected to differ significantly.

3.1 Introduction

The broadcast ephemeris accurately reconstructs the predicted GPS orbit during the hour in which it is current. If the ephemeris is used outside the original four-hour fit interval, then the ephemeris will be substantially in error, perhaps hundreds of kilometers, within half an orbit. A continuous supply of new ephemerides comes from the Master Control Station (MCS) to keep all the satellite positions current. If the MCS were no longer able to provide the ephemerides or if autonomous operation of a receiver is desired, a method to update old ephemerides using current pseudorange measurements would be required. The process of updating the broadcast ephemeris is the subject of this chapter.

The process used for the ephemeris update was a linearized, least squares, batch estimator with the Broadcast Ephemeris Algorithm as the model [Van Dierendonck, et.al., 1978]. As suggested by Ananda, et.al., [1984], the estimator processed a subset of the fifteen parameters, to produce the updated ephemeris and clock parameters. The six Keplerian parameters and two clock parameters a_0 and a_1 (satellite clock bias and drift

rate), constituted the state:

$$X = [M_0 \ e \ \sqrt{A} \ \Omega_0 \ \omega \ i \ a_0 \ a_1]^T$$

This reduction in the number of estimated parameters greatly simplified the estimator for fast, smooth convergence.

Results from this study show that a variety of conditions caused a wide spectrum of accuracies in the updated ephemerides. By using the actual broadcast ephemerides as truth, it was possible to judge the updated ephemerides in four criteria: the RMS of residuals and the parameter one sigma values from the least squares fitting process, the ECF position differences, and the individual parameter changes from the broadcast to the updated ephemerides.

As shown in Section 3.5, the RMS of residuals from the fitting process were all between 1.6 and 10.0 meters, demonstrating the ability of the model to fit the observations. The parameter one sigma values varied with the magnitude of the parameter, but were consistent between test cases and showed confidence in the updated parameters.

On the other hand, the ECF position differences (position error) between the broadcast ephemeris position and the updated ephemeris position exhibited a large

degree of inconsistency and some large errors between test cases. For instance, the smallest position error in the validation test was 145 meters for satellite SV09. Typical position errors ranged from 1000 to about 30,000 meters for the long-range ephemeris updates. The largest position error was 203,127 meters for SV12.

Finally, the individual parameter changes between the broadcast Keplerian parameters and the updated Keplerian parameters were generally small throughout the test cases ranging from 0.000014 percent of the broadcast value for \sqrt{A} to one percent of the broadcast value of e . The two clock parameters, however, changed considerably during the tests, revealing adjustments in the timing of the problem, particularly variations in the satellite time standards. Table 3-1 lists the ranges of values for the four criteria used to judge accuracy of the updated ephemerides.

Table 3-1
Range of Values for the Accuracy Criteria

Criteria	Range		
RMS of Residuals	1.6 to 10.0 (meters)		
Parameter One Sigma			
M_o	9.8E-7	to	3.0E-2 (rads)
e_o	2.4E-7	to	2.4E-5
\sqrt{A}	2.4E-7	to	4.7E-2 (meters) ^{1/2}
Ω_o	2.1E-6	to	1.0E-4 (rads)
i	1.9E-6	to	8.3E-5 (rads)
ω	4.4E-5	to	5.1E-4 (rads)
a_o	2.4E-8	to	7.5E-7 (secs)
a_1	1.2E-14	to	1.2E-10 s/s)
Parameter Changes			
M_o	0.001	to	0.13 %
e_o	0.025	to	1.0 %
\sqrt{A}	0.00009	to	0.0004 %
Ω_o	0.002	to	0.01 %
i	0.004	to	0.18 %
ω	0.01	to	0.22 %
a_o	0.3	to	90.0 %
a_1	0.49	to	1003.0 %
ECF Position Error			
SV06	547	to	73,146 meters
SV08	2265	to	62,411 meters
SV09	145	to	26,916 meters
SV11	298	to	12,896 meters
SV12	382	to	203,127 meters
SV13	994	to	19,067 meters

The conditions that caused the larger errors can be arranged in two categories: specific test conditions and algorithm characteristics. The test conditions that tended to increase the updated ephemeris errors were small measurement sets caused by short passes of certain

satellites and the lack of measurements on several long passes, probably due to receiver malfunctions (see Tables 3-2 and 3-3). The algorithm characteristics that affected the updates were 1) the lack of elevation masking and measurement smoothing, 2) normal matrix ill-conditioning caused by the high correlation of the M_0 and w parameters, and 3) an observability problem with one or two short passes over a single site (see Section 3.4). Realizing that the test conditions and algorithm characteristic affected the results, it was possible to study the various test cases to gain an understanding of the ephemeris update process. This ephemeris update process is the first step in the navigation accuracy study in Chapter Five.

Another study of navigation accuracy using updated ephemerides was published by the Aerospace Corporation, Ananda, et.al, [1988], but it did not discuss the accuracy of the updated ephemerides. However, the updated ephemerides were probably more consistently accurate because a Kalman Filter was used to update the ephemerides, with elevation masking and measurement smoothing, an adjusted parameter set that avoided the correlation between M_0 and w , long satellite passes and an a priori covariance matrix to guarantee observability. Other comparisons between the two studies are presented

in Chapter Five. This chapter, then, describes the ephemeris update algorithm with a minor modification to the model, the pseudorange measurements with corrections, and the estimator validation and test cases. The updated ephemeris, which is produced, is an input to the navigation procedure in Chapter Five.

3.2 The Broadcast Ephemeris Update Algorithm

The mathematical model was the BEA, with a small adjustment in the coordinate system. This adjustment was required because the estimator used actual range measurements from the operational GPS tests which used slightly different coordinates than the BEA system. The operational GPS coordinate system in the 1985 tests was the World Geodetic System (WGS) 72 coordinates[Seppelin, 1974]. The WGS 72 system used the x axis 0.54" east of the prime meridian, the z axis was the earth spin vector averaged from 1900 to 1905, and the y axis completed a right hand system. The adjustment to the BEA was 0.54" subtracted from the longitude of the ascending node calculation. This correction affected the results very little but brought the estimator up to date with the GPS operations. The rest of the model remained as outlined previously.

The first step in the ephemeris update algorithm was

to compute residuals by subtracting the calculated from the observed pseudorange:

$$y = p_o - p_c, \quad (3-1)$$

where p_o is the observed and p_c is the calculated pseudorange. Corrections to both pseudoranges adjust for clock errors, ionospheric delay, tropospheric delay, and relativistic effects. The basis for the calculated pseudorange is the slant range which comes from the geometry of the i^{th} satellite and the receiver site:

$$p_{\text{geom}_i} = \sqrt{(x_i - x_r)^2 + (y_i - y_r)^2 + (z_i - z_r)^2}, \quad (3-2)$$

where x_i, y_i, z_i are the i^{th} satellite coordinates, computed from the mathematical model at the time of the pseudorange measurement, and x_r, y_r, z_r are the known receiver coordinates, all in the ECF system. Knowing the exact receiver coordinates is critical to updating the ephemeris accurately, because the number of unknowns would be too large in the estimator if receiver coordinates were also estimated.

The clock bias errors at the satellite and the receiver affect the calculated range directly. Both the satellite clock and the receiver clock are synchronized by offsets or biases to GPS system time, kept by the MCS. The satellite clock difference from the MCS standard is

transmitted with the ephemerides, whereas the receiver clock bias is estimated by the update algorithm. To prevent timing errors in the update algorithm all calculations were done at the pseudorange measurement time (signal reception time). Because the signal travels at the speed of light, the two clock biases multiplied by the speed of light form the corrections to the geometric range:

$$p_{cc_i} = p_{geom_i} - c\Delta t_{sv_i} + c\Delta t_u \quad (3-3)$$

where $c = 2.99792458 \times 10^8$ meters/sec, Δt_{sv_i} and Δt_u are the i^{th} satellite and receiver (user) clock errors, respectively.

The observed pseudorange signal actually passes through the atmosphere, so it is corrected for ionospheric delay. The ionospheric delay is frequency dependent, so the satellites transmit messages on two frequencies simultaneously to facilitate computing the delay:

$$p_{cid} = \frac{p_{L_2} - p_{L_1}}{1 - \gamma_1} \quad (3-4)$$

where p_{cid} is the pseudorange corrected for ionospheric delay, p_{L_2} and p_{L_1} are the pseudorange measurements for the two frequencies L_2 and L_1 , and γ is a frequency factor, given by $\gamma = (f_{L_1}/f_{L_2})^2 = 1.64694$. The quantities

f_{L_1} and f_{L_2} are the standard GPS frequencies: $L_1 = 1575.42$ MHz and $L_2 = 1227.6$ MHz [Moller, 1984]. For the validation tests the ionospheric delay correction was applied to the pseudorange data file before reading the data, but normal operations and the other test cases apply the correction during the pseudorange processing.

The tropospheric delay also affects the observed pseudorange. This delay depends on the distance the signal travels in the troposphere, given by the elevation of the satellite and the density of the atmosphere. The delay is large when the satellite is at a low elevation and the signal is travelling through a dense atmosphere, determined by the temperature, pressure, and humidity near the receiver. A subroutine entitled TROP, provided by Goad [private communication, 1985], computes this signal delay. Thus,

$$P_{ctd} = P_o - \Delta p_{trop} \quad , \quad (3-5)$$

where p_{ctd} is the pseudorange corrected for tropospheric delay, p_o is the observed pseudorange and Δp_{trop} is the tropospheric correction.

Finally, the general and special relativistic effects on the satellite time must be corrected. According to Van Dierendonck, et.al., [1978], the satellite time drifts because the satellite clock is located at a

different gravitational potential than the user clock and is travelling at a much higher speed. The combined effect is a secular and periodic drift in the satellite clocks. Knowing the orbit altitude and speed allows the secular drift to be corrected by an offset to the clock frequency before launch. The periodic drift may have an amplitude of 70 nanoseconds and is corrected by the following expression from Moller[1984]:

$$\Delta t_r = F e (A)^{1/2} \sin(E_k) \quad (3-6)$$

where $F = -4.442809305 \times 10^{-10} \text{ sec}/(\text{meter})^{1/2}$

e - eccentricity

$(A)^{1/2}$ - square root of the semimajor axis

E_k - eccentric anomaly calculated in the BEA.

Thus, the observed pseudorange is computed from the two timed signals from the satellite and corrected for ionospheric and tropospheric delays as well as relativistic effects. The calculated pseudorange is formed from the slant range which is adjusted for the satellite and user clock errors. By subtracting the calculated pseudoranges from the observed pseudoranges, the residuals are found (Equation 3-1). The residuals are used in the normal equation when calculating the state corrections.

The measurement sensitivity matrix is also required

for the estimation process. It consists of the partial derivatives of the pseudorange with respect to the eight elements of the state, evaluated on the reference trajectory, X^* . The reference trajectory is the current-hour broadcast ephemeris, and

$$H = \frac{\partial G(X^*, t)}{\partial X} , \quad (3-7)$$

where $G(X, t) = p_c$, the calculated pseudorange.

The partial derivatives form a (1×8) matrix describing the sensitivity of the pseudorange, p_c , to small changes in the state X ,

$$H = \left[\frac{\partial p_c}{\partial M_0} \quad \frac{\partial p_c}{\partial e} \quad \dots \quad \frac{\partial p_c}{\partial a_1} \right] . \quad (3-8)$$

The elements of H are similar enough to the elements of H in Chapter Two, that by using the chain rule of differentiation these elements are obtained. For example,

$$\frac{\partial p_c}{\partial M_0} = \frac{\partial p_c}{\partial x_k} \frac{\partial x_k}{\partial M_0} + \frac{\partial p_c}{\partial y_k} \frac{\partial y_k}{\partial M_0} + \frac{\partial p_c}{\partial z_k} \frac{\partial z_k}{\partial M_0} , \quad (3-9)$$

where $\frac{\partial x_k}{\partial M_0}$, $\frac{\partial y_k}{\partial M_0}$, and $\frac{\partial z_k}{\partial M_0}$ are the same as in Chapter Two, which are presented in Appendix C. The other partial derivatives for H are in Appendix D. As in Equation 2-25, the H and H^T matrices combine with the residual to

form the normal equation[Tapley and Born, 1985]:

$$\hat{x} = (H^T H)^{-1} H^T y . \quad (3-10)$$

The normal equation gives the state correction vector.

Just as in section 2.2.B, the state correction vector, \hat{x} , is the solution to the normal equation and represents the difference between X and X^* . Because \hat{x} consists of only eight elements, it does not correct the nine perturbation terms from the input ephemeris. Instead, the updated ephemeris consists of six updated Keplerian elements, nine of the original perturbation parameters, and two updated satellite clock terms. In this form, the updated ephemeris is used in the navigation routine of Chapter Five.

The state transition matrix has the same characteristics as in Chapter Two. Because X is constant and \dot{X} equals zero, the $\Phi(t, t_k)$ matrix is the identity matrix. The state propagates forward to each measurement time by means of the rate terms in the ephemeris ($n, \dot{\Omega}, di/dt$). This method simplifies computations and provides a constant ephemeris at each epoch, t_{oe} .

Again, like the estimator in Chapter Two, this processor is linearized about X^* and iterates to a solution. Iterations end when the relative difference in the RMS of

the residuals drops below the specified tolerance.

The covariance matrix, the (8×8) inverse of the normal matrix, is one measure of the accuracy of the updated ephemerides. The weighting matrix in the normal equation was the identity matrix, so the standard deviations are for a one unit standard. Then, small values for the diagonal elements suggest that the estimated ephemerides can be considered accurate. See Section 3.5 for typical covariance results.

The estimator output is the updated, eight-parameter satellite state, X , at epoch hour, t_{oe} . The first six parameters represent the corrected Keplerian terms from the 15-parameter broadcast ephemeris. The last two parameters are the corrected satellite clock parameters. For navigation purposes, the updated parameters are combined with the old perturbation parameters to form a full ephemeris.

3.3 Test Data

The old broadcast ephemerides to be updated along with the pseudorange measurements came from the Phase One tests organized by the Jet Propulsion Laboratory in 1985. These tests consisted of GPS receivers located around the United States collecting data that included broadcast ephemerides and pseudorange measurements for a variety of

investigations. Seven test satellites were in orbit but only six were available for accurate data transmission during these tests. By their pseudo-random number (PRN) code, the satellites were PRN04, PRN06, PRN08, PRN09, PRN11, PRN12, and PRN13, which, for convenience will be addressed as Space Vehicle (SV) numbers. Thus PRN06 will be referred to as SV06 in the following discussion. Satellite SV04 had an inaccurate crystal clock and was not used for this study.

The data transmitted by each satellite which was necessary for this study included the fifteen-parameter broadcast ephemeris and two satellite clock parameters, a_0 , clock bias, and a_1 , clock drift rate. The broadcast message format included a time of transmission which allowed the receivers to calculate a pseudorange distance between the transmitting satellite and the receiver, since the receivers kept accurate clocks also. A Hydrogen Maser Oscillator was connected to some of the GPS receivers, thereby providing a highly stable oscillator reference. All of the data was collected in a normal GPS scenario with satellites continuously broadcasting their stored one-hour ephemerides which had been created and uploaded by the MCS. The work in this paper used data from two of the receivers on several dates, first to validate the software, then to update old ephemerides.

The first validation cases were examined with data received from the six test satellites on the first through the fifth of April at receiver sites in Fort Davis, Texas, and Richmond, Florida. Other validation cases were examined at Fort Davis, Texas, with data from 20 and 21 November. Finally, long-range update cases were compared using broadcast ephemerides in June, August, September, and October that were obtained from GPS Archives in Yuma, Arizona [Chasko, private communication, 1987] and updated with the pseudoranges from 20 November. All of the data from Fort Davis and Richmond were received on Texas Instruments 4100 GPS Receiver Sets [Texas Instruments, 1982] located near Very Long Baseline Interferometer reference points with corrections applied for the exact antenna locations. These GPS antenna phase center coordinates in the ECF system are listed below:

Fort Davis, Texas (Harvard RM 4 Site):

x = -1,324,192.043 meters

y = 5,332,060.634 meters

z = 3,232,044.050 meters

Richmond, Florida (Timer Site):

x = 961,319.584 meters

y = -5,674,055.766 meters

$$z = 2,740,564.177 \text{ meters}$$

[Abusali, private communication, 1985]

The equipment at each site included the Texas Instruments 4100 receiver, a Hydrogen Maser Oscillator (except at Richmond in November), a processor and a recorder. The processor used the GESAR 22.0 software [Kurtin, private communication, 1987]. Most of the data was collected, stored and made available through the Applied Research Laboratory at the University of Texas at Austin [Scott, 1983]. As mentioned, the "old" ephemerides for long range updates came from the GPS Archives in Yuma, Arizona.

The broadcast ephemerides were composed of the same fifteen constants as in Chapter Two: six Keplerian, M_0 , e , \sqrt{A} , Ω_0 , i_0 , ω , and nine perturbations, Δn , $\dot{\Omega}$, di/dt , C_{uc} , C_{us} , C_{rc} , C_{rs} , C_{ic} , C_{is} . In addition, there were two clock parameters: the satellite clock bias, a_0 , and drift rate, a_1 . For daily operation each satellite clock operated independently, with its own characteristic bias from GPS system time and drift rate. Estimates of these two quantities were computed by the MCS and included in the upload message to each satellite. This timing process coordinates the ephemerides broadcast by the satellites with the GPS system time at the MCS. The benefit to the user is that epoch times and

pseudorange times reference only one standard clock[Russell and Schaibly, 1978].

The epoch times for the broadcast ephemerides in this study were similar to those in Chapter Two, referencing the beginning of an hour as the number of seconds past 00:00 Sunday. The updated ephemerides described here use the same type of epochs.

The estimator was initialized with the broadcast ephemeris for one satellite at a given epoch. The fifteen ephemeris and two clock parameters came from the test data, actually transmitted by the specified satellite. For a typical example, at epoch time, $t_{oe} = 284,400$ seconds (Wednesday, 3 Apr 85, 0700 hours), for an hour, satellite SV09 sent the following values:

$$\begin{aligned}
 M_o &= .9266238889 \text{ rads} \\
 \Delta n &= .1254 \times 10^{-8} \text{ rads/sec} \\
 e &= .0107720089 \\
 \sqrt{A} &= .5153697346 \times 10^4 \text{ meters}^{1/2} \\
 \Omega_o &= -2.832466585 \text{ rads} \\
 i &= 1.114525777 \text{ rads} \\
 \omega &= 1.225491443 \text{ rads} \\
 \dot{\Omega} &= -.6461341 \times 10^{-8} \text{ rads/sec} \\
 di/dt &= .5386 \times 10^{-9} \text{ rads/sec} \\
 C_{uc} &= .45877 \times 10^{-5} \text{ rads}
 \end{aligned}$$

$$C_{us} = .11383 \times 10^{-4} \text{ rads}$$

$$C_{rc} = 234.91 \text{ meters}$$

$$C_{rs} = 89.188 \text{ meters}$$

$$C_{ic} = -.89407 \times 10^{-7} \text{ rads}$$

$$C_{is} = .65193 \times 10^{-7} \text{ rads}$$

$$a_o = .2997946 \times 10^{-3} \text{ seconds}$$

$$a_1 = .10982 \times 10^{-9} \text{ seconds/second}$$

After initialization, the estimator accepted the pseudorange measurements.

The pseudorange measurements provided the information to be used to update the ephemeris. The test data included raw pseudorange measurements from all six satellites to the two receiver sites, taking only one satellite and one site at a time. Measurements occurred every 30 seconds for the entire time a satellite was visible to a site. No elevation masking was used. The estimator tested for and eliminated measurements that were out of set bounds, but did no data smoothing. Typical observation sets included one to three days of data with one or two passes per day over the site, each pass lasting from two to five hours. Ephemeris updates were made with 600 and 750 observations for each satellite at Fort Davis and with 750 observations at Richmond. The details of the observation sets are included in Tables 3-2 and 3-3.

Table 3-2
Observation Sets - Fort Davis, TX - April 1985

Satellite	SV08	SV09	SV11	SV12	SV13
April Dates	1-3	1-2	1-2	1-2	1-2
Passes per Day	1	2	1	2	1
Obs/Pass 1	437	447	720	375	422
/Pass 2	31	195	235	376	408
/Pass 3	471	192	730	417	423
April Dates	3-4	3-4	3-4	3-4	3-4
Passes per Day	1	2	1	2	1
Obs/Pass 1	471	448	730	375	423
/Pass 2	479	195	730	376	422
/Pass 3	0	448	720	371	415

Table 3-3
Observation Sets - Richmond, FL - April 1985

Satellite	SV08	SV09	SV11	SV12	SV13
April Dates	3-4	3-4	3-4	3-4	3-4
Passes per Day	1	2	1	2	1
Obs on Pass 1	265	370	731	332	464
Pass 2	470	408	885	342	467
Pass 3	472	371	883	332	467

Another characteristic of the observation sets was their proximity to the update epochs. The update epochs were sequential, set to the beginning of each hour a satellite was visible to the site. As the epochs, t_{oe} , advanced in time for a new estimate, the observation set slid forward, similar to the Chapter Two process, to insure that the observation times included the epoch

time. This process made the updated ephemeris a product of recent observations.

These observations had unknown statistical characteristics. Consequently, the estimator assumed that the random observation errors were uncorrelated in time and normally distributed with zero mean. No receiver bias was known, so the weighting matrix for the observations was the identity matrix. With this system, the estimator operated smoothly and accurately, producing updated ephemerides.

3.4 Update Algorithm Observability

Observability for the update algorithm is mathematically similar to that in Chapter Two; namely, the normal matrix must be full rank for a solution to exist. However, because the observations came from actual satellite passes of varying lengths, obtaining enough linearly independent observations was often difficult. As shown by Tapley and Born[1985], a set of observations from a single satellite pass over a single station may render a system unobservable. An attempt to insure observability was made by using one full pass and at least part of a second pass in all but three of the test cases. Tables 3-2 and 3-3 show that to obtain 600 and 750 observations for the test cases, two and sometimes three passes were

used, except for SV11 which had enough observations on one pass for 600 observations. The test results show that the observability problem may have caused some of the large position errors in the updated ephemerides.

Another method to prevent observability problems would have been to add an a priori covariance matrix in the normal equation. However, this study did not use an a priori covariance matrix.

3.5 Experiments with the Ephemeris Update Estimator

The Ephemeris Update Estimator operated effectively using pseudorange measurements from the April and November 1985 tests organized by Jet Propulsion Laboratory. It converged smoothly in eight iterations or less for most of the cases. The updated parameters were close to the actual broadcast parameters at the same epoch, thus demonstrating the ability to correct the old ephemerides with current pseudorange measurements. The test cases were divided into two parts: validation tests using April and November ephemerides, and long range, update cases where ephemerides were brought forward to November from dates in April, June, August, September, and October.

In all these experiments, the normal equation was solved by the method of Gentleman, using the same GIVLIB

library of subroutines mentioned in section 2.2.D. The Cholesky method produced nearly identical results in well-conditioned cases, therefore only GIVLIB was used. Also, the measurement sensitivity matrix was obtained using the analytic partial derivatives only.

All test cases used one satellite at a time, with pseudorange measurements at one receiver site. This simulated a lone operator updating the GPS constellation, starting with old ephemerides, in case the MCS did not create new ephemerides for the satellites to broadcast. Most of these cases ran at Fort Davis, Texas, but for comparison several validation tests were run at Richmond, Florida. Because the satellites were visible for varying amounts of time, the number of observations per satellite pass varied. Consequently, the test cases used a variety of observation sets. Other variations in the constellation that affect the update cases are presented after the validation cases.

A. Validation Tests

The validation tests ran for satellite passes on 1, 2, and 3 April 1985, inclusive, for 3, 4, and 5 April 1985 inclusive, and for 20 and 21 November 1985, inclusive. The actual broadcast ephemeris transmitted by

a satellite was used to initiate the estimator, then pseudorange range measurements were used to update the six Keplerian and two clock terms at the same epoch. The difference between the broadcast position and the update position is reported as position error. This position error is due partly to errors in the update position and partly to errors in the broadcast position, since the broadcast ephemeris is an estimate also. However, the broadcast ephemeris position is considered truth in this study. Satellites SV04 and SV06 had insufficient observations on the first and second of April for accurate tests, so only five satellites were examined during that time. Generally, two passes on one day provided the best results in terms of the RMS of residuals and covariance elements. One pass yielded very good RMS of residual values but the variances of the state were larger than the two-pass cases. For two or three passes over two days, the RMS of residuals grew slightly. However, all of the RMS of residuals are less than ten meters.

Another measure of accuracy is a comparison of the actual satellite broadcast position and the updated position in the xyz space. For this comparison the broadcast and updated ephemerides at the same epoch are used in the BEA to compute xyz positions. The difference between the two positions is reported as position error in the xyz

space as well as in the radial(R), transverse(T), and normal(N) directions (RTN space) relative to the satellite path. The position error represents the difference between the MCS-generated broadcast position and the updated position.

One example of the results in the validation tests is SV09. Using two passes on 1 April (600 observations), SV09 produces RMS of residual values equal to 2.8 meters for several epochs in sequence. At epoch $t_{oe} = 111,600$ seconds, the position error is 302.3 meters. In the xyz and RTN spaces, the position error vector is given in meters by:

$$\bar{p}_{SV09} = \begin{bmatrix} 285 \text{ m} \\ -84 \text{ m} \\ -58 \text{ m} \end{bmatrix}_{xyz} = \begin{bmatrix} 110 \text{ m} \\ 166 \text{ m} \\ 228 \text{ m} \end{bmatrix}_{RTN}$$

With 750 observations over two passes, the RMS of residuals ranges from 2.9 meters to 3.1 meters and the variances reduce by one to five orders of magnitude for all the parameters. The position error vector is given by:

$$\bar{p}_{SV09} = \begin{bmatrix} -50 \text{ m} \\ 130 \text{ m} \\ 45 \text{ m} \end{bmatrix}_{xyz} = \begin{bmatrix} -10 \text{ m} \\ -143 \text{ m} \\ -22 \text{ m} \end{bmatrix}_{RTN}$$

the magnitude being 145 meters. The improvement in the variances indicates a higher confidence in the updated state. These good results are attributed to SV09 having two passes per day compared with one pass per day for

most of the others. This means for SV09 the observation blocks are spaced more closely than the others, yielding a better fit of the orbit perturbations by the constant parameters. Satellite SV12 is also visible to Fort Davis twice a day in the April data. Results for SV12 are also very good for one and two passes, with RMS of residual values between one and four meters, and position errors between 1,100 and 1,200 meters.

The other satellites with only one pass per day produce RMS of residual accuracies from 1.8 meters for SV11 (600 observations on one pass) to 8.1 meters for SV13 (750 observations on two passes). Position errors vary from 145 meters for SV09 (750 observations on two passes) to 20,184 meters for SV08 (750 observations on three passes over three days, because there were only 31 observations on 2 April 1985). Table 3-4 lists the satellite test results with 600 and 750 observations in April 1985. The results of the RMS of residuals, the one sigma value of M_0 , and the position error are shown to demonstrate accuracy. Differences in the individual parameters are shown in Table 3-7. Satellite SV04 is omitted due to its marginal clock performance and lack of observations during several test periods. Satellite SV06 is also omitted due to lack of observations.

Table 3-4
Validation Tests - Fort Davis, TX - Apr 1985

Satellite	SV08	SV09	SV11	SV12	SV13
April Dates	1-3	1-2	1-2	1-2	1-2
No. of Obs.	600	600	600	600	600
RMS Residuals(m)	4.5	2.8	1.9	1.9	2.6
σM (rads)	1.9E-4	7.0E-6	1.7E-3	1.8E-5	2.9E-4
Posit err.(m)	7484	302	6209	1165	7313
No. of Obs.	750	750	750	750	750
RMS Residuals(m)	5.9	2.9	2.4	2.0	8.1
σM (rads)	1.8E-4	1.1E-6	1.1E-4	1.6E-5	2.8E-4
Posit err.(m)	20,184	145	298	1083	19,067
April Dates	3-4	3-4	3-4	3-4	3-4
No. of Obs.	600	600	600	600	600
RMS Residuals(m)	2.0	2.4	2.8	2.2	3.2
σM (rads)	1.8E-4	7.2E-6	1.7E-3	1.8E-5	3.1E-4
Posit err.(m)	2265	505	12,260	1204	2945
No. of Obs.	750	750	750	750	750
RMS Residuals(m)	2.4	5.1	5.6	2.3	7.0
σM (rads)	1.7E-4	9.8E-7	1.5E-4	1.4E-5	2.6E-4
Posit err.(m)	2410	787	3794	1211	4258

Validation tests at Richmond, Florida, for five satellites, were run for 3-5 April to compare with results at Fort Davis, Texas. Results are very similar to Table 3-4. For example, the smallest RMS of the residuals is 2.6 meters for SV11 using 750 observations from one pass and part of a second. Parameter variances are slightly smaller for the Richmond case with SV11, indicating better confidence in the Richmond updated ephemeris.

erides than the Fort Davis cases. The position errors range from 382 meters to 11,729 meters. (SV08 had a short pass on 3 April at Richmond, so three passes were required over three days to get 750 observations, and the accuracy decreased). The position error vectors for SV12 and SV08 are given by:

$$\bar{p}_{SV12} = \begin{vmatrix} 30 \text{ m} \\ 315 \text{ m} \\ 213 \text{ m} \end{vmatrix}_{xyz} = \begin{vmatrix} 41 \text{ m} \\ 379 \text{ m} \\ 22 \text{ m} \end{vmatrix}_{RTN}$$

$$\bar{p}_{SV08} = \begin{vmatrix} -2277 \text{ m} \\ 9004 \text{ m} \\ 7163 \text{ m} \end{vmatrix}_{xyz} = \begin{vmatrix} 576 \text{ m} \\ -7705 \text{ m} \\ 8824 \text{ m} \end{vmatrix}_{RTN}$$

The results are presented in Table 3-5, with SV04 and SV06 omitted due to lack of data.

Table 3-5 Validation Tests - Richmond, FL, Apr 1985					
Satellite	SV08	SV09	SV11	SV12	SV13
April Date	3-4	3-4	3-4	3-4	3-4
No. of Obs.	750	750	750	750	750
RMS Residuals(m)	8.2	5.6	2.6	4.8	5.5
σM_0 (rads)	7.6E-4	1.0E-5	4.6E-5	2.6E-6	4.5E-5
pos't err.(m)	11,729	756	1686	382	1456

The close comparison of Table 3-5 with the second half of Table 3-4 indicates the repeatability in the estimator operation. Operating with the same input ephemerides at the same epoch times but with observations at physically

separated sites affords estimator verification, since the results are alike.

Similar validation tests were run for 20 November data at Fort Davis with very similar results. Updates to broadcast ephemerides on 20 November were computed using one and two passes per day over a single site at Fort Davis, Texas. One difference in the November updates was in the computer that ran the algorithm. The April tests were run on the Dual Cyber computers at the University of Texas using single precision (15 significant digits). The November updates were all run on the USAF Academy Burroughs computer using double precision (22 significant digits). The single precision on the Burroughs computer caused much less accuracy than the Cyber while the Burroughs double precision provided more than enough accuracy. There were no noticeable differences between the Cyber single precision results and the Burroughs double precision results.

In these November 1985 tests, satellites SV08 and SV12 had very short passes with low peak elevations, so there were fewer observations for them and some accuracy was lost in their updated parameters. They produced highest accuracy with 500 and 400 observations respectively, over two passes. The position error vectors for SV08 and SV12 are:

$$\bar{P}_{SV08} = \begin{bmatrix} 455 \text{ m} \\ 3844 \text{ m} \\ -6546 \text{ m} \end{bmatrix}_{xyz} = \begin{bmatrix} 999 \text{ m} \\ -7527 \text{ m} \\ -418 \text{ m} \end{bmatrix}_{RTN},$$

$$\text{and } \bar{P}_{SV12} = \begin{bmatrix} 2579 \text{ m} \\ -2663 \text{ m} \\ 2827 \text{ m} \end{bmatrix}_{xyz} = \begin{bmatrix} 598 \text{ m} \\ 731 \text{ m} \\ 4566 \text{ m} \end{bmatrix}_{RTN}.$$

Table 3-6 displays the results from 20 November.

Table 3-6
Validation Tests - Fort Davis, TX, Nov 1985

Satellite	SV06	SV08	SV09	SV11	SV12	SV13
Nov. Date	20-21	20-21	20-21	20	20-21	20-21
No. of Obs.	600	500	600	600	400	600
RMS Res.(m)	1.62	1.89	2.10	2.03	3.10	1.97
σM (rads)	1.6E-3	6.0E-3	2.5E-4	1.8E-4	3.0E-2	4.9E-4
Posit err.(m)	547	7605	1693	4868	4662	2930

Another characteristic of the validation tests that demonstrated accuracy was the relative change in the eight parameters between the broadcast and the updated ephemerides. For the Phase One tests, the broadcast ephemerides were created daily by the MCS, so the updated ephemerides, which used pseudoranges on the same day, were very close.

For instance, for SV11 with 750 observations on 3-4 April at Fort Davis, the parameter \sqrt{A} changed from the broadcast 5153.6580 meter^{1/2} to the updated 5153.6349 meters^{1/2}, which is a 0.0231 meters^{1/2} change, or a 0.00044 percent change. This is equivalent to a 238

meter change in the semimajor axis, which, because the orbit is nearly circular, appears as part of the radial component of the position error, given by:

$$P_{SV11} = \begin{bmatrix} 1771 \text{ m} \\ 1024 \text{ m} \\ -3195 \text{ m} \end{bmatrix}_{xyz} = \begin{bmatrix} 917 \text{ m} \\ 3663 \text{ m} \\ -363 \text{ m} \end{bmatrix}_{RTN}$$

Other parameter changes were similar and are shown in Tables 3-7 through 3-9 for SV11 at Fort Davis and Richmond on 3-4 April, and Fort Davis on 20 November.

The argument of latitude at epoch (u_0) is included in the tables to indicate that although the updated M_0 and u may differ from the broadcast values individually, their combination, u_0 , is closer to the combined broadcast value. The high correlation between the two parameters continues to be manifest as it was in Chapter Two. The magnitude of the u_0 difference is somewhat deceiving, though, because very small differences can cause kilometer-size position errors. For instance, the 0.000165 radian difference for u_0 in Table 3-7 amounts to a 4,382 meter position error at the orbit altitude, in the transverse direction. However, as will be shown in Chapters Four and Five, the navigation accuracy depends more on the radial position error than the transverse position error. Thus, the small differences in \sqrt{A} tend to aid the navigation process, while the large position

errors caused by the u_o differences tend not to inhibit the navigation process.

Table 3-7
SV11 Parameter Differences (750 obs) Ft Davis 3 Apr 1985

Parameter	Broadcast	Updated	Difference	% Difference
T_{oe} (sec)	277200	277200		
M_o (rads)	3.03500	3.03179	.00321	.1058
e	.0105571	.0105348	.0000223	.2112
\sqrt{A} (\sqrt{m})	5153.6580	5153.6349	.0231	.00044
Ω (rads)	-.7132025	-.7132681	.0000656	.00919
i (rads)	1.097112	1.096928	.000184	.01677
ω (rads)	-2.799288	-2.796243	.003045	.1088
a_o (sec)	.6631E-3	.6611E-3	.0020E-3	.3016
a_1 (s/s)	.4900E-10	.2503E-10	.2397E-10	.4892
u_o (rads)	.235712	.235547	.000165	.0700

Table 3-8
SV11 Parameter Differences (750 obs) Richmond 3 Apr 1985

Parameter	Broadcast	Updated	Difference	% Difference
T_{oe} (sec)	277200	277200		
M_{oe} (rads)	3.03500	3.03374	.00126	.0415
e	.0105571	.0105470	.0000101	.0957
$\sqrt{A} (\sqrt{m})$	5153.6580	5153.6397	.0183	.00035
Ω (rads)	-.7132025	-0.7132747	.0000722	.01012
i (rads)	1.097112	1.097046	.000066	.00601
u (rads)	-2.799288	-2.798055	.001233	.04404
a_o (sec)	.6631E-3	.6624E-3	.0007E-3	.1056
a_1 (s/s)	.4900E-10	.3438E-10	.1462E-10	29.98
u_o (rads)	.235712	.235685	.000027	.01145

Table 3-9
SV11 Parameter Differences (750 obs) Ft Davis 20 Nov 1985

Parameter	Broadcast	Updated	Difference	% Difference
T_{oe} (sec)	320400	320400		
M_{oe} (rads)	-1.34089	-1.34280	.0019	.0014
e	.0108427	.0108292	.0000135	.1245
$\sqrt{A} (\sqrt{m})$	5153.7242	5153.7292	.0050	.00009
Ω (rads)	1.469856	1.469817	.000039	.00265
i (rads)	1.096948	1.096807	.000141	.01285
u (rads)	-2.775411	-2.773555	.001856	.0669
a (sec)	.1431E-3	.1788E-4	.1252E-3	87.51
a_1 (s/s)	.6025E-11	.2004E-10	.1402E-10	232.6
u_o (rads)	-4.116303	-4.116359	.000056	.000014

The covariance matrix elements help confirm the accuracy of the ephemeris updates, also. The diagonal elements, or variances, represent uncertainty in the state variables. The small values for all the variances manifest good confidence in the converged state. For example, the variance for $\sqrt{|\bar{A}|}$ with SV11 using 600 observations in April at Fort Davis is 0.0022 meters, which converts to a one sigma value of 0.047 meters^{1/2}. Since the nominal value for $\sqrt{|\bar{A}|}$ is 5153.658 meters^{1/2}, this one sigma value implies high accuracy (68.3% of the estimated semimajor axes lie within 485 meters of nominal). The variances also show a definite trend toward improved accuracy with increased observations. The one sigma values for SV11 with 750 and 900 observations are 0.0012 meters^{1/2} and 0.000025 meters^{1/2}, respectively. The latter case establishes 68.3% of the estimated semimajor axes within 0.26 meters of nominal. The other state parameters have similar variances, indicating the confidence in the updated ephemerides. Tables 3-10 through 3-12 exhibit typical one sigma values for all the SV11 parameters at Fort Davis and Richmond in April, and Fort Davis in November. Following these tables is a discussion of the ill-conditioning.

Table 3-10
Updated SV11 Parameter One Sigma Values
Fort Davis, TX - 3-4 Apr 1985

No. of obs	600	750	900
M_o (rads)	1.74E-3	1.52E-4	1.07E-4
e_o	2.36E-5	1.05E-6	8.09E-7
$\sqrt{ \bar{A}(\sqrt{ \bar{m}})}$	4.74E-2	1.19E-3	2.53E-5
Ω (rads)	1.03E-4	3.14E-6	1.71E-6
i (rads)	8.29E-5	8.20E-6	6.11E-6
w (rads)	5.10E-4	1.44E-4	1.01E-4
a_o (secs)	7.47E-7	7.56E-8	4.30E-8
a_1 (s/s)	1.18E-10	1.80E-12	3.40E-14

Table 3-11
Updated SV11 Parameter One Sigma Values
Richmond, FL - 3-4 Apr 1985

No. of obs	750
M_o (rads)	4.63E-5
e_o	2.39E-7
$\sqrt{ \bar{A}(\sqrt{ \bar{m}})}$	2.39E-7
Ω (rads)	2.12E-6
i (rads)	1.85E-6
w (rads)	4.39E-5
a_o (secs)	2.41E-8
a_1 (s/s)	2.05E-12

Table 3-12
Updated SV11 Parameter One Sigma Values
Fort Davis, TX - 20 Nov 1985

No. of obs	600	750	900
M_o (rads)	1.75E-4	1.28E-4	1.20E-4
e_o	1.63E-6	9.95E-7	9.26E-7
$\sqrt{ \bar{A} }(\sqrt{ \bar{m} })$	6.33E-3	4.67E-5	1.09E-5
Ω (rads)	7.61E-6	2.56E-6	2.38E-6
i (rads)	9.24E-6	7.52E-6	7.00E-6
u (rads)	1.52E-4	1.22E-4	1.14E-4
a_o (secs)	8.05E-7	5.58E-8	5.13E-8
a_1 (s/s)	8.77E-12	5.89E-14	1.16E-14

Evidence of ill-conditioning exists as described in Chapter Two. The high correlation between M_o and u for the near-circular GPS orbits causes the ill-conditioning. For all the test cases the correlation coefficient, $\mu_{1,6}$, is nearly -1.0 (see section 2.2.D). The other indicators are large condition numbers related to near-zero eigenvalues for the normal matrices. The condition numbers vary from 10^7 to 10^{12} with the larger values associated with fewer observations. The larger values are caused by eigenvalues of the normal matrix near zero; actually ranging from 10^{-3} to 10^3 , again, with the worst cases coming from fewer observations. To compensate for the ill-conditioning the estimator used the Givens orthogonalization (avoiding matrix inversion), retained as many significant digits as possible (15 for the April cases and 22 for the November cases), and used as many

observations as possible, 400 to 900 being ideal.

The estimator operated smoothly with 600 observations, (500, and 400 for SV08 and SV12 in November) in spite of the ill-conditioning. Convergence was smooth in eight or less iterations. The small values for the RMS of residuals, some position errors, the parameter changes, and the variances of the state verify the estimator accuracy. Chapter Five navigation results will demonstrate the performance of the updated ephemerides.

B. Long Range Ephemeris Updates.

The validation tests used update epochs that were the same as the actual broadcast epochs, e.g., $T_{oe} = 277,200$ seconds in April. For the long range updates, epochs varied from one to seven months old and were updated to 20 November. This time separation simulated the loss of the MCS for an extended period. Except for propagating the old parameters forward, the estimator was identical to the batch estimator just validated. Results were also very similar to the validation cases; the RMS of residuals, the position errors, the parameter changes, and the covariance elements indicated the accuracy.

To propagate the old parameters to the update epoch, the estimator multiplied the ephemeris rate terms, \dot{n} and $\dot{\Omega}$, by the number of seconds between the epochs. The ECF

coordinate system was also updated to the new epoch. All other parameters were held constant. (see Appendix E for propagating the two parameters and the coordinate system.) This method provided initial conditions sufficiently accurate to permit quick convergence in all cases.

The initial conditions produced by propagating the old broadcast ephemerides introduced varying degrees of error in the xyz position at the start of the update algorithm. To determine this error the propagated positions were compared to the broadcast ephemeris positions at the update epoch. The position errors ranged from 16 kilometers to over 2,000 kilometers; the errors growing with the longer propagation times. For example, the SV11 propagated position errors are presented in Table 3-13, first in ECF coordinates, then in RTN coordinates. Notice the best accuracy is in the radial coordinate, suggesting the importance of the accuracy of the radial component.

Table 3-13
Propagated Ephemeris Position Errors
Before Applying the Ephemeris Update Algorithm-SV11(m)

Date	5 Apr	11 Jun	13 Aug	13 Sep	11 Oct
x	1,222,100	678,500	196,200	-11,100	-11,800
y	447,600	295,300	122,100	20,500	3,500
z	-839,600	-427,600	-104,400	17,200	10,300
R	-34,200	-5,900	640	-570	-560
T	1,545,300	854,600	249,800	-10,600	-13,400
N	-93,000	7,900	43,600	27,000	8,800
mag	1,548,000	855,000	254,000	29,000	16,000

A portion of the initial condition error was produced by the nine perturbation parameters which remained constant from the old ephemeris to the updated ephemeris. As shown in Chapter Two, the nine perturbation terms are periodic with bounded amplitudes. So, depending on the epoch time, the perturbation parameters from the old ephemeris could have values anywhere between their maximum and minimum points. When held constant from the old ephemeris to the initial conditions for the update processor which could span several months, these nine parameters introduced a certain amount of position error. To isolate this position error, hybrid ephemerides were created, composed of the six Keplerian and two clock parameters from the 20 November epoch and the nine

perturbation parameters from the old ephemerides. Then the hybrid positions were compared to the broadcast positions at the same epoch on 20 November. In other words, the six Keplerian and two clock parameters were held constant for the comparison, so the source of position error was the combined differences in the perturbation parameters. Table 3-14 presents the position errors introduced by holding the perturbation terms for SV11 constant in the update process. The position errors range from 8.8 meters for the 5 April parameters to 107 meters using the 13 September parameters. No attempt was made to determine individual parameter effects on the position error or to minimize the effects of any set of perturbation parameters. Gaining an idea of the magnitude of the position error produced by holding the perturbation parameters constant was the goal of this study.

Table 3-14
Position Errors Caused by Holding the Perturbation
Parameters Constant to 20 November - SV11 - (meters)

Date	11 Oct	13 Sep	13 Aug	11 Jun	5 Apr
x	-2.3	10.8	57.5	12.3	6.1
y	30.8	49.2	23.4	-12.0	6.4
z	61.2	-94.5	-33.0	26.0	.4
R	-56.4	-78.9	2.5	30.3	1.8
T	39.1	72.3	70.2	7.1	6.8
N	.5	-.5	.7	.2	5.3
mag	68.6	107.1	70.3	31.2	8.8

The first update cases used the propagated ephemerides from 11 October 1985 to initiate the estimator. A typical satellite was SV11 with an initial epoch at 489,600 seconds on 11 October. With 600 observations on 20 November 1985, the 11 October ephemeris was updated to epoch 320,400 seconds on 20 November. Convergence occurred in five iterations to an RMS of residuals of 2.13 meters, suggesting a satisfactory fit of the pseudorange observations.

The position error, however, for the converged ephemeris compared to the broadcast ephemeris at the same epoch was 9,281 meters, or in vector form:

$$\bar{p}_{SV11} = \begin{bmatrix} 1416 \text{ m} \\ 9146 \text{ m} \\ 697 \text{ m} \end{bmatrix}_{xyz} = \begin{bmatrix} -1584 \text{ m} \\ 3848 \text{ m} \\ 8296 \text{ m} \end{bmatrix}_{RTN}$$

Compared with the initial condition position error of 16,000 meters, this is nearly a 7,000 meter improvement. The M_0 parameter changed from the propagated value of 4.94446 radians to 4.93766 radians, a change of 0.0068 radians which is a 0.1375 percent change, equivalent to a position error of 180,608 meters. The u_0 difference was 0.000147 radians, accounting for 3,904 meters of position error in the transverse direction. The radial component of the position error was -1584 meters, composed of 115 meter change in the semimajor axis and the remainder due most likely to the timing adjustments. The other satellites had similar results except SV08 and SV12.

Satellites SV08 and SV12 had low elevation, short passes on 20 November, so they provided only 318 and 239 observations per pass, compared with 597 for SV11. Consequently, their accuracy was degraded in parameter updates, position errors, and one sigma values. Also, their accuracy was very sensitive to the number of observations used for the update, probably due to the marginal observability and ill-conditioning in the normal matrix. To update the 11 October ephemerides, best accuracy occurred with 400 observations over two passes. For SV08, the RMS of residuals was 1.93 meters, but the position error was 55,503 meters, the change in M_0 was 0.03625 radians, or 1.11 percent, and the one sigma value

for M_0 was 5.37×10^{-3} radians; the last three quantities being slightly worse than for SV11. The same quantities for SV12 were: RMS of residuals = 4.99 meters, position error = 60,705 meters, change in M_0 = 0.019706 radians or 0.005711 percent, and one sigma for M_0 = 3.11×10^{-2} radians. These results reveal the reduction in accuracy for SV08 and SV12. The inaccuracies are characteristic of the test constellation and will not occur for the full constellation with at least four satellites visible on high elevation passes at all times.

Tables 3-15 through 3-17 show the results for the test satellites using 600 and 750 observations (400 observations for SV08 and SV12).

Table 3-15 11 Oct Ephemeris Updates on 20 Nov - Ft Davis						
Sat.	SV06	SV08	SV09	SV11	SV12	SV13
Obs.	600	400	600	600	400	600
RMS (m)	2.12	1.93	2.16	2.13	4.99	1.86
σM_0 (r)	1.6E-3	5.4E-3	2.5E-4	1.8E-4	3.1E-2	4.9E-4
pos ^o err (m)	24,208	55,503	3486	9274	60,705	2601
Obs	750		750	750		750
RMS (m)	7.79		5.36	2.56		4.79
σM_0 (r)	1.46E-3		9.6E-4	1.3E-4		4.7E-4
pos ^o err (m)	46,990		7005	4064		8437

Table 3-16
Updated SV11 Parameter Differences (600 obs) 11 Oct 1985

Parameter	Broadcast 20 Nov	Updated 20 Nov	Difference	% Difference
T_{oe} (secs)	320400	320400		
M_o (rads)	4.94229	4.93766	.00463	.0937
e	.0108427	.0108077	.000035	.3228
\sqrt{A} (\sqrt{m})	5153.7242	5153.7354	.0112	.00022
Ω (rads)	1.469857	1.469763	.000094	.0064
i (rads)	1.096948	1.096629	.000319	.0291
w (rads)	-2.775411	-2.770926	.00449	.1616
a_o (secs)	.1431E-3	.1761E-4	.1255E-3	87.69
a_1 (s/s)	.6025E-11	.6855E-11	.830E-12	13.78
u_o (rads)	2.166882	2.166735	.000147	.00678

Table 3-17
Updated SV11 Parameter One Sigma Values - 11 Oct 1985

No. of Obs	600	750
M_o (rads)	1.75E-4	1.28E-4
e	1.63E-6	9.96E-7
\sqrt{A} (\sqrt{m})	6.34E-3	4.67E-5
Ω (rads)	7.62E-6	2.56E-6
i (rads)	9.25E-6	7.52E-6
w (rads)	1.53E-4	1.22E-4
a_o (secs)	8.06E-7	5.58E-8
a_1 (s/s)	8.78E-12	5.89E-14

These data show the estimator's accuracy; updating broadcast ephemerides over six weeks and producing position errors between 2601 meters and 60,705 meters. These position errors are the same order of magnitude as most of the same-day updates in the validation tests, demonstrating the ability to update old ephemerides. Test conditions and update algorithm characteristics continue to cause the large position errors. The next update covers ten weeks.

The second test case involved ephemerides from 13 September updated on 20 November. The results were very similar to the 11 October case, in the values for the RMS of residuals, the position errors, the changes in the parameters and the one sigma values. The results are shown in Tables 3-18 through 3-20, using 600 and 750 observations for each satellite, except SV08 and SV12(400 observations).

Table 3-18
13 Sep Ephemeris Updates on 20 Nov - Ft Davis

Sat	SV06	SV08	SV09	SV11	SV12	SV13
Obs	600	400	600	600	400	600
RMS (m)	2.45	1.90	2.30	2.22	5.70	1.79
$\sigma M(r)$	1.6E-3	5.7E-3	2.5E-4	1.8E-4	3.4E-2	4.8E-4
pos ^o err (m)	15,243	33,082	19,913	12,896	203,127	5268

Obs	750	750	750	750
RMS (m)	10.0	6.04	2.48	5.17
$\sigma M(r)$	1.5E-3	3.1E-4	1.3E-4	4.7E-4
pos ^o err (m)	70,884	4794	8763	9031

Table 3-19
Updated SV11 Parameter Differences (600 Obs) 13 Sep 1985

Parameter	Broadcast 20 Nov	Updated 20 Nov	Difference	% Difference
T_{oe} (secs)	320400	320400		
M_o (rads)	4.94229	4.93596	.00633	.1281
e	.0108427	.0107941	.0000486	.4482
$\sqrt{A} (\sqrt{m})$	5153.7242	5153.7418	.0176	.000342
Ω (rads)	1.469857	1.469732	.000124	.00844
i (rads)	1.096948	1.096491	.000457	.0417
ω (rads)	-2.775411	-2.769268	.00614	.2213
a_o (secs)	.1431E-3	.1761E-4	.1255E-3	87.69
a_i (s/s)	.6025E-11	-.2170E-11	.8195E-11	136.02
u_o (rads)	2.166882	2.166696	.000186	.00858

Table 3-20
Updated SV11 Parameter One Sigma Values - 13 Sep 1985

No. of Obs.	600	750
M_o (rads)	1.76E-4	1.29E-4
e_o	1.63E-6	9.92E-7
\sqrt{A} (\sqrt{m})	6.34E-3	4.67E-5
Ω (rads)	7.62E-6	2.56E-6
i (rads)	9.25E-6	7.52E-6
u (rads)	1.53E-4	1.22E-4
a_o (secs)	8.07E-7	5.58E-8
a_1 (s/s)	8.78E-12	5.89E-14

Comparing the one sigma values for the 13 September and 11 October updates, Tables 3-20 and 3-17, respectively, emphasizes how similar the cases are. None of the values differ by more than four in the third significant digit. This pattern repeats for all the long range updates. The next update, from 13 August, exhibits the same characteristics as the September and October cases. The update characteristics are presented in Tables 3-21 through 3-23.

Table 3-21
13 Aug Ephemeris Updates on 20 Nov - Ft Davis

Sat	SV06	SV08	SV09	SV11	SV12	SV13
Obs	600	400	600	600	400	600
RMS (m)	1.73	1.93	2.13	2.08	3.05	4.08
$\sigma M_o(r)$	1.6E-3	7.4E-3	2.5E-4	1.7E-4	3.3E-2	4.8E-4
pos ^o err (m)	21,185	62,411	21,408	7097	16,534	9853

Obs	750	750	750	750
RMS (m)	6.08	3.17	2.87	5.04
$\sigma M_o(r)$	1.5E-3	9.8E-5	1.3E-4	4.8E-4
pos ^o err (m)	73,146	12,748	12,323	9914

Table 3-22
Updated SV11 Parameter Differences (600 Obs) 13 Aug 1985

Parameter	Broadcast 20 Nov	Updated 20 Nov	Difference	% Difference
T_{oe} (secs)	320400	320400		
M_{oe} (rads)	4.94229	4.940073	.00222	.0449
e_o	.0108427	.01083999	.0000027	.0250
\sqrt{A} (\sqrt{m})	5153.7242	5153.7009	.0233	.00045
Ω (rads)	1.469857	1.469905	.000048	.00327
i (rads)	1.096948	1.096748	.00020	.1823
ω (rads)	-2.775411	-2.773431	.00198	.07134
a_o (secs)	.1431E-3	.1404E-4	.1291E-3	90.19
a_1 (s/s)	.6025E-11	.6648E-10	.6046E-10	1003.4
u_o (rads)	2.166882	2.166643	.000239	.01103

Table 3-23
Updated SV11 Parameter One Sigma Values - 13 Aug 1985

No. of Obs.	600	750
M_0 (rads)	1.75E-4	1.29E-4
e_0	1.63E-6	9.89E-7
\sqrt{A} (\sqrt{m})	6.33E-3	4.67E-5
Ω (rads)	7.61E-6	2.56E-6
i (rads)	9.24E-6	7.52E-6
u (rads)	1.52E-4	1.23E-4
a_0 (secs)	8.05E-7	5.57E-8
a_1 (s/s)	8.76E-12	5.89E-14

These first three ephemeris updates exhibit very similar accuracies that should enable accurate navigation. One may think that accuracy decreased as the time from 20 November increased. Such was not the case with the update algorithm. Because the input ephemeris acted only as initial conditions, it did not significantly affect the accuracy. The parameters M_0 and Ω were propagated farther and were less precise, but, once initialized, the estimator ran smoothly with accurate results back as far as seven months. A look at five and seven month old ephemerides will demonstrate this accuracy.

The next ephemeris, 11 June 1985, displays similar results which are reported in Tables 3-24 through 3-26.

Table 3-24
11 Jun Ephemeris Updates on 20 Nov - Ft Davis

Sat	SV06	SV08	SV09	SV11	SV12	SV13
Obs	600	400	600	600	400	600
RMS (m)	1.62	1.90	2.09	2.02	3.24	1.79
$\sigma M_o(r)$	1.5E-3	5.8E-3	2.5E-4	1.7E-4	2.9E-2	4.9E-4
pos ^o err (m)	1865	27,046	10,396	2436	22,052	1021

Obs	750	750	750	750
RMS (m)	3.53	2.74	2.15	4.19
$\sigma M_o(r)$	1.5E-3	9.7E-5	1.3E-4	4.8E-4
pos ^o err (m)	25,622	3131	5554	10,859

Table 3-25
Updated SV11 Parameter Differences (600 obs) 11 Jun 1985

Parameter	Broadcast 20 Nov	Updated 20 Nov	Difference	% Difference
T_{oe} (secs)	320400	320400		
M_o (rads)	4.942293	4.942529	.000236	.00478
e	.0108427	.0108532	.0000105	.9684
\sqrt{A} (\sqrt{m})	5153.7242	5153.7098	.0144	.00028
Ω (rads)	1.469857	1.469904	.000047	.00320
i (rads)	1.096948	1.096999	.000051	.00465
ω (rads)	-2.775411	-2.775713	.000302	.01088
a_o (secs)	.1431E-3	.1681E-4	.1263E-3	88.25
a_1 (s/s)	.6025E-11	.4549E-10	.3947E-10	655.02
u_o (rads)	2.166882	2.166816	.0000657	.00303

Table 3-26
Updated SV11 Parameter One Sigma Values - 11 Jun 1985

No. of Obs	600	750
M_o (rads)	1.74E-4	1.25E-4
e_o	1.63E-6	1.00E-6
\sqrt{A} (\sqrt{m})	6.33E-3	4.67E-5
Ω (rads)	7.61E-6	2.56E-6
i (rads)	9.24E-6	7.52E-6
w (rads)	1.52E-4	1.21E-4
a_o (rads)	8.05E-7	5.58E-8
a_1 (s/s)	8.77E-12	5.89E-14

The last ephemeris to be updated was broadcast during the April 1985 Test on 5 April. Again, the 5 April update is as accurate as the others even though the time between epochs is 19,818,000 seconds (nearly 33 weeks). Tables 3-27 through 3-29 list the results.

Table 3-27
5 Apr Ephemeris Updates on 20 Nov - Ft Davis

Sat	SV06	SV08	SV09	SV11	SV12	SV13
Obs	600	400	600	600	400	600
RMS (m)	1.87	1.91	2.12	2.04	5.02	2.92
σ_M (r)	1.6E-3	5.6E-3	2.4E-4	1.7E-4	3.1E-2	4.9E-4
pos err (m)	27,277	41,305	26,916	2571	59,199	994

Obs	750	750	750	750
RMS (m)	5.36	6.58	2.48	9.10
σ_M (r)	1.4E-3	9.5E-5	1.3E-4	4.9E-4
pos err (m)	15,943	18,708	4642	13,773

Table 3-28
Updated SV11 Parameter Differences(600 obs) 5 Apr 1985

Parameter	Broadcast 20 Nov	Updated 20 Nov	Difference	% Difference
T_{oe} (secs)	320400	320400		
M_o (rads)	4.942293	4.940852	.00144	.02916
e_o	.0108427	.0108385	.0000042	.3874
\sqrt{A} (\sqrt{m})	5153.7242	5153.7191	.0051	.0000990
Ω (rads)	1.469857	1.469893	.000036	.00245
i (rads)	1.096948	1.096901	.000047	.00428
u (rads)	-2.775411	-2.774081	.00133	.04792
a_o (secs)	.143E-3	.1757E-4	.1255E-3	87.722
a_1 (s/s)	.6025E-11	.2714E-10	.2112E-10	350.46
u_o (rads)	2.166882	2.166771	.000111	.005123

Table 3-29
Updated SV11 Parameter One Sigma Values - 5 Apr 1985

No. of Obs	600	750
M_o (rads)	1.75E-4	1.28E-4
e_o	1.63E-6	1.00E-6
\sqrt{A} (\sqrt{m})	6.33E-3	4.67E-5
Ω (rads)	7.61E-6	2.56E-6
i (rads)	9.24E-6	7.53E-6
u (rads)	1.52E-4	1.21E-4
a_o (secs)	8.06E-7	5.59E-8
a_1 (s/s)	8.77E-12	5.89E-14

This concludes the tables of figures which compare the long range updates. Figures that show the relative stability of the updates across the seven months are shown in Figures 3-1 through 3-4 for representative satellites. There are significant patterns in the accuracy of the updates over the long term. Satellites SV08 and SV12 reveal how the lack of accuracy in the RMS of residual value and one sigma value is manifest in the position error. Whereas, SV11 maintains steady accuracies. In Figure 3-1, SV12 exhibits a near doubling of the RMS of residuals from November to September. Figure 3-2 shows that the position error climbs to over 200,000 meters in the same time period. Finally, Figure 3-3 shows the lack of confidence in the M_0 parameter for SV12 compared to SV11. The SV08 shows very steady RMS of residual values, but the position errors and the one sigma values reveal the reduced accuracy due to the low elevation, short passes on 20 November. Satellite SV11 demonstrates the steady accuracy achievable over seven months.

Figure 3-4 shows the behavior of the percent change in M_0 , \sqrt{A} , and u_0 for SV11. The reasonably steady values for these quantities further demonstrate the accuracy possible in updating the broadcast ephemerides over a long time.

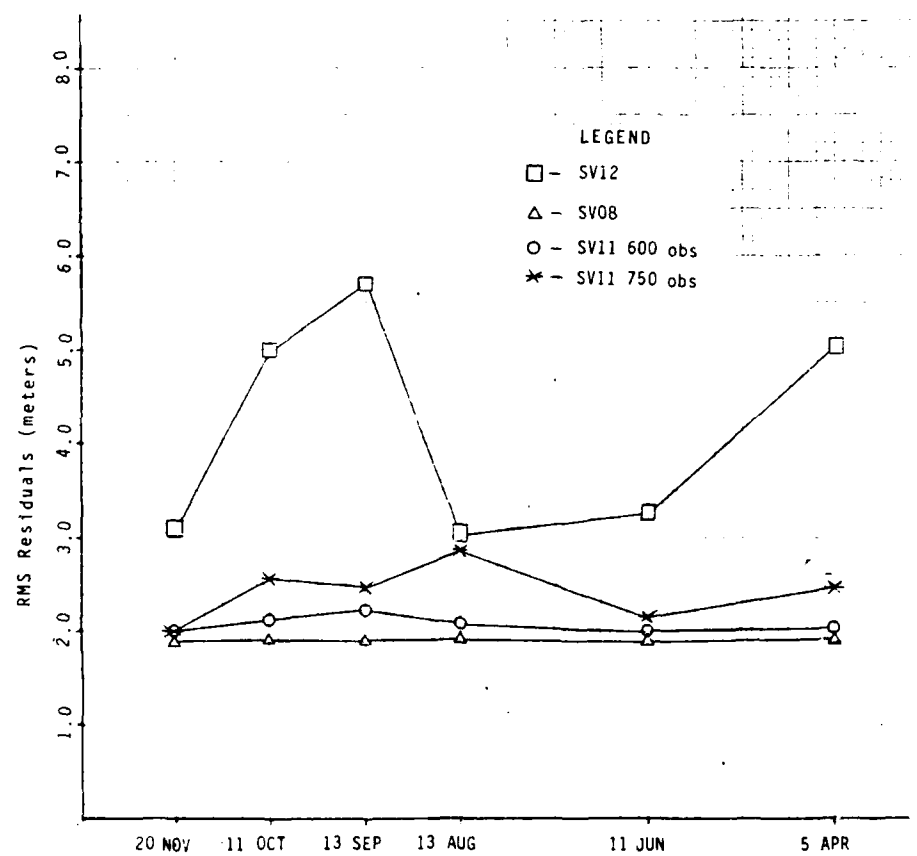


FIGURE 3-1 RMS OF RESIDUALS (METERS)

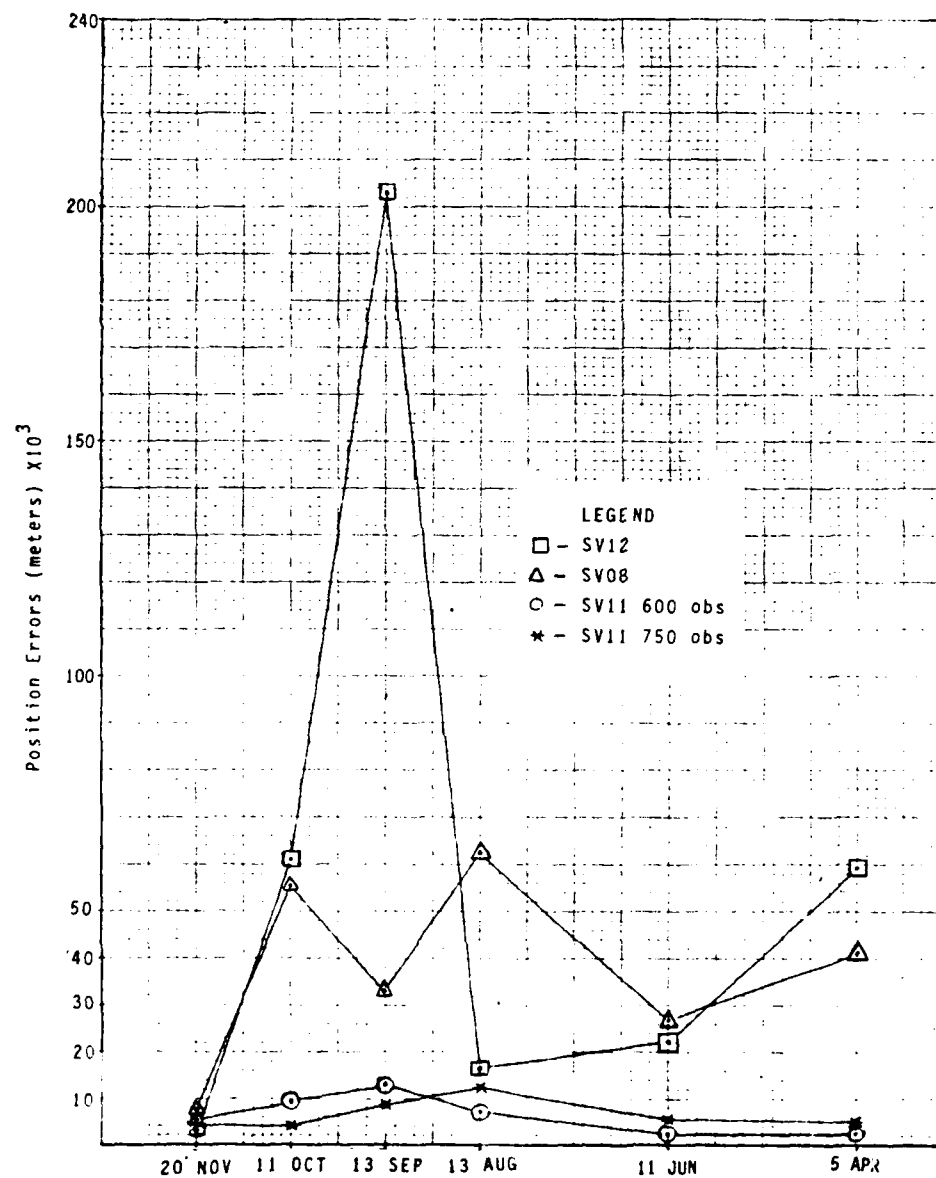
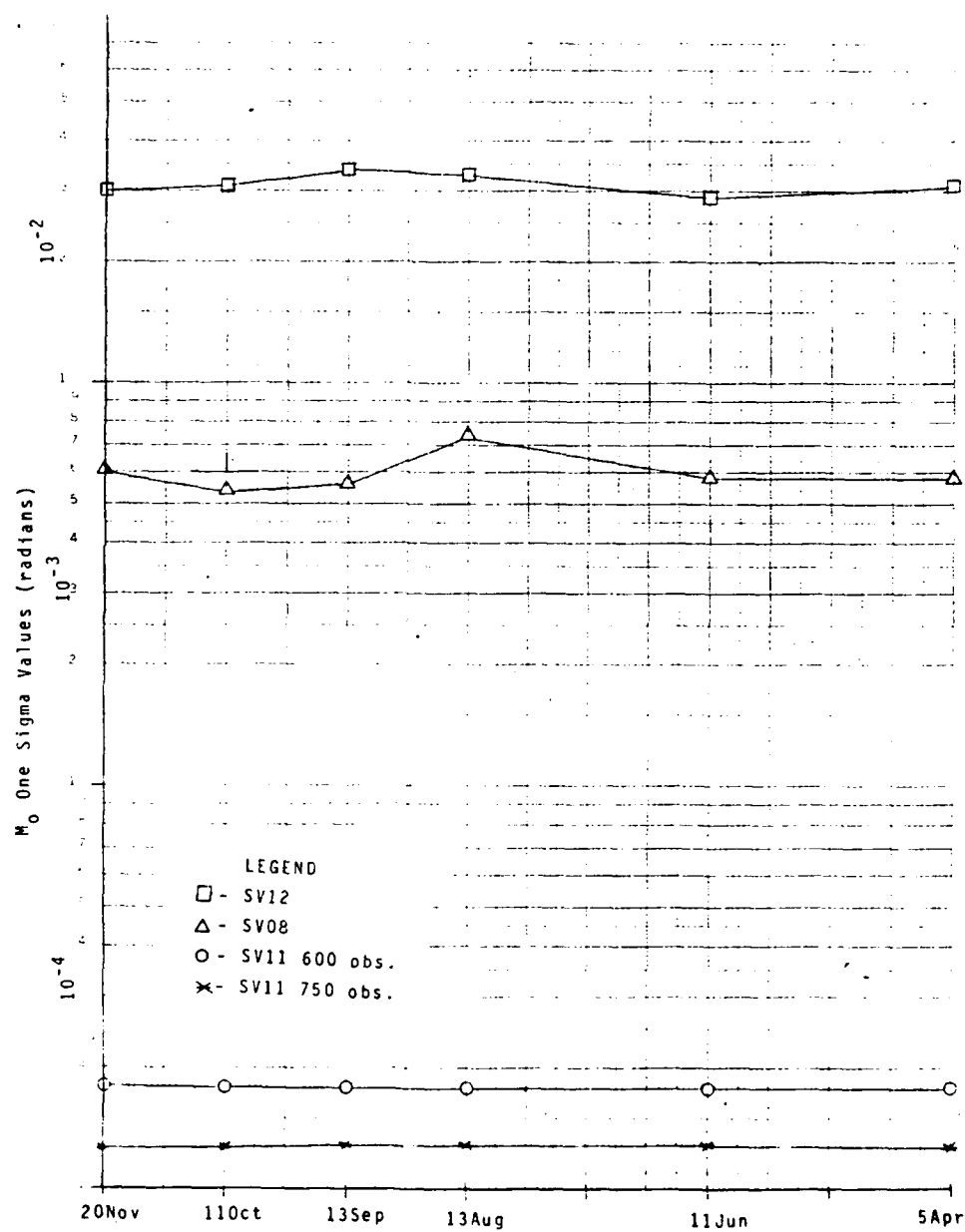


FIGURE 3-2 POSITION ERRORS (METERS)

FIGURE 3-3 M_O ONE SIGMA VALUES (RADIAN)

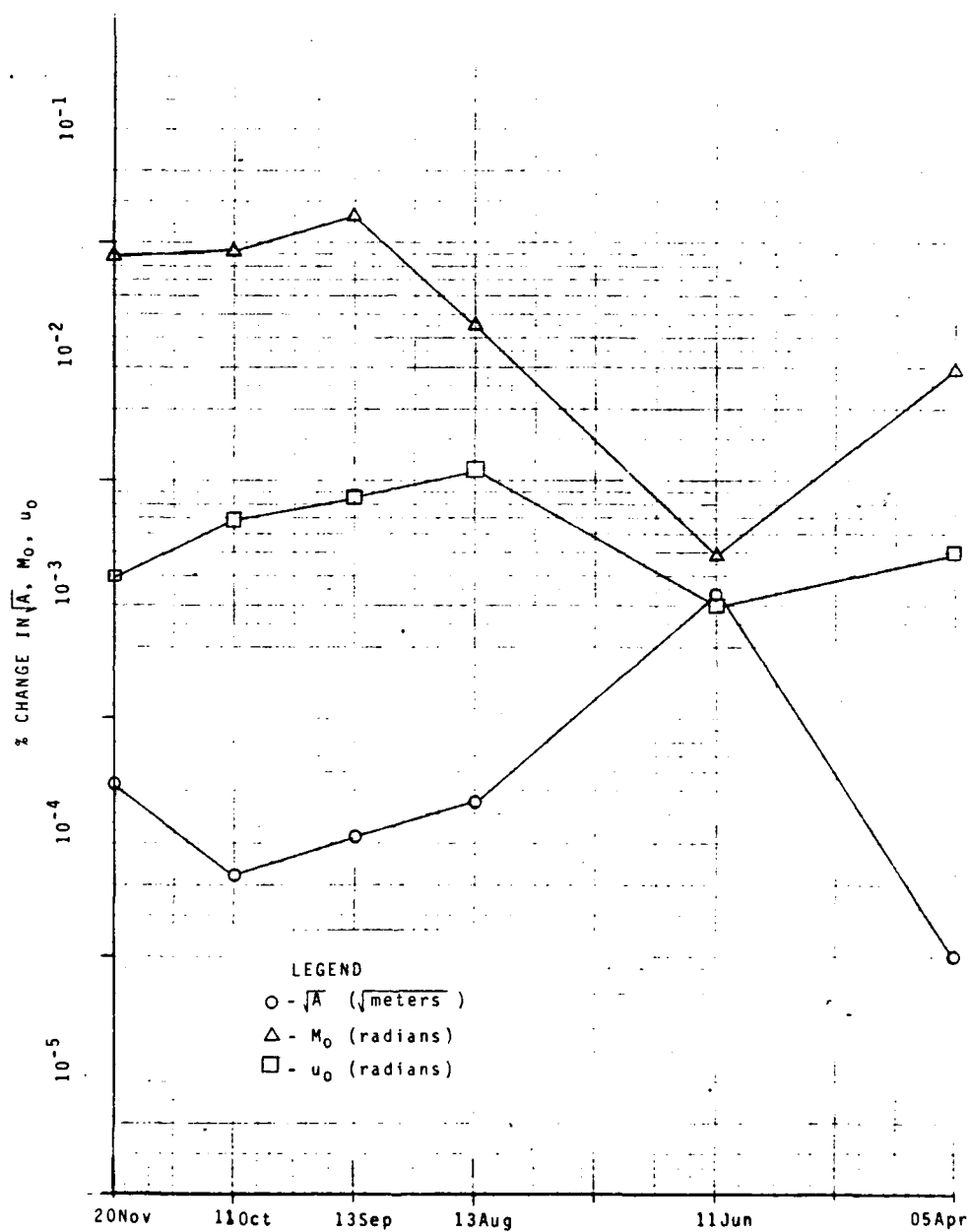


FIGURE 3-4 PERCENT DIFFERENCE IN \bar{A} , M_0 , and u_0
(UPDATED - BROADCAST)

3.6 Summary

In conclusion, these results indicate that updating old ephemerides with current pseudorange measurements is possible. If the MCS were unable to generate new ephemerides for the satellites, then a relatively simple least squares, batch estimator can compute updated ephemerides. The input broadcast ephemerides can be as old as seven months and possibly older. This estimator is sensitive to the number of passes per day and the number of pseudoranges per pass; the best accuracy coming from satellites with two daily passes, totalling over 400 measurements. The estimator is insensitive to the age of the broadcast ephemeris; updates from April to November produce accuracies nearly identical to the updates from October to November. Finally, the choice of the parameter set that includes the highly correlated M_0 and w terms, affects the estimator by causing some ill-conditioning. The algorithm converges smoothly in spite of the ill-conditioning and produces ephemerides which can be used for navigation as described in Chapter Five.

A summary of the assumptions used in the ephemeris update process is presented in Table 3-30:

Table 3-30
Ephemeris Update Estimator Assumptions

1. The Broadcast ephemeris Algorithm accurately modelled the GPS orbital motion.
2. Only eight of the ephemeris parameters needed to be updated; six Keplerian and two satellite clock parameters. The nine perturbation parameters remain uncorrected from their original broadcast values.
3. The receiver antenna location must be known accurately.
4. The receiver must use an atomic time standard that can be synchronized with the satellite time to form pseudorange measurements from the satellite transmissions.
5. The pseudorange measurement errors were uncorrelated in time and normally distributed with a zero mean. All measurements were weighted equally.
6. The broadcast ephemerides were the most accurate representation of the true satellite position and could be used to evaluate the accuracy of the updated ephemerides.
7. For validating the update processor an actual broadcast ephemeris from one epoch was updated at the same epoch using pseudorange measurements in close proximity to that epoch.
8. System observability required a long satellite pass or two short passes and no a priori covariance matrix was required.
9. Long range update cases could be initialized within the estimator's radius of convergence by propagating the old broadcast ephemerides to the update epoch using the rate terms \dot{n} and $\dot{\Omega}$.

Several of the most significant results are listed in Table 3-31:

Table 3-31
Significant Results of the Ephemeris Update Algorithm

1. Old broadcast ephemerides can be updated after several months, using current pseudorange measurements. The accuracy of the update ephemerides is reasonably constant from short range to long range updates.
2. A single receiver collecting measurements over one short (two hour) satellite pass, will render the update process marginally unobservable.
3. The ephemeris parameters M_0 and w are highly correlated and estimating them separately causes ill-conditioning in the normal matrix.
4. The radial component of the updated ephemeris is more accurate than the transverse and normal components.
5. Initial conditions within 1,548,000 meters of the broadcast position allowed convergence of the ephemeris update processor.

Before discussing navigation with updated ephemerides in Chapter Five, the navigation algorithm is presented in Chapter Four, investigating accuracy with the real-time broadcast ephemerides.

Chapter Four - User Navigation Algorithm

4.1 Introduction

The first three chapters discussed the origin and characteristics of the broadcast ephemeris. These fifteen constant parameters accurately represent the perturbed orbit for each hour in which they are applicable. They permit users worldwide to calculate the satellite ECF position to use in navigation routines. This chapter describes the processing of current ephemerides and pseudorange measurements for user navigation. Again, the Phase One test satellites transmitted the data to three receiver sites: Fort Davis, Texas, Richmond, Florida, and Haystack, Massachusetts. The analysis included a start-up algorithm for initialization, and the Extended Kalman Filter (EKF). The results were position estimates of surveyed sites. This navigation process sets the stage for Chapter Five: navigation using old, but updated, ephemerides.

The GPS System provides users with at least four simultaneous sets of ephemerides and pseudorange measurements for navigating. With four sets the user can solve for his ECF position and the time. For this study the initial solution comes from a simple, four-element,

linearized, differential correction estimator (DCA), which acted to initialize the EKF after the first DCA solution was computed. Four simultaneous satellite transmissions provided the necessary information for computing the four state corrections in the DCA, so four satellites must be visible to the receiver. The DCA calculated corrections to the initial state guess directly with no filtering, so, because of signal noise, the DCA solution at the first time point (time tag) was often inaccurate. The EKF took over on the second time tag and reduced the solution inaccuracies. Therefore, data editing and sequential filtering are suggested. This chapter does not review data editing, but does show the effect of signal noise on the navigation solution. This chapter also demonstrates the accuracy of the Extended Kalman Filter.

4.2 The Differential Correction Algorithm

The user navigation solution began with a linearized, differential correction estimator, suggested by Noe and Myers[1976], using Hotelling's iterative method to update the measurement sensitivity matrix. The DCA computed one solution, then reverted to the EKF for subsequent solutions. The inputs to the DCA were four simultaneous pseudorange measurements and the current hour

ephemerides from four satellites. The output was the user state (ECF position and clock bias) and the covariance matrix, both being required to start the EKF.

The filter state was represented by the following:

$$X = \begin{bmatrix} x_u \\ y_u \\ z_u \\ b_u \end{bmatrix} \quad (4-1)$$

The position was an estimate of the stationary receiver at one test site. The clock bias was an estimate of the difference between the site atomic clock and the GPS system time kept by the MCS.

The mathematical model for the DCA and the EKF was, again, the ephemeris representation of the Keplerian and perturbation parameters, described in Section 2.2.B. Because the processors used actual data, the same coordinate system correction was applied as described in Section 3.2, namely, 0.54 arc seconds subtracted from the longitude of the ascending node. This correction aligned the Broadcast Ephemeris Algorithm with the WGS 72 coordinates. After setting the model and coordinates, the variables were initialized.

The initial conditions were set close to the actual receiver site, but convergence occurred with initial conditions over 10,000 km from the actual site, without

using any a priori covariance matrix. This insensitivity to initial conditions indicated that users need not have a good estimate of their position before using the GPS system. Typical values for the initial state at Fort Davis were:

$$x_u = -.13 \times 10^7 \text{ (meters)} \quad (4-2)$$

$$y_u = -.53 \times 10^7 \text{ (meters)}$$

$$z_u = .32 \times 10^7 \text{ (meters)}$$

$$b_u = .5 \times 10^5 \text{ (meters) (seconds} \times \text{speed of light)}$$

This was approximately 51.4 km from the surveyed receiver location. After initialization the filter accepted the broadcast ephemerides and pseudorange measurements.

Since the filter simulated the actual navigation process, it accepted the current hour ephemerides and a single pseudorange measurement from each of four satellites. The pseudorange measurements had the ionospheric correction (Equation 3-4) already applied by a preprocessor. All four of the pseudoranges had the same reception time, or time tag, simulating four receivers accepting simultaneous measurements. This timing simplified the solution by not requiring time tag adjustment. The solution was formed at approximately the same time tag as the

measurement. Filter timing is explained next.

Proper timing occurred when the navigation process was synchronized with the official GPS time, kept by the MCS. The first step in the synchronization was to relate the user clock reception time tag back to the satellite clock transmission time by using the pseudorange measurement:

$$t_{sv_i} = t_u - p_i/c \quad (4-3)$$

where t_{sv_i} - approximate i^{th} satellite clock transmission time (not yet corrected for bias and drift) (seconds since 00:00 Sunday)

t_u - user clock reception time (corrected for user clock bias) (seconds since 00:00 Sunday)

p_i - pseudorange measurement from i^{th} satellite (meters)

c - speed of light (see Section 2.2.B).

Then the filter computed the time since epoch to adjust for the relativity effect:

$$t_{k_i} = t_{sv_i} - t_{oe_i} \quad (4-4)$$

where t_{k_i} - time since epoch (not adjusted for relativity) (seconds)

t_{sv_i} - approximate i^{th} satellite clock transmission time (still not corrected for bias and drift) (seconds since 00:00 Sunday)

t_{oe_i} - epoch time when the broadcast ephemeris is correct. (seconds after 00:00 Sunday)

Knowing t_k , the filter computed the general and special relativity correction, Equation (3-6). The relativity correction added to the satellite clock bias and drift and became the i^{th} satellite clock correction, Δt_{sv_i} :

$$\Delta t_{sv_i} = a_{0_i} + a_{1_i} t_{k_i} + \Delta t_{r_i} \quad (4-5)$$

Where a_{0_i} - i^{th} satellite clock bias

a_{1_i} - i^{th} satellite clock drift rate

Δt_{r_i} - relativity correction for the i^{th} satellite clock.

The Δt_{sv_i} adjusted the i^{th} satellite clock to coincide with GPS system time, and

$$t_{sv_i} = t_{sv_i} - \Delta t_{sv_i} \quad (4-6)$$

The time since epoch was recalculated with the new t_{sv_i} as

$$t_{k_i} = t_{sv_i} - t_{oe_i} \quad (4-7)$$

Note that t_{k_i} was required in the Δt_{r_i} calculation and Δt_{r_i} corrected t_{k_i} . Although this appeared as an iterative path, the Δt_{r_i} changed the value of t_{k_i} very little so that recalculating Δt_{r_i} a second time did not change

t_{k_i} significantly [Moller, 1984]. Now that a synchronized t_k was computed for one satellite, that satellite ECF position was calculated using the BEA. (see Section 2.2.B) The next step was computing the residuals.

With the i^{th} satellite position and the latest state estimate, the filter calculated the pseudorange.

$$p_i = \sqrt{(x_i - x_u)^2 + (y_i - y_u)^2 + (z_i - z_u)^2} + cb_u \quad (4-8)$$

p_i - the calculated pseudorange, i^{th} satellite,
 x_i, y_i, z_i - the ECF position, i^{th} satellite,
 x_u, y_u, z_u, b_u - the latest state estimate,
 c - speed of light.

This calculated pseudorange was subtracted from the observed pseudorange to form the residual for the i^{th} satellite.

$$y_i = p_i - \hat{p}_i \quad (4-9)$$

Here the \hat{p}_i is the transmitted pseudorange corrected for ionospheric and tropospheric delays as in Equations 3-4 and 3-5, respectively.

The calculated pseudorange should have matched the observed, yielding a small residual. Differences in the two pseudoranges, identified by large residuals indicated an error in the state estimate. These errors were removed in the DCA through the differential correction

which is the solution to the equation:

$$\delta p = \left| \frac{\partial p}{\partial X} \right| \delta X, \quad (4-10)$$

which came from expanding Equation 4-8 in a Taylor series about the nominal and keeping the linear terms [Noe and Myers, 1976]. The term, $\frac{\partial p}{\partial X}$, is the measurement sensitivity matrix which is next.

The measurement sensitivity matrix was the 4 x 4 matrix of partial derivatives of the four pseudoranges with respect to the state, evaluated on the four reference trajectories. The reference trajectories were the current best estimates of the satellites states.

$$H_i = \frac{\partial G_i(X^*, t)}{\partial X} \quad (4-11)$$

where $G_i(X, t) = p_i$, the calculated pseudorange. The partials described the sensitivity of the calculated pseudoranges to small changes in the state: X^* .

$$H_i = \begin{vmatrix} \frac{\partial p_i}{\partial x_u} & \frac{\partial p_i}{\partial y_u} & \frac{\partial p_i}{\partial z_u} & \frac{\partial p_i}{\partial cb_u} \end{vmatrix} \quad (4-12)$$

This equation represents four rows, one for each satellite, thus providing the 4 x 4 matrix needed for a solution.

$$\text{Here, } \frac{\partial p_i}{\partial x_u} = \frac{x_u - x_i}{p_i - cb_u}, \quad (4-13)$$

$$\frac{\delta p_i}{\delta y_u} = \frac{y_u - y_i}{p_i - cb_u} , \quad (4-14)$$

$$\frac{\delta p_i}{\delta z_u} = \frac{z_u - z_i}{p_i - cb_u} , \quad (4-15)$$

$$\frac{\delta p_i}{\delta cb_u} = 1.0 . \quad (4-16)$$

Unlike the previous chapters that used least squares solutions, the normal matrix, $H^T H$, was not formed in the DCA to compute the state correction terms. Instead, the DCA calculated H^{-1} , which sufficed.

Because the Taylor series was linearized, the solution to Equation 4-10 was:

$$\delta x = H^{-1} \delta p , \quad (4-17)$$

or in terms of state corrections, \hat{x} , and residuals, y :

$$\hat{x} = H^{-1} y . \quad (4-18)$$

Since the solution was approximate, caused by the Taylor series truncation, the algorithm required iteration until the RMS of the residuals from successive iterations reached a preset tolerance.

During the iteration process, instead of inverting H each time, the DCA used the Hotelling approximation to H^{-1} [Noe and Myers, 1976]. The following equation for B_m represents iterative approximations of H^{-1} :

$$B_m = B_{m-1} (2I - H B_{m-1}) \quad m = 1, 2, 3, \dots \quad (4-19)$$

The B_0 term is the initial inversion of H . Successive terms, B_1, B_2, B_3 , approach the exact value of H^{-1} [Noe, Myers, and Wu, 1978]. During actual operation, however, a single calculation of B_m produced the required accuracy to form the next estimate of the state corrections. Thus, the computer operations decreased and the accuracy was unchanged.

Note that the H matrix must be full rank to obtain a solution. This requirement was satisfied by partial derivatives that were linearly independent. Analysis of the geometry of the four satellite constellation will provide a measure of the linear independence, Geometric Dilution of Precision (GDOP).

The GDOP is defined as the square root of the trace of the covariance matrix, P [Fang, 1980]. To solve for \hat{x} , the filter did not compute P , but to check that a solution existed, P was calculated. The matrix P was formed by $(H^T H)^{-1}$, which depended on the relative geometry of the user and the four satellites (see Equations 4-13 through 4-16). Then, GDOP represented a measure of that geometry. In practice, when the four satellites were spread far apart (ideally, one overhead and the others spaced evenly along the horizon) the GDOP was best

(small), yielding a good navigation solution. However, if the satellites were grouped together or situated along a line, then GDOP was large and a solution may not have been available[Fang, 1980]. Thus, the value of GDOP was vital to the availability of a solution.

Note that with a 21 satellite GPS constellation, there may be several sets of four satellites available. The value of GDOP may be used for choosing the best set, that is, the set with the lowest GDOP. For this study, however, the test constellations had only four satellites available and GDOP served to guarantee the inverse of H for the navigation solution. Since the filter calculated the covariance matrix to find GDOP, the covariance matrix was available for other purposes as well.

The covariance matrix, P , was formed to find GDOP but also served to verify the accuracy of the solution and to initialize the Extended Kalman Filter. The 4×4 inverse of the normal matrix has diagonal components that are variances of the state solution and off-diagonal covariances. As in Chapters Two and Three, the weighting matrix was the identity matrix since the measurement statistics were unknown. The observations were assumed to have random errors, uncorrelated in time, with a normal distribution around a zero mean. Thus, the P matrix was assumed to accurately reflect the variances of the

state; small values indicating high confidence in the solution [Tapley and Born, 1985]. Section 4.2.A provides experimental values for the variances.

The P matrix was also propagated forward to form the initial \bar{P} required for the first iteration of the EKF. The EKF was not self-starting, but required a propagated state vector, \bar{x} , and covariance matrix, \bar{P} . The propagation matrix was another constant state transition matrix, Φ , similar to the one in Section 2.2.C. As expressed by Equation 2-31, the Φ matrix permitted the use of the converged state and covariance matrix as the propagated quantities for starting the EKF. Before the EKF is presented, however, results of the Differential Correction Algorithm are reviewed.

A. Experiments with Differential Correction Algorithm

To verify the differential correction user navigation algorithm, various experiments were conducted using data from the Spring 1985 System Test as described in Chapter Three. Rather than analyzing just one navigation solution at a time, these experiments used a continuous filter, solving for the user state every 30 seconds for approximately one hour. Each solution was independent of the last solution, except the old converged state became the new initial conditions when four new data sets were

read. The results were very good for the RMS of residuals and covariance values, however, random discontinuities in the estimated state revealed the presence of measurement noise.

The position error in the state estimate was the straight line distance between the surveyed and estimated receiver locations. With accurate site clocks and good constellation geometry, position errors under ten meters were possible. However, typical values from the DCA solution proposed by Noe and Myers[1976] varied from eight meters to 81.8 meters at Fort Davis, from 4.1 meters to a spike of 330.8 meters at Richmond, and from 2.8 meters to 68.3 meters at Haystack. Figures 4-1 through 4-3 plot the position errors between time tags 115,829 seconds and approximately 119,000 seconds. In each figure satellites SV09, SV11, SV12, and SV13 provided the initial navigation information. Note that at Fort Davis there was a five and a half minute span starting at time tag 118,469 seconds with no solution available because satellite SV11 pseudoranges were erroneous. Also, at Fort Davis and Richmond there were breaks in the transmitted pseudoranges just before time tags 119,000 seconds and 118,000 seconds, respectively, indicating that satellite SV09 set and satellite SV04 rose. Satellite SV04 produced large position errors due to the

reduced accuracy in the satellite clock[Conley, private communication, 1986].

All three figures clearly show the random discontinuities in the estimated positions caused by measurement noise. In Figure 4-1 only eleven time tags have accuracies under ten meters. Figure 4-2 has nine and Figure 4-3, 22. To improve the accuracy and smooth the discontinuities, the EKF can be used as described later in this chapter.

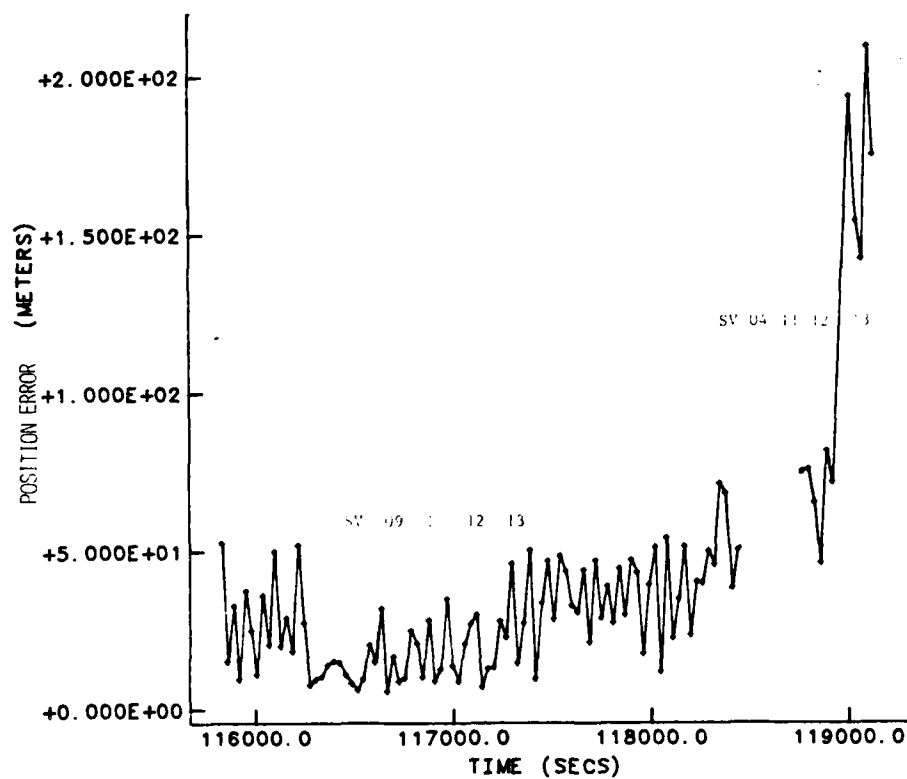


FIGURE 4-1 POSITION ERROR vs TIME - FT DAVIS

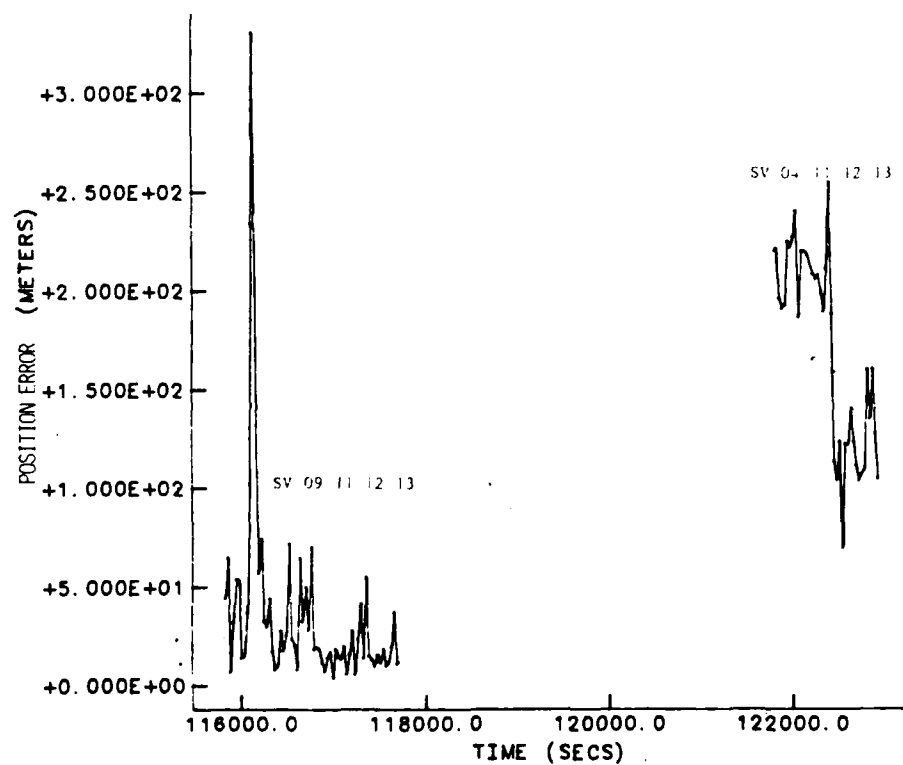


FIGURE 4-2 POSITION ERROR vs TIME - RICHMOND

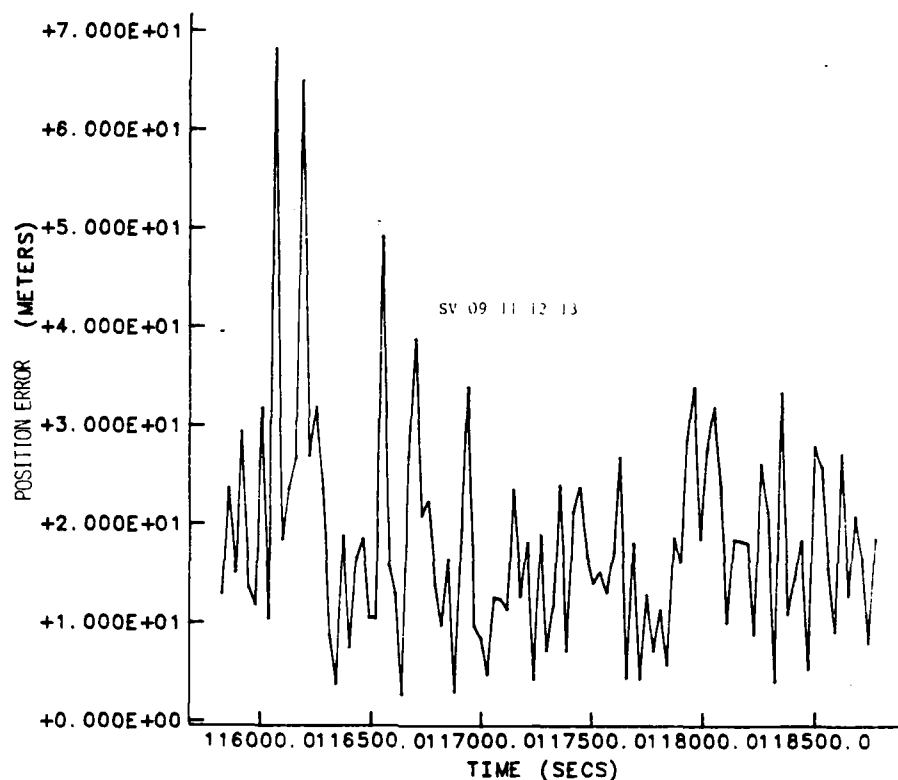


FIGURE 4-3 POSITION ERROR vs TIME - HAYSTACK

The user clock biases at the three sites are plotted in Figures 4-4 through 4-6. These estimated biases synchronized the user clock with the GPS system time. The clocks at Fort Davis, Richmond, and Haystack were hydrogen masers. The Fort Davis, clock produced biases between 50 and 350 nanoseconds whereas, the Richmond clock biases were more consistent than at Fort Davis, but significantly higher at about 5,000 nanoseconds. The clock biases at Haystack showed an unusual linear growth, indicating either a possible clock malfunction or that the receiver operated on a crystal oscillator during the test. Each of these user clock biases represented a

potentially large error in the pseudorange if it were ignored. For instance, the 350 nanosecond bias at Fort Davis could produce a 105 meter error in the pseudorange which could greatly reduce accuracy in the position estimate. Also note that the clock bias values change randomly in the Fort Davis and Richmond plots. These jumps correlate highly with the changes in the position error plots, demonstrating that the navigation accuracy depends on the user clock synchronization. This dependency is expected in the GPS system because the pseudorange measurement is computed as the difference between the transmission time on the satellite clock and the reception time on the user clock. When the clocks are synchronized then the measurements are accurate. The large discontinuities in the clock bias diminish in the EKF.

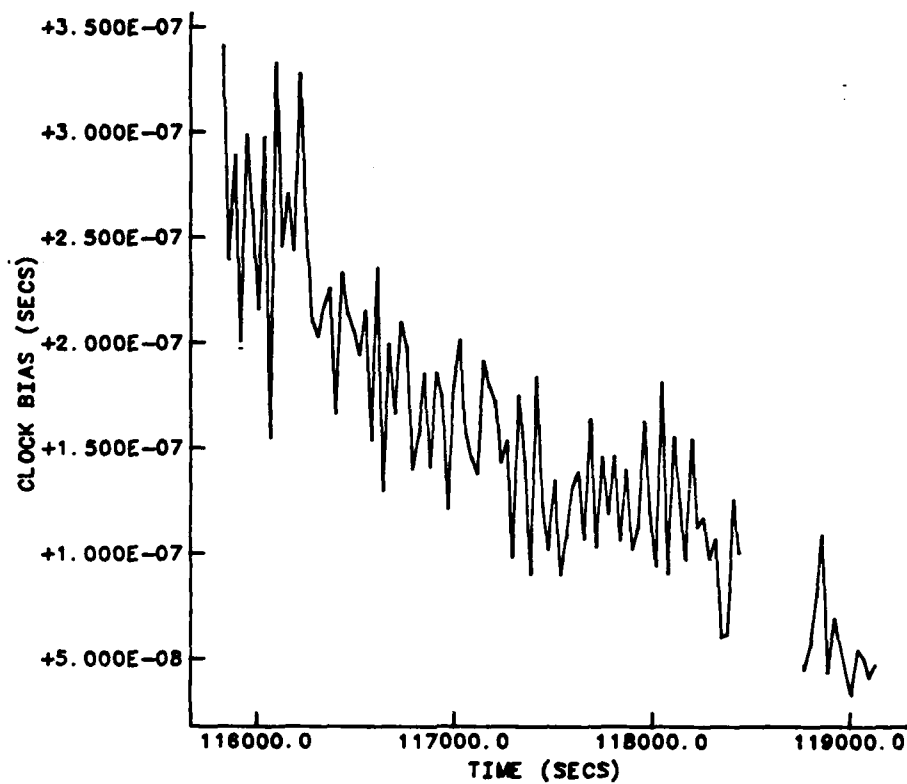


FIGURE 4-4 USER CLOCK BIAS vs TIME - FT DAVIS

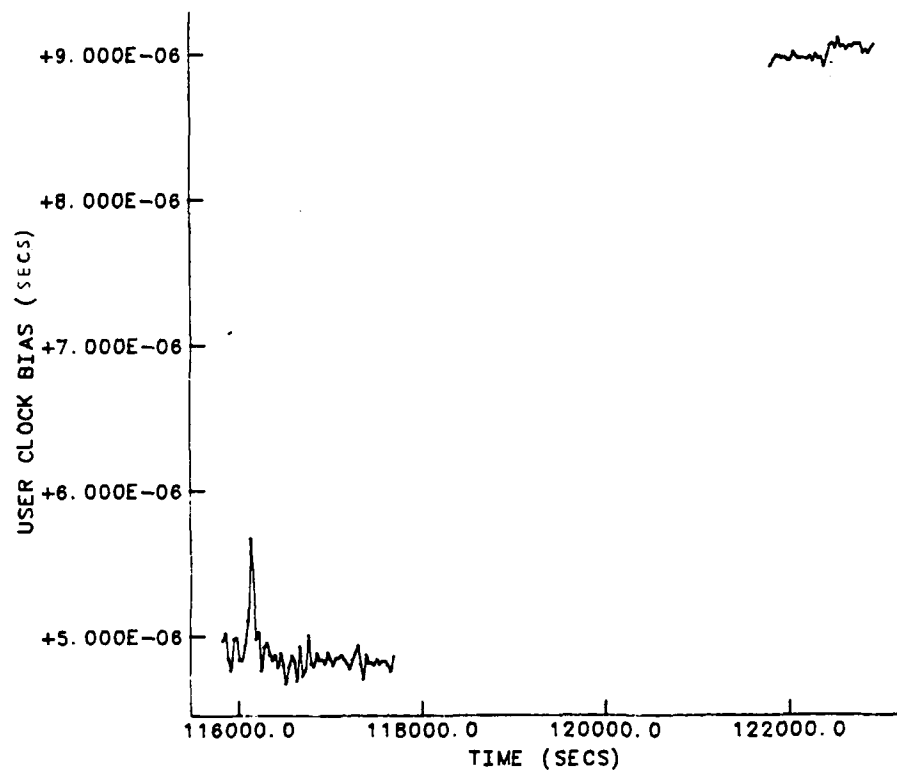


FIGURE 4-5 USER CLOCK BIAS vs TIME - RICHMOND

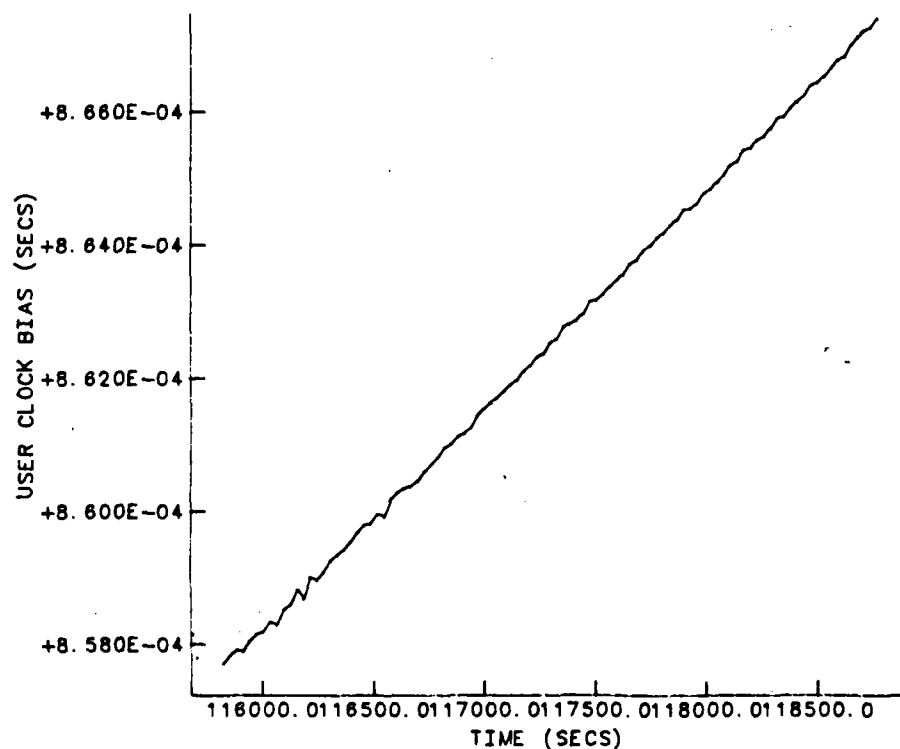


FIGURE 4-6 USER CLOCK BIAS vs TIME - HAYSTACK

This navigation algorithm produced results with an RMS of the residuals on the order of 10^{-6} meters and smaller for the three sites. This accuracy was expected because the filter did not use least squares but instead, formed the state corrections, \hat{x} , directly from $H^{-1} y$. The H^{-1} matrix was accurate to the limit of the computer inverse algorithm, approximately 12 significant decimal digits. Further, the residuals, y , were formed from the accurate model of the pseudorange measurement. Together, they formed the highly accurate \hat{x} vector which corrected the state, so the residuals from successive iterations improved rapidly. Thus, in three iterations, small values for the RMS of residuals resulted.

The satellite motion within the test constellation and the combined variances of the state are reflected in the GDOP plots, Figures 4-7 through 4-9. GDOP began slightly large (about 14 meters) at each site, indicating that the geometry was not ideal for a navigation solution. The large GDOP also denoted large values for the variances of the state. Consequently, initial confidence in the solution was low. As time progressed and the geometry improved, the GDOP values decreased to slightly under eight meters at Fort Davis and Haystack, and slightly under nine meters for Richmond. This improvement was expected since the four test satellites

initially rose above the western horizon in close proximity, yielding a large GDOP, then passed over the test sites in a reasonably good geometry. The best GDOP values were 7.41 meters at Fort Davis, 8.54 meters at Richmond, and 7.63 meters at Haystack. The individual variances of the state also reflected this improvement as they decreased from the initial time to the final time. Table 4-1 lists the initial and final variances for the estimated user positions, using the DCA.

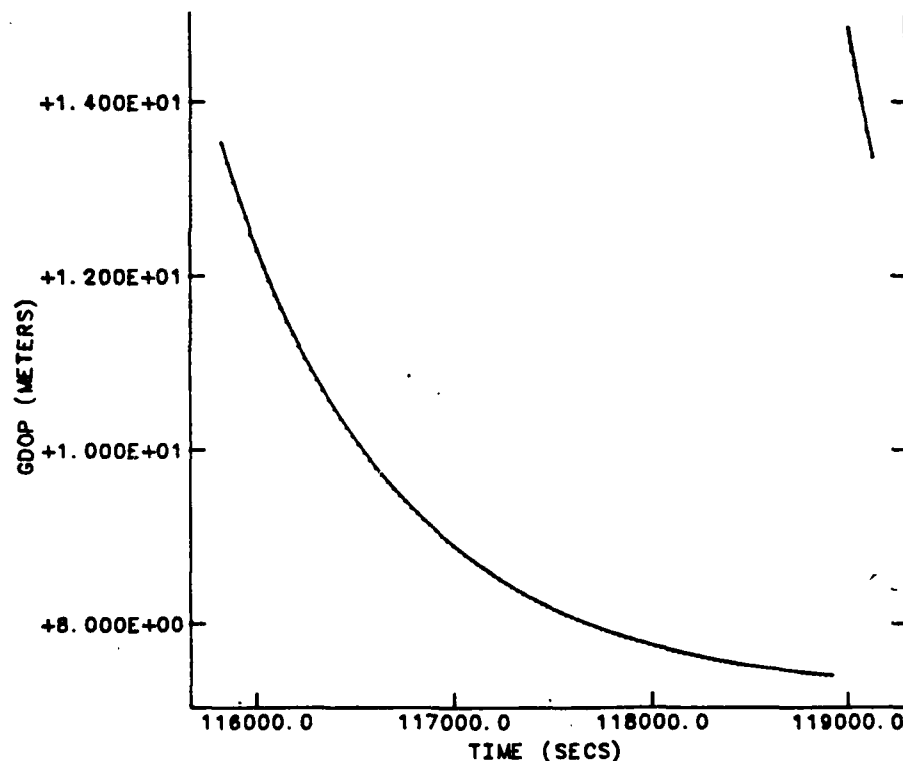


FIGURE 4-7 GDOP vs TIME - FT DAVIS

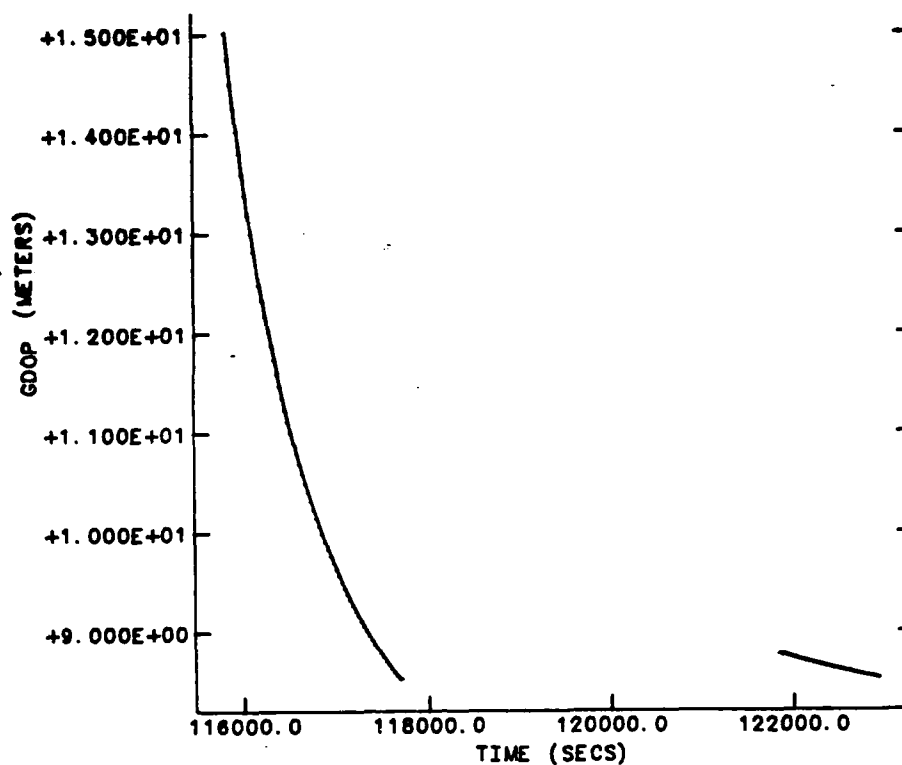


FIGURE 4-8 GDOP vs TIME - RICHMOND

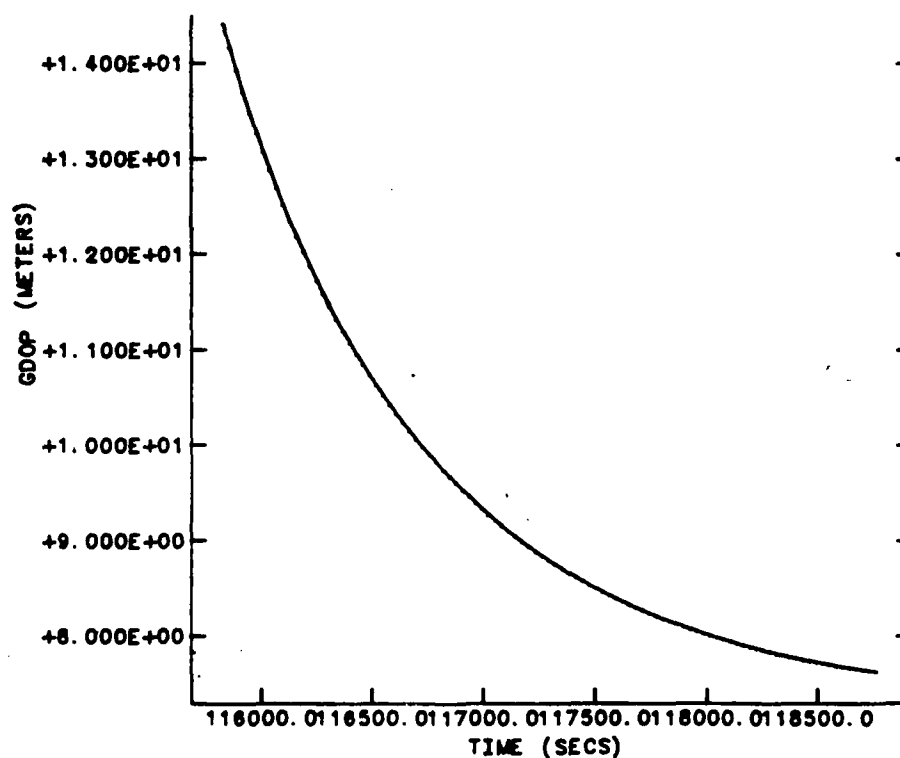


FIGURE 4-9 GDOP vs TIME - HAYSTACK

Table 4-1
Initial and Final Variances of the State (meter²)

	Fort Davis		Richmond		Haystack	
	Initial	Final	Initial	Final	Initial	Final
x_u	2.13	1.81	4.83	1.24	5.50	1.25
y_u	35.9	31.6	41.3	31.7	45.1	34.7
z_u	76.5	8.83	93.9	19.4	79.1	8.74
cb_u	68.7	12.7	85.9	20.5	78.1	13.5

The User Navigation Algorithm to this point has used the differential correction estimator. The output has revealed various characteristics of the solution, the most obvious being random changes in the estimated site position caused by measurement noise. The high correlation between the position error and the clock bias emphasizes the need for accurate clocks to minimize the error in the calculated pseudorange. Finally, the GDOP values represent the constellation geometry and the confidence in the solution accuracy. Next, the Extended Kalman Filter will be used to improve several of these characteristics and produce position estimates within ten meters of the surveyed site.

4.3 The Extended Kalman Filter

The Extended Kalman Filter (EKF) used the output of the Differential Correction Algorithm (DCA) for initialization, then operated independently to form navigation solutions from the broadcast ephemerides and pseudorange measurements from four satellites. The EKF filtered the measurement noise so that the position estimates did not change in direct response to the measurement noise. Instead, plots of the test cases show much smoother results with position errors under ten meters possible. The filter began by initializing X and P with values from the DCA.

The Noe and Myers[1976] DCA produced the state, X and covariance matrix P at a time tag, t_k . As mentioned, the X_k and P_k were propagated forward by the state transition matrix which was identity, forming \bar{X}_{k+1} and \bar{P}_{k+1} . These two quantities along with pseudorange measurements from four satellites were inputs to the EKF. Although all six inputs may have been affected by measurement noise, they initialized the EKF which quickly filtered the noise. The algorithm was relatively simple with the first step being to define the state.

The initial state was the propagated site position and user clock bias:

$$\bar{X}_{k+1} = \begin{bmatrix} x_u \\ y_u \\ z_u \\ b_u \end{bmatrix}_{k+1} \quad (4-20)$$

This also represented the initial reference trajectory, X_{k+1}^* , which was updated at each measurement time. Because the site was fixed in the ECF coordinate system the state equation of motion was simple:

$$\dot{\bar{X}}_{k+1}(t) = F(\bar{X}, t) = [0], \quad (4-21)$$

where $\bar{X}(t_k) = \hat{X}_k$, which implies \bar{X}_{k+1} was a constant. This means integration between measurement times was not required, greatly simplifying the operation. Since the estimated quantities are constant, the partial derivatives of the equations of motion with respect to the state are:

$$A(t) = \frac{\partial F(\bar{X}, t)}{\partial X} = [0]. \quad (4-22)$$

The consequence of Equation (4-22) was a simple differential equation for the state transition matrix:

$$\dot{\Phi}(t, t_k) = A(t)\Phi(t, t_k) = [0] \quad (4-23)$$

Since the initial condition for Φ was:

$$\Phi(t_k, t_k) = I, \quad (4-24)$$

then $\Phi = I$ always. The next step in the EKF was forming the filter gain.

The filter gain, K_{k+1} , depended on the propagated covariance matrix, \bar{P}_{k+1} , the measurement sensitivity matrix, H_{k+1} , and the measurement weights, W_{k+1} :

$$K = \bar{P}H^T[H\bar{P}H^T + W^{-1}]^{-1} \text{ at } t_{k+1} \quad (4-25)$$

(See Appendix E for derivation of the filter gain) As mentioned, measurements were weighted equally because measurement statistics were unknown. Random errors were assumed to be uncorrelated in time, with a normal distribution about a zero mean.

$$\text{Thus, } W_{k+1} = [I] \quad (4-26)$$

The H_{k+1} matrix was the same 4x4 as given by matrix Equation (4-12) with elements given by Equation (4-13) through (4-16). The state corrections were formed next.

The filter gain was multiplied by the measurement residual vector to form the state corrections, \hat{x}_{k+1} :

$$\hat{x}_{k+1} = K_{k+1}y_{k+1} \quad (4-27)$$

The corrections were added to the reference trajectory to form the new state and reference trajectory:

$$\hat{x}_{k+1} = x_{k+1}^* + \hat{x}_{k+1} \quad (4-28)$$

$$x_{k+2}^* = \hat{x}_{k+1} \quad (4-29)$$

Also required with the new state was the new covariance matrix, \hat{P}_{k+1} :

$$\hat{P}_{k+1} = [I - K_{k+1} H_{k+1}] \bar{P}_{k+1} \quad (4-30)$$

(See Appendix E for derivation of \hat{P}_{k+1}) This quantity, \hat{P}_{k+1} , was propagated forward by the identity state transition matrix to form the initial conditions for filter operation with the next set of four pseudorange measurements. Note that there was no propagation of the state correction vector, \hat{x} , meaning $\bar{x} = 0$, and there was no need for iteration since the new state was the best estimate. Therefore, a significant amount of computing time was saved with no accuracy degradation.

One of the inherent problems with the EKF was filter divergence caused by the filter gain decreasing close to zero, resulting in the filter ignoring new residuals. By ignoring the new residuals, the filter could allow model error and truncation error to build so that divergence might occur. Mathematically, the covariance elements normally decrease as the filter models the trajectory better with new observations. Since the P elements became the \bar{P} elements in this filter, then from Equation (4-25), the decreasing \bar{P} elements will cause the K values

to decrease. Eventually the K values might approach zero which when multiplied by the new residuals, y_{k+1} , produces near-zero state corrections in Equation (4-27). Thus, the new residuals have very little effect on the estimated state and errors in the mathematical model increase, yielding larger residuals at the next observation. Over many observations, the covariance elements and filter gain asymptotically approach zero, often causing filter divergence. Correcting the divergence is possible by adding process noise to the state dynamics [Tapley and Born, 1985]. The state noise compensator, as it is called, can complicate filter operation, particularly, in the determination of the process noise parameters. However, for this simple EKF, the state noise was added, as a constant, to the diagonal elements of the \bar{P} matrix whenever the trace of the \bar{P} matrix was below 1.0 meters²:

$$\bar{P}_{i,i} = \bar{P}_{i,i} + C \quad i = 1, 2, 3, 4 \quad (4-31)$$

According to Tapley and Born [1985], the equations for determining \hat{x} are not changed when state noise is included. Consequently, Equation (4-31) sufficed to prevent filter divergence by establishing a lower bound on the covariance matrix.

Thus, the EKF used the state and covariance matrix

from the DCA for initialization, then used pseudorange measurements and ephemerides to form navigation solutions. The random changes in the DCA solutions were smoothed and accuracy improved. The problem with filter divergence was avoided by adding a constant state noise to the covariance matrix.

A. Experiments with the Extended Kalman Filter

A variety of test cases were examined with the EKF, using the Spring 1985 System Test Data. The EKF was implemented as outlined in the previous section with the best state noise constant, C , determined by trial and error, set to 0.5 meters (other values caused a decrease in accuracy). Navigation solutions are presented for April 1-3 at the Fort Davis receiver site, and April 1 at the Richmond and Haystack sites. The tests ran for several hours, sufficiently long to demonstrate several events that occurred in the GPS test constellation affecting the solutions. Events such as satellites rising and setting, and inadequate geometry formations were analyzed. Other considerations such as non-current ephemerides and individual satellite characteristics also affected the solutions. When all the adverse characteristics of the test data were eliminated or accounted for, the position error from the surveyed sites was

typically under ten meters. The values for the RMS of the residuals were also under ten meters, indicating accurate modelling of the problem.

The position error in the state estimate is the straight line distance between the actual and the estimated receiver site. Expected results in the position errors were under ten meters. However, the plots show some variations from this expectation. Typical values range from 1.8 meters at Fort Davis on April 2, to over 400 meters associated with a large GDOP at Haystack on April 1. Figures 4-10 through 4-14 plot the results of the position errors at the three sites, with solutions formed every 30 seconds. The plots show a variety of characteristics which are discussed next.

Figures 4-10 through 4-12 are plots of position error at Fort Davis on the April 1, 2, and 3, 1985, respectively. They all show the smoothing trait of the EKF when compared to the differential correction solutions of Figures 4-1 through 4-3, since measurement noise is filtered. In each of these first three EKF plots the initial point is the Noe and Myers[1976] DCA solution which is large. Then, the EKF solutions that follow show improvement, but are still outside the ten meter criteria. Several factors affect the accuracies. First of all, each of the position error peaks are caused by

deteriorating constellation geometry. On April 1, Figure 4-10, the GDOP rises to over 1000 meters at 108,689 seconds and 114,419 seconds, causing the gradual climbs in position error. Figure 4-11 has one peak associated with a large GDOP at 200,579 seconds, and Figure 4-12 has two peaks at 281,009 seconds and 286,739 seconds. Comparisons of these results with the corresponding GDOP results reveal the correlation between large GDOP values and large position errors. Note that the position errors maintain consistent values while the GDOP increased considerably. This steadiness is an EKF characteristic resulting from the covariance matrix propagation. Also note that the peaks in GDOP occur in the test constellation and will not be so large nor as frequent in the full constellation [Porter, 1978].

The next factor affecting the results is the timeliness of the ephemeris epochs. Because the data was taken from the 1985 system test storage tapes, after the fact, not all of the broadcast ephemerides are current with the pseudorange time tags. For instance, the initial constellation in Figure 4-10 is composed of satellites SV06, SV08, SV09 and SV11 with corresponding ephemeris epochs of 104,400 seconds for all satellites, except SV09 with an epoch of 111,600 seconds. This means that the SV09 data does not have a current broadcast ephemeris included

with its initial pseudorange measurements (from time tag 105,509 seconds to 111,119 seconds). (Note, this discrepancy can not occur with a real time test since the satellites broadcast their ephemerides at the current epoch.) At the next epoch, 108,000 seconds, satellites SV06, SV08, and SV11 update to that epoch, making the SV09 epoch only one hour ahead. Then SV06 and SV08 set before the next epoch, 111,600 seconds. When SV12 and SV13 rise to form a constellation of four again, their broadcast ephemeris epochs are ahead by two hours each, at 118,800 seconds. At time tag 115,200 seconds, SV09 and SV11 update, leaving SV12 and SV13 ahead by one hour. Finally, at time tag 118,800 seconds, SV09 and SV11 update again so all four satellites have the current ephemeris epoch. Unfortunately, SV09 sets at 118,919 seconds, after only four solutions. Then, SV04 rises and, because of errors in its clock, the position error climbs very high.

Similar conditions exist in Figure 4-11, where, initially all four satellites, (SV09, SV11, SV12, and SV13), have epochs that are two hours ahead of the first pseudorange (epoch times are 205,200 seconds: the first pseudorange is 199,349 seconds). This condition continues until time tag 201,600 seconds when all four epochs update and are one hour ahead. Then, at time tag 205,079

seconds, SV09 sets and, 90 seconds later, SV04 rises with an ephemeris epoch one hour ahead of the others and SV13 one hour ahead. So, at no time do all the satellites have epochs that are current with the pseudoranges. (Note that SV04 does not decrease the navigation accuracy as it does in all the other navigation cases, but position errors improve steadily to 1.8 meters: unusual behavior for the solutions that include SV04 data.)

In Figure 4-12 slightly better results occur when three satellites broadcast the current epoch and one satellite epoch is only one hour ahead. Initially, satellites SV06, SV08, SV09, and SV11 form the constellation, with the SV09 epoch being two hours ahead of the other three. The epochs for SV06, SV08, and SV11 update at time tag 280,800 seconds, putting SV09 only one hour ahead. The position errors begin to improve rapidly (with an improvement in GDOP, also), levelling near 14.0 meters. Then SV06 and SV08 set at time tag 283,439 seconds. Note the marked improvement when only one satellite epoch is in error by one hour. At time tag 284,939 seconds SV12 and SV13 rise; SV12 with a broadcast ephemeris epoch two hours ahead of the others and SV13 one hour ahead. The growing GDOP causes a peak in the position error but then, after the GDOP peak, SV09 and SV11 update their epoch to the same as SV13. This leaves

only SV12 in error by one hour and the results are very good. The position error steadily decreases to 7.4 meters. Shortly afterward SV09 sets and SV04 rises, causing much worse position errors.

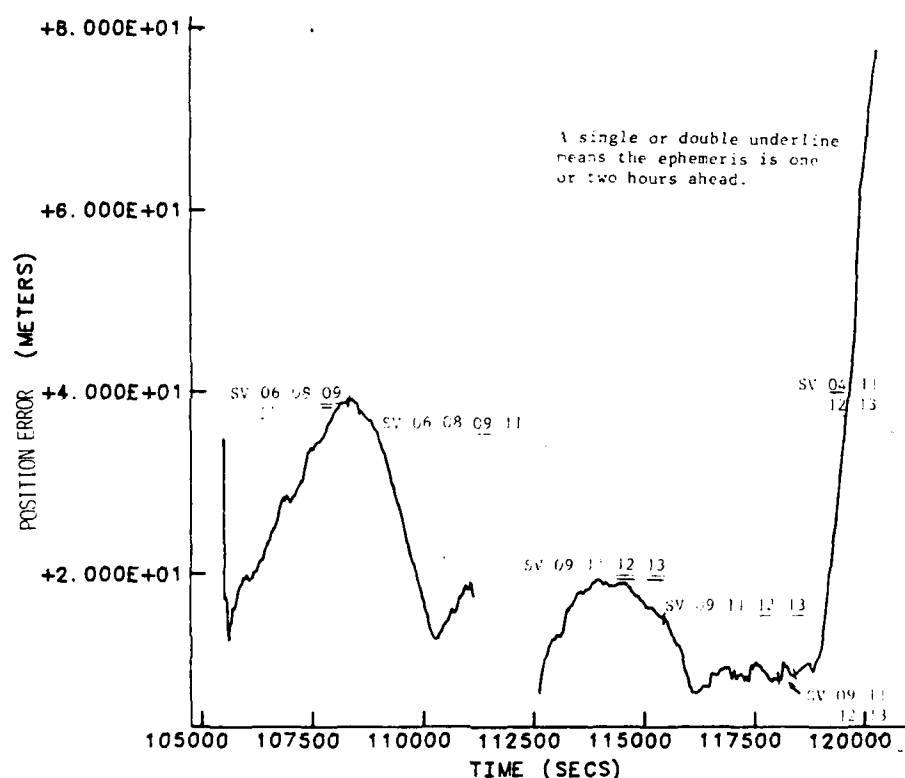


FIGURE 4-10 POSITION ERROR AT FT DAVIS - APRIL 1, 1985

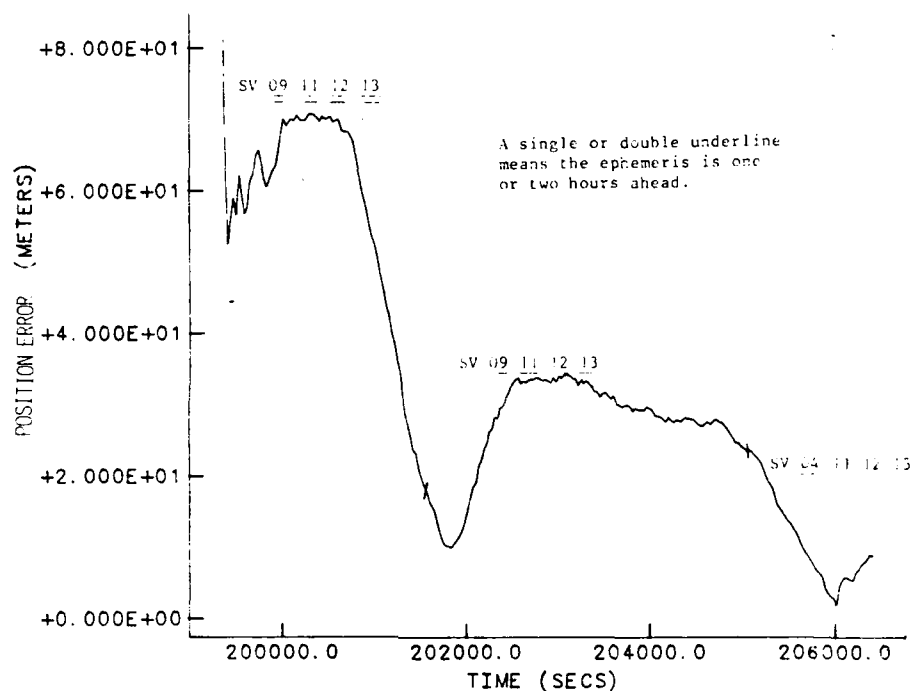


FIGURE 4-11 POSITION ERROR AT FT DAVIS - APRIL 2, 1985

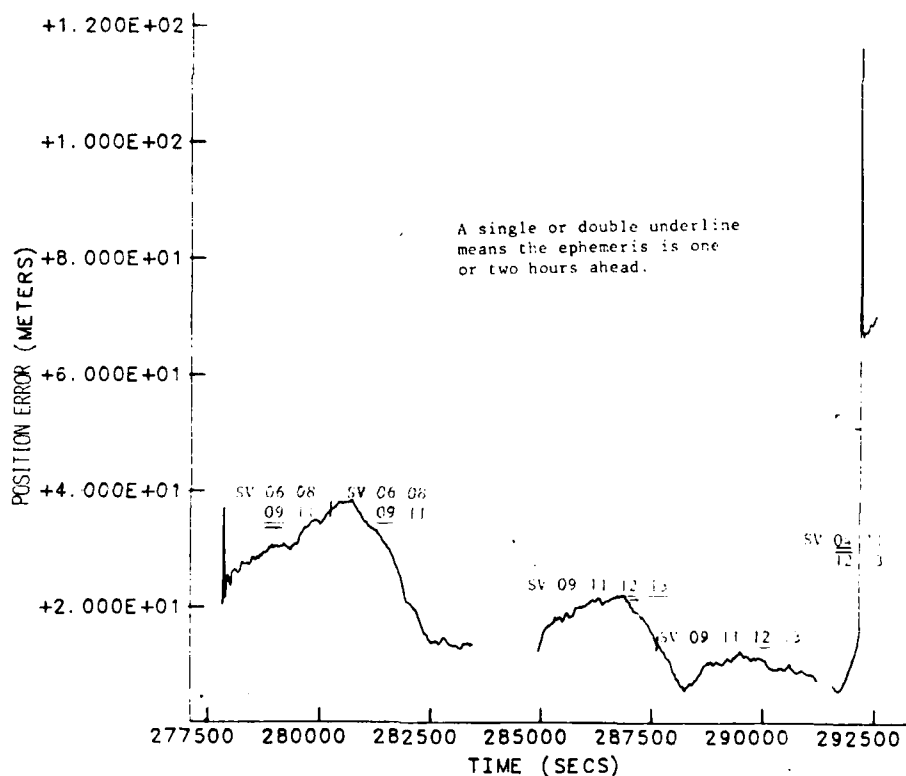


FIGURE 4-12 POSITION ERROR AT FT DAVIS - APRIL 3, 1985

The last two position error plots, Figures 4-13 at Richmond and 4-14 at Haystack, exhibit the same characteristics as Figures 4-10 through 4-12. In Figure 4-13 the constellation starts with SV06, SV08, SV09 and SV11 in a poor geometry, causing GDOP to grow to over 1000 meters at 108,719 seconds. The large GDOP causes large position errors initially. Also, the epoch for SV09 is two hours ahead of the others until the others update at 108,000 seconds. After the GDOP peak and the epoch updates, the position errors fall to values between 16.2 meters at 109,739 seconds and 33.4 meters just before SV06 and SV08 set at 111,059 seconds. When SV12 and SV13 rise, forming the four satellite constellation again, their epochs are two hours ahead of SV09 and SV11. The GDOP value is slightly high initially, 31.63 meters, but decreases quickly. Then SV09 and SV11 update their epochs at 115,200 seconds. Position errors remain steady until 116,129 seconds when two consecutive pseudoranges from SV12 are unusually large (they change the computed satellite position by 12,000 meters), causing the position error to jump to 45.9 meters. After the discontinuity, the pseudoranges return to normal and position errors steadily decrease to 13.5 meters at 117,689 seconds when SV09 sets. No solutions are computed with all four satellite epochs current with the pseudoranges.

The final 3000 seconds of the plot show the effect of SV04 joining the constellation. The GDOP is good, 8.78 meters, but the position error rises quickly to over 200 meters. Note in the plot of user clock bias, Figure 4-21, the estimate of the user clock rises rapidly, attempting unsuccessfully to compensate for the errors in the satellite clock.

In Figure 4-14 the constellation is formed with SV06, SV08, SV09, and SV11. Satellite SV09 has an epoch two hours ahead of the other three and the GDOP rises early, the combination causing the position error to rise to over 400 meters. Then, the geometry improves and three satellites update their epochs, so SV09 is only one hour ahead. The position errors reduce to under ten meters, generally, and continue until SV06 and SV08 set at 111,119 seconds. SV12 and SV13 rise with epochs two hours ahead of SV09 and SV11. The initial geometry is poor, then improves and the epochs for SV09 and SV11 update. Position errors decline into the range 20.0 meters to 40.0 meters until 118,800 seconds, when all four satellites have the current epoch and the position error drops to 9.9 meters for two solutions. The last two solutions before SV09 sets have position errors of 22.2 and 24.7 meters, with no apparent reason for the sudden rise (pseudoranges appear normal). One minute

after SV09 sets, SV04 rises with the epoch two hours ahead of the others, resulting in a slight rise in the GDOP and a large rise in the position error. Again, the SV04 clock causes the position error discontinuity.

To summarize the five position error plots, there is an expected correlation between the rise in GDOP and growth in position errors. Each spike in GDOP yields a peak in position error. Also, the timeliness of the satellite ephemeris epochs affect the plot. When all four satellites have epochs that are current with the pseudoranges, the position errors generally remain under ten meters. When one satellite has an epoch one hour ahead of the others, the position error is generally under 20 meters. When one epoch is two hours ahead of the others, or two satellites have epochs ahead by an hour or two, the position errors climb to almost 40 meters. This dependence on the current epoch is logical because the orbit parameters are constants for one hour and must be referenced to the navigation solution time. The farther the parameters are moved in time, the less current and thus, the less accurate, they will be. So for these test cases that have some broadcast ephemerides at different epoch times than the pseudorange measurement times, it can be concluded that, the closer the broadcast ephemerides are to the current epoch for as many satellites as

possible, the better the navigation solution. Note, for the full 21 satellite constellation, broadcasting current epochs, this differing-epoch problem will not exist and the solutions should be consistently under ten meters.

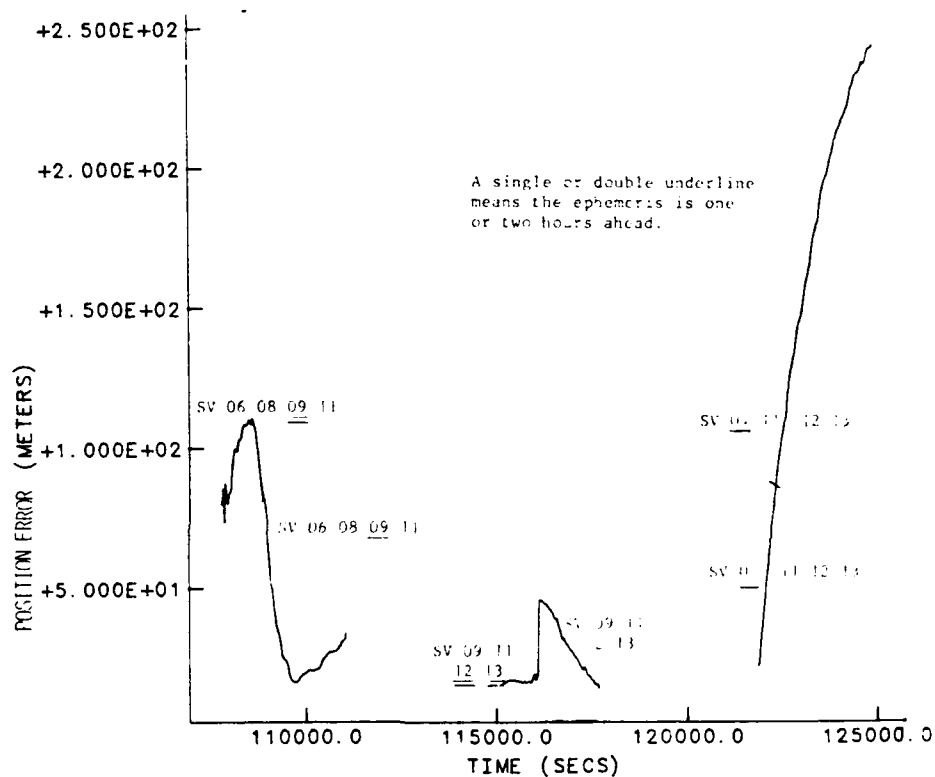


FIGURE 4-13 POSITION ERROR AT RICHMOND - APRIL 1, 1985

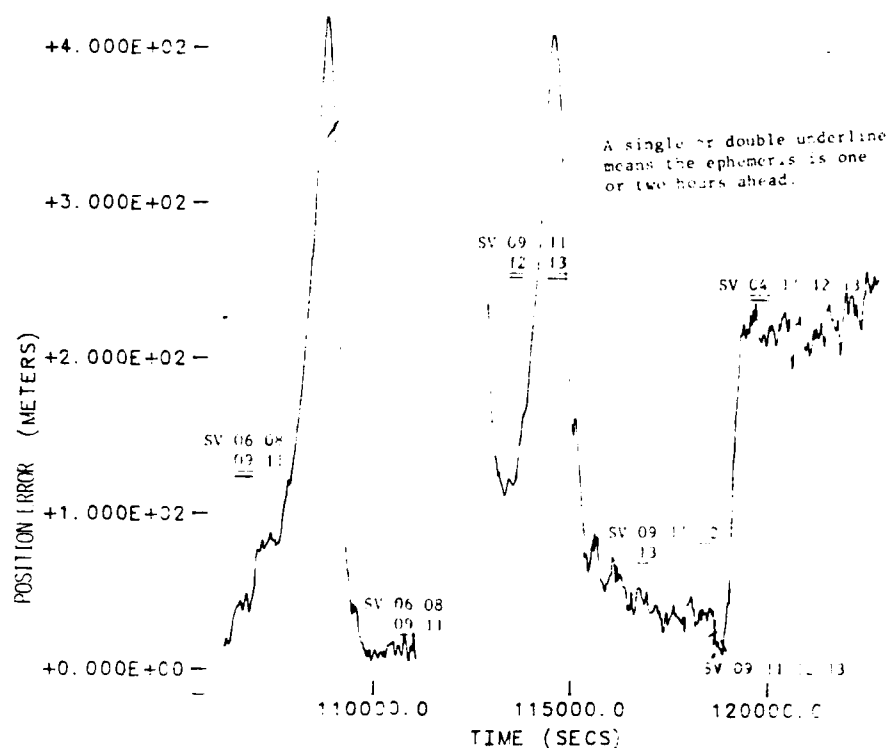


FIGURE 4-14 POSITION ERROR AT HAYSTACK - APRIL 1, 1985

The next figures, 4-15 through 4-24, plot the GDOP and User Clock Bias for the same times and locations as the position errors just presented. The two main characteristics are the GDOP spikes and the correlation between user clock bias and the position error. Only the user clock bias at Haystack exhibits unusual behavior (nearly linear growth), as described previously. The GDOP plots all display the smooth transitioning of the test constellation through various geometries including the spikes where position errors grow excessively. The user clock bias plots show that when the geometry is poor, the biases decrease much like the position errors increase.

This high correlation is expected because the position errors are dependent on the pseudoranges and the pseudoranges are a function of the user clock bias estimates. These plots complete the discussion of the position error, GDOP, and user clock bias.

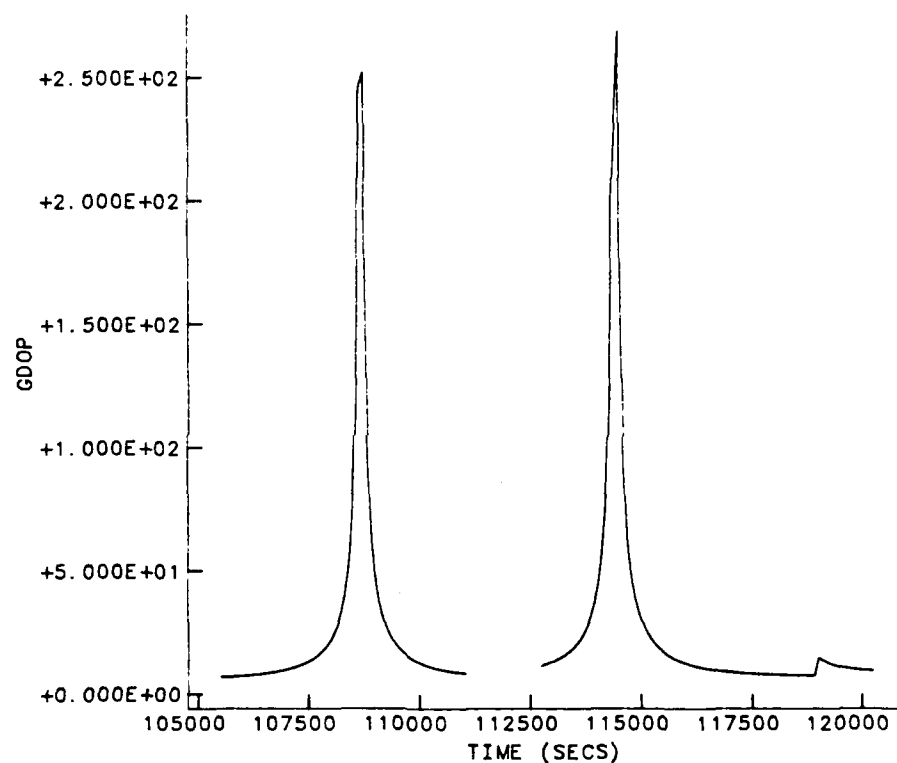


FIGURE 4-15 GDOP AT FORT DAVIS - APRIL 1, 1985

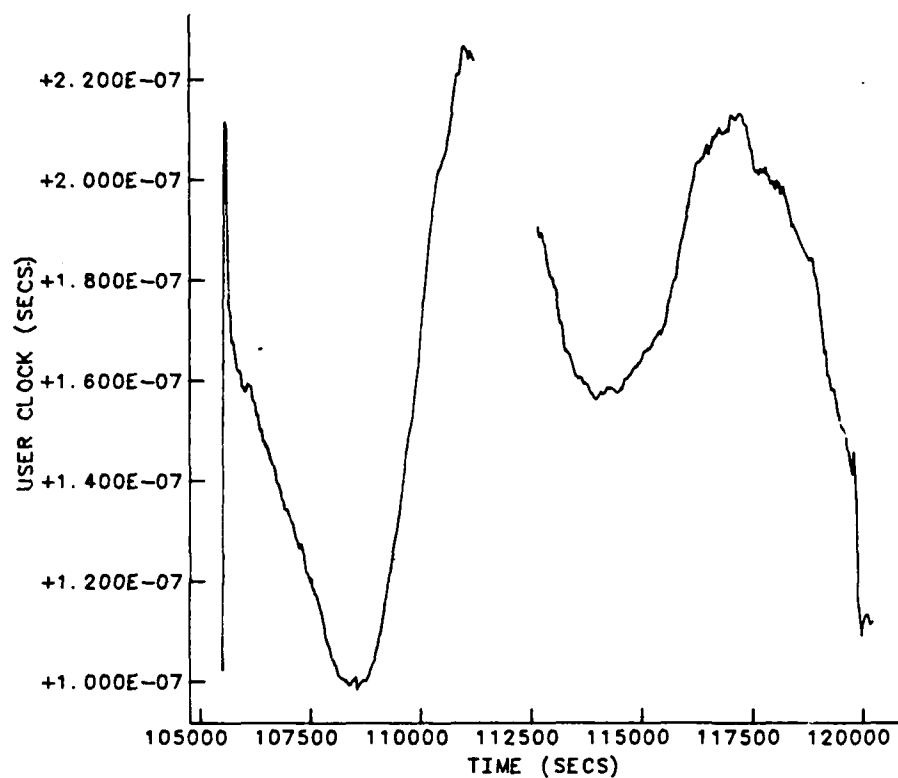


FIGURE 4-16 CLOCK BIAS AT FORT DAVIS - APRIL 1, 1985

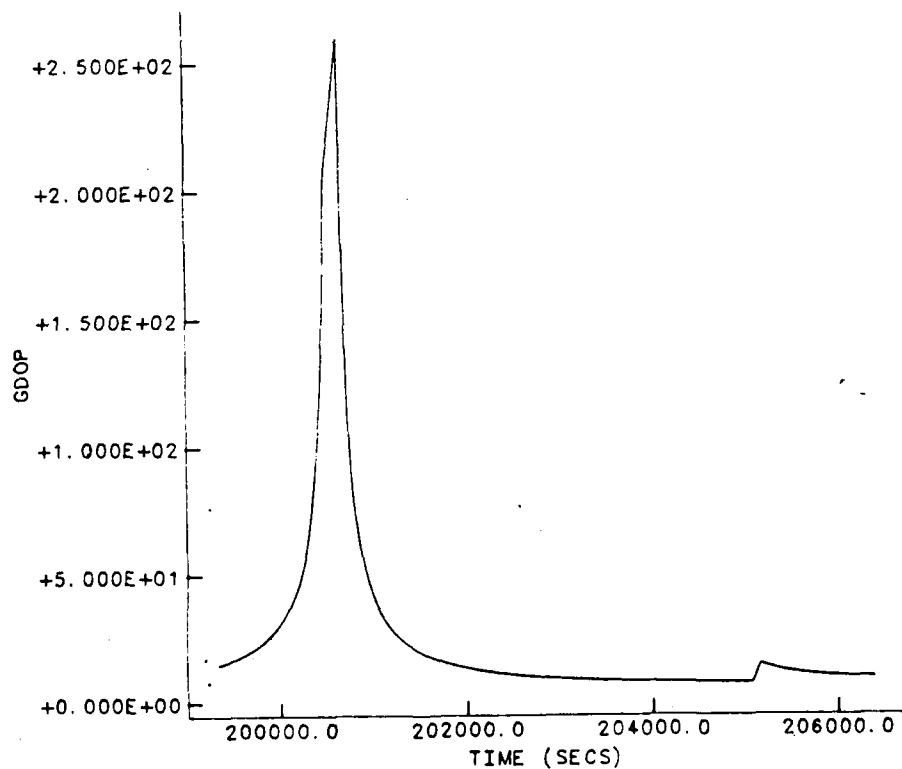


FIGURE 4-17 GDOP AT FORT DAVIS - APRIL 2, 1985

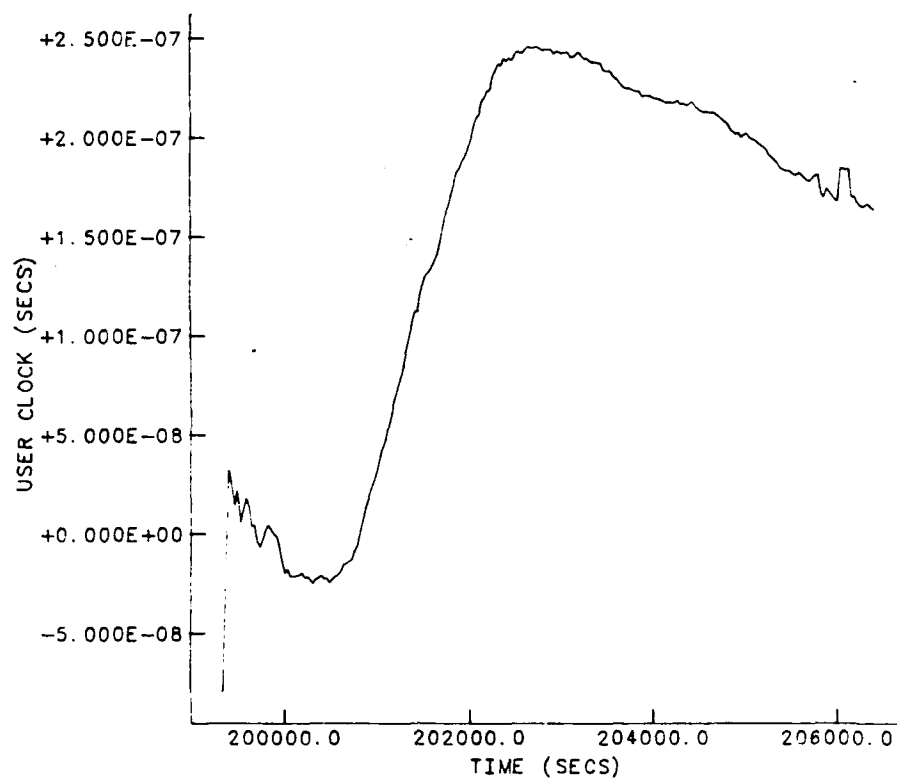


FIGURE 4-18 CLOCK BIAS AT FORT DAVIS - APRIL 2, 1985

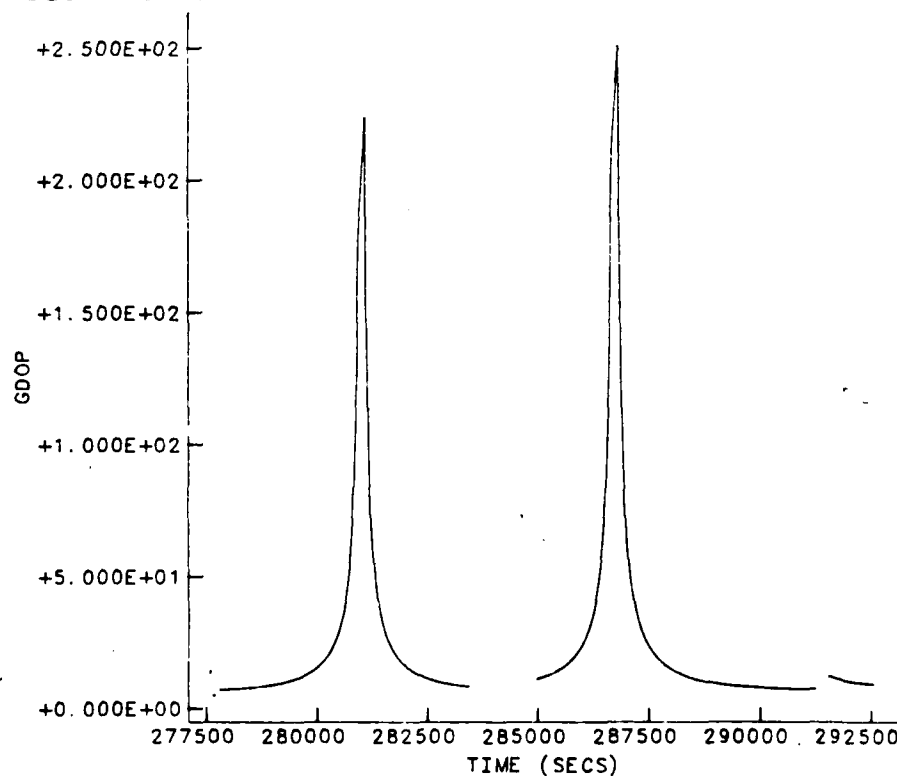


FIGURE 4-19 GDOP AT FORT DAVIS - APRIL 3, 1985

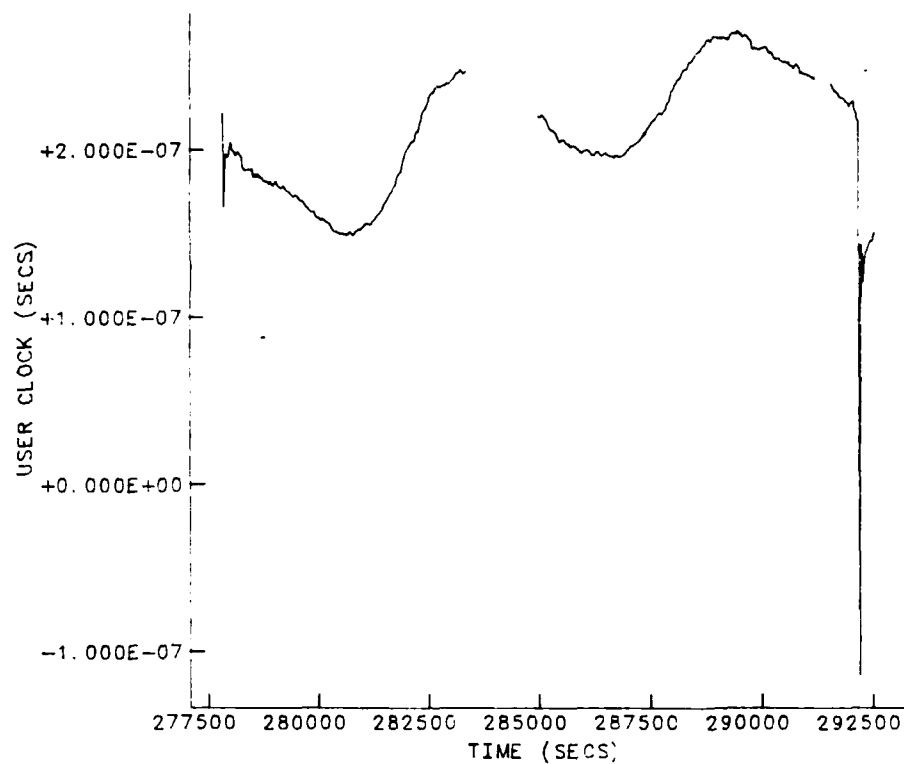


FIGURE 4-20 CLOCK BIAS AT FORT DAVIS - APRIL 3, 1985

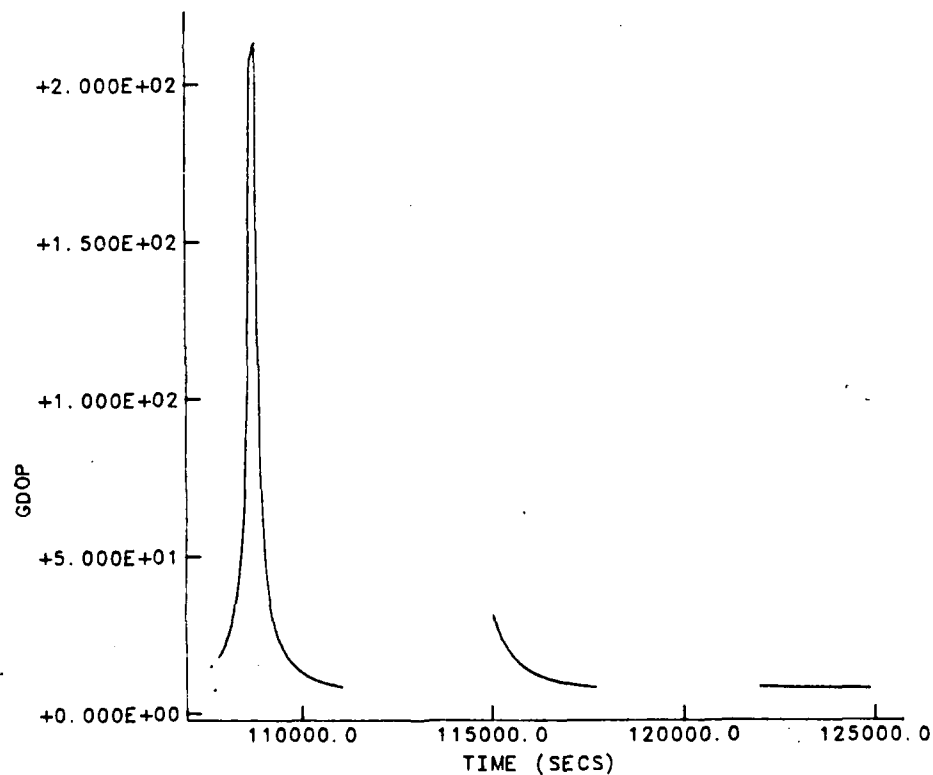


FIGURE 4-21 GDOP AT RICHMOND - APRIL 1, 1985

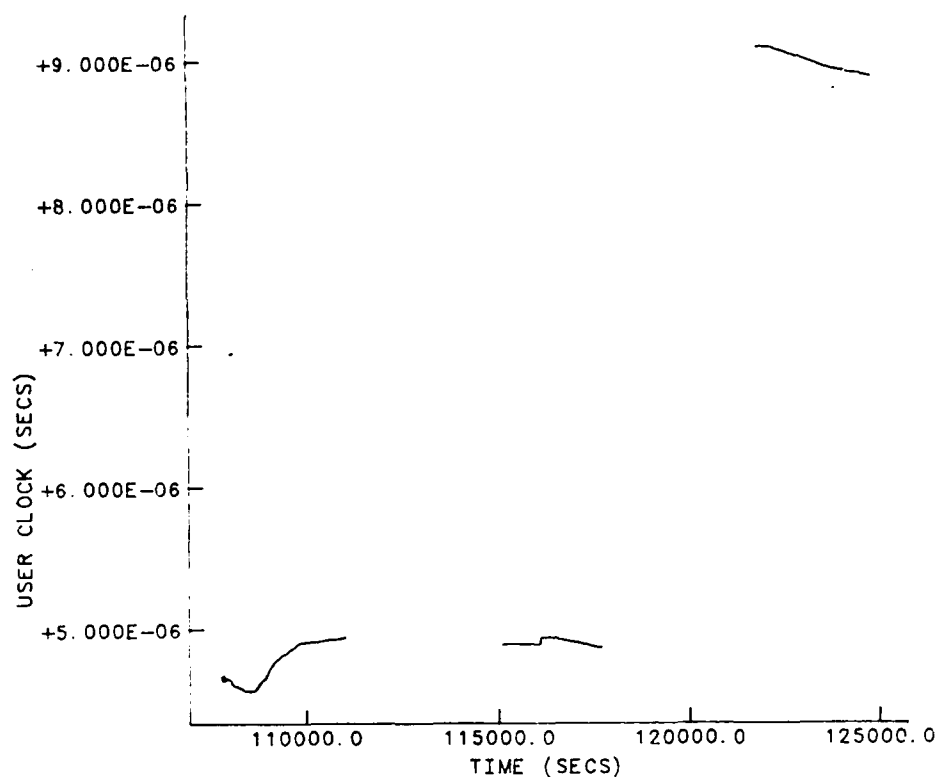


FIGURE 4-22 CLOCK BIAS AT RICHMOND - APRIL 1, 1985

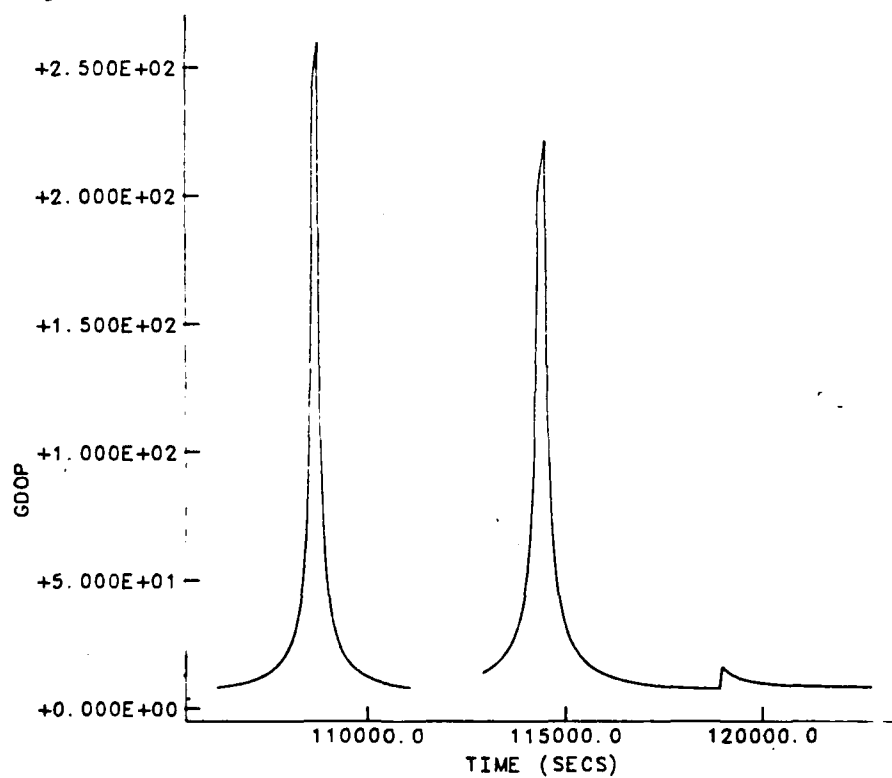


FIGURE 4-23 GDOP AT HAYSTACK - APRIL 1, 1985

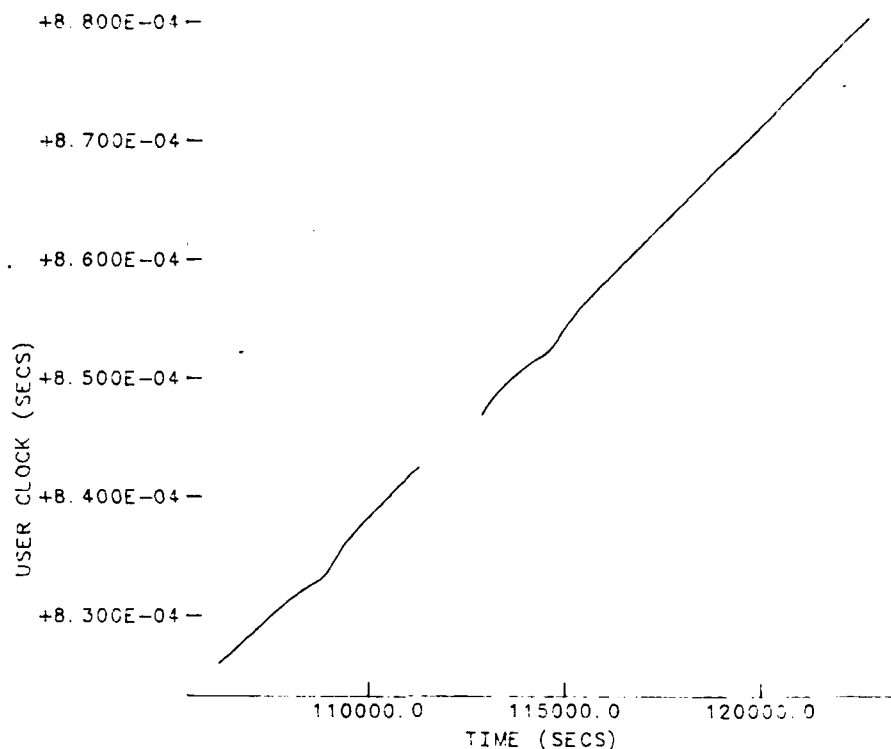


FIGURE 4-24 CLOCK BIAS AT HAYSTACK - APRIL 1, 1985

As mentioned, the RMS of residuals all remain under ten meters for all the test cases. Typical navigation solutions converge in two to four iterations (four to six iterations at Haystack) to an RMS of residuals between 0.20 meters and 9.55 meters. These RMS of residual values are composed of the residuals of the four pseudoranges required for the solution. The low values for the RMS of the residuals indicate accurate modelling of the actual pseudorange data (see Section 4.2 for a discussion of the residuals). Because of the accurate modelling, navigation solutions are assumed to accurately indicate the system capabilities. Another indicator of

accuracy is the covariance matrix, computed with each navigation solution.

The covariance matrix diagonal elements represent the statistical accuracy of the solution as far as the system is modelled accurately. The model accuracy from Chapter Two is time varying because of the constant ephemeris parameters, but bounded by ten meters in the xyz reference frame. Realizing this accuracy, then, as described in Section 4.2, the diagonal elements are the variances of the state. For this EKF, with the state noise compensator, the variances include the 0.5 meter^2 constant added to each diagonal element whenever the trace of the matrix drops below 1.0 meters^2 .

Table 4-2 displays the x-position variances for the first ten solutions at Fort Davis, Richmond and Haystack on April 1. These variances reveal the steady decline that represents improving confidence in the accuracy of the solution. At Fort Davis and Richmond the variances for all four state variables decrease like the x-position variance to below 1.0 meter^2 and remain there for most of the solutions.

Table 4-2
 x_u Position Variances (meters²), April 1, 1985

Estimate	Fort Davis	Richmond	Haystack
1	12.0	15.6	13.6
2	11.9	3.17	3.25
3	2.95	2.28	2.48
4	1.96	1.79	2.28
5	.973	1.47	2.17
6	.832	1.26	2.13
7	.726	1.10	2.11
8	.643	.977	2.09
9	.577	.881	2.08
10	.523	.804	2.07

The state noise constant, 0.5 meters², is added regularly at both sites. The Haystack variances, however, never reach a sufficiently small value to enable the state noise. Typical variances at Haystack are between 2.0 and 10.0 meters² for all four state variables, indicating slightly less confidence in the solution accuracy. A summary of these experiments with the EKF conclude this chapter.

4.4 Summary

The EKF navigation results show important characteristics of the GPS System which are nearly identical at the different receiver sites on different days. First of all, the values for the RMS of residuals are all below

ten meters, suggesting that the modelling of the system is good; i.e., the corrections to the calculated pseudoranges represent real effects in the transmitted pseudoranges. Another characteristic which demonstrates the solution accuracy is the covariance matrix; small variances indicating high confidence in the solutions realizing the ten meter accuracy limit in the orbit model. A third characteristic is the constellation geometry. When GDOP rises excessively the position errors also rise, to over 400 meters in two cases.

The next effect to be examined is the loss of accuracy caused by non-current ephemeris epochs. When one broadcast ephemeris epoch out of four is not current with the pseudoranges by one hour, then solution accuracy changes from under ten meters to under twenty meters. A further decrease in accuracy results when more than one satellite ephemeris epoch is different from the pseudorange measurement time by an hour or more. Finally, individual satellite characteristics affect the solutions, particularly SV04 with its inaccurate clock. In all but one case, when SV04 joins the constellation the position errors rise rapidly. The next chapter will describe navigation test cases using updated ephemerides from Chapter Three.

Chapter Five Navigation Accuracy With Updated Ephemeris

5.1 Introduction

The previous Chapters have established the foundation for investigating GPS navigation accuracy using old ephemerides which are updated with current pseudorange measurements. The ephemeris update algorithm and the sequential navigation algorithm from Chapters Three and Four can operate together to estimate the receiver position. This process simulates the loss of the Master Control Station (MCS) which normally uploads the satellite broadcast ephemerides. Without the MCS uploads, the satellites will continue to broadcast the stored, hourly ephemerides until their computer memory is empty. Each operational satellite can carry about a two-week supply of ephemerides. After their two-week memory is exhausted, the satellites will continue to broadcast "empty" messages, so a user can still receive pseudorange measurements but no useful ephemeris data will be transmitted. With the pseudorange measurements and outdated ephemerides from four visible satellites, a lone receiver can produce accurate position information. Tests of this process at Fort Davis, Texas, and Richmond, Florida, are the subject of this chapter. Also included

is a test of the effect that the variable Earth rate has on the navigation accuracy.

5.2 System and Algorithm Characteristics

Chapters Two through Four described the GPS ephemeris parameters, the update algorithm and the navigation process, respectively. In combination, under the Phase One Test conditions, they can produce surprisingly accurate navigation results. The best results occurred under conditions that will be routine for the full constellation, but were fairly specific for the test constellation. These test conditions are described in the following paragraphs.

The test constellation consisted of six satellites: SV06, SV08, SV09, SV11, SV12, and SV13. Data from three other satellites were excluded: SV04 had an inaccurate clock and satellites SV03 and SV07 were launched during the test period. Consequently, because of orbit timing only four satellites were visible to the receiver site; during any time block.

The test conditions were very similar to those in Chapter Three for updating old ephemerides and those in Chapter Four for estimating the receiver location(navigating). First, broadcast ephemerides and pseudorange measurements from the Phase One Tests on 20

and 21 November at Fort Davis and Richmond were used to establish a level of navigation accuracy possible on those dates. Then old broadcast ephemerides from previous months were updated using the pseudorange measurements on 20 and 21 November and the navigation process reinitiated with the updated ephemerides. The results show certain algorithm and system characteristics as well as the effect of the variable Earth rate on the navigation accuracy. Finally, the accuracy of navigating at Richmond with ephemerides updated at Fort Davis is shown.

On the test days of November 20-21, 1985, satellites SV08 and SV12 had short, low-elevation passes at Fort Davis and Richmond, causing degraded accuracy in their ephemeris updates (see Chapter Three). As a consequence, finding a time period with four, long-pass satellites in a good geometry, limited the test time to less than one hour per day. Satellites SV06, SV09, SV11, and SV13 formed a constellation that fit the criteria on 21 November. With a suitable constellation, it was possible to consider the GPS system characteristics that would affect the navigation accuracy.

Several system characteristics were considered in the navigation accuracy tests, including the perturbation parameter accuracy and GPS orbit adjustments. When the broadcast ephemerides were updated, only the Keplerian

and clock parameters were updated. The perturbation terms were not updated, so their inaccuracy introduced some error in the satellite position calculation. This error in the satellite position may have been a major error in the navigation solution. As reported in Section 3.5.B, satellite position errors caused by the old perturbation parameter values ranged from 8.8 meters to 107.1 meters for SV11, with the radial components often being large. However, another system characteristic tended to negate individual satellite position errors: four satellites were used simultaneously, so the error in one parameter of one satellite had less effect on the whole navigation solution than on the individual satellite location. That is, although the individual satellite positions may have been in error, the four-satellite triangulation process cancelled some of the error.

Updating the ephemerides over a month or more required the consideration of natural and programmed orbit changes. The natural changes resulted from the primary perturbations, both gravitational and nongravitational forces. One nongravitational perturbation is solar activity which can have large effects on a low altitude orbit but has very little effect on the GPS orbits. During the months July through November 1985, there were five major and fourteen minor solar events,

as reported by the 4th Weather Wing[Hayward, 1987]. As shown in the test results, any orbit changes caused by the solar events were not noticeable.

Another nongravitational perturbation on GPS satellites is called y bias due to its characteristic acceleration along the satellite y axis. According to Fliegel,et.al.,[1985], this acceleration is on the order of 0.2×10^{-9} meters per second squared along the solar panel beam(y axis). Attempts to model the acceleration suggest that a combination of spacecraft thermal radiation, solar panel and sensor misalignment, and control bias contribute to the y bias. Changes in the GPS orbits due to the y bias during the Phase One Tests were probable, however, the magnitude of the effect was not known.

Other unmodelled orbit changes may have resulted from programmed orbit corrections or from momentum dumping. The General Dynamics Services Corporation[Chasko, private communication, 1987], indicated no large orbit corrections or asymmetric momentum dumps during the ephemeris update times in this study. However, it can be noted that from approximately November 1986 through April 1987, at least one satellite was programmed to change its position in orbit one degree per day as part of a test constellation correction[Rhodus, private communication, 1987]. Consequently, large, unmodelled orbit changes can

occur.

Understanding these system characteristics was important to this study and any future studies. However, understanding the various effects was limited because they were difficult to quantify. The perturbation parameter inaccuracies affected the satellite positions during navigation but because there were nine uncorrected parameters in each of four ephemerides, the size of the individual effect was not clear. The orbit adjustments also affected the satellite positions, but in an unknown manner. Solar pressure and asymmetric momentum dumping could have affected any of the parameters by a significant amount. Consequently, the solution precision relied largely on the pseudorange measurements on the test dates to provide an accurate basis for updating the six Keplerian parameters and two clock parameters from the old ephemerides.

Three algorithm characteristics influenced the navigation accuracy most, two in a positive manner while the other in a negative manner. The negative effect was the ill-conditioning in the ephemeris update algorithm. Although the updated ephemerides compared closely with the actual broadcast ephemerides, there was some error. Because the normal matrix condition numbers were so large in the update solution a slight variation in the initial

conditions may have resulted in significant changes in the updated ephemerides (see Chapter Three). Satellite position errors ranging from 839 meters to 13,533 meters resulted from these parameter differences on the 21 November updates. Any error in the computed satellite position affected the navigation accuracy.

One positive influence on accuracy was the EKF, used for the navigation solution. As described in Chapter Four, the sequential algorithm smoothed some large changes in the solution caused by measurement noise. Thus, the position error was characterized by fairly steady behavior over long periods, as shown in Section 5.3. The other positive factor was navigating at the same receiver site that was used to update the ephemerides. Because the ephemeris update algorithm required the precise receiver site coordinates, the navigation results at the same site using updated ephemerides were very good. Validation of the navigation process with updated ephemerides was possible by this means. Navigation at Richmond, Florida, using updated ephemerides from Fort Davis, Texas, showed the accuracy that was possible in a more general case.

These GPS system characteristics and algorithm characteristics indicate that many variables exist in the navigation tests that can influence navigation accuracy.

Establishing a controlled set of experiments was difficult, however, using the four satellites with long passes on 21 November produced very accurate and consistent results which allowed several significant conclusions about navigation accuracy using updated ephemerides. These results and conclusions are presented in the next section dealing with the actual experiments.

Another system error source is the fact that the Earth rotation rate is not a constant and although it changes very slowly, over long time periods the change must be accounted for in some processes. The correction term for the variable Earth rate is the quantity UT1-UTC, or ΔUT1 , which is the difference between Coordinated Universal Time (UTC) and Universal Time corrected for the observed motion of the geographic pole (UT1)[Almanac, 1986]. As tabulated by the Astronomical Almanac, UT1-UTC shows a long-term decrease in the Earth rate. For updating the broadcast ephemerides the variable Earth rate may play a significant part, growing in significance with longer times between updates. To test this hypothesis, updates were run with and without the UT1-UTC correction and the navigation accuracy was compared. According to Dr. Raynor L. Duncombe[private communication, 1985] and Dr. Dennis McCarthy[private communication, 1985], the Earth rate correction manifests itself in the measurement

times from the GPS satellites. Consequently, the difference between the UT1-UTC for the input broadcast ephemeris time and the update ephemeris time was added to the measurement time in the update algorithm. For instance, UT1-UTC for 13 September 1985 was 0.4947 seconds and for 21 November it was 0.3754 seconds. The difference in the UT1-UTC values on those dates, $\Delta(\text{UT1-UTC}) = -0.1193$ seconds, represented the difference in the Earth rate that might have affected the accuracy of the updated ephemerides if it were not included in the update algorithm. The $\Delta(\text{UT1-UTC})$ value was added to each measurement time to correct for the variable Earth rate. For instance, the first measurement time on 21 November was 399,899.74 seconds past 00:00 Sunday, 17 November. The corrected time was 399,899.6207 seconds. To show the variable Earth rate effect, two sets of updated ephemerides were tested in the navigation algorithm, one with and one without the Earth rate correction. The results for the navigation on 21 November showed that the variable Earth rate need not be included. The experiments with the navigation algorithm and updated ephemerides are presented next.

5.3 Experiments in Navigation Using Updated Ephemerides

The navigation accuracy tests were conducted with data from November 20-21, 1985 with the best results occurring on 21 November. Updated ephemerides from Fort Davis on 5 April, 11 June, 13 August, 13 September, 11 October, and 21 November were used to navigate at Fort Davis to test the consistency of the results and evaluate the effect of the variable Earth rate. Updated ephemerides from Fort Davis were used to navigate at Richmond to demonstrate the effect of a physical separation between the ephemeris update site and the navigation site. To set a basis for comparison, the position error and GDOP using the actual broadcast ephemerides on 21 November were determined. These broadcast ephemerides were updated on the same day and the position error determined. Next, old ephemerides were updated at Fort Davis, once with and once without the Earth rate corrections, and position error for Fort Davis was obtained. Finally, the updated ephemerides from Fort Davis were used for navigation at Richmond.

A. Navigation Accuracy with Broadcast Ephemerides on 21 November

The first navigation case used the broadcast ephem-

erides and pseudoranges that were received at Fort Davis on 21 November to determine the expected navigation accuracy on that date. The first two solutions were the differential correction estimates described in Chapter Four. The DCA estimates of the state and covariance matrix were then input to the EKF for the subsequent solutions. The initial conditions were the exact receiver antenna phase center coordinates and the user clock bias listed in Chapter Three. Perturbed initial conditions are not described because the results demonstrated no change in the navigation accuracy.

Figures 5-1 and 5-2 show the navigation position error and GDOP for the first case. The position error is defined as the straight line distance between the surveyed site and the position estimate. As described in Chapter Four, because the broadcast data came from the Phase One Test storage tapes, the broadcast ephemeris epochs were sometimes more than an hour different from the measurement times. For instance, where the position error reached 60 meters, at 402,389 seconds, the ephemeris epochs for SV06 and SV11 were 6,389 seconds behind the measurements times. As described in Chapter Four, having the ephemeris epochs different than the measurement time caused some increase in the position error. Note the very small rise in the position error caused by

the GDOP spike at 397,000 seconds. Usually the rise was much more pronounced but in this case the EKF remained steady.

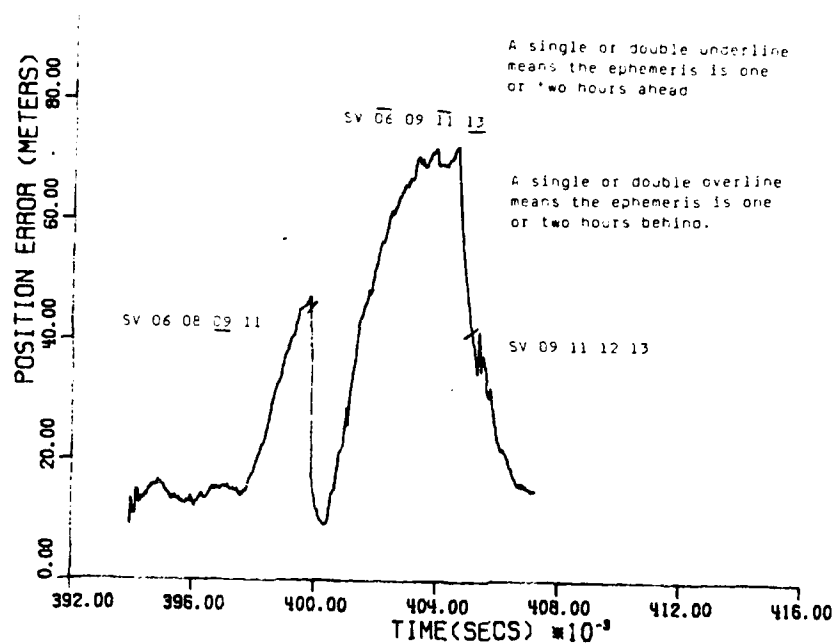


FIGURE 5-1 POSITION ERROR - BROADCAST EPHEMERIDES 21 NOV

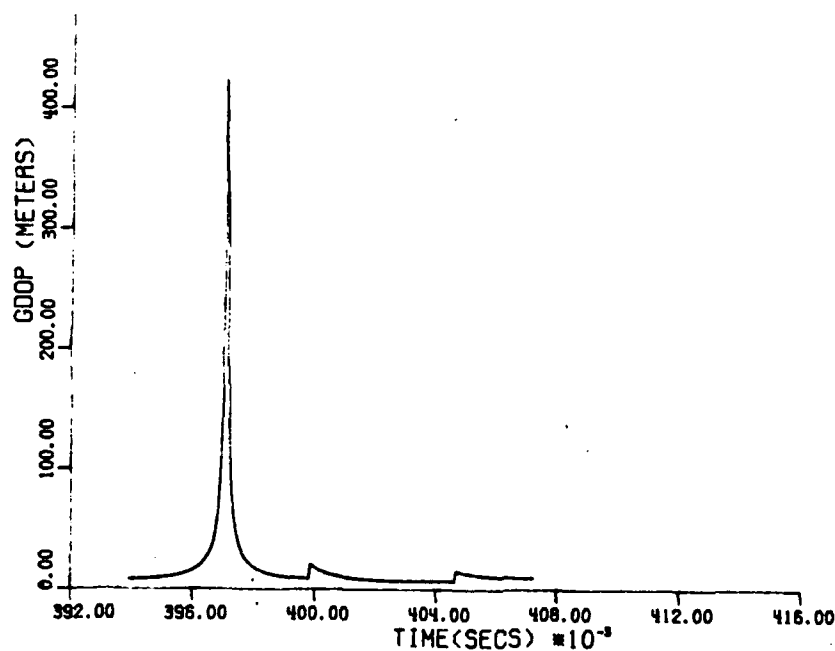


FIGURE 5-2 GDOP - BROADCAST EPHEMERIDES 21 NOV

B. Navigation Accuracy with Updated Ephemerides on 21 November

Figure 5-3 shows the position error after updating the ephemerides for SVO6, SVO9, SV11, and SV13. The time span was the same as the middle time period on Figure 5-1, from approximately 400,000 seconds to 405,000 seconds past 00:00 Sunday, 17 November. Figure 5-3 indicates that excellent accuracy was possible when navigating at the same site where the ephemeris updates were made. Some of the improvement was attributed to having all four ephemeris epochs updated to the same hour, 399,600 seconds, so navigation occurred with the current-hour ephemerides. Also, some improvement came from using current pseudoranges for the ephemeris updates since the broadcast ephemerides were based on measurements over a week. This first case did not test the Earth rate correction because the updates were on the same day as the broadcast ephemerides.

The confidence in the position estimate, as shown in the covariance matrix diagonal terms, was the same order of magnitude as the position error and improved slightly with new estimates. The first estimated position had a combined x, y, z position one sigma value of 7.77 meters. The tenth position estimate one sigma was 7.11 meters,

and the trend toward increased confidence continued with time.

Analyzing the accuracy of the updated ephemerides indicated the same characteristics as described in Chapter Three: the RMS of residual values were under ten meters using 600 observations, the parameters differed very little from the actual broadcast parameters (u_0 for SV11 differed by 0.0002514 percent), and the covariance

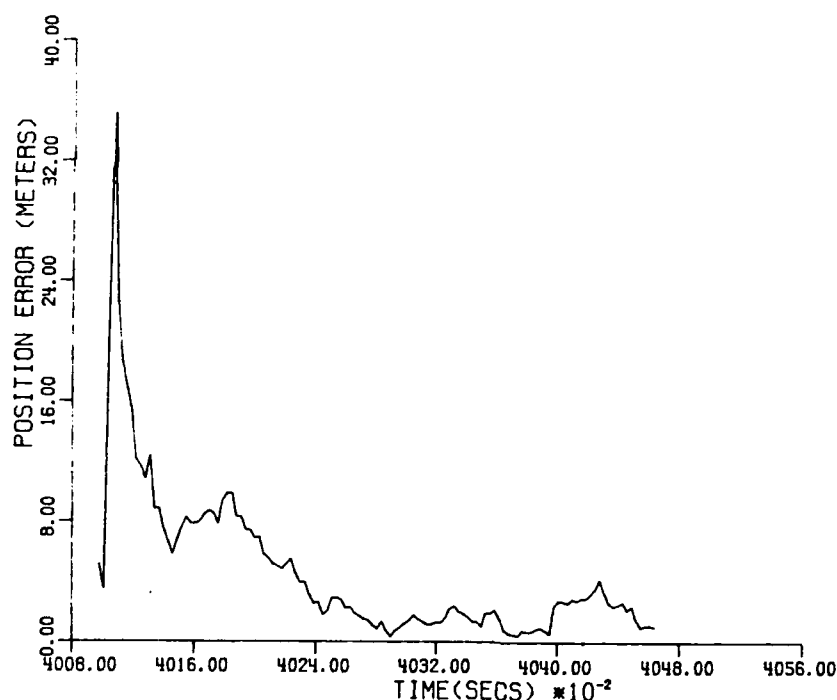


FIGURE 5-3 POSITION ERROR - UPDATED EPHEMERIDES 21 NOV

one sigma values were small ($1.58E-4$ radians for M_0 for SV11). The four satellite position errors were

1145 meters, 1918 meters, 839 meters, and 1651 meters for SV06, SV09, SV11, and SV13, respectively. However, their radial position errors were an order of magnitude smaller; 166 meters, 139 meters, 47 meters, and -255 meters, respectively. These radial position errors give an indication of the precision required for accurate navigation solutions.

B.1. 11 October Ephemerides Updated on 21 November

The second test used updated ephemerides from 11 October and produced navigation solutions at the same times as the previous case. Figure 5-4 shows the position error without the Earth rate correction and Figure 5-5 includes the correction ($\Delta(\text{UT1-UTC}) = -0.0767$ seconds, between 11 October and 21 November). The consistent position error under ten meters in Figure 5-4 represents successful navigation with the updated ephemerides. The accuracy is reduced in Figure 5-5, clearly indicating that the $\Delta(\text{UT1-UTC})$ values adversely affected the position accuracy.

The updated ephemerides were almost as accurate as the previous case. The position estimate one sigma values for these two cases remained nearly identical to each other as well as to the previous case. The satellite position errors were larger than the previous case.

but the radial components were good enough to produce the accurate navigation results. The position errors were 13,533 meters, 2006 meters, 8293 meters, and 3016 meters, while the radial components were 1674 meters, 144 meters, 284 meters, and 233 meters, for SV06, SV09, SV11, and SV13, respectively. Although the radial component for SV06 was much larger than previously, the navigation process produced very accurate results.

Comparing the Earth-rate corrected updated ephemerides with the updated ephemerides not corrected for the variable Earth rate revealed how the $\Delta(\text{UT1-UTC})$ affected the satellite ephemerides. The updated parameter values were identical to 12 significant digits for the four parameters that do not have rate terms: e , \sqrt{A} , i , and ω . The two parameters with rate terms: M_0 and Ω were different in the fifth and sixth significant digits and the clock bias and rate parameters differed in the eighth and ninth significant digit, respectively. The difference in the M_0 values (0.0000108 radians) amounted to a 289 meter in-plane correction at the orbit radius. Thus when compared to the M_0 value uncorrected for Earth rate, the M_0 term for the Earth-rate-corrected case added a 289 meter in-plane error to the satellites' positions. The Ω_0 difference caused out-of-plane error and the two clock parameter

differences caused minor variations in the combined error. Further discussion of this phenomenon is given later.

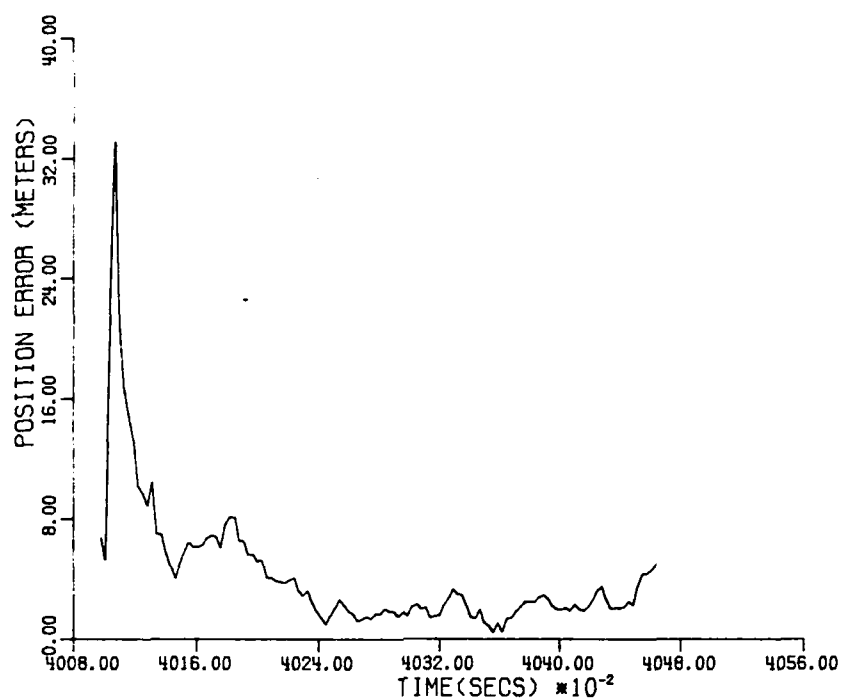


FIGURE 5-4 POSITION ERROR - UPDATED EPHEMERIDES 11 OCT
NO EARTH RATE CORRECTION

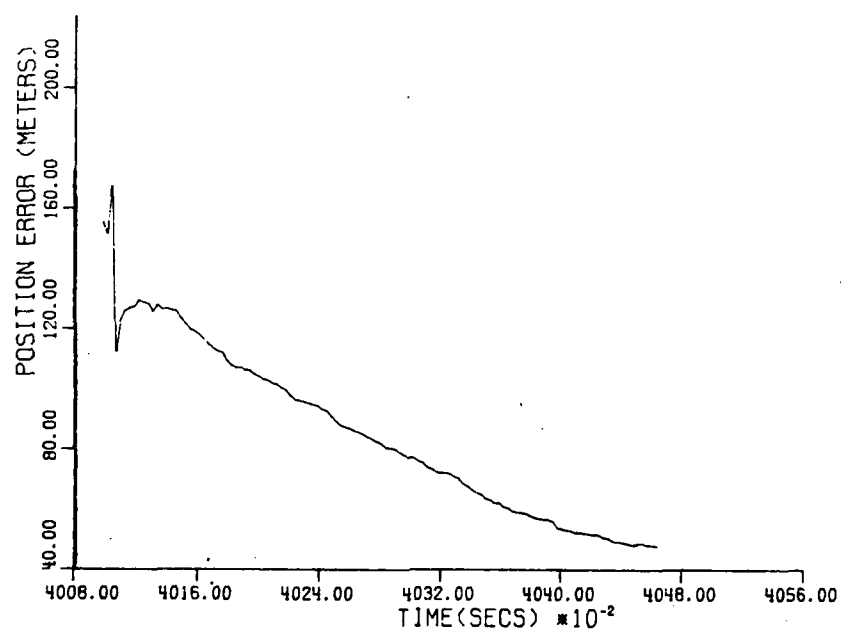


FIGURE 5-5 POSITION ERROR - UPDATED EPHEMERIDES 11 OCT
WITH EARTH RATE CORRECTION

B.2. 13 September Ephemerides Updated on 21 November

The next case used updated ephemerides from 13 September. Moving the four satellites' ephemerides forward ten weeks to 21 November produced the navigation position errors in Figures 5-6 and 5-7. Again, these position errors without the Earth rate correction, Figure 5-6, were better than those with the correction, Figure 5-7. The accuracy with the Earth rate correction was worse on 13 September than on 11 October, by a constant ratio. That is, the ratio of the Earth rate corrections between 11 October and 13 September was 0.65, and the ratio of the two initial position errors was 0.64, indicating a strong connection between the Earth rate correction and the increase in navigation position error.

The position errors in Figure 5-6 did not fall below ten meters until 404,339.7 seconds. This was unusual since the case was so similar to the 11 October case except for the input broadcast ephemerides to the update algorithm. The most likely cause is the ill-conditioning in the update solutions. The ill-conditioning added to the individual satellite position errors which ranged from 5688 meters to 13,332 meters. The radial components were much better at 1313 meters, 185 meters, 426 meters, and -495 meters, respectively, for the same four satel-

lites as the previous cases. These radial components of the satellite position errors were slightly larger than the previous case, but the navigation position errors were significantly larger. Because of the many variables in these tests, it was difficult to identify a definite cause for the large navigation errors. The other accuracy criteria from the ephemeris update algorithm were nearly identical to the last two cases: the RMS of residuals, the one sigma values for the updated parameters, etc. However, the next three cases return to excellent navigation position accuracy and demonstrate consistency in the navigation.

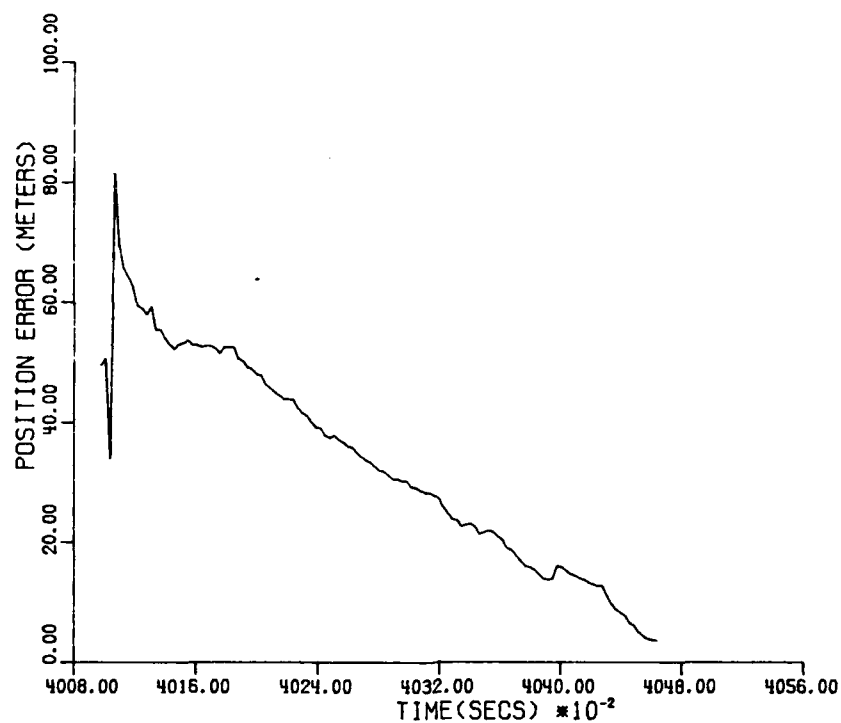


FIGURE 5-6 POSITION ERROR - UPDATED EPHEMERIDES 13 SEP
NO EARTH RATE CORRECTION

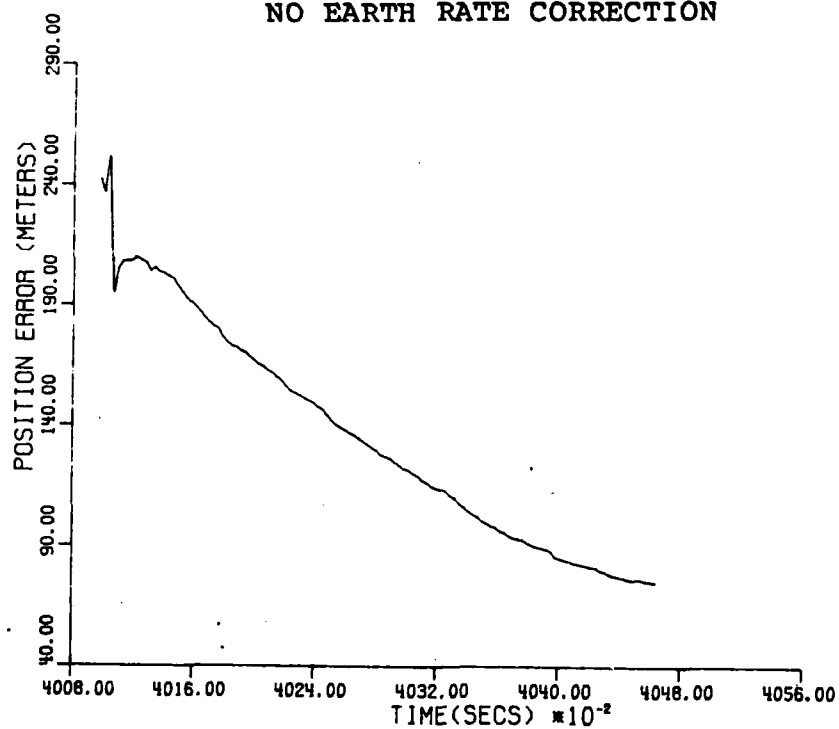


FIGURE 5-7 POSITION ERROR - UPDATED EPHEMERIDES 13 SEP
WITH EARTH RATE CORRECTION

B.3. Three, Five, and Seven Month Old Ephemerides Updated on 21 November

The cases with update ephemerides from 13 August, 11 June, and 5 April are presented in Figures 5-8 through 5-13. The similarities in Figures 5-8, 5-10, and 5-12 to Figures 5-3 and 5-4 indicate the repeatability of the navigation accuracy. Consistent results were possible with updates of seven months, and possibly longer. The growing inaccuracies in Figures 5-9, 5-11, and 5-13 show that as the value for $\Delta(\text{UT1-UTC})$ grew so did the navigation position error by the same ratio (between 11 October and 5 April, the ratio of the $\Delta(\text{UT1-UTC})$ values was 0.2495 and ratio of the initial navigation position errors was 0.2492).

For these three cases the satellite position errors remained at the kilometer level while the radial components were an order of magnitude or two smaller. Table 5-1, which is presented after the 20 November cases, compares the satellite position errors, the radial components, and the navigation position errors. The only conclusions about navigation accuracy available from Table 5-1 are that large satellite position errors tend to cause large navigation position errors and the smaller radial components of the satellite position errors con-

tribute to the better navigation accuracies. However, the ability to produce accurate navigation results with updated satellite ephemerides is demonstrated.

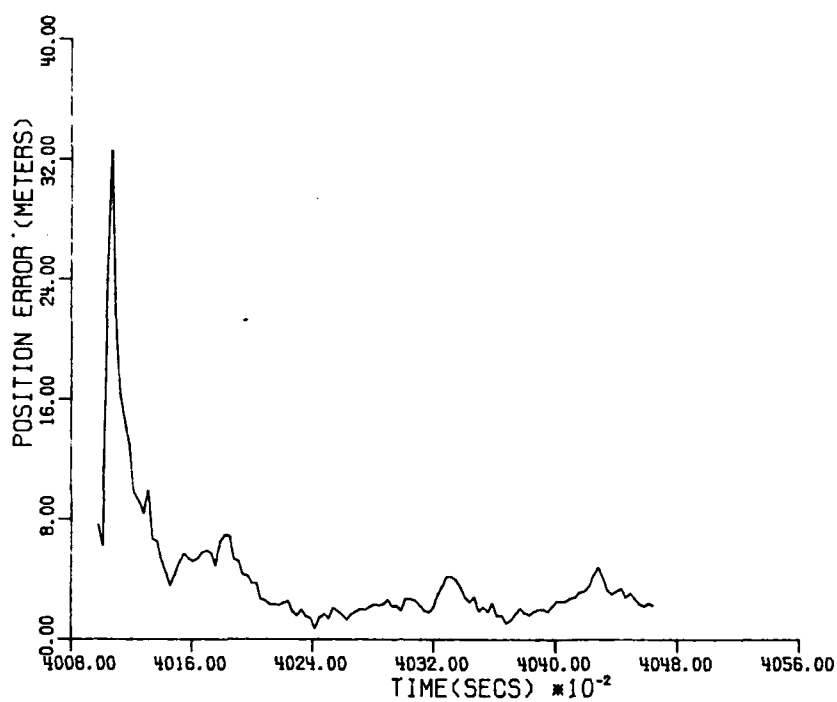


FIGURE 5-8 POSITION ERROR - UPDATED EPHEMERIDES 13 AUG
NO EARTH RATE CORRECTION

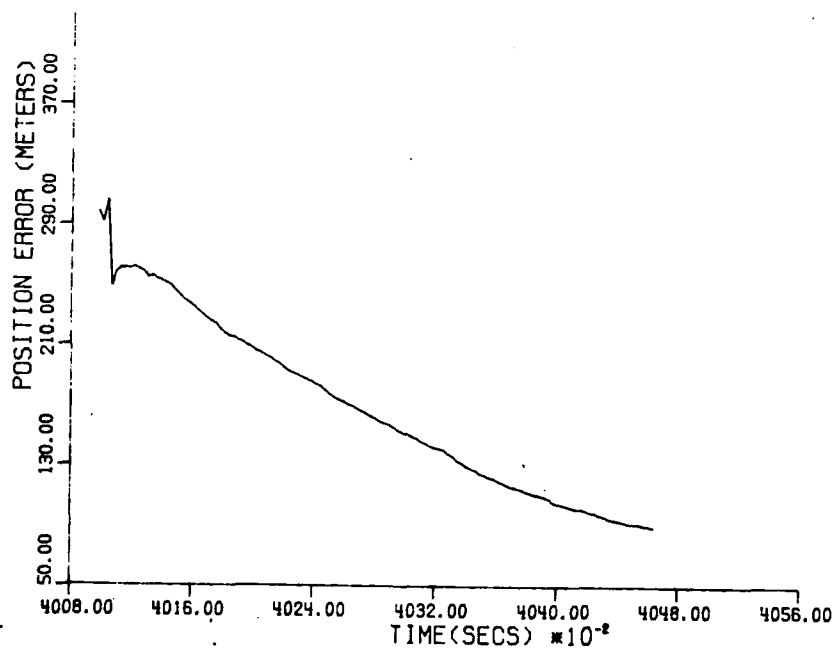


FIGURE 5-9 POSITION ERROR - UPDATED EPHEMERIDES 13 AUG
WITH EARTH RATE CORRECTION

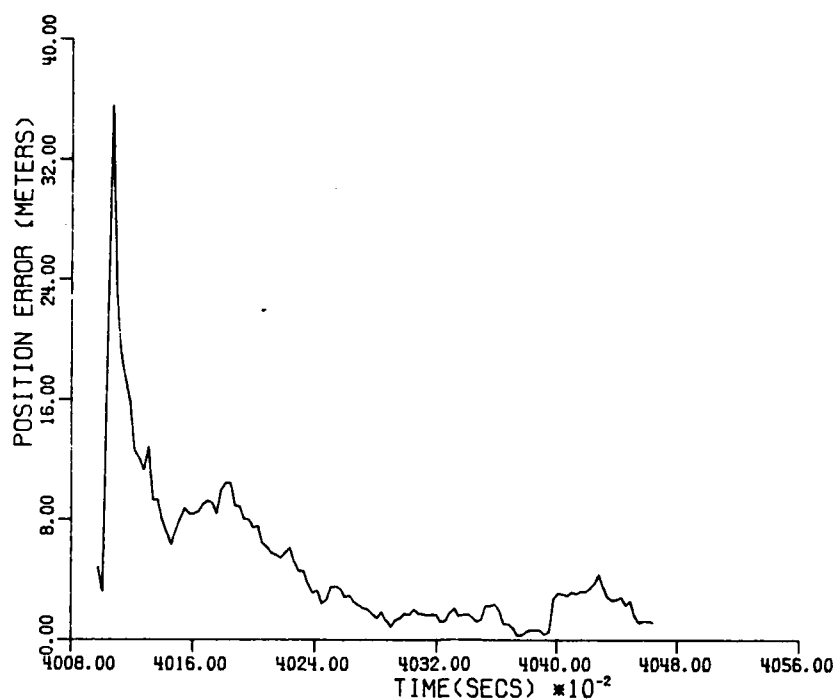


FIGURE 5-10 POSITION ERROR - UPDATED EPHEMERIDES 11 JUN
NO EARTH RATE CORRECTION

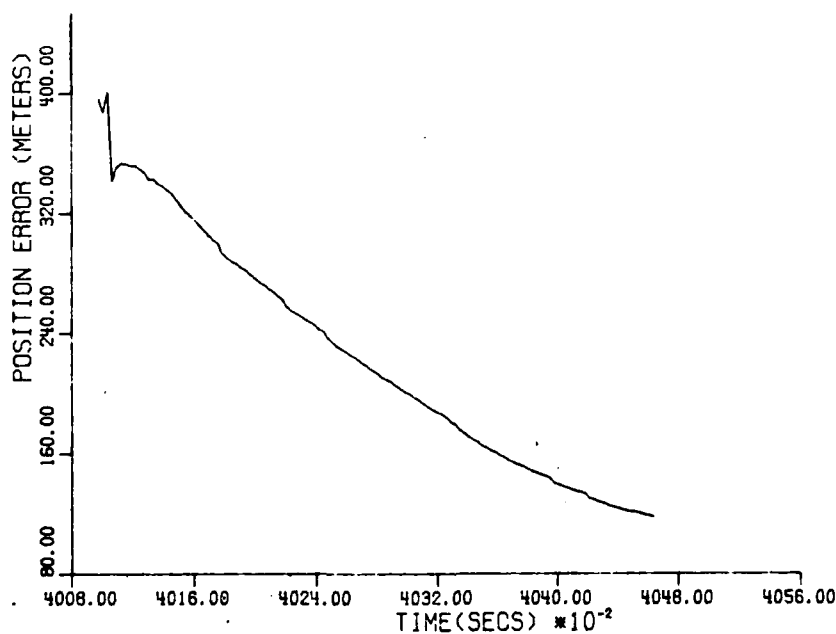


FIGURE 5-11 POSITION ERROR - UPDATED EPHEMERIDES 11 JUN
WITH EARTH RATE CORRECTION

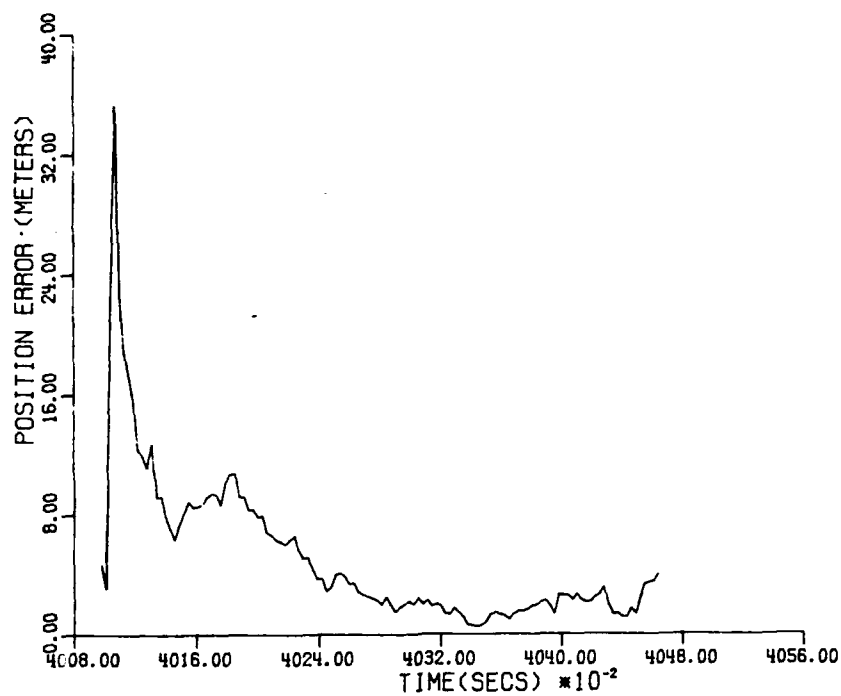


FIGURE 5-12 POSITION ERROR - UPDATED EPHEMERIDES 5 APR
NO EARTH RATE CORRECTION

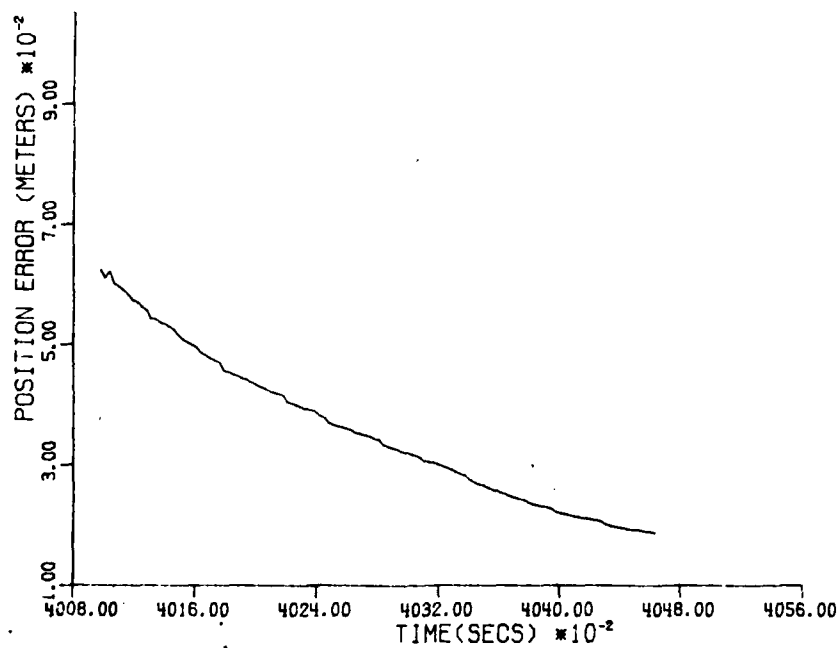


FIGURE 5-13 POSITION ERROR-UPDATED EPHEMERIDES 5 APR
WITH EARTH RATE CORRECTION

These positive results represent the high accuracy achievable with the updated ephemerides. By accounting for the system and algorithm characteristics and by choosing an appropriate test constellation it was possible to get position errors which compared with real time results. The variable Earth rate correction did not improve the results in the short or long term. In fact, the Earth-rate-corrected results showed just the opposite; that is, correcting for the variable rate reduced accuracy. The reason for this situation lay in the ephemeris update algorithm: the old broadcast ephemerides acted only as initial conditions to the processor. The algorithm converged to similar values with any input ephemeris that was within its convergence criteria, bearing in mind that the ill-conditioning may have affected the converged parameter values. Using current pseudorange measurements was the key to updating the ephemerides to the current time. The current pseudoranges represented actual ranges, corrected for various conditions, and, as such, included the current Earth rate, probably absorbed in the longitude of the ascending node parameter, Ω_0 . Thus, the variable Earth rate should not be included in the update algorithm to achieve the highest navigation accuracy.

C. Navigation Accuracy with the Broadcast Ephemerides on 20 November

Another navigation case used the actual broadcast ephemerides and pseudoranges that were received at Fort Davis on 20 November 1985. This 20 November case used the same software as the 21 November cases but a different satellite constellation was chosen to investigate the effect of a low elevation pass on the navigation accuracy. As with the 21 November cases, several hours of navigation solutions were created with the actual broadcast ephemerides to determine the accuracy possible on that date.

The navigation position error is shown in Figure 5-14 for three combinations of satellites. The first combination (SV06, SV08, SV09, and SV11) creates navigation accuracy from approximately 100 meters to about 55 meters. Note that SV09 has an ephemeris epoch that is two hours ahead of the pseudorange time. At time 313,900 seconds, satellite SV08 sets and SV13 rises with an ephemeris epoch that is three hours ahead of the current pseudorange time. Satellites SV06 and SV11 are one hour behind in their epochs. The navigation position errors start at 40 meters, decrease to under five meters, then increase again to about 35 meters, when SV06 sets.

Finally, SV12 rises at time 318,000 seconds with an ephemeris epoch that is two hours ahead of the pseudorange time. Satellites SV09 and SV11 do not have new ephemerides during this test, so their ephemeris epochs fall two and three hours behind, respectively. The satellite SV13 epoch is two hours ahead. The navigation position errors are very small for this third set of satellites (under ten meters), so this is the set chosen to investigate the low elevation pass of SV12.

These navigation position errors on 20 November compare favorably with the 21 November case with the actual broadcast ephemerides (Figure 5-1). Navigation position errors ranging from near zero meters to 100 meters are typical. The variations in accuracy resulted from the test constellation geometry and the broadcast ephemeris epochs differing from the pseudorange measurement times due to the lack of data on the Phase One Test storage tapes. In Figure 5-14 there was a GDOP spike at approximately 309,000 seconds causing the large position errors at the beginning. Other indicators of precision were very similar to the 21 November data: the first position estimate one sigma value was 7.74 meters and the RMS of the residual values remained under ten meters. Based on the navigation accuracy achieved using satellites SV09, SV11, SV12, and SV13, as shown in Figure 5-14, the

navigation accuracy using the updated ephemerides should have shown improvement like the 21 November updated cases, but these cases didn't show that improvement.

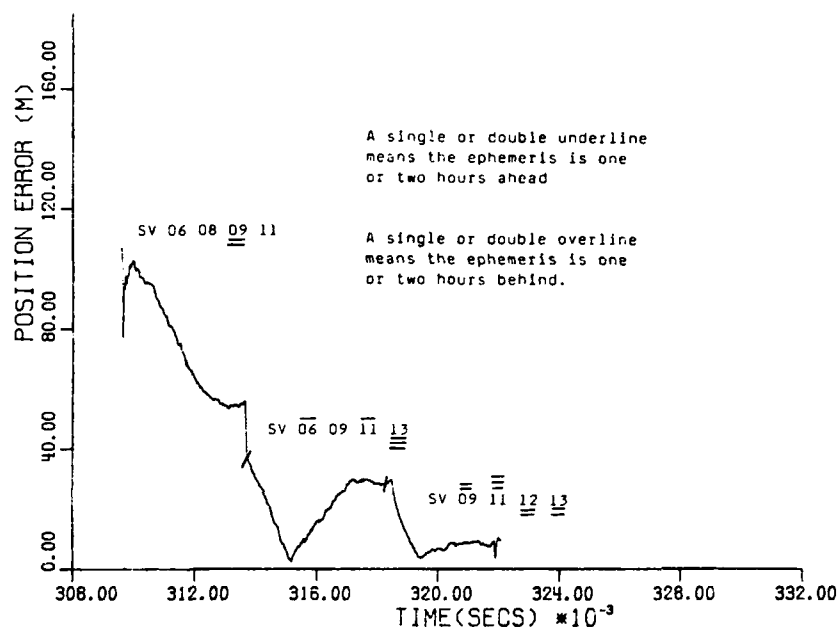


FIGURE 5-14 POSITION ERROR - BROADCAST EPHEMERIDES 20 NOV

D. Navigation Accuracy with Updated Ephemerides on 20 November

These navigation cases used updated ephemerides and pseudoranges to produce navigation solutions at 320,400 seconds on 20 November 1985 at Fort Davis, TX. Unlike the cases for updated ephemerides on 21 November, these cases showed a decrease in navigation accuracy due to

large satellite position errors, particularly the radial components. The navigation position errors are shown together in Figure 5-15 with no Earth rate correction, since the Earth rate correction produced a negative effect on navigation accuracy in previous cases.

The software for these cases was identical to the 21 November cases. However, the constellation was chosen to include SV09, SV11, SV12, and SV13 which passed over Fort Davis starting at 319,650 seconds. The pass for SV12 was low elevation and short, so only 400 observations were used to update its ephemeris, resulting in very large satellite position errors. Here, satellite position truth is taken as the satellite position calculated from the actual broadcast ephemerides from each of the four satellites at epoch 320,400 seconds on 20 November. Satellites SV09 and SV11 used 750 observations and also evidenced larger position errors than the 21 November case, possibly indicating a variation in the data collection process or another result of ill-conditioning in the ephemeris update algorithm. Satellite SV13 produced typical position errors using 750 observations and the radial components were very similar to the 21 November case. Table 5-1 compares the individual satellite position errors, the radial component, and the navigation position errors for the 20 and 21 November cases.

The first case on 20 November updated the actual broadcast satellite ephemerides on 20 November. The satellite position errors were 2044 meters, 3969 meters, 22,860 meters, and 11,168 meters, with radial components -898 meters, -633 meters, 1938 meters, and 386 meters, respectively. These satellite positions resulted in the first navigation position error being 79 meters, considerably larger than the 5 meter navigation error on 21 November. It is evident that larger radial components of the satellites position error caused larger navigation position errors, but predicting the magnitude of the navigation position error was difficult due to the large number of variables in the process. The Extended Kalman Filter overcame some of the error-inducing variables in the process since the navigation solutions steadily improved with time, as expected, to approximately 20 meters.

D.1. 11 October Ephemerides Updated on 20 November

The second test on 20 November used updated ephemerides from 11 October for the same four satellites and produced navigation solutions at Fort Davis for the same times as the previous case. Figure 5-15 shows the navigation position errors which start at 133 meters and steadily decrease to about 55 meters. From Table 5-1 the

satellite position errors for SV09 and SV12 are significantly larger than the previous case, as are their radial components. Satellite SV11 had slightly larger position errors and SV13 slightly smaller position errors. This combination of satellite position errors increased the navigation error by about 1.7 times. Again, large satellite radial position errors tended to cause large navigation errors, but predicting the magnitude of the navigation errors from the radial errors was difficult.

D.2. 13 September Ephemerides Updated on 20 November

The next case used 13 September ephemerides, updating them and navigating on 20 November at Fort Davis. As shown in Figure 5-15 the navigation solutions were slightly worse than the 11 October case, even though the satellite position errors and radial components were significantly larger for SV11 and SV12. Of course, the radial components for the other two satellites compensated slightly by decreasing. The navigation algorithm combined the four satellite positions in such a way as to reduce the effect of one or two satellites being grossly in error from the truth model.

D.3. Three, Five, and Seven Month Old Ephemerides
Updated on 20 November

The next three cases updated ephemerides from 13 August, 11 June, and 5 April on 20 November and composed navigation solutions at Fort Davis. The navigation position errors are shown in Figure 5-15 with the 13 August case producing the best accuracy, starting at a 60 meter error, decreasing to approximately five meters, then rising to 20 meters. The satellite position errors are all large but the radial components are an order of magnitude smaller than the position error magnitude for each satellite.

The 11 June case exhibited a navigation position error 1.5 times larger than the 13 August case but much better satellite position errors and radial components, violating the suggestion that the larger the radial position errors, the larger the navigation position errors. This case serves to emphasize that predicting the magnitude of the navigation error from the radial components of the satellite position error was difficult. However, when compared to the five meter navigation error in the 21 November cases, the 93 meter error supported the previous suggestion that larger radial position errors contributed to larger navigation errors.

The 5 April case concludes the navigation cases at Fort Davis. Here, three satellites had large position errors, SV09, SV12, and SV13, but only two had large radial components of the position error, SV09 and SV12. This combination of satellite positions created the largest of the navigation errors, starting at 162 meters and steadily decreasing to approximately 80 meters. Again, the navigation algorithm reduced the effect of individual satellite position errors to compute moderately accurate receiver position estimates.

This ability of the navigation algorithm to compensate for the satellite position errors was evident throughout this study, and is presented as a characteristic of the GPS system. Because the user must solve for his position as the intersection of four spheres, centered at each of the four satellites, the satellites' transverse and normal position errors are not as critical to the solution as the range to the satellites (the radii of the spheres). Also, the user navigation algorithm maintains some control over the range to the satellites by estimating the user clock bias along with the user position.

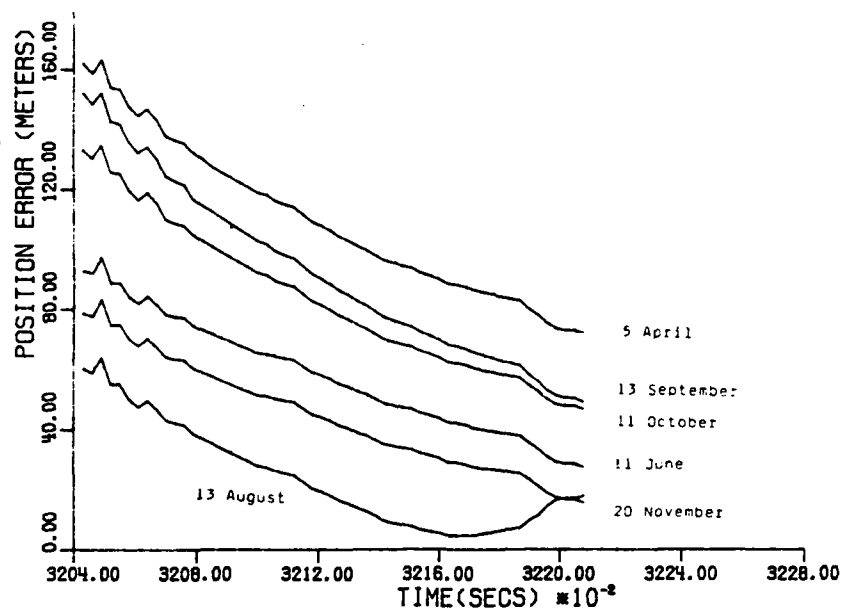


FIGURE 5-15 POSITION ERROR - UPDATED EPHEMERIDES
NO EARTH RATE CORRECTION

Table 5-1
Satellite Updated Position Errors, Radial
Component, and Subsequent Navigation Position Error

Ephemeris Date		Satellite Position Error (meters)					First Nav Error
Broad- cast	Update	SV06	SV09	SV11	SV12	SV13	
21 Nov	21 Nov	1145	1918	839	-	1651	5m
Radial		116	139	47	-	-255	
20 Nov	20 Nov	-	2044	3969	22,860	11,168	79m
Radial		-	-898	-633	1938	386	
11 Oct	21 Nov	13,533	2006	8295	-	3016	7m
Radial		1674	144	-284	-	-233	
11 Oct	20 Nov	-	7005	4064	60,705	8437	133m
Radial		-	-2049	-682	6160	255	
13 Sep	21 Nov	13,332	5696	11,582	-	5688	50m
Radial		1313	185	426	-	-495	
13 Sep	20 Nov	-	4794	8763	203127	9031	152m
Radial		-	-1257	-1375	22,712	152	
13 Aug	21 Nov	11,002	12,213	4054	-	9138	8m
Radial		1710	-285	-111	-	1189	
13 Aug	20 Nov	-	12,748	12,323	169534	9914	60m
Radial		-	1475	-1875	18,453	113	
11 Jun	21 Nov	1260	3398	1221	-	1102	5m
Radial		-305	311	39	-	-221	
11 Jun	20 Nov	-	3131	5554	22,052	10,859	93m
Radial		-	-1072	499	-3009	374	
5 Apr	21 Nov	16,619	11,638	2266	-	1373	5m
Radial		-2494	877	-91	-	-42	
5 Apr	20 Nov	-	18,708	4642	59,199	13,773	162m
Radial		-	-4113	463	6401	398	

E. Navigation Accuracy at Richmond, FL, with Broadcast Ephemerides on 21 November

The final tests for navigation accuracy were run at Richmond, Florida, on 21 November using the updated ephemerides from Fort Davis, Texas on the same date. These tests formed a more general case where the receiver site was known accurately for updating old ephemerides but the navigation site was assumed not to be known. Pseudorange measurements from the Richmond site and updated ephemerides from the Fort Davis site were inputs to the EKF and position errors between the estimated and the actual Richmond site were plotted. To demonstrate the accuracy possible at Richmond, results are shown in Figure 5-16 that used the actual broadcast ephemerides for satellites SV06, SV09, SV11, and SV13 pseudorange measurements at Richmond starting at 400,900 seconds. The large navigation position errors were partly due to the broadcast epoch times for satellites SV06 and SV11 being 4,900 seconds behind the initial pseudorange time, a characteristic of the data collected during the Phase One Tests. The epoch times for SV09 and SV13 were one hour ahead of the other two, at 399,600 seconds.

Other reasons for the large navigation position errors using the actual broadcast ephemerides are those

described in Chapter Four, namely, no elevation masking and no data editing. Also contributing, was the lack of a hydrogen maser oscillator at Richmond during the November tests. Without a precision oscillator, the receiver naturally added some random measurement noise to the pseudorange measurements.

Figures 5-18 and 5-19 show the GDOP and clock bias values for the broadcast ephemerides case. These two plots show the same characteristic as the plots in Chapter Four, namely, GDOP starts large but smoothly declines to about 7.90 meters, and the clock bias correlates highly with the position error.

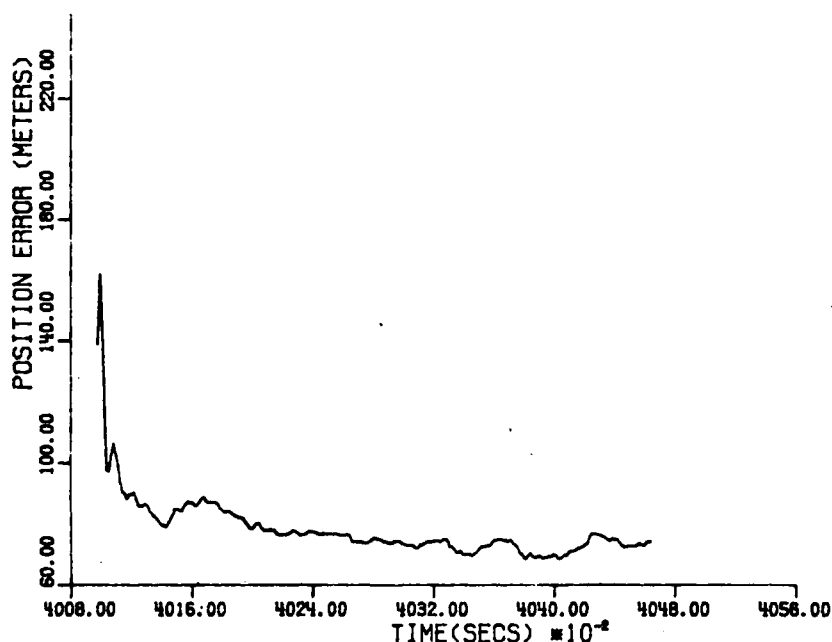


FIGURE 5-16 POSITION ERROR - RICHMOND
BROADCAST EPHEMERIDES - 21 NOV

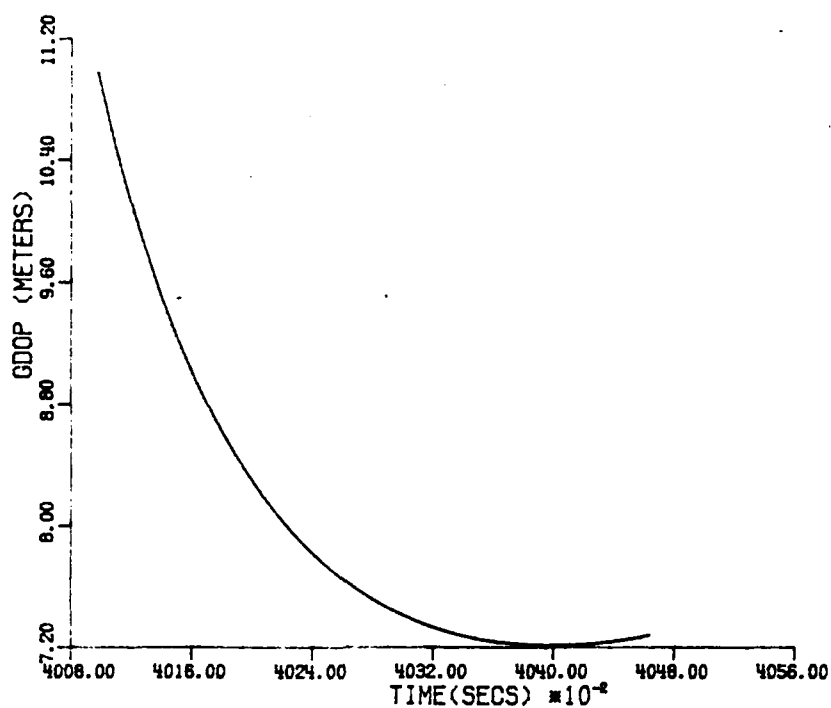


FIGURE 5-17 GDOP - RICHMOND - BROADCAST
EPHEMERIDES 21 NOV

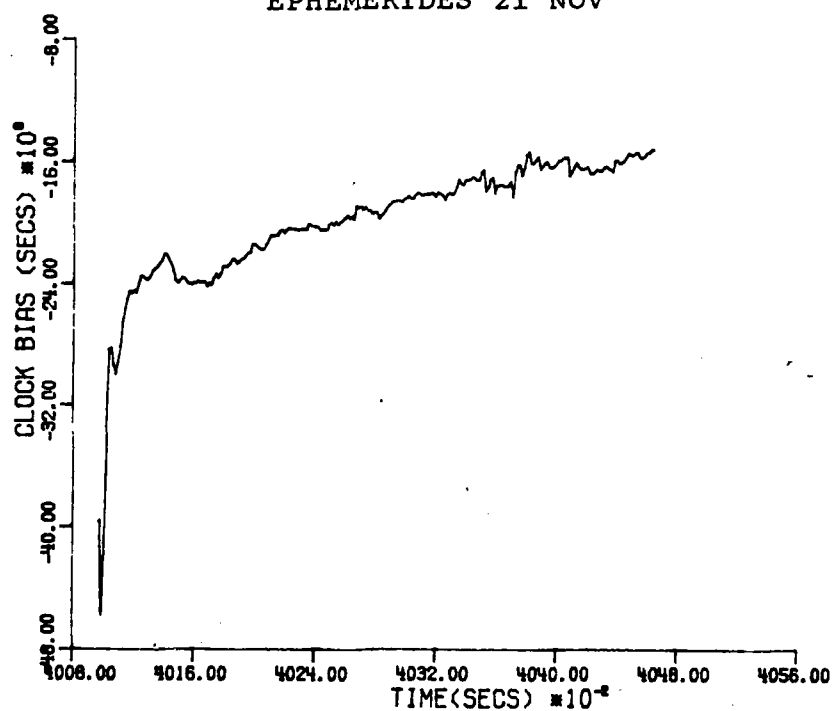


FIGURE 5-18 CLOCK BIAS - RICHMOND - BROADCAST
EPHEMERIDES 21 NOV

E.1. Navigation Accuracy at Richmond, with Updated Ephemerides from Fort Davis

The next case used the four 21 November broadcast ephemerides updated on 21 November at Fort Davis to navigate at Richmond, Figure 5-20. The updated ephemerides were the same that produced navigation position errors under eight meters at Fort Davis Figure 5-3. These results at Richmond demonstrated how the receiver site location affects the navigation accuracy, since this case used the same software and identical ephemerides for the same four satellites as the Fort Davis case. The only known differences were the initial conditions at Richmond (2,362,640 meters from Fort Davis) and the pseudorange measurements. So, unless there were unreported data collection anomalies, the large distance between Fort Davis and Richmond caused about a three-fold increase in the navigation error. Though the navigation errors are larger than the previous cases, they may be very satisfactory for many applications.

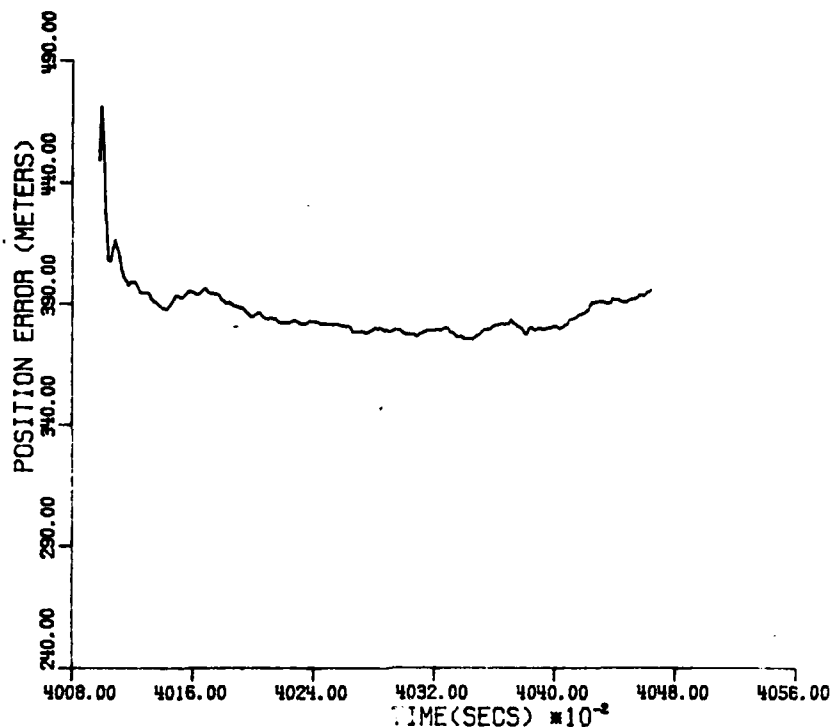


FIGURE 5-19 POSITION ERRORS - UPDATED EPHEMERIDES
RICHMOND 21 NOV

E.2 One to Seven Month Old Ephemerides Updated on 21 November at Fort Davis and Used at Richmond

The last five cases are very similar to one another using the same software and updated ephemerides from 11 October, 13 September, 13 August, 11 June, and 5 April at Fort Davis that were used in Sections B.1 to B.3, and navigating at Richmond. Again, only the initial conditions and the pseudorange measurements were different. The results were navigation position errors ranging from hundreds of meters to nearly three kilometers, Figures 5-20 to 5-24. These errors are much larger than previously, however, the ability to navigate at a location

other than the update site using updated ephemerides has been demonstrated. It is possible that navigation accuracy would increase with a navigation receiver that was connected to a hydrogen maser oscillator or located closer to the ephemeris update site. Again, for many applications, the final results may be satisfactory.

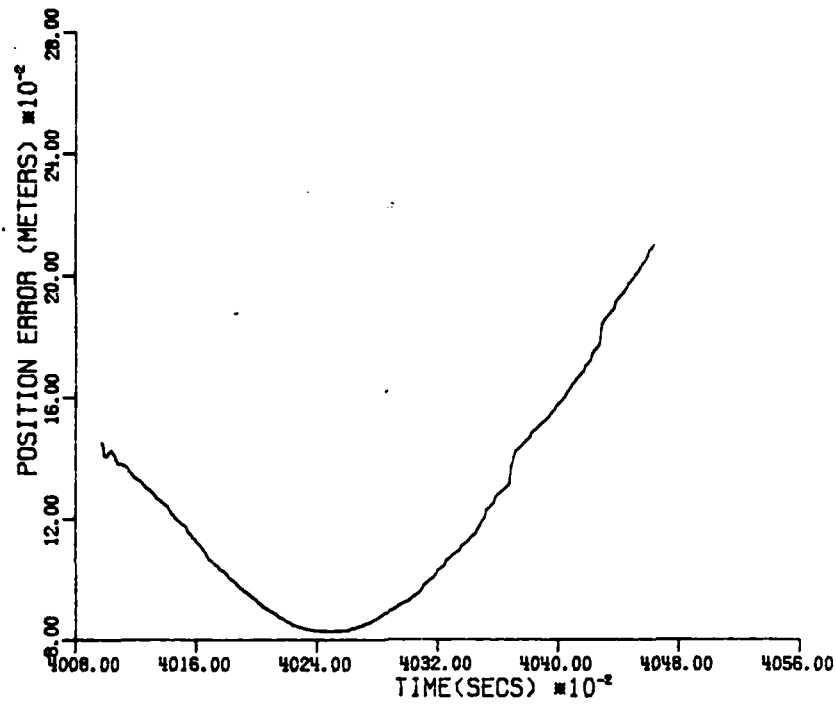


FIGURE 5-20 POSITION ERROR - UPDATED EPHEMERIDES
RICHMOND 11 OCT

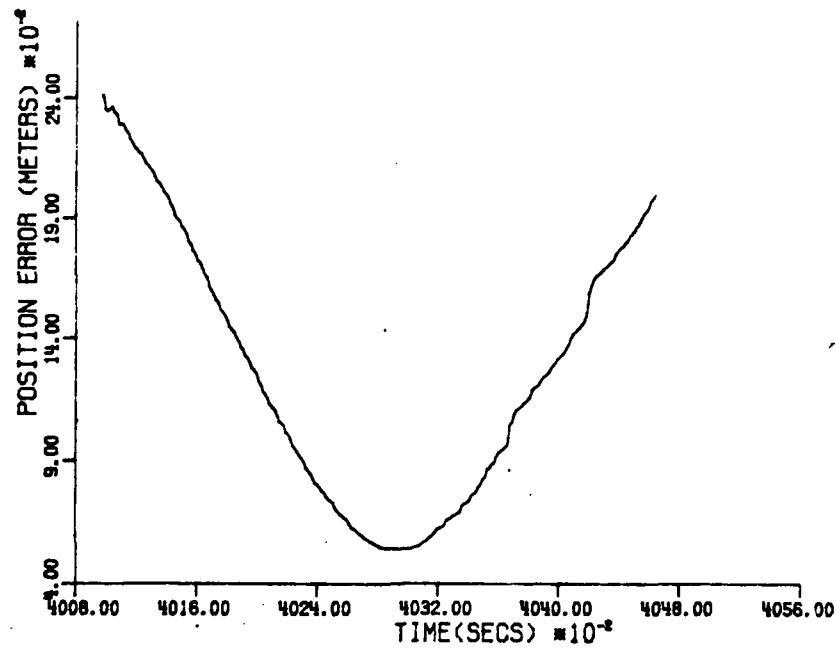


FIGURE 5-21 POSITION ERROR - UPDATED EPHEMERIDES
RICHMOND 13 SEP

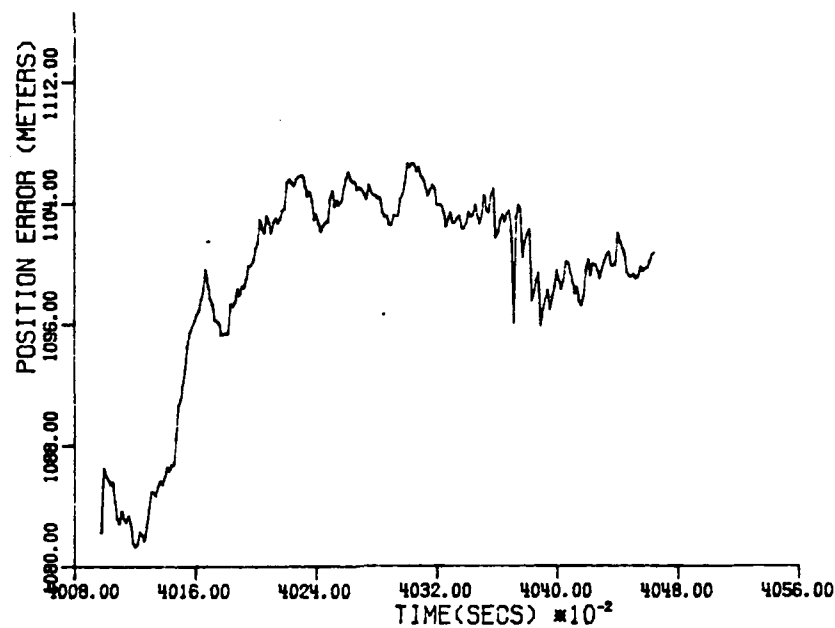


FIGURE 5-22 POSITION ERROR - UPDATED EPHEMERIDES
RICHMOND 13 AUG

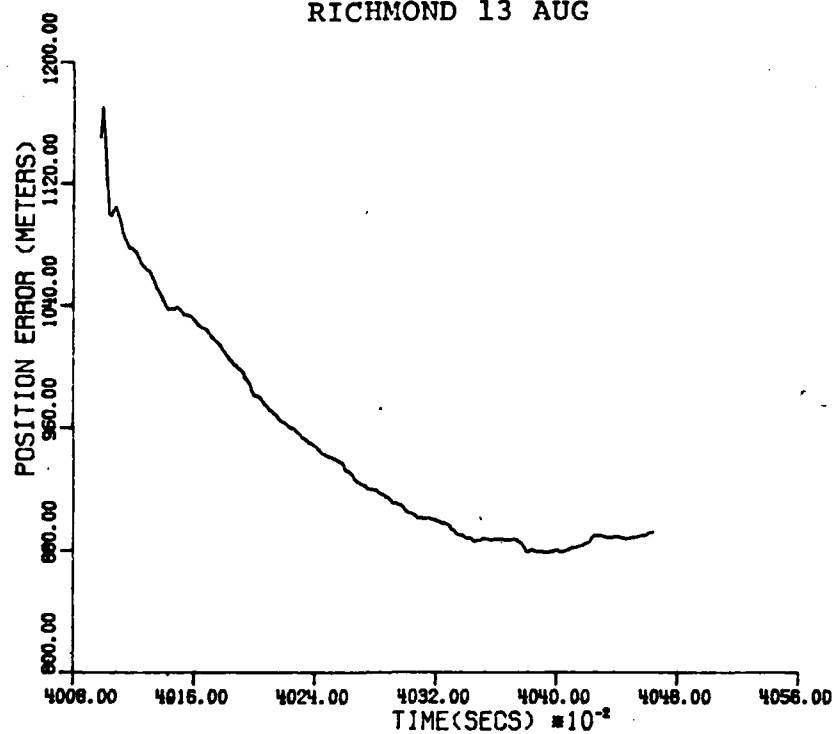


FIGURE 5-23 POSITION ERROR - UPDATED EPHEMERIDES
RICHMOND 11 JUN

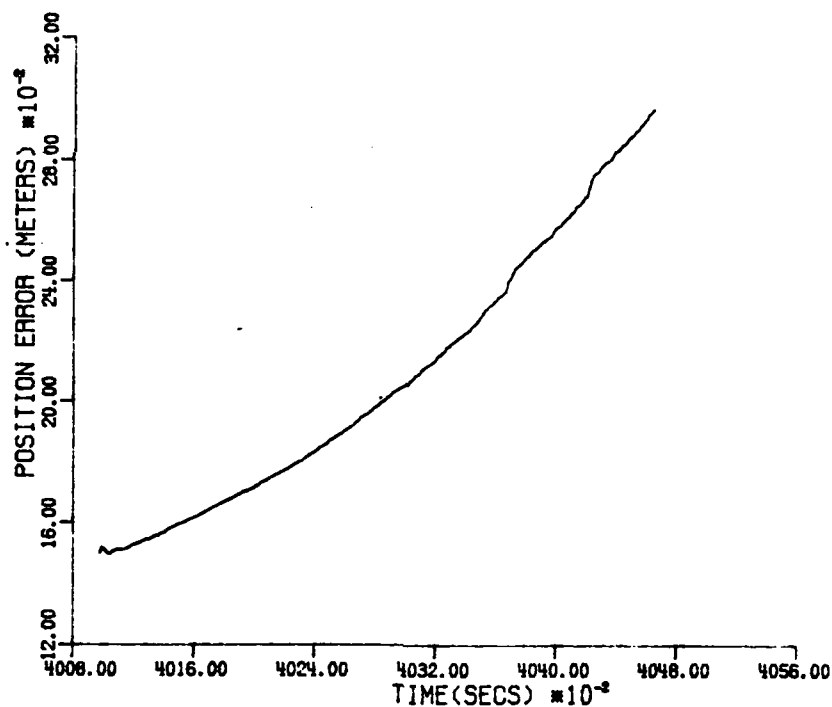


FIGURE 5-24 POSITION ERROR - UPDATED EPHEMERIDES
RICHMOND 5 APR

5.4 Summary

This chapter has demonstrated the capability to navigate using old ephemerides and current pseudorange measurements. The "empty" messages from four visible satellites were used to update the old ephemerides and then serve as measurements in the navigation algorithm. Navigation accuracies under ten meters were obtained, but GPS system characteristics and the update algorithm ill-conditioning also caused near kilometer-size navigation position errors. No generalization can be made about the repeatability of the results on different dates, with different satellites and different receiver sites. These

results demonstrated a navigation capability and further testing is required to generalize the results. Test results with the variable Earth rotation rate showed that the Earth rate correction was not necessary since the pseudorange measurements are current and include the current Earth rate, probably in the longitude of the ascending node parameter. Several adjustments in the ephemeris update algorithm should solve the ill-conditioning problem and make highly accurate positioning possible at all times. These algorithm adjustments are suggested in Chapter Six.

5-5 Aerospace Corporation Autonomous User Study

The Aerospace Corporation performed another study in 1986 of six month navigation accuracy without daily uploaded ephemerides. In this study the GPS satellites were presumed to store six months of predicted ephemerides that were created by the MCS and uploaded prior to the loss of the MCS. The ephemeris update algorithm was a Kalman Filter that used the predicted ephemeris and smoothed pseudorange and delta pseudorange measurements to update eight ephemeris parameters. The updated parameters coupled with the uncorrected parameters formed the ephemeris for each of four satellites. These updated ephemerides and smoothed pseudoranges and delta

pseudoranges were inputs to the navigation algorithm.

The Aerospace Corporation performed various experiments with their Autonomous User system. The closest in format to this study is described here. First, the predicted ephemerides were created by the Aerospace Corporation using a method similar to the MCS operation. Then, at the Yuma Proving Ground, the predicted ephemerides were updated using a Kalman Filter. The updated ephemerides were transmitted to a mobile test van at Washington, D.C., where the navigation test was accomplished.

The test results were very accurate, demonstrating navigation position errors under ten meters. There was no discussion of satellite position errors caused by the ephemeris update algorithm, but a high degree of accuracy was expected, similar to the best satellite position accuracies in Chapter Five of this study.

When compared to the Aerospace Corporation navigation results, the results in Chapter Five of this study reveal the importance of several accuracy-enhancing techniques. As mentioned in Chapter Three, smoothing the pseudorange measurements over 15 minutes aided the ephemeris update process and the navigation process. The Aerospace Corporation reduced measurement noise significantly by including the accumulated delta pseudoranges

which were not available for this study. Elevation masking was another technique that reduced measurement errors for the Aerospace Corporation study. The primary enhancement, however, was the modified parameter set used by Aerospace Corporation. By combining the M_0 and u terms, and estimating another term, $e \sin u$, the ephemeris update algorithm virtually eliminated the ill-conditioning caused by the high correlation between M_0 and u . The modified parameter set prevented large changes in the updated ephemeris parameters, thus improving satellite position accuracy. The Kalman Filter with an a priori covariance matrix that the Aerospace Corporation used in the ephemeris update process may have aided the satellite position accuracy, but similar accuracy was expected from the batch, least squares estimator used in Chapters Three and Five [Ananda, et.al., 1988].

Chapter Six Conclusions and Recommendations

6.1 Conclusions

The conclusions drawn from the preceding chapters are summarized as follows:

1. The broadcast ephemeris parameters have periodic characteristics caused by the orbit perturbations on the semi-synchronous satellites. Amplitudes of several of the periodic characteristics compare closely with analytic results considering the J_2 and the lunar-solar gravity perturbations. Several parameters absorb more than one perturbation during the ephemeris estimation process.

2. Broadcast ephemerides from previous dates can be updated to a current date by using current pseudorange measurements to a known site. Updated satellite position errors range from several hundred meters to several hundred kilometers with the best results coming from satellites with two high-elevation passes per day, yielding over 400 measurements. The batch estimator is insensitive to the age of the input broadcast ephemerides.

3. The broadcast parameter set that includes the mean anomaly at epoch, M_0 , and argument of perigee, w , causes ill-conditioning in the parameter update algorithm due to the correlation between the two parameters for the

near-circular GPS orbits.

4. Navigation accuracy can be under ten meters when using four satellites in a favorable geometry indicated by a small Geometric Dilution of Precision and with all four broadcast epochs current with the pseudorange measurements as will be the case for normal, full constellation navigation.

5. Navigation accuracy with updated ephemerides can be under ten meters when using ephemerides that have been updated with over 400 measurements from high-elevation passes. Navigating at the same receiver site where the ephemerides are updated, and using ephemeris epochs that are current with the pseudorange measurements, increase accuracy.

6. Accounting for the variable Earth rotation rate is not necessary when updating the broadcast ephemerides and navigating, because the current pseudorange measurements include the Earth rotation rate and the effect is absorbed into the estimate of Ω_0 , thereby compensating for the effect. During the update process, the variable Earth rate is accounted for when updating over seven months and possibly longer.

6.2 Recommendations

The following recommendations are made concerning

the previous material:

1. Further study of the broadcast ephemeris estimation process is warranted, particularly the high correlation between the mean anomaly and the argument of perigee parameters.

2. A continued analysis of broadcast ephemeris update test cases may reveal other causes of the large satellite position errors. Studies with either M_0 or w held fixed may eliminate much of the ill-conditioning in the update process. Investigating test cases with input ephemerides more than seven months old may disclose a limit on the age of the input ephemerides.

3. Investigation of the navigation algorithm with more current broadcast ephemerides and smoothing of the pseudorange measurements is needed to consistently reach the advertised GPS system accuracy.

4. Many more tests of the navigation routine with updated ephemerides are required to analyze the navigation accuracy under various conditions, such as, at the same receiver site where the ephemerides are updated, at sites close by, at later times, and at far away sites.

APPENDIX A

FORMULATION OF THE LONGITUDE OF ASCENDING NODE IN THE ECF COORDINATE SYSTEM

This appendix derives the equation for the longitude of the ascending node in the rotating, Earth-Centered, Earth-Fixed Coordinate System (ECF). Figure A-1 shows the relationships that lead to the equation used by Van Dierendonck, et.al.[1978], in the Broadcast Ephemeris Algorithm;

$$\Omega_k = \Omega_0 + (\dot{\Omega} - \dot{\Omega}_e)t_k - \dot{\Omega}_e t_{oe}, \quad (A-1)$$

where Ω_k is the longitude of the ascending node in the ECF system, at time t_k past the epoch time, Ω_0 (a GPS ephemeris parameter) is the longitude of the ascending node at epoch time, t_{oe} , in the ECF system, measured from the ECF x axis at 00:00 Sunday,

$\dot{\Omega}$ is the node rate due orbit perturbations,

$\dot{\Omega}_e$ is the Earth rotation rate ,

t_{oe} is the epoch time, given as the number of seconds past 00:00 Sunday. It is reset to zero each week and is always given at the beginning of an hour,

t_k is the time, in seconds, since epoch.

APPENDIX B

SUMMARY OF THE BROADCAST EPHEMERIS ALGORITHM

The Broadcast Ephemeris Algorithm (BEA) is the mathematical model for the GPS system and is described in some detail in Chapter Two. Inputs to the BEA are the 15 constant parameters that form the GPS broadcast ephemeris and two times: the time of epoch t_{oe} , and the time since epoch t_k . The output is the Earth-Centered, Earth-fixed (ECF) position (x_k, y_k, z_k) of the GPS satellite at time t_k . The epoch time, t_{oe} , is the beginning of a one-hour period during which the constant parameters are valid, expressed in seconds past 00:00 Sunday, GPS time. The following is a summary of the BEA equations.

$$A = (\sqrt{\bar{A}})^2 \quad (B-1)$$

$$n_o = \sqrt{\frac{\mu_e}{A^3}} \quad (B-2)$$

$$n = n_o + \Delta n \quad (B-3)$$

$$M_k = M_o + nt_k \quad (B-4)$$

Kepler's equation is solved by Newton iteration for eccentric anomaly, E_k .

$$\psi_k = \arccos [(\cos E_k - e)/(1 - e \cos E_k)] \quad (B-5)$$

To check the true anomaly quadrant, another form of the equation is also used:

$$\psi_k = \arcsin[\sqrt{1-e^2} \sin E_k / (1 - e \cos E_k)] \quad (B-6)$$

$$\phi_k = \psi_k + \omega \quad (B-7)$$

$$\delta u_k = C_{uc} \cos 2\phi_k + C_{us} \sin 2\phi_k \quad (B-8)$$

$$\delta r_k = C_{rc} \cos 2\phi_k + C_{rs} \sin 2\phi_k \quad (B-9)$$

$$\delta i_k = C_{ic} \cos 2\phi_k + C_{is} \sin 2\phi_k \quad (B-10)$$

$$u_k = \phi_k + \delta u_k \quad (B-11)$$

$$r_k = A(1 - e \cos E_k) + \delta r_k \quad (B-12)$$

$$i_k = i_0 + \delta i_k + \frac{di}{dt} t_k \quad (B-13)$$

$$x'_k = r_k \cos u_k \quad (B-14)$$

$$y'_k = r_k \sin u_k \quad (B-15)$$

$$\Omega_k = \Omega_0 + (\dot{\Omega} - \dot{\Omega}_e) t_k - \dot{\Omega}_e t_{oe} \quad (B-16)$$

$$x_k = x'_k \sin \Omega_k + y'_k \cos i_k \sin \Omega_k \quad (B-17)$$

$$y_k = x'_k \sin \Omega_k + y'_k \cos i_k \cos \Omega_k \quad (B-18)$$

$$z_k = y'_k \sin i_k \quad (B-19)$$

This concludes the summary of the BEA.

APPENDIX C

THE MEASUREMENT SENSITIVITY MATRIX FOR THE BROADCAST EPHEMERIS ALGORITHM

The H matrix consists of analytic partial derivatives of the ECF position coordinates (x,y,z) with respect to the 15 filter parameters, evaluated on the reference trajectory. The general form for H is:

$$H = \frac{\partial G(X^*, t)}{\partial X}$$

where $G(X, t) = \begin{vmatrix} x \\ y \\ z \end{vmatrix}$ calculated

This (3 x 15) H matrix describes the sensitivity of the position, G, to small changes in the state, X. The specific elements are given by:

$$H = \begin{vmatrix} \frac{\partial x_k}{\partial M_0} & \frac{\partial x_k}{\partial \Delta n} & \dots & \frac{\partial x_k}{\partial C_{is}} \\ \frac{\partial y_k}{\partial M_0} & \frac{\partial y_k}{\partial \Delta n} & \dots & \frac{\partial y_k}{\partial C_{is}} \\ \frac{\partial z_k}{\partial M_0} & \frac{\partial z_k}{\partial \Delta n} & \dots & \frac{\partial z_k}{\partial C_{is}} \end{vmatrix}$$

This appendix presents all of these partials as programmed for the Broadcast Ephemeris Algorithm. On first inspection the partials appear to be straightforward and well-known with respect to the Keplerian parameters. However, because of the perturbation corrections in the

Van Dierendonck algorithm, the partials need additional terms which increase their complexity. The well-known partials which form the bases for many of the H matrix elements have references indicated.

A list of variables used in the partial derivatives is given first.

x_k, y_k, z_k - satellite position in the Earth centered, Earth fixed coordinates at time, t_k .

x_p, y_p - satellite position in an intermediate coordinate system that has its origin at the Earth's center, the x_p axis collocated with the ascending node vector, and the y_p axis in the orbit plane, 90 degrees from the x_p axis in the direction of motion.

M_o - mean anomaly at epoch, t_{oe} .

i_k - inclination at time, t_k .

Ω_k - longitude of the ascending node at time, t_k .

r_k - radius to the satellite at time, t_k .

u_k - argument of latitude at time, t_k .

A - semimajor axis

e - eccentricity

E_k - eccentric anomaly at time, t_k .

δr_k - correction to the radius at time, t_k .

ϕ_k - intermediate argument of latitude at time, t_k .

V_k - true anomaly at time, t_k .

$C_{uc}, C_{us}, C_{rc}, C_{rs}, C_{ic}, C_{is}$ - amplitudes of the cosine and sine harmonic correction terms.

δu_k - correction to the argument of latitude at time, t_k .

δi_k - correction to the inclination at time, t_k .

Δn - change in mean motion.

M_k - mean anomaly at time, t_k .

\sqrt{A} - square root of the semimajor axis.

t_k - seconds past the epoch time, t_{oe} .

n_o - mean motion at epoch, t_{oe} .

Ω_o - longitude of the ascending node at epoch, t_{oe} .

i_o - inclination at epoch, t_{oe} .

ω - argument of perigee.

$\dot{\Omega}$ - longitude of the ascending node rate.

$\frac{di}{dt}$ - inclination rate.

The first element, $\frac{\partial x_k}{\partial M_o}$, consists of three, chain-rule parts:

$$\frac{\partial x_k}{\partial M_o} = \frac{\partial x_k}{\partial x_p} \frac{\partial x_p}{\partial M_o} + \frac{\partial x_k}{\partial y_p} \frac{\partial y_p}{\partial M_o} + \frac{\partial x_k}{\partial i_k} \frac{\partial i_k}{\partial M_o} \quad (C-1)$$

where $\frac{\partial x_k}{\partial x_p} = \cos(\Omega_k) \quad (C-2)$

$$\frac{\partial x_k}{\partial y_p} = -\cos(i_k) \sin(\Omega_k) \quad (C-3)$$

$$\frac{\partial x_k}{\partial i_k} = r_k \sin(u_k) \sin(i_k) \sin(\Omega_k) \quad (C-4)$$

$$\text{and } \frac{\partial x}{\partial M_o^p} = \frac{\partial x_p}{\partial r_k} \frac{\partial r_k}{\partial M_o} + \frac{\partial x_p}{\partial u_k} \frac{\partial u_k}{\partial M_o} \quad (C-5)$$

$$\text{where } \frac{\partial x_p}{\partial r_k} = \cos(u_k) \quad (C-6)$$

$$\frac{\partial r_k}{\partial M_o} = \frac{A e \sin(E_k)}{1 - e \cos(E_k)} + \frac{\partial \delta r_k}{\partial \phi_k} \frac{\partial \phi_k}{\partial V_k} \frac{\partial V_k}{\partial M_o} \quad (C-7)$$

where the Keplerian partial comes from Broucke[1970],

$$\text{with } \frac{\partial \delta r_k}{\partial \phi_k} = 2 C_{rs} \cos(2\phi_k) - 2 C_{rc} \sin(2\phi_k) \quad (C-8)$$

$$\frac{\partial \phi_k}{\partial V_k} = 1 \quad (C-9)$$

$$\frac{\partial V_k}{\partial M_o} = \frac{(1 - e^2)^{\frac{1}{2}}}{(1 - e \cos(E_k))^2} \quad (C-10)$$

here, the Keplerian partial is from Brouwer and Clemence[1961].

Now, back to the factors in equation C-5:

$$\frac{\partial x_p}{\partial u_k} = -r_k \sin(u_k) \quad (C-11)$$

$$\frac{\partial u_k}{\partial M_o} = \frac{\partial V_k}{\partial M_o} + \frac{\partial \delta u_k}{\partial \phi_k} \frac{\partial \phi_k}{\partial V_k} \frac{\partial V_k}{\partial M_o} \quad (C-12)$$

with $\frac{\partial V_k}{\partial M_o}$ given above as equation C-10 and recognizing

that $\frac{\partial u_k}{\partial \delta u_k}$ and $\frac{\partial \phi_k}{\partial V_k}$ are unity. For equation C-12:

$$\frac{\partial \delta u_k}{\partial \phi_k} = 2 C_{us} \cos(2\phi_k) - 2 C_{uc} \sin(2\phi_k) \quad (C-13)$$

From equation C-1, the quantity $\frac{\partial y_p}{\partial M_o}$ is similar to $\frac{\partial x_p}{\partial M_o}$:

$$\frac{\partial y_p}{\partial M_o} = \frac{\partial y_p}{\partial r_k} \frac{\partial r_k}{\partial M_o} + \frac{\partial y_p}{\partial u_k} \frac{\partial u_k}{\partial M_o} \quad (C-14)$$

where $\frac{\partial y_p}{\partial r_k} = \sin(u_k),$ (C-15)

and $\frac{\partial y_p}{\partial u_k} = r_k \cos(u_k)$ (C-16)

The other components for equation C-14 are equations C-7 and C-12. The final part of the first element of H is $\frac{\partial i_k}{\partial M_o}$:

$$\frac{\partial i_k}{\partial M_o} = \frac{\partial \delta i_k}{\partial \phi_k} \frac{\partial \phi_k}{\partial M_o} \quad (C-17)$$

where $\frac{\partial \delta i_k}{\partial \phi_k} = 2 C_{is} \cos(2\phi_k) - 2 C_{ic} \sin(2\phi_k)$ (C-18)

along with equation C-10 form equation C-17, recognizing that $\frac{\partial i_k}{\partial \delta i_k}$ and $\frac{\partial \phi_k}{\partial \phi_k}$ are unity. This completes Equation C-1.

The second element of the H matrix is $\frac{\partial x_k}{\partial \Delta n}$:

$$\frac{\partial x_k}{\partial \Delta n} = \frac{\partial x_k}{\partial x_p} \frac{\partial x_p}{\partial \Delta n} + \frac{\partial x_k}{\partial y_p} \frac{\partial y_p}{\partial \Delta n} + \frac{\partial x_k}{\partial i_k} \frac{\partial i_k}{\partial \Delta n} \quad (C-19)$$

Equations C-2, C-3, and C-4 provide $\frac{\partial x_k}{\partial x_p}$, $\frac{\partial x_k}{\partial y_p}$, and $\frac{\partial x_k}{\partial i_k}$, respectively.

Next, $\frac{\partial x_p}{\partial \Delta n} = \frac{\partial x_p}{\partial r_k} \frac{\partial r_k}{\partial \Delta n} + \frac{\partial x_p}{\partial u_k} \frac{\partial u_k}{\partial \Delta n}$ (C-20)

where equations C-6 and C-11 give $\frac{\partial x_p}{\partial r_k}$ and $\frac{\partial x_p}{\partial u_k}$, respec-

tively.

$$\text{Then, } \frac{\partial r_k}{\partial \Delta n} = \frac{\partial r_k}{\partial M_o} \frac{\partial M_k}{\partial n} + \frac{\partial \phi_k}{\partial \phi_k} \frac{\partial V_k}{\partial M_o} \frac{\partial M_k}{\partial n} \quad (\text{C-21})$$

Recognize that $\frac{\partial M_o}{\partial M_k}$, $\frac{\partial r_k}{\partial r_k}$, $\frac{\partial \phi_k}{\partial V_k}$ and $\frac{\partial n}{\partial \Delta n}$ are left out of equation C-21 because they are unity.

$$\text{Now, } \frac{\partial M_k}{\partial n} = t_k \quad (\text{C-22})$$

and from equation C-20

$$\frac{\partial u_k}{\partial \Delta n} = \frac{\partial V_k}{\partial M_o} \frac{\partial M_k}{\partial \Delta n} + \frac{\partial \phi_k}{\partial \phi_k} \frac{\partial V_k}{\partial M_o} \frac{\partial M_k}{\partial \Delta n} \quad (\text{C-23})$$

Again with $\frac{\partial M_o}{\partial M_k}$, $\frac{\partial \phi_k}{\partial V_k}$, $\frac{\partial u_k}{\partial \phi_k}$ and $\frac{\partial n}{\partial \Delta n}$ being unity. From equation C-19, $\frac{\partial y_p}{\partial \Delta n}$ is similar to $\frac{\partial x_p}{\partial \Delta n}$:

$$\frac{\partial y_p}{\partial \Delta n} = \frac{\partial y_p}{\partial r_k} \frac{\partial r_k}{\partial \Delta n} + \frac{\partial y_p}{\partial u_k} \frac{\partial u_k}{\partial \Delta n} \quad (\text{C-24})$$

Equations C-15, C-21, C-16, and C-23 form the parts of equation C-24; $\frac{\partial y_p}{\partial r_k}$, $\frac{\partial r_k}{\partial \Delta n}$, $\frac{\partial y_p}{\partial u_k}$, and $\frac{\partial u_k}{\partial \Delta n}$, respectively.

Finally, from equation C-19:

$$\frac{\partial i_k}{\partial \Delta n} = \frac{\partial \phi_k}{\partial \phi_k} \frac{\partial V_k}{\partial M_o} \frac{\partial M_k}{\partial n}, \quad (\text{C-25})$$

where the three components are equations C-18, C-10, and C-22, respectively, with $\frac{\partial i_k}{\partial \phi_k}$, $\frac{\partial \phi_k}{\partial V_k}$, $\frac{\partial M_o}{\partial M_k}$, and $\frac{\partial n}{\partial \Delta n}$ being unity.

This completes Equation C-19.

The third element of the first row of H is $\frac{\partial x_k}{\partial e}$

$$\frac{\partial x_k}{\partial e} = \frac{\partial x_k}{\partial x_p} \frac{\partial x_p}{\partial e} + \frac{\partial x_k}{\partial y_p} \frac{\partial y_p}{\partial e} + \frac{\partial x_k}{\partial i_k} \frac{\partial i_k}{\partial e} \quad (C-26)$$

where $\frac{\partial x_k}{\partial x_p}$, $\frac{\partial x_k}{\partial y_p}$, and $\frac{\partial x_k}{\partial i_k}$ are equations C-2, C-3, and C-4, respectively.

$$\text{Then, } \frac{\partial x_p}{\partial e} = \frac{\partial x_p}{\partial r_k} \frac{\partial r_k}{\partial e} + \frac{\partial x_p}{\partial u_k} \frac{\partial u_k}{\partial e} \quad (C-27)$$

where $\frac{\partial x_p}{\partial r_k}$ is equation C-6 and $\frac{\partial x_p}{\partial u_k}$ is equation C-11.

$$\text{Then } \frac{\partial r_k}{\partial e} = -A \cos(E_k) + \frac{A e \sin^2(E_k)}{1 - e \cos(E_k)} + \frac{\partial \delta r_k}{\partial e} \quad (C-28)$$

The first two components come from Broucke[1970].

$$\text{Here } \frac{\partial \delta r_k}{\partial e} = \frac{\partial \delta r_k}{\partial \phi_k} \frac{\partial \phi_k}{\partial e} \quad (C-29)$$

Where $\frac{\partial \delta r_k}{\partial \phi_k}$ is equation C-8, and

$$\frac{\partial \phi_k}{\partial e} = \left(\frac{1}{1 - e \cos(E)} + \frac{1}{1 - e^2} \right) \sin(\phi_k) \quad (C-30)$$

This partial comes from Brouwer and Clemence[1961]. From

C-29, $\frac{\partial \phi_k}{\partial \phi_k}$ is omitted since it is unity. From equation

C-27,

$$\frac{\partial u_k}{\partial e} = \frac{\partial \phi_k}{\partial e} + \frac{\partial \delta u_k}{\partial \phi_k} \frac{\partial \phi_k}{\partial e} \quad (C-31)$$

with $\frac{\partial u_k}{\partial \sqrt{v_k}}$, $\frac{\partial u_k}{\partial \delta u_k}$ and $\frac{\partial \phi_k}{\partial \sqrt{v_k}}$ being unity.

Equations C-30 and C-13 provide $\frac{\partial \sqrt{v_k}}{\partial e}$ and $\frac{\partial \delta u_k}{\partial \phi_k}$, respectively.

From equation C-26,

$$\frac{\partial y_p}{\partial e} = \frac{\partial y_p}{\partial r_k} \frac{\partial r_k}{\partial e} + \frac{\partial y_p}{\partial u_k} \frac{\partial u_k}{\partial e} \quad (C-32)$$

with these partials being supplied by equations C-15, C-28, C-16 and C-31, respectively. Finally, $\frac{\partial i_k}{\partial e}$ completes equation C-26.

$$\frac{\partial i_k}{\partial e} = \frac{\partial \delta i_k}{\partial \phi_k} \frac{\partial \sqrt{v_k}}{\partial e} \quad (C-33)$$

Where $\frac{\partial \delta i_k}{\partial \phi_k}$ is equation C-18, $\frac{\partial \sqrt{v_k}}{\partial e}$ is equation C-30, and $\frac{\partial i_k}{\partial \delta i_k}$ and $\frac{\partial \phi_k}{\partial \sqrt{v_k}}$ are unity. This concludes Equation C-26.

The fourth element in the first row of H is $\frac{\partial x_k}{\partial \sqrt{A}}$:

$$\frac{\partial x_k}{\partial \sqrt{A}} = \frac{\partial x_k}{\partial x_p} \frac{\partial x_p}{\partial \sqrt{A}} + \frac{\partial x_k}{\partial y_p} \frac{\partial y_p}{\partial \sqrt{A}} + \frac{\partial x_k}{\partial i_k} \frac{\partial i_k}{\partial \sqrt{A}} \quad (C-34)$$

where $\frac{\partial x_k}{\partial x_p}$, $\frac{\partial x_k}{\partial y_p}$, and $\frac{\partial x_k}{\partial i_k}$ are equations C-2, C-3, and C-4 respectively.

$$\text{Then } \frac{\partial x_p}{\partial \sqrt{A}} = \frac{\partial x_p}{\partial r_k} \frac{\partial r_k}{\partial \sqrt{A}} + \frac{\partial x_p}{\partial u_k} \frac{\partial u_k}{\partial \sqrt{A}} \quad (C-35)$$

Here $\frac{\partial x_p}{\partial r_k}$ and $\frac{\partial x_p}{\partial u_k}$ are equations C-6 and C-11, respectively. And,

$$\frac{\partial r_k}{\partial \sqrt{A}} = 2\sqrt{A} (1-e \cos(E_k)) + \frac{\partial \delta r_k}{\partial \sqrt{A}} + \frac{\partial r_k}{\partial E_k} \frac{\partial E_k}{\partial \sqrt{A}} \quad (C-36)$$

$$\text{where } \frac{\partial \delta r_k}{\partial \sqrt{A}} = \frac{\partial \delta r_k}{\partial \phi_k} \frac{\partial \phi_k}{\partial \sqrt{A}} \quad (C-37)$$

with $\frac{\partial r_k}{\partial \delta r_k}$ and $\frac{\partial \phi_k}{\partial \phi_k}$ being unity. Equation C-8 provides $\frac{\partial \delta r_k}{\partial \phi_k}$, and

$$\frac{\partial \phi_k}{\partial \sqrt{A}} = \frac{\partial \phi_k}{\partial E_k} \frac{\partial E_k}{\partial \sqrt{A}} \quad (C-38)$$

$$\text{Where } \frac{\partial \phi_k}{\partial E_k} = \frac{(1-e^2)^{\frac{1}{2}}}{1-e \cos(E_k)} \quad (C-39)$$

which comes from Brouwer and Clemence[1961]

$$\text{and } \frac{\partial E_k}{\partial \sqrt{A}} = \frac{-3 t_k n_0}{\sqrt{A} (1-e \cos(E_k))} \quad (C-40)$$

which completes equation C-37. For equation C-36,

$$\frac{\partial r_k}{\partial E_k} = A e \sin(E_k) + \frac{\partial \delta r_k}{\partial E_k}, \quad (C-41)$$

the first part coming from Smart[1953]

$$\text{where } \frac{\partial \delta r_k}{\partial E_k} = \frac{\partial \delta r_k}{\partial \phi_k} \frac{\partial \phi_k}{\partial E_k} \quad (C-42)$$

Here $\frac{\partial \delta r_k}{\partial \phi_k}$ is equation C-8, $\frac{\partial \phi_k}{\partial E_k}$ is equation C-39, and

$\frac{\partial r_k}{\partial \delta r_k}$ and $\frac{\partial \phi_k}{\partial \psi_k}$ are unity. Now, from equation C-35 we need $\frac{\partial u_k}{\partial \sqrt{A}}$.

$$\frac{\partial u_k}{\partial \sqrt{A}} = \frac{\partial \psi_k}{\partial \sqrt{A}} + \frac{\partial \delta u_k}{\partial \sqrt{A}} \quad (C-43)$$

where $\frac{\partial \psi_k}{\partial \sqrt{A}}$ is equation C-38, with $\frac{\partial u_k}{\partial \phi_k}$, $\frac{\partial u_k}{\partial \delta u_k}$ and $\frac{\partial \phi_k}{\partial \psi_k}$ being unity.

$$\text{Also, } \frac{\partial \delta u_k}{\partial \sqrt{A}} = \frac{\partial \delta u_k}{\partial \phi_k} \frac{\partial \psi_k}{\partial \sqrt{A}} \quad (C-44)$$

with $\frac{\partial \delta u_k}{\partial \phi_k}$ given by equation C-13, $\frac{\partial \psi_k}{\partial \sqrt{A}}$ given by equation C-38, and $\frac{\partial \phi_k}{\partial \psi_k}$ being unity, which completes equation C-35.

From equation C-34, there is $\frac{\partial y_p}{\partial \sqrt{A}}$:

$$\frac{\partial y_p}{\partial \sqrt{A}} = \frac{\partial y_p}{\partial r_k} \frac{\partial r_k}{\partial \sqrt{A}} + \frac{\partial y_p}{\partial u_k} \frac{\partial u_k}{\partial \sqrt{A}} \quad (C-45)$$

where these partials are given by equations C-15, C-36, C-16, and C-43, respectively. Finally, $\frac{\partial i_k}{\partial \sqrt{A}}$ completes equation C-34.

$$\frac{\partial i_k}{\partial \sqrt{A}} = \frac{\partial \delta i_k}{\partial \phi_k} \frac{\partial \psi_k}{\partial \sqrt{A}} \quad (C-46)$$

where, $\frac{\partial \delta i_k}{\partial \phi_k}$ is equation C-18, $\frac{\partial \psi_k}{\partial \sqrt{A}}$ is equation C-38, and

$\frac{\partial i_k}{\partial \delta i_k}$ and $\frac{\partial \phi_k}{\partial \psi_k}$ are unity. This concludes Equation C-34.

The next element is $\frac{\partial x_k}{\partial \Omega_0}$.

$$\frac{\partial x_k}{\partial \Omega_0} = \frac{\partial x_k}{\partial x_p} \frac{\partial x_p}{\partial \Omega_0} + \frac{\partial x_k}{\partial y_p} \frac{\partial y_p}{\partial \Omega_0} + \frac{\partial x_k}{\partial i_k} \frac{\partial i_k}{\partial \Omega_0} + \frac{\partial x_k}{\partial \Omega_0} \quad (C-47)$$

Here, $\frac{\partial x_p}{\partial \Omega_0}$, $\frac{\partial y_p}{\partial \Omega_0}$, and $\frac{\partial i_k}{\partial \Omega_0}$ are all zero, leaving only $\frac{\partial x_k}{\partial \Omega_0}$:

$$\frac{\partial x_k}{\partial \Omega_0} = -r_k \cos(u_k) \sin(\Omega_k) - r_k \sin(u_k) \cos(i_k) \cos(\Omega_k) \quad (C-48)$$

where $\frac{\partial \Omega_k}{\partial \Omega_0}$ is unity. This concludes Equation C-47.

The sixth element is $\frac{\partial x_k}{\partial i_0}$:

$$\frac{\partial x_k}{\partial i_0} = \frac{\partial x_k}{\partial x_p} \frac{\partial x_p}{\partial i_0} + \frac{\partial x_k}{\partial y_p} \frac{\partial y_p}{\partial i_0} + \frac{\partial x_k}{\partial i_k} \frac{\partial i_k}{\partial i_0} \quad (C-49)$$

Here $\frac{\partial x_p}{\partial i_0}$ and $\frac{\partial y_p}{\partial i_0}$ are zero, leaving only $\frac{\partial x_k}{\partial i_k}$:

$$\frac{\partial x_k}{\partial i_k} = r_k \sin(u_k) \sin(i_k) \sin(\Omega_k) \quad (C-50)$$

recognizing that $\frac{\partial i_k}{\partial i_0} = 1$. This concludes Equation C-49.

The next element is $\frac{\partial x_k}{\partial \omega}$.

$$\frac{\partial x_k}{\partial \omega} = \frac{\partial x_k}{\partial x_p} \frac{\partial x_p}{\partial \omega} + \frac{\partial x_k}{\partial y_p} \frac{\partial y_p}{\partial \omega} + \frac{\partial x_k}{\partial i_k} \frac{\partial i_k}{\partial \omega} \quad (C-51)$$

where $\frac{\partial x_k}{\partial x_p}$, $\frac{\partial x_k}{\partial y_p}$, and $\frac{\partial x_k}{\partial i_k}$ are equations C-2, C-3, and C-4, respectively.

$$\text{Then } \frac{\partial x_p}{\partial u} = \frac{\partial x_p}{\partial r_k} \frac{\partial \delta r_k}{\partial \phi_k} + \frac{\partial x_p}{\partial u_k} \frac{\partial u_k}{\partial u} \quad (\text{C-52})$$

recognizing that the omissions, $\frac{\partial r_k}{\partial \delta r_k}$ and $\frac{\partial \phi_k}{\partial u}$ are both unity.

$$\text{Here, } \frac{\partial u_k}{\partial u} = 1 + \frac{\partial \delta u_k}{\partial \phi_k} \quad (\text{C-53})$$

where $\frac{\partial u_k}{\partial \delta u_k}$ and $\frac{\partial \phi_k}{\partial u}$ are omitted because they are unity.

$$\text{Then } \frac{\partial y_p}{\partial u} = \frac{\partial y_p}{\partial r_k} \frac{\partial \delta r_k}{\partial \phi_k} + \frac{\partial y_p}{\partial u_k} \frac{\partial u_k}{\partial u} \quad (\text{C-54})$$

where $\frac{\partial y_p}{\partial r_k}$, $\frac{\partial \delta r_k}{\partial \phi_k}$, $\frac{\partial y_p}{\partial u_k}$, and $\frac{\partial u_k}{\partial u}$ are equations C-15, C-8, C-16, and C-53 respectively. Finally, the factor $\frac{\partial i_k}{\partial u}$ is:

$$\frac{\partial i_k}{\partial u} = \frac{\partial \delta i_k}{\partial \phi_k}, \quad (\text{C-55})$$

with $\frac{\partial \delta i_k}{\partial \phi_k}$ being equation C-18, noting that $\frac{\partial i_k}{\partial \delta i_k}$ and $\frac{\partial \phi_k}{\partial u}$ are unity. This finishes Equation C-51.

The eighth element is $\frac{\partial x_k}{\partial \Omega}$.

$$\frac{\partial x_k}{\partial \Omega} = \frac{\partial x_k}{\partial x_p} \frac{\partial x_p}{\partial \Omega} + \frac{\partial x_k}{\partial y_p} \frac{\partial y_p}{\partial \Omega} + \frac{\partial x_k}{\partial i_k} \frac{\partial i_k}{\partial \Omega} + \frac{\partial x_k}{\partial \Omega_k} \frac{\partial \Omega_k}{\partial \Omega} \quad (\text{C-56})$$

Here, the partials $\frac{\partial x_p}{\partial \Omega}$, $\frac{\partial y_p}{\partial \Omega}$, and $\frac{\partial i_k}{\partial \Omega}$ are zero. Then $\frac{\partial x_k}{\partial \Omega_k}$ is equation C-47, noting that $\frac{\partial \Omega_o}{\partial \Omega_k}$ is unity. Finally,

$$\frac{\partial \Omega_k}{\partial \Omega} = t_k \quad (C-57)$$

This concludes Equation C-56.

The next element is $\frac{\partial x_k}{\partial i}$:

$$\frac{\partial x_k}{\partial i} = \frac{\partial x_k}{\partial x_p} \frac{\partial x_p}{\partial i} + \frac{\partial x_k}{\partial y_p} \frac{\partial y_p}{\partial i} + \frac{\partial x_k}{\partial i_k} \frac{\partial i_k}{\partial i} \quad (C-58)$$

Here, $\frac{\partial x_p}{\partial i} = \frac{\partial y_p}{\partial i} = 0$, $\frac{\partial x_k}{\partial i_k}$ is equation (C-50), and

$$\frac{\partial i_k}{\partial i} = t_k \quad (C-59)$$

which completes Equation C-58.

The tenth element is $\frac{\partial x_k}{\partial C_{uc}}$:

$$\frac{\partial x_k}{\partial C_{uc}} = \frac{\partial x_k}{\partial x_p} \frac{\partial x_p}{\partial C_{uc}} + \frac{\partial x_k}{\partial y_p} \frac{\partial y_p}{\partial C_{uc}} + \frac{\partial x_k}{\partial i_k} \frac{\partial i_k}{\partial C_{uc}} \quad (C-60)$$

Here, the partials $\frac{\partial x_k}{\partial x_p}$, $\frac{\partial x_k}{\partial y_p}$, and $\frac{\partial x_k}{\partial i_k}$ are equations C-2, C-3, and C-4, respectively.

$$\text{Then, } \frac{\partial x_p}{\partial C_{uc}} = \frac{\partial x_p}{\partial u_k} \frac{\partial u_k}{\partial C_{uc}} \quad (C-61)$$

The partial $\frac{\partial x_p}{\partial u_k}$ is equation C-11 and

$$\frac{\partial u_k}{\partial C_{uc}} = \frac{\partial \delta u_k}{\partial C_{uc}} = \cos (2\phi_k) \quad (C-62)$$

noting that $\frac{\partial u_k}{\partial \delta u_k}$ is unity.

$$\text{Then, } \frac{\partial y_p}{\partial C_{uc}} = \frac{\partial y_p}{\partial u_k} \frac{\partial u_k}{\partial C_{uc}} \quad (C-63)$$

where $\frac{\partial y_p}{\partial u_k}$ is equation C-16 and $\frac{\partial u_k}{\partial C_{uc}}$ is equation C-62.

This concludes Equation C-60, since $\frac{\partial i_k}{\partial C_{uc}}$ is zero.

The next element of the H matrix is $\frac{\partial x_k}{\partial C_{us}}$:

$$\frac{\partial x_k}{\partial C_{us}} = \frac{\partial x_k}{\partial x_p} \frac{\partial x_p}{\partial C_{us}} + \frac{\partial x_k}{\partial y_p} \frac{\partial y_p}{\partial C_{us}} + \frac{\partial x_k}{\partial i_k} \frac{\partial i_k}{\partial C_{us}} \quad (C-64)$$

Again, equations C-2, C-3, and C-4 are the partials, $\frac{\partial x_k}{\partial x_p}$, $\frac{\partial x_k}{\partial y_p}$, and $\frac{\partial x_k}{\partial i_k}$, respectively.

$$\text{Then, } \frac{\partial x_p}{\partial C_{us}} = \frac{\partial x_p}{\partial u_k} \frac{\partial u_k}{\partial C_{us}}, \quad (C-65)$$

where $\frac{\partial x_p}{\partial u_k}$ is given by equation C-11 and

$$\frac{\partial u_k}{\partial C_{us}} = \frac{\partial \delta u_k}{\partial C_{us}} = \sin (2\phi_k) \quad (C-66)$$

noting that $\frac{\partial u_k}{\partial \delta u_k}$ is unity. Next, from equation C-64,

$\frac{\partial y_p}{\partial C_{us}}$ is needed:

$$\frac{\partial y_p}{\partial C_{us}} = \frac{\partial y_p}{\partial u_k} \frac{\partial u_k}{\partial C_{us}} \quad (C-67)$$

where $\frac{\partial y_p}{\partial u_k}$ is equation C-16 and $\frac{\partial u_k}{\partial C_{us}}$ is equation C-66.

Noting that the partial, $\frac{\partial i_k}{\partial C_{us}}$ is zero, completes Equation C-64.

The next element is $\frac{\partial x_k}{\partial C_{rc}}$:

$$\frac{\partial x_k}{\partial C_{rc}} = \frac{\partial x_k}{\partial x_p} \frac{\partial x_p}{\partial C_{rc}} + \frac{\partial x_k}{\partial y_p} \frac{\partial y_p}{\partial C_{rc}} + \frac{\partial x_k}{\partial i_k} \frac{\partial i_k}{\partial C_{rc}} \quad (C-68)$$

Here, the partials, $\frac{\partial x_k}{\partial x_p}$, $\frac{\partial x_k}{\partial y_p}$, and $\frac{\partial x_k}{\partial i_k}$ are equations C-2, C-3, and C-4, respectively.

$$\text{Then } \frac{\partial x_p}{\partial C_{rc}} = \frac{\partial x_p}{\partial r_k} \frac{\partial r_k}{\partial C_{rc}} \quad (C-69)$$

with $\frac{\partial x_p}{\partial r_k}$ being equation C-6 and

$$\frac{\partial r_k}{\partial C_{rc}} = \frac{\partial \delta r_k}{\partial C_{rc}} = \cos(2\phi_k) \quad (C-70)$$

noting that $\frac{\partial r_k}{\partial \delta r_k}$ is unity. Next from equation C-68,

$$\frac{\partial y_p}{\partial C_{rc}} = \frac{\partial y_p}{\partial r_k} \frac{\partial r_k}{\partial C_{rc}} \quad (C-71)$$

where $\frac{\partial y_p}{\partial r_k}$ is equation C-15 and $\frac{\partial r_k}{\partial C_{rc}}$ is equation C-70.

Finally, $\frac{\partial i_k}{\partial C_{rc}}$ is zero, which completes Equation C-68.

The thirteenth element is $\frac{\partial x_k}{\partial C_{rs}}$,

$$\frac{\partial x_k}{\partial C_{rs}} = \frac{\partial x_k}{\partial x_p} \frac{\partial x_p}{\partial C_{rs}} + \frac{\partial x_k}{\partial y_p} \frac{\partial y_p}{\partial C_{rs}} + \frac{\partial x_k}{\partial i_k} \frac{\partial i_k}{\partial C_{rs}} \quad (C-72)$$

where the partials, $\frac{\partial x_k}{\partial x_p}$, $\frac{\partial x_k}{\partial y_p}$, and $\frac{\partial x_k}{\partial i_k}$ refer to equations C-2, C-3, and C-4, respectively.

$$\text{Then, } \frac{\partial x_p}{\partial C_{rs}} = \frac{\partial x_p}{\partial r_k} \frac{\partial r_k}{\partial C_{rs}} \quad (C-73)$$

where $\frac{\partial x_p}{\partial r_k}$ is equation C-6 and

$$\frac{\partial r_k}{\partial C_{rs}} = \frac{\partial \delta r_k}{\partial C_{rs}} = \sin (2\phi_k) \quad (C-74)$$

again, noting that $\frac{\partial r_k}{\partial \delta r_k}$ is unity. Next, from equation C-72,

$$\frac{\partial y_p}{\partial C_{rs}} = \frac{\partial y_p}{\partial r_k} \frac{\partial r_k}{\partial C_{rs}} \quad (C-75)$$

where $\frac{\partial y_p}{\partial r_k}$ is equation C-15 and $\frac{\partial r_k}{\partial C_{rs}}$ is equation C-74.

The component $\frac{\partial i_k}{\partial C_{rs}}$ is zero and Equation C-72 is complete.

The next element is $\frac{\partial x_k}{\partial C_{ic}}$:

$$\frac{\partial x_k}{\partial C_{ic}} = \frac{\partial x_k}{\partial x_p} \frac{\partial x_p}{\partial C_{ic}} + \frac{\partial x_k}{\partial y_p} \frac{\partial y_p}{\partial C_{ic}} + \frac{\partial x_k}{\partial i_k} \frac{\partial i_k}{\partial C_{ic}} \quad (C-76)$$

Here $\frac{\partial x_p}{\partial C_{ic}}$ and $\frac{\partial y_p}{\partial C_{ic}}$ are zero, leaving $\frac{\partial x_k}{\partial i_k}$ (C-4) and $\frac{\partial i_k}{\partial C_{ic}}$:

$$\frac{\partial i_k}{\partial C_{ic}} = \frac{\partial \delta i_k}{\partial C_{ic}} = \cos (2\phi_k) \quad (C-77)$$

noting that $\frac{\partial i_k}{\partial \delta i_k}$ is unity. This ends the Equation C-76.

The final element in the first row is $\frac{\partial x_k}{\partial C_{is}}$:

$$\frac{\partial x_k}{\partial C_{is}} = \frac{\partial x_k}{\partial x_p} \frac{\partial x_p}{\partial C_{is}} + \frac{\partial x_k}{\partial y_p} \frac{\partial y_p}{\partial C_{is}} + \frac{\partial x_k}{\partial i_k} \frac{\partial i_k}{\partial C_{is}} \quad (C-78)$$

Again, the partials $\frac{\partial x_p}{\partial C_{is}}$ and $\frac{\partial y_p}{\partial C_{is}}$ are zero, with $\frac{\partial x_k}{\partial i_k}$ being equation C-4 and $\frac{\partial i_k}{\partial C_{is}}$ being :

$$\frac{\partial i_k}{\partial C_{is}} = \frac{\partial \delta i_k}{\partial C_{is}} = \sin (2\phi_k) \quad (C-79)$$

Where, again, $\frac{\partial i_k}{\partial \delta i_k}$ is unity. This completes Equation C-78, and the first row of the H matrix. As will be seen, the other two rows follow the same pattern. The first element of the second row is $\frac{\partial y_k}{\partial M_o}$:

$$\frac{\partial y_k}{\partial M_o} = \frac{\partial y_k}{\partial x_p} \frac{\partial x_p}{\partial M_o} + \frac{\partial y_k}{\partial y_p} \frac{\partial y_p}{\partial M_o} + \frac{\partial y_k}{\partial i_k} \frac{\partial i_k}{\partial M_o} \quad (C-80)$$

The new partials for this element are:

$$\frac{\partial y_k}{\partial x_p} = \sin (\Omega_k), \quad (C-81)$$

$$\frac{\partial y_k}{\partial y_p} = \cos (i_k) \cos (\Omega_k), \quad (C-82)$$

$$\text{and } \frac{\partial y_k}{\partial i_k} = -r_k \sin (u_k) \sin (i_k) \cos (\Omega_k) \quad (C-83)$$

The other partials in Equation C-80 are discussed previ-

ously, as indicated below:

$$\frac{\partial x_p}{\partial M_o} \quad (C-5) \quad , \quad \frac{\partial y_p}{\partial M_o} \quad (C-14),$$

$$\text{and } \frac{\partial i_k}{\partial M_o} \quad (C-17).$$

For the second through fourth elements in the second row,

$$\frac{\partial y_k}{\partial \Delta n}, \frac{\partial y_k}{\partial e}, \text{ and } \frac{\partial y_k}{\partial \sqrt{A}}, \text{ all the partials are complete:}$$

$$\frac{\partial y_k}{\partial \Delta n} = \frac{\partial y_k}{\partial x_p} \frac{\partial x_p}{\partial \Delta n} + \frac{\partial y_k}{\partial y_p} \frac{\partial y_p}{\partial \Delta n} + \frac{\partial y_k}{\partial i_k} \frac{\partial i_k}{\partial \Delta n} \quad (C-84)$$

$$\frac{\partial y_k}{\partial x_p} \quad (C-81) \quad , \quad \frac{\partial x_p}{\partial \Delta n} \quad (C-20),$$

$$\frac{\partial y_k}{\partial y_p} \quad (C-82) \quad , \quad \frac{\partial y_p}{\partial \Delta n} \quad (C-24),$$

$$\frac{\partial y_k}{\partial i_k} \quad (C-83) \quad , \quad \frac{\partial i_k}{\partial \Delta n} \quad (C-25);$$

$$\frac{\partial y_k}{\partial e} = \frac{\partial y_k}{\partial x_p} \frac{\partial x_p}{\partial e} + \frac{\partial y_k}{\partial y_p} \frac{\partial y_p}{\partial e} + \frac{\partial y_k}{\partial i_k} \frac{\partial i_k}{\partial e} \quad (C-85)$$

$$\frac{\partial y_k}{\partial x_p} \quad (C-81) \quad , \quad \frac{\partial x_p}{\partial e} \quad (C-27),$$

$$\frac{\partial y_k}{\partial y_p} \quad (C-82) \quad , \quad \frac{\partial y_p}{\partial e} \quad (C-32),$$

$$\frac{\partial y_k}{\partial i_k} \quad (C-83) \quad , \quad \frac{\partial i_k}{\partial e} \quad (C-33);$$

$$\frac{\partial y_k}{\partial \sqrt{A}} = \frac{\partial y_k}{\partial x_p} \frac{\partial x_p}{\partial \sqrt{A}} + \frac{\partial y_k}{\partial y_p} \frac{\partial y_p}{\partial \sqrt{A}} + \frac{\partial y_k}{\partial i_k} \frac{\partial i_k}{\partial \sqrt{A}} \quad (C-86)$$

$$\frac{\partial y_k}{\partial x_p} \quad (C-81) \quad , \quad \frac{\partial x_p}{\partial \sqrt{A}} \quad (C-35) ,$$

$$\frac{\partial y_k}{\partial y_p} \quad (C-82) \quad , \quad \frac{\partial y_p}{\partial \sqrt{A}} \quad (C-45) ,$$

$$\frac{\partial y_k}{\partial i_k} \quad (C-83) \quad , \quad \frac{\partial i_k}{\partial \sqrt{A}} \quad (C-46) .$$

Now, the fifth element in the second row is $\frac{\partial y_k}{\partial \Omega_0}$, which adds one new partial.

$$\frac{\partial y_k}{\partial \Omega_0} = \frac{\partial y_k}{\partial x_p} \frac{\partial x_p}{\partial \Omega_0} + \frac{\partial y_k}{\partial y_p} \frac{\partial y_p}{\partial \Omega_0} + \frac{\partial y_k}{\partial i_k} \frac{\partial i_k}{\partial \Omega_0} + \frac{\partial y_k}{\partial \Omega_0} \quad (C-87)$$

$$\frac{\partial y_k}{\partial \Omega_0} = r_k \cos(u_k) \cos(\Omega_k) - r_k \sin(u_k) \cos(i_k) \sin(\Omega_k) \quad (C-88)$$

noting that $\frac{\partial x_p}{\partial \Omega_0} = \frac{\partial y_p}{\partial \Omega_0} = \frac{\partial i_k}{\partial \Omega_0} = 0$

The sixth element in the second row, $\frac{\partial y_k}{\partial i_0}$, also adds one new partial:

$$\frac{\partial y_k}{\partial i_0} = \frac{\partial y_k}{\partial x_p} \frac{\partial x_p}{\partial i_0} + \frac{\partial y_k}{\partial y_p} \frac{\partial y_p}{\partial i_0} + \frac{\partial y_k}{\partial i_k} \frac{\partial i_k}{\partial i_0} \quad (C-89)$$

$$\frac{\partial y_k}{\partial i_0} = -r_k \sin(u_k) \sin(i_k) (\cos \Omega_k) \quad (C-90)$$

again, noting that $\frac{\partial x_p}{\partial i_0} = \frac{\partial y_p}{\partial i_0} = 0$ and $\frac{\partial i_k}{\partial i_0}$ is unity.

The seventh through fifteenth elements are complete with

the partials referenced to their equations below:

$$\frac{\partial y_k}{\partial u} = \frac{\partial y_k}{\partial x_p} \frac{\partial x_p}{\partial u} + \frac{\partial y_k}{\partial y_p} \frac{\partial y_p}{\partial u} + \frac{\partial y_k}{\partial i_k} \frac{\partial i_k}{\partial u} \quad (C-91)$$

$$\frac{\partial y_k}{\partial x_p} \quad (C-81) \quad , \quad \frac{\partial x_p}{\partial u} \quad (C-52)$$

$$\frac{\partial y_k}{\partial y_p} \quad (C-82) \quad , \quad \frac{\partial y_p}{\partial u} \quad (C-54)$$

$$\frac{\partial y_k}{\partial i_k} \quad (C-83) \quad , \quad \frac{\partial i_k}{\partial u} \quad (C-55)$$

$$\frac{\partial y_k}{\partial i} = \frac{\partial y_k}{\partial x_p} \frac{\partial x_p}{\partial i} + \frac{\partial y_k}{\partial y_p} \frac{\partial y_p}{\partial i} + \frac{\partial y_k}{\partial i_k} \frac{\partial i_k}{\partial i} \quad (C-92)$$

$$\text{Where, } \frac{\partial x_p}{\partial i} = \frac{\partial y_p}{\partial i} = 0 \quad ,$$

$$\text{and, } \frac{\partial y_k}{\partial i_k} \quad (C-83) \quad , \quad \frac{\partial i_k}{\partial i} \quad (C-59)$$

$$\frac{\partial y_k}{\partial C_{uc}} = \frac{\partial y_k}{\partial x_p} \frac{\partial x_p}{\partial C_{uc}} + \frac{\partial y_k}{\partial y_p} \frac{\partial y_p}{\partial C_{uc}} + \frac{\partial y_k}{\partial i_k} \frac{\partial i_k}{\partial C_{uc}} \quad (C-93)$$

$$\frac{\partial y_k}{\partial x_p} \quad (C-81) \quad , \quad \frac{\partial x_p}{\partial C_{uc}} \quad (C-61) \quad ,$$

$$\frac{\partial y_k}{\partial y_p} \quad (C-82) \quad , \quad \frac{\partial y_p}{\partial C_{uc}} \quad (C-63) \quad ,$$

$$\text{and } \frac{\partial i_k}{\partial C_{uc}} \text{ is zero.}$$

$$\frac{\partial y_k}{\partial C_{us}} = \frac{\partial y_k}{\partial x_p} \frac{\partial x_p}{\partial C_{us}} + \frac{\partial y_k}{\partial y_p} \frac{\partial y_p}{\partial C_{us}} + \frac{\partial y_k}{\partial i_k} \frac{\partial i_k}{\partial C_{us}} \quad (C-94)$$

$$\frac{\partial y_k}{\partial x_p} \quad (C-81) \quad , \quad \frac{\partial x_p}{\partial C_{us}} \quad (C-65) ,$$

$$\frac{\partial y_k}{\partial y_p} \quad (C-82) \quad , \quad \frac{\partial y_p}{\partial C_{us}} \quad (C-67) ,$$

and $\frac{\partial i_k}{\partial C_{us}}$ is zero.

$$\frac{\partial y_k}{\partial C_{rc}} = \frac{\partial y_k}{\partial x_p} \frac{\partial x_p}{\partial C_{rc}} + \frac{\partial y_k}{\partial y_p} \frac{\partial y_p}{\partial C_{rc}} + \frac{\partial y_k}{\partial i_k} \frac{\partial i_k}{\partial C_{rc}} \quad (C-95)$$

$$\frac{\partial y_k}{\partial x_p} \quad (C-81) \quad , \quad \frac{\partial x_p}{\partial C_{rc}} \quad (C-69) ,$$

$$\frac{\partial y_k}{\partial y_p} \quad (C-82) \quad , \quad \frac{\partial y_p}{\partial C_{rc}} \quad (C-71) ,$$

and $\frac{\partial i_k}{\partial C_{rc}}$ is zero.

$$\frac{\partial y_k}{\partial C_{rs}} = \frac{\partial y_k}{\partial x_p} \frac{\partial x_p}{\partial C_{rs}} + \frac{\partial y_k}{\partial y_p} \frac{\partial y_p}{\partial C_{rs}} + \frac{\partial y_k}{\partial i_k} \frac{\partial i_k}{\partial C_{rs}} \quad (C-96)$$

$$\frac{\partial y_k}{\partial x_p} \quad (C-81) \quad , \quad \frac{\partial x_p}{\partial C_{rs}} \quad (C-73) ,$$

$$\frac{\partial y_k}{\partial y_p} \quad (C-82) \quad , \quad \frac{\partial y_p}{\partial C_{rs}} \quad (C-75) ,$$

and $\frac{\partial i_k}{\partial C_{rs}}$ is zero.

$$\frac{\partial y_k}{\partial C_{ic}} = \frac{\partial y_k}{\partial x_p} \frac{\partial x_p}{\partial C_{ic}} + \frac{\partial y_k}{\partial y_p} \frac{\partial y_p}{\partial C_{ic}} + \frac{\partial y_k}{\partial i_k} \frac{\partial i_k}{\partial C_{ic}} \quad (C-97)$$

$$\text{Here, } \frac{\partial x_p}{\partial C_{ic}} = \frac{\partial y_p}{\partial C_{ic}} = 0 \quad , \quad \text{and } \frac{\partial y_k}{\partial i_k} \quad (C-83) \quad , \quad \frac{\partial i_k}{\partial C_{ic}} \quad (C-77)$$

$$\frac{\partial y_k}{\partial C_{is}} = \frac{\partial y_k}{\partial x_p} \frac{\partial x_p}{\partial C_{is}} + \frac{\partial y_k}{\partial y_p} \frac{\partial y_p}{\partial C_{is}} + \frac{\partial y_k}{\partial i_k} \frac{\partial i_k}{\partial C_{is}} \quad (C-98)$$

Here again, $\frac{\partial x_p}{\partial C_{is}} = \frac{\partial y_p}{\partial C_{is}} = 0$

and $\frac{\partial y_k}{\partial i_k}$ (C-83) , $\frac{\partial i_k}{\partial C_{is}}$ (C-79)

This completes the fifteen elements in the second row of the H matrix. The third row is very similar.

The first element of the third row is $\frac{\partial z_k}{\partial M_o}$:

$$\frac{\partial z_k}{\partial M_o} = \frac{\partial z_k}{\partial x_p} \frac{\partial x_p}{\partial M_o} + \frac{\partial z_k}{\partial y_p} \frac{\partial y_p}{\partial M_o} + \frac{\partial z_k}{\partial i_k} \frac{\partial i_k}{\partial M_o} \quad (C-99)$$

The new partials for the third row are:

$$\frac{\partial z_k}{\partial x_p} = 0$$

$$\frac{\partial z_k}{\partial y_p} = \sin(i_k) \quad (C-100)$$

and $\frac{\partial z_k}{\partial i_k} = r_k \sin(u_k) \cos(i_k) \quad (C-101)$

The other partials are complete, as indicated by the reference equations: $\frac{\partial x_p}{\partial M_o}$ (C-5), $\frac{\partial y_p}{\partial M_o}$ (C-14), and $\frac{\partial i_k}{\partial M_o}$ (C-17).

The other fourteen elements in the third row introduce no new partials. Because the partial $\frac{\partial z_k}{\partial x_p}$ is zero, all the

third row elements are shortened by that term. For example, the second element is $\frac{\partial z_k}{\partial \Delta n}$:

$$\frac{\partial z_k}{\partial \Delta n} = \frac{\partial z_k}{\partial y_p} \frac{\partial y_p}{\partial \Delta n} + \frac{\partial z_k}{\partial i_k} \frac{\partial i_k}{\partial \Delta n}, \quad (C-102)$$

where

$$\frac{\partial z_k}{\partial y_p} \quad (C-100) \quad , \quad \frac{\partial y_p}{\partial \Delta n} \quad (C-24)$$

$$\frac{\partial z_k}{\partial i_k} \quad (C-101) \quad , \quad \frac{\partial i_k}{\partial \Delta n} \quad (C-25)$$

Element three is $\frac{\partial z_k}{\partial e}$:

$$\frac{\partial z_k}{\partial e} = \frac{\partial z_k}{\partial y_p} \frac{\partial y_p}{\partial e} + \frac{\partial z_k}{\partial i_k} \frac{\partial i_k}{\partial e} \quad (C-103)$$

$$\frac{\partial z_k}{\partial y_p} \quad (C-100) \quad , \quad \frac{\partial y_p}{\partial e} \quad (C-32)$$

$$\frac{\partial z_k}{\partial i_k} \quad (C-101) \quad , \quad \frac{\partial i_k}{\partial e} \quad (C-33)$$

The next element is $\frac{\partial z_k}{\partial \sqrt{A}}$:

$$\frac{\partial z_k}{\partial \sqrt{A}} = \frac{\partial z_k}{\partial y_p} \frac{\partial y_p}{\partial \sqrt{A}} + \frac{\partial z_k}{\partial i_k} \frac{\partial i_k}{\partial \sqrt{A}} \quad (C-104)$$

$$\frac{\partial z_k}{\partial y_p} \quad (C-100) \quad \frac{\partial y_p}{\partial \sqrt{A}} \quad (C-45)$$

$$\frac{\partial z_k}{\partial i_k} \quad (C-101) \quad \frac{\partial i_k}{\partial \sqrt{A}} \quad (C-46)$$

The partial, $\frac{\partial z_k}{\partial \Omega_0}$, is next; however, both factors are zero:

$$\frac{\partial z_k}{\partial \Omega_0} = \frac{\partial z_k}{\partial y_p} \frac{\partial y_p}{\partial \Omega_0} + \frac{\partial z_k}{\partial i_k} \frac{\partial i_k}{\partial \Omega_0} \quad (C-105)$$

Where $\frac{\partial y_p}{\partial \Omega_0} = \frac{\partial i_k}{\partial \Omega_0} = 0$

so $\frac{\partial z_k}{\partial \Omega_0}$ is a constant zero.

Next is $\frac{\partial z_k}{\partial i_0}$:

$$\frac{\partial z_k}{\partial i_0} = \frac{\partial z_k}{\partial y_p} \frac{\partial y_p}{\partial i_0} + \frac{\partial z_k}{\partial i_k} \frac{\partial i_k}{\partial i_0} \quad (C-106)$$

here, $\frac{\partial y_p}{\partial i_0}$ is zero, leaving only $\frac{\partial z_k}{\partial i_0}$ (C-101), noting that $\frac{\partial i_k}{\partial i_0}$ is unity.

The seventh element is $\frac{\partial z_k}{\partial u}$:

$$\frac{\partial z_k}{\partial u} = \frac{\partial z_k}{\partial y_p} \frac{\partial y_p}{\partial u} + \frac{\partial z_k}{\partial i_k} \frac{\partial i_k}{\partial u} \quad (C-107)$$

where $\frac{\partial z_k}{\partial y_p}$ (C-100) $\frac{\partial y_p}{\partial u}$ (C-54)

$\frac{\partial z_k}{\partial i_k}$ (C-101) $\frac{\partial i_k}{\partial u}$ (C-55)

The next element in row three is $\frac{\partial z_k}{\partial \Omega}$:

$$\frac{\partial z_k}{\partial \Omega} = \frac{\partial z_k}{\partial y_p} \frac{\partial y_p}{\partial \Omega} + \frac{\partial z_k}{\partial i_k} \frac{\partial i_k}{\partial \Omega}, \quad (C-108)$$

where both factors are zero, so $\frac{\partial z_k}{\partial \Omega}$ is a constant zero.

Next is $\frac{\partial z_k}{\partial i}$:

$$\frac{\partial z_k}{\partial i} = \frac{\partial z_k}{\partial y_p} \frac{\partial y_p}{\partial i} + \frac{\partial z_k}{\partial i_k} \frac{\partial i_k}{\partial i} \quad (C-109)$$

where $\frac{\partial y_p}{\partial i}$ is zero, $\frac{\partial z_k}{\partial i_k}$ (C-101), and $\frac{\partial i_k}{\partial i}$ (C-59).

The last six elements are all very similar:

$$\frac{\partial z_k}{\partial C_{uc}} = \frac{\partial z_k}{\partial y_p} \frac{\partial y_p}{\partial C_{uc}} + \frac{\partial z_k}{\partial i_k} \frac{\partial i_k}{\partial C_{uc}} \quad (C-110)$$

$$\frac{\partial z_k}{\partial y_p} \quad (C-100) \quad , \quad \frac{\partial y_p}{\partial C_{uc}} \quad (C-63)$$

and $\frac{\partial i_k}{\partial C_{uc}}$ is zero.

$$\frac{\partial z_k}{\partial C_{us}} = \frac{\partial z_k}{\partial y_p} \frac{\partial y_p}{\partial C_{us}} + \frac{\partial z_k}{\partial i_k} \frac{\partial i_k}{\partial C_{us}} \quad (C-111)$$

$$\frac{\partial z_k}{\partial y_p} \quad (C-100) \quad , \quad \frac{\partial y_p}{\partial C_{us}} \quad (C-67),$$

and $\frac{\partial i_k}{\partial C_{us}}$ is zero.

$$\frac{\partial z_k}{\partial C_{rc}} = \frac{\partial z_k}{\partial y_p} \frac{\partial y_p}{\partial C_{rc}} + \frac{\partial z_k}{\partial i_k} \frac{\partial i_k}{\partial C_{rc}} \quad (C-112)$$

$$\frac{\partial z_k}{\partial y_p} \quad (C-100) \quad , \quad \frac{\partial y_p}{\partial C_{rc}} \quad (C-71)$$

and $\frac{\partial i_k}{\partial C_{rc}}$ is zero.

$$\frac{\partial z_k}{\partial C_{rs}} = \frac{\partial z_k}{\partial y_p} \frac{\partial y_p}{\partial C_{rs}} + \frac{\partial z_k}{\partial i_k} \frac{\partial i_k}{\partial C_{rs}} \quad (C-113)$$

$$\frac{\partial z_k}{\partial y_p} \quad (C-100) \quad , \quad \frac{\partial y_p}{\partial C_{rs}} \quad (C-75)$$

and $\frac{\partial i_k}{\partial C_{rs}}$ is zero.

$$\frac{\partial z_k}{\partial C_{ic}} = \frac{\partial z_k}{\partial y_p} \frac{\partial y_p}{\partial C_{ic}} + \frac{\partial z_k}{\partial i_k} \frac{\partial i_k}{\partial C_{ic}} \quad (C-114)$$

Here, $\frac{\partial y_p}{\partial C_{ic}}$ is zero, $\frac{\partial z_k}{\partial i_k} \quad (C-101) \quad , \quad$ and $\frac{\partial i_k}{\partial C_{ic}} \quad (C-77) .$

$$\frac{\partial z_k}{\partial C_{is}} = \frac{\partial z_k}{\partial y_p} \frac{\partial y_p}{\partial C_{is}} + \frac{\partial z_k}{\partial i_k} \frac{\partial i_k}{\partial C_{is}} \quad (C-115)$$

Again, $\frac{\partial y_p}{\partial C_{is}}$ is zero, $\frac{\partial z_k}{\partial i_k} \quad (C-101) , \quad$ and $\frac{\partial i_k}{\partial C_{is}} \quad (C-79)$

This completes the third row and consequently finishes the forty-five elements of the H matrix. These elements form a subroutine called HCALC in the Broadcast Ephemeris Algorithm.

APPENDIX D

THE MEASUREMENT SENSITIVITY MATRIX FOR THE EPHEMERIS UPDATE ALGORITHM

This appendix derives the H matrix for the broadcast ephemeris update algorithm. The elements of the 1x8 matrix are partial derivatives of the pseudorange with respect to the eight elements of the state, evaluated on the reference trajectory.

$$H = \frac{\partial G(X^*, t)}{\partial X}$$

where $G(X, t) = p_c$ the calculated pseudorange.

The elements of the H matrix are:

$$H = \begin{vmatrix} \frac{\partial p_c}{\partial M_0} & \frac{\partial p_c}{\partial e} & \dots & \frac{\partial p_c}{\partial a_1} \end{vmatrix}$$

This appendix presents each of the partial derivatives as programmed in the Ephemeris Update Algorithm.

The elements of H are very similar to the corresponding elements in Appendix C, so that the chain rule of differentiation simplifies their formulation. However, the two partials with respect to the satellite clock parameters do not have corresponding elements in Appendix C, so they are separate. The equation which forms the basis for the partials is the pseudorange equation:

$$p_c = [(x_i - x_r)^2 + (y_i - y_r)^2 + (z_i - z_r)^2]^{\frac{1}{2}} - a_0 c - a_1 t_k c, \quad (D-1)$$

where x_i , y_i , and z_i are the i^{th} satellite coordinates, and x_r , y_r , and z_r are the known receiver coordinates, all in the ECF coordinate system. The other quantities are:

a_0 - clock bias (secs)

a_1 - clock drift rate (secs/sec)

c - speed of light (m/sec)

t_k - time (seconds since epoch, t_{oe})

The first partial is $\frac{\partial p_c}{\partial M_0}$:

$$\frac{\partial p_c}{\partial M_0} = \frac{\partial p_c}{\partial x_k} \frac{\partial x_k}{\partial M_0} + \frac{\partial p_c}{\partial y_k} \frac{\partial y_k}{\partial M_0} + \frac{\partial p_c}{\partial z_k} \frac{\partial z_k}{\partial M_0} \quad (D-2)$$

$$\text{where } \frac{\partial p_c}{\partial x_k} = \frac{(x_i - x_r)}{cp} \quad (D-3)$$

$$\text{and } cp = [(x_i - x_r)^2 + (y_i - y_r)^2 + (z_i - z_r)^2]^{\frac{1}{2}}. \quad (D-4)$$

The partial $\frac{\partial x_k}{\partial M_0}$ is equation (C-1) in Appendix C.

$$\text{Now, } \frac{\partial p_c}{\partial y_k} = \frac{(y_i - y_r)}{cp} \quad (D-5)$$

and $\frac{\partial y_k}{\partial M_0}$ is equation (C-80).

The last factors in equation D-2 are $\frac{\partial p_c}{\partial z_k}$ and $\frac{\partial z_k}{\partial M_0}$.

$$\frac{\partial p_c}{\partial z_k} = \frac{(z_i - z_r)}{cp} \quad (D-6)$$

and $\frac{\partial z_k}{\partial M_o}$ is equation (C-99).

The second element in H is $\frac{\partial p_c}{\partial e}$:

$$\frac{\partial p_c}{\partial e} = \frac{\partial p_c}{\partial x_k} \frac{\partial x_k}{\partial e} + \frac{\partial p_c}{\partial y_k} \frac{\partial y_k}{\partial e} + \frac{\partial p_c}{\partial z_k} \frac{\partial z_k}{\partial e} \quad (D-7)$$

$$\frac{\partial p_c}{\partial x_k} \text{ (D-3), } \frac{\partial x_k}{\partial e} \text{ (C-26)}$$

$$\frac{\partial p_c}{\partial y_k} \text{ (D-5), } \frac{\partial y_k}{\partial e} \text{ (C-85)}$$

$$\frac{\partial p_c}{\partial z_k} \text{ (D-6), } \frac{\partial z_k}{\partial e} \text{ (C-103)}$$

The next element is $\frac{\partial p_c}{\partial \sqrt{A}}$:

$$\frac{\partial p_c}{\partial \sqrt{A}} = \frac{\partial p_c}{\partial x_k} \frac{\partial x_k}{\partial \sqrt{A}} + \frac{\partial p_c}{\partial y_k} \frac{\partial y_k}{\partial \sqrt{A}} + \frac{\partial p_c}{\partial z_k} \frac{\partial z_k}{\partial \sqrt{A}} \quad (D-8)$$

$$\frac{\partial p_c}{\partial x_k} \text{ (D-3), } \frac{\partial x_k}{\partial \sqrt{A}} \text{ (C-34)}$$

$$\frac{\partial p_c}{\partial y_k} \text{ (D-5), } \frac{\partial y_k}{\partial \sqrt{A}} \text{ (C-86)}$$

$$\frac{\partial p_c}{\partial z_k} \text{ (D-6), } \frac{\partial z_k}{\partial \sqrt{A}} \text{ (C-104)}$$

The fourth element is $\frac{\partial p_c}{\partial \Omega_o}$:

$$\frac{\partial p_c}{\partial \Omega_o} = \frac{\partial p_c}{\partial x_k} \frac{\partial x_k}{\partial \Omega_o} + \frac{\partial p_c}{\partial y_k} \frac{\partial y_k}{\partial \Omega_o} + \frac{\partial p_c}{\partial z_k} \frac{\partial z_k}{\partial \Omega_o} \quad (D-9)$$

$$\frac{\partial p_c}{\partial x_k} \text{ (D-3), } \frac{\partial x_k}{\partial \Omega_o} \text{ (C-47)}$$

$$\frac{\partial p_c}{\partial y_k} \text{ (D-5), } \frac{\partial y_k}{\partial \Omega_o} \text{ (C-87)}$$

$$\frac{\partial p_c}{\partial z_k} \text{ (D-6), } \frac{\partial z_k}{\partial \Omega_o} \text{ (C-105)}$$

Next is the partial, $\frac{\partial p_c}{\partial i_o}$:

$$\frac{\partial p_c}{\partial i_o} = \frac{\partial p_c}{\partial x_k} \frac{\partial x_k}{\partial i_o} + \frac{\partial p_c}{\partial y_k} \frac{\partial y_k}{\partial i_o} + \frac{\partial p_c}{\partial z_k} \frac{\partial z_k}{\partial i_o} \quad (\text{D-10})$$

$$\frac{\partial p_c}{\partial x_k} \text{ (D-3), } \frac{\partial x_k}{\partial i_o} \text{ (C-49)}$$

$$\frac{\partial p_c}{\partial y_k} \text{ (D-5), } \frac{\partial y_k}{\partial i_o} \text{ (C-89)}$$

$$\frac{\partial p_c}{\partial z_k} \text{ (D-6), } \frac{\partial z_k}{\partial i_o} \text{ (C-106)}$$

The sixth element is $\frac{\partial p_c}{\partial \omega}$:

$$\frac{\partial p_c}{\partial \omega} = \frac{\partial p_c}{\partial x_k} \frac{\partial x_k}{\partial \omega} + \frac{\partial p_c}{\partial y_k} \frac{\partial y_k}{\partial \omega} + \frac{\partial p_c}{\partial z_k} \frac{\partial z_k}{\partial \omega} \quad (\text{D-11})$$

$$\frac{\partial p_c}{\partial x_k} \text{ (D-3), } \frac{\partial x_k}{\partial \omega} \text{ (C-51)}$$

$$\frac{\partial p_c}{\partial y_k} \text{ (D-5), } \frac{\partial y_k}{\partial \omega} \text{ (C-91)}$$

$$\frac{\partial p_c}{\partial z_k} \text{ (D-6), } \frac{\partial z_k}{\partial \omega} \text{ (C-107)}$$

The partials with respect to the satellite clock parameters are next:

$$\frac{\partial p_c}{\partial a_o} = -c \quad (D-12)$$

$$\text{and} \quad \frac{\partial p_c}{\partial a_1} = -t_k c \quad (D-13)$$

The algorithm actually normalizes these last two partials with the speed of light, so that the partials are:

$$\frac{\partial p_c}{\partial a_o c} = -1.0 \quad (D-14)$$

$$\text{and} \quad \frac{\partial p_c}{\partial a_1 c} = -t_k \quad (D-15)$$

This concludes the partial derivatives for the H matrix in the Ephemeris Update Algorithm.

APPENDIX E

PROPAGATING THE BROADCAST PARAMETERS TO THE UPDATE TIME

This appendix describes the method for moving the mean anomaly at epoch, M_0 , the longitude of the ascending node at epoch, Ω_0 , and the Earth-Centered, Earth-Fixed (ECF) Coordinate System from any date to another. This method is used in the Broadcast Ephemeris Update Algorithm to provide initial conditions that are within its convergence criteria.

The time, in seconds, between the original broadcast epoch and the desired update epoch is determined first. Because the time of epoch is reset to zero each Sunday at 00:00, the time between epochs must include the number of resets. For instance, to find the time between the epoch at 489,600 seconds on 11 October 1985 (1600 hours on Friday) and the epoch at 320,400 seconds on 20 November 1985 (1700 hours on Wednesday), the number of resets is six. Five full weeks, plus the last part of the 11 October week, plus the first part of the 20 November week combine for a total of 3,459,600 seconds. This Δt is multiplied by the corrected mean motion, n , and the node rate, $\dot{\Omega}$, then these products are added to M_0 and Ω_0 , respectively, to obtain the two corrected parameters. For instance,

the mean motion for SV11 on 11 October is calculated to be 1.4585058×10^{-4} radians per second. The mean motion correction (another ephemeris parameter), $\Delta n = 1.6411397 \times 10^{-9}$ radians per second, is added to n before multiplying by the Δt . The product, $n\Delta t$, produces a ΔM_0 of 504.59034 radians, which is added to the broadcast M_0 , 3.0089462 radians, to get 507.599286 radians. Reducing this M_0 value to below two pi radians yields 4.944466 radians for the initial condition which is close to the broadcast M_0 at 320400 seconds on 20 November: 4.9422925 radians. The same process to update Ω_0 on 20 November starts with the 11 October parameters: $\Omega_0 = 2.2143991$ radians and $\dot{\Omega} = 6.3049051 \times 10^{-9}$ radians per second. Then $\dot{\Omega}\Delta t$ is -2.181245×10^{-2} radians, which is added to Ω_0 to get the initial condition at 320,400 seconds on 20 November: 2.1925867 radians. The broadcast Ω_0 for the same time is 1.469856512 radians, which appears to be quite inaccurate until the coordinate system correction is applied.

The ECF coordinate system must be updated because the ephemeris parameters are measured from the instantaneous coordinate position at 00:00 Sunday each week. Consequently, multiplying the Earth rotation rate by the number of seconds between the Sunday axis updates will move the coordinates close enough to their proper

orientation. For instance, the six Sunday updates between 11 October and 20 November cover 3,628,800 seconds, which produces a total Earth rotation of 264.61627 radians, or equivalently, 0.72248985 radians. This angle is subtracted from the longitude of the ascending node to account for the rotating axis. The resulting Ω_0 is 1.4700969, which compares accurately with the broadcast value. This completes the updates that are required to initiate the ephemeris update algorithm.

APPENDIX F

DERIVATION OF THE FILTER GAIN AND COVARIANCE MATRIX FOR THE EXTENDED KALMAN FILTER

This appendix derives the filter gain, K_k , and the covariance matrix P_k for the Extended Kalman Filter (EKF). The derivation begins with the batch, weighted, least squares estimate of the state corrections,

$$\hat{x}_k = (H_k^T W_k H_k)^{-1} H_k^T W_k y_k \quad (F-1)$$

where \hat{x}_k is the best estimate of the state corrections,

H_k, H_k^T are the measurement sensitivity matrix, and

its transpose,

W_k is the measurement weighting matrix, and

y_k are the measurements, all referenced time k .

The state variances and covariances from the estimate at time k are available in the covariance matrix, P_k

$$P_k = (H_k^T W_k H_k)^{-1}. \quad (F-2)$$

When new measurements, y_{k+1} are available at time $k+1$, the state and covariance matrix are propagated forward by

the state transition matrix, $\Phi(t_{k+1}, t_k)$,

$$\bar{x}_{k+1} = \Phi(t_{k+1}, t_k) \hat{x}_k, \quad (F-3)$$

$$\text{and } \bar{P}_{k+1} = \Phi(t_{k+1}, t_k) P_k \Phi^T(t_{k+1}, t_k), \quad (F-4)$$

where the bar notation indicates a propagated quantity. With the propagated state and covariance matrix, the new measurements are included in the batch, sequential estimate of the state corrections,

$$\hat{x}_{k+1} = (H_{k+1}^T W_{k+1} H_{k+1} + \bar{P}_{k+1}^{-1})^{-1} (H_{k+1}^T W_{k+1} y_{k+1} + \bar{P}_{k+1}^{-1} \bar{x}_{k+1}) \quad (F-5)$$

By relating the first term in parentheses in equation F-5, with the first term in parentheses in equation F-1, it is seen that the new covariance matrix which contains the information from times t_k and t_{k+1} , is given by

$$P_{k+1} = (H_{k+1}^T W_{k+1} H_{k+1} + \bar{P}_{k+1}^{-1})^{-1} \quad (F-6)$$

If the batch of measurements contains only one measurement, then the algorithm can be rewritten as a purely sequential processor (Kalman Filter). The first step in the change to the Kalman Filter is to reset the time $k+1$ to time k , then manipulate Equation F-6 to get P_k in a form that requires the inversion of a scalar instead of the matrix. The manipulation begins by inverting both

sides of Equation F-6

$$P_k^{-1} = H_k^T W_k H_k + \bar{P}_k^{-1}. \quad (F-7)$$

Then pre-multiply by P_k , followed by post-multiplying by \bar{P}_k to get:

$$\bar{P}_k = P_k H_k^T W_k H_k \bar{P}_k + P_k, \quad (F-8)$$

or rearranged:

$$P_k = \bar{P}_k - P_k H_k^T W_k H_k \bar{P}_k. \quad (F-9)$$

Post-multiplying (F-8) by $H_k^T W_k$ yields:

$$\bar{P}_k H_k^T W_k = P_k H_k^T W_k H_k \bar{P}_k H_k^T W_k + P_k H_k^T W_k. \quad (F-10)$$

The next step is to factor $P_k H_k^T W_k$ from the right side of (F-10):

$$\bar{P}_k H_k^T W_k = P_k H_k^T W_k [H_k \bar{P}_k H_k^T W_k + I]. \quad (F-11)$$

Factoring W_k from the right side of (F-11) gives:

$$\bar{P}_k H_k^T W_k = P_k H_k^T W_k [H_k \bar{P}_k H_k^T + W_k^{-1}] W_k. \quad (F-12)$$

Next post-multiply (F-12) by W_k^{-1} to get:

$$\bar{P}_k H_k^T = P_k H_k^T W_k [H_k \bar{P}_k H_k^T + W_k^{-1}]. \quad (F-13)$$

Finally, solve for $P_k H_k^T W_k$ in (F-13) to substitute into (F-9):

$$P_k H_k^T W_k = \bar{P}_k H_k^T [H_k \bar{P}_k H_k^T + W_k^{-1}]^{-1}. \quad (F-14)$$

When the substitution is done, Equation (F-9) provides the form for P_k that requires inverting a matrix with the same dimensions as the number of observations (a scalar inversion in the Kalman Filter):

$$P_k = \bar{P}_k - \bar{P}_k H_k^T [H_k \bar{P}_k H_k^T + W_k^{-1}]^{-1} H_k \bar{P}_k \quad (F-15)$$

This equation is referred to as the Schurr Identity (Tapley and Born, 1985).

The filter gain, K_k is defined as:

$$K_k = \bar{P}_k H_k^T [H_k \bar{P}_k H_k^T + W_k^{-1}]^{-1}, \quad (F-16)$$

which is the same as the right side of (F-14), providing a shorter form for K_k :

$$K_k = P_k H_k^T W_k. \quad (F-17)$$

Equation (F-16) substituted into (F-15) simplifies the equation for P_k :

$$P_k = [I - K_k H_k] \bar{P}_k. \quad (F-18)$$

To obtain the solution for the Kalman Filter, Equation (F-6) must be substituted in (F-5):

$$\hat{x}_k = P_k [H_k^T W_k y_k + \bar{P}_k^{-1} \bar{x}_k], \quad (F-19)$$

or in expanded form:

$$\hat{x}_k = P_k H_k^T W_k y_k + P_k \bar{P}_k^{-1} \bar{x}_k \quad (F-20)$$

Using Equations (F-17) and (F-18) in (F-20) provides the Kalman solution:

$$\hat{x}_k = K_k y_k + [I - K_k H_k] \bar{P}_k \bar{P}_k^{-1} \bar{x}_k, \quad (F-21)$$

which is simplified to the following:

$$\hat{x}_k = \bar{x}_k + K_k [y_k - H_k \bar{x}_k]. \quad (F-22)$$

This equation gives the best estimate of the state corrections when given the propagated (or a priori) state and covariance matrix, and the single measurement, y_k [Tapley and Born, 1985].

The Extended Kalman Filter is very similar to the Kalman Filter except that the EKF updates the reference

trajectory after each observation. This update minimizes the effect of errors due to dropping higher order terms when linearizing the state dynamics and the observation-state relationship. Mathematically, the reference trajectory, x^* , is updated by the latest estimate of the state corrections,

$$\hat{x}_k = x_k^* + \hat{x}_k, \quad (F-23)$$

then the reference trajectory is integrated forward using \hat{x}_k as the new initial condition. This new process eliminates the need to propagate the state corrections, so there is no \bar{x}_k which reduces the EKF solution to

$$\hat{x}_k = K_k y_k. \quad (F-24)$$

The need to propagate the P_k matrix still exists and the equations for the P_{k+1} and K_{k+1} matrices stay the same. Overall, convergence for the EKF is more rapid than the Kalman Filter because of the reduction in errors introduced during the linearization, and implementation is simpler.

References

Abusali, PAM, Private Communication, Post-graduate Engineer, University of Texas at Austin, TX, 1985.

Ananda, Mohan P., Harold Bernstein, R.W. Bruce, K.E. Cunningham, W.A. Feess, P.S. Jorgensen, M. Menn, and C.M. Price, "Autonomous Navigation of the Global Positioning System Satellites," The Aerospace Corporation, El Segundo, CA, AIAA Paper No. 84-1863-CP, Aug 1984.

Ananda, Mohan P., Harold Bernstein, William A. Feess, and Thomas C. Paugstat, "The Global Positioning System (GPS) Autonomous User System," The Aerospace Corporation, El Segundo, CA, Jan 1988.

Bate, Roger R., Donald D. Mueller, and Jerry E. White, Fundamental of Astronautics, Dover Publications, Inc., New York, 1971.

Broucke, Roger A., "On the Matrizant of the Two-Body Problem," Astronautics and Astrophysics, Vol. 6, 1970.

Brouwer, D., and G.M. Clemence, Methods of Celestial Mechanics. New York, Academic Press, 1961.

Brown, Donald, Private Communication, Chief of the Navigation Analysis Section, 2 Satellite Control Squadron, Falcon AFS, CO, May 1987.

Chasko, Andy, Private Communication, General Dynamics Services, Yuma, AZ, Feb 1987.

Cholesky Subroutine on IMSL, International Mathematical Statistical Library, NBC Building, Houston, TX, 1985.

Conley, Rob, Private Communication, Chief of Test and Integration Branch, GPS Liaison Office, Detachment 4, Space Division, Falcon AFS, CO, Aug 1986, Feb 1987.

Davidson, Jeff., C.L. Thornton, T.H. Dixon, C.J. Vegas, L.E. Young, and T.P. Yunck, "The March 1985 Demonstration of the Fiducial Network Concept for GPS Geodesy: A Preliminary Report," TDA Progress Report 42-85, Jet Propulsion Laboratory, Pasadena, CA, 15 May 1986.

Decker, Louis B., "World Geodetic System 1984", Defense Mapping Agency Aerospace Center, Saint Louis, MO, 1986.

Duncombe, Raynor L., Private Communication, Professor of Aerospace Engineering, The University of Texas at Austin, Austin, TX, Sep 1985.

Easton, Roger L., "The Timation Navigation Satellites," Principles and Operational Aspects of Precision Determination Systems, AGARD-AG-245, Technical Editing and Reproduction, Ltd, Harford House, London, July 1979.

Faddeva, V.N., Computational Methods of Linear Algebra, Dover Publications, Inc., NY, 1959, Trans. by Curtis D. Benster.

Fang, Bertrand T., "Geometric Dilution of Precision in Global Positioning System Navigation", AIAA Journal of Guidance and Control, Vol. 4, No. 1, 1980.

Fliegel, H.F., W.A. Feess, W.C. Layton, and N.W. Rhodus, "The GPS Radiation Force Model," Proceedings of the First International Symposium on Precise Positioning with the Global Positioning System, Rockville, MD, April 1985.

Gentleman, W. Morven, "Least Squares Computations by Givens Transformations Without Square Roots," Journal of the Institute of Mathematical Applications, Vol. 12, 1973.

Goad, Clyde, Private Communication, NOAA/NOS/C15, Rockville, Md, 1985.

Glazer, B.G., "GPS Receiver Operation," Global Positioning System, The Institute of Navigation, Washington, D.C., 1980.

Hayward, Jonathan K, Solar and Geomagnetic Event Summary Letter, Chief of the Weather Support Division, Headquarters 4th Weather Wing, Peterson Air Force Base, CO, February 1987.

Hotelling, H., "Some New Methods in Matrix Calculation," Annual Mathematical Statistics, Vol. 4, 1943.

Hurley, M.J., J.L. Kramer, and D.D. Thornburg, "Master Control Station," Principles and Operational Aspects of Precision Determination Systems, AGARD-AG-245, Technical Editing and Reproduction, Ltd, Harford House, London, July 1979.

International Mathematical Systems Library (Computer Code), IMSL, NBC Building, Houston, TX.

Joint Program Office, "User's Overview," Deputy for Space Navigation Systems, Navstar Global Positioning System, Los Angeles, CA, September, 1984.

Kaula, William M., Theory of Satellite Geodesy, Blaisdell Publishing Company, Waltham, MA, 1966.

Kopitzke, E.R., Private Communication, Magnavox Corporation, Torrance, CA, August 1986.

Kozai, Yoshihide, "On the Effects of the Sun and the Moon upon the Motion of a Close-Earth Satellite," Smithsonian Contributions to Astrophysics, Vol. 6, Smithsonian Institution, Washington, D.C., 1963.

Kruh, Pierre, "The Navstar Global Positioning System Six-Plane, 18 - Satellite Constellation." The 1981 National Telecommunications Conference of the IEEE, IEEE Press, New York, November, 1981.

Kurtin, Duane, Private Communication, Computer Programmer, Satellite and Geophysics Division, Applied Research Laboratory, The University of Texas at Austin, Austin, TX, 1987.

Marquardt, Donald W., "Comment," Journal of the American Statistical Association, Washington, D.C., Vol. 75, Number 369, March 1980.

McCarthy, Dennis D., Private Communication, Chief of the Orientation Parameters Division, Time Service Department, US Naval Observatory, Washington, D.C., October 1985.

Milliken, R.J. and C.J. Zoller, "Principle of Operation of NAVSTAR System Characteristics," Global Positioning System, The Institute of Navigation, Washington, D.C., 1980.

Moller, V., "NAVSTAR GPS Space Segment/Navigation User Interfaces," ICD-GPS-200, Rockwell International Corporation, Downey, CA, September 1984.

Noe, Philip S., and Kenneth A. Meyers, "A Position Fixing Algorithm for the Low-Cost GPS Receiver," IEEE Transactions on Aerospace and Electronic Systems, Vol AES-12, No.2, March 1976.

Noe, Philip S., Kenneth A. Meyers, and T. K. Wu, "A Navigation Algorithm for the Low-Cost GPS Receiver," Navigation: Journal of the Institute of Navigation, Vol. 25, No. 2, Summer 1978.

Porter, J., Col., P. Kruh, Sq. Ldr. B. Sprosen, "GPS NAVSTAR System Overview," Navigation: Journal of the Institute of Navigation, Washington, D.C., Vol 25, No. 2, Summer 1978.

Rhodus, Wayne, Private Communication, Aerospace Corporation, El Segundo, CA, 1987.

Russell, S.S. and J.H. Schaibly, "Control Segment and User Performance," Navigation: Journal of the Institute of Navigation, Washington, D.C., Vol. 25, No. 2, Summer 1978.

Schutz, B.E. and B.D. Tapley, "UTOPIA: University of Texas Orbit Processor TR 80-1", Center for Space Research, University of Texas at Austin, Austin, TX, 1980.

Scott, V. Dan, "Standardized Exchange Format for NAVSTAR GPS Geodetic Data", Applied Research Laboratories, The University of Texas at Austin, Austin, TX, 24 March 1983.

Sentman, O.L. Lt Cmdr, Robert J. Danchik, and Lauren J. Rueger, "Joint Paper on the Navy Navigation Satellite System (TRANSIT) Status and Plans," Proceedings of the Fourth International Symposium on Satellite Positions, Austin, TX, April 1986.

Seppelin, Thomas O., "The Department of Defense World Geodetic System 1972", Defense Mapping Agency, Washington, D.C., May 1974.

Smart, W.M., Celestial Mechanics. New York, Longmans, 1953.

Stansell, Thomas A., Jr, "TRANSIT-The Current Satellite Navigation System," Principles and Operational Aspects of Precision Determination Systems, AGARD-AG-245, Technical Editing and Reproduction, Ltd, Harford House, London, July 1979.

Strang, Gilbert, Linear Algebra and Its Applications, Second Edition, Academic Press, New York, NY, 1980.

Tapley, Byron D. and George H. Born, "Statistical Orbit Determination Theory," Center for Space Research, University of Texas, Austin, TX, Jan 1985.

Texas Instruments TI 4100 GEOSTAR, "Interface Control Document for the Advanced Geodetic Receiver Application of the TI 4100 NAVSTAR Navigator", October 1982.

The Astronomical Almanac, U.S. Government Printing Office, 1985.

Van Dierendonck, A.J., S.S. Russell, E.R. Kopitzke, and M. Birnbaum, "The GPS Navigation Message", Navigation: Journal of the Institute of Navigation Washington, D.C., Vol. 25, No. 2, Summer 1978.

Wilson, Thomas., User's Reference Guide for the University of Texas Orbit Processor, Master's Thesis, The University of Texas at Austin, December 1976.

Wilson, Thomas, "GIVLIB," Computer Library for the Cyber 170 Computer, The University of Texas at Austin, May 1979.

VITA

Douglas Hayward Kirkpatrick was born [REDACTED]
[REDACTED] the son of [REDACTED]
[REDACTED] Kirkpatrick and [REDACTED] Kirkpatrick, Sr. He
completed work at [REDACTED] High School, [REDACTED]
[REDACTED] in 1966, then entered the United
States Air Force Academy where he graduated in 1970 with
a Bachelor of Science degree in Engineering Science. He
then attended Purdue University, finishing a Master of
Science degree in Aeronautics, Astronautics, and
Engineering Science in January, 1971. He entered Under-
graduate Pilot Training for the United States Air Force
in March, 1971, earning his wings in February, 1972. He
flew for the Air Force four years before becoming an
Instructor, then Assistant Professor, of Astronautical
Engineering at the United States Air Force Academy in
December, 1975. After two and a half years of teaching,
he flew for three more years then entered Graduate School
at The University of Texas at Austin in August, 1982. He
married [REDACTED] in February, 1971, [REDACTED]
[REDACTED] and they have six children: [REDACTED]
[REDACTED]

Permanent Address: [REDACTED]
[REDACTED]